Regulation of carbon polymer accumulation in *Synechocystis* sp. PCC 6803

Dissertation
der Mathematisch-Naturwissenschaftlichen Fakultät
der Eberhard Karls Universität Tübingen
zur Erlangung des Grades eines
Doktors der Naturwissenschaften
(Dr. rer. nat.)

vorgelegt von

Hauf, Waldemar
aus Zelinograd, Kasachstan

Tübingen
2016

Tag der mündlichen Qualifikation:	10.11.2016
Dekan:	Prof. Dr. Wolfgang Rosenstiel
1. Berichterstatter:	Prof. Dr. Karl Forchhammer
2. Berichterstatter:	Prof. Dr. Dieter Jendrossek

Contents

1 Zusammenfassung

Cyanobakterien sind eines der ältesten bakteriellen Phyla mit vielen metabolischen Fähigkeiten. Ihre Nährstoffansprüche sind gering, denn kleinere Mengen an Mineralsalzen, gute CO_2 Versorgung und Beleuchtung sind ausreichend um Wachstum sicherzustellen. Deshalb ist die Anwendung von Cyanobakterien als Biokatlysatoren für Kohlenstoffspeichertechnologien und Synthese von Feinchemikalien vorstellbar. Das CO_2 der Atmosphäre wird von Cyanobakterien normalerweise in metabolischen Stoffwechselwegen fixiert und benutzt um Wachstum und Produktion von Biomasse sicherzustellen. Die Umleitung der metabolischen Flüsse zur Produktion von Chemikalien für industrielle Anwendungen ist dabei ein aktives Forschungsfeld, mit möglichen kommerziellen und ökologischen Nutzen. Cyanobakterielle Biokatalysatoren könnten dabei eine neue grüne Revolution einleiten, indem Kohlenstoffspeichertechnologien mit der Synthese von chemischen Verbindungen gekoppelt werden.
Eine dieser chemisch interessanten Verbindungen ist das Biopolymer Polyhydroxybuttersäure (PHB) das biologisch abbaubar, nicht giftig ist und ähnliche Materialeigenschaften aufweist wie das aus fossilen Brennstoffen hergestellte Polypropylen. Das Cyanobakterium *Synechocystis* sp. PCC 6803 synthetisiert PHB bei ungünstigen Wachstumsbedingungen, jedoch ist die Regulation dieses Prozesses nicht vollständig geklärt. Um PHB biotechnologisch herstellen zu können, müssen die zugrundeliegenden regulatorischen Prozesse verstanden werden, so dass es möglich wird Kohlenstoffflüsse effizient für die PHB Synthese umzulenken. Diese Arbeit beschreibt die metabolischen Veränderungen, die mit PHB Synthese einhergehen und identifiziert metabolische Grundvoraussetzungen die erfüllt werden müssen um effiziente PHB Synthese in *Synechocystis* zu ermöglichen. Sie untersuchte dabei die Rolle des Stickstoff regulatorischen Proteins P_{II} (GlnB) in der Regulation des acetyl-CoA Stoffwechsels, dem Vorläufer für PHB Synthese. Sie beschreibt ein regulatorisches Protein das an der PHB Oberfläche assoziiert ist, dass dazu benutzt werden kann die Polymerkettenlänge zu beeinflussen und untersucht die Oberflächenzusammensetzung des PHB Granulums *in vivo*. Die hier gewonnen Erkenntnisse können genutzt werden um Biokatalysatoren auf Basis von *Synechocystis* zu entwickeln, die eine erhöhte PHB Produktion aufweisen.

2 Abstract

Cyanobacteria constitute one of the oldest bacterial phyla with high metabolic plasticity. Nutritional requirements for growth are simple and can be achieved with low amounts of salt, good CO_2 supply and illumination. Hence, application of cyanobacteria as biocatalysts for carbon capture technologies and production of fine chemicals can be envisioned. CO_2 from the atmosphere is usually fixed in metabolic pathways to foster growth and generate biomass. Redirection of metabolic pathways to produce chemical compounds of interest for industrial application is an active field of research with potential economical and ecological benefits. Thereby cyanobacterial biocatalysts could spark a new green revolution, coupling carbon capture technologies with synthesis of chemical compounds of interest.

One compound of interest is the biopolymer polyhydroxybutyrate (PHB) which is biodegradable, non-toxic and has similar material properties as polypropylene, a fossil fuel derived polymer. The cyanobacterium *Synechocystis* sp. PCC 6803 synthesizes PHB upon adverse growth conditions but the regulation of this process is not fully understood. For biotechnological PHB production knowledge of the underlying regulatory mechanisms is required to efficiently redirect carbon flux towards PHB synthesis. This work describes the metabolic alterations occurring upon PHB synthesis and identifies metabolic prerequisites that have to be met for efficient PHB production in *Synechocystis*. It investigates the role of the nitrogen regulatory protein P_{II} (GlnB) in the regulation of acetyl-CoA metabolism, the precursor of PHB synthesis. It describes a regulatory protein associated to the PHB surface, which can be used to manipulate polymer chain length and investigates the surface composition of the PHB granule *in vivo*. The insight gained through this work can be used to design biocatalysts based on *Synechocystis*, which show increased PHB production.

3 Introduction

3.1 Ecology and evolution of Cyanobacteria

Cyanobacteria are Gram negative prokaryotes, occupying diverse ecological niches. They can be found from soil crusts in deserts, to aquatic systems like the ocean, lakes, hot springs, rivers and temporary moist rocks to arctic and alpine environments (Whitton and Potts, 2000; Zakhia et al., 2008). Even though the ecological niches are diverse, all cyanobacteria can be grouped into five sections based on their morphology (Rippka et al., 1979). Section I cyanobacteria are unicellular and reproduce by binary fission or budding. Section II cyanobacteria are also unicellular, reproduce by multiple fission which give rise to small daughter cells the baeocyte. Section III cyanobacteria are filamentous bacteria without specialized cells. The section IV cyanobacteria form filaments, divide in only one plane and develop heterocysts, a specialized cell to fix atmospheric nitrogen. Section V cyanobacteria grow as filaments, divide in more than one plane and form heterocyst. All of these morphological diverse bacteria perform oxygenic photosynthesis and synthesize chlorophyll *a* which classifies them as one phylum the *Cyanophyta* (Whitton and Potts, 2000; Carr and Whitton, 1982). The present morphological diversity is thought to have evolved during the Archean period (3.8 - 2.9 Ga) and the evolution of multicellularity might have played a key role for the evolutionary success of cyanobacteria. Culminating in the great oxygenation event 2.4 Ga ago substantially changing the earths atmosphere (Schirrmeister et al., 2015).

3.2 Energy metabolism of *Synechocystis* sp. PCC 6803

Synechocystis sp. PCC 6803 is a unicellular cyanobacterium and belongs to the group *Chroococcales* (Rippka et al., 1979). It is able to grow photoautotrophically with CO_2 as sole carbon source, however some strains can also utilize acetate or glucose and grow photoheterotrophically. It is not able to fix atmospheric nitrogen and relies on combined nitrogen in the medium for growth.

3.2.1 Photosynthetic and respiratory electron flow

3.2.1.1 Photosyntheis

Light energy captured through light harvesting complexes is channeled through excitone transfer to the photosynthetic reaction centers. Chlorophyll *a* in the photosynthetic reaction center of photosystem II (PSII) is excited, which leads to charge separation. One electron of the chlorophyll *a* is transferred through several electron acceptors within the photosystem to plastoquinone reducing it to plastoquinol. Electrons abstracted from chlorophyll are resupplied by a manganese cluster in the oxygen evolving complex (OEC). Once four electrons were abstracted from the manganese cluster water is oxidized to oxygen and four protons are released in the thylakoid lumen contributing to the acidification of the thylakoid lumen (Shen, 2015). Plastoquinol is released from PSII into the membrane and is oxidized through the cytochrome b_6f complex to plastoquinon, contributing to the proton gradient through the Q-cycle. Electrons from the two electron carrier plastoquinol are transferred by the cytochrome b_6f complex to the single electron carrier plastocyanine in the thylakoid lumen. Plastocyanine can be used as electron donor by

PSI to reduce oxidized chlorophyll *a*. Light induced charge separation at PSI is used to generate reduced ferredoxin, which can be used for anabolic reactions or to generate NADPH through ferridoxin-$NADP^+$ reductase (FNR).

3.2.1.2 Respiration

The main difference of respiratory electron flow to photosynthetic electron flow is that plastoquinol is generated by either the NDH1 complex or succinate dehydrogenase (Cooley et al., 2000). The NDH1 complex of cyanobacteria is special in respect to the tasks it can perform. It is not only involved in respiration (as complex I) but can perform cyclic electron flow around PSI to increase the ATP/NADP ratio. In addition it is involved in high and low affinity CO_2 uptake (Battchikova et al., 2011). The cytochrome b_6f complex is also utilized during respiratory electron flow and transfers electrons on plastocyanine and cytochrome c_6. Terminal oxidases (aa_3 cytochrome-, b_0 quinol oxidase) use the electrons provided by the electron carriers to reduce oxygen to water (Peschek et al., 2011). The proton motive force generated by either photosynthesis or respiration is used to drive ATP synthesis through ATP synthase.

The primary source for ATP and reducing equivalents is photosynthesis if sufficient light is available. When light is limiting or in darkness cyanobacteria catabolize sugars to generate ATP and reducing equivalents. Electron transfer processes that lead to the generation of a proton motive force for ATP synthesis, occurring during light and dark periods, are summarized in figure 3.1.

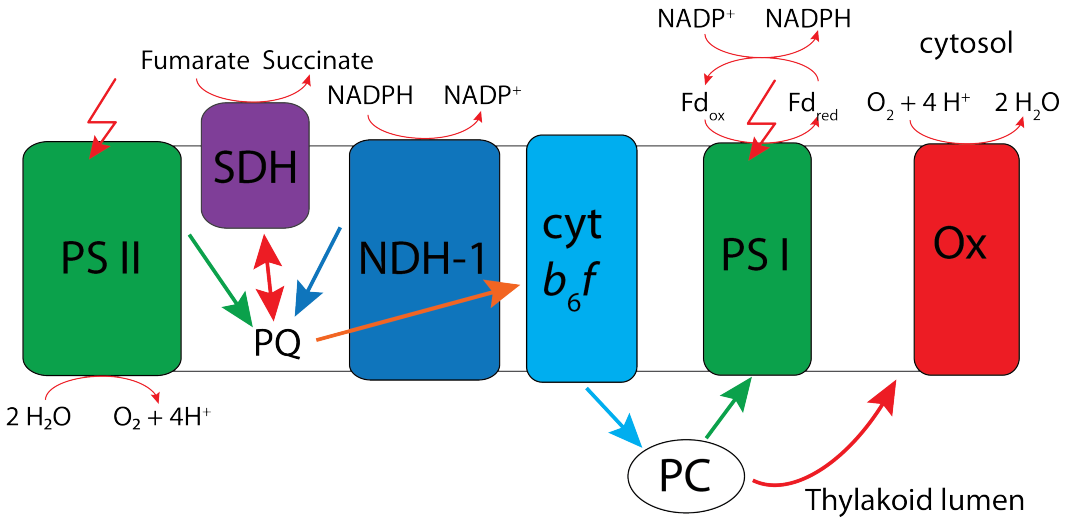

Fig. 3.1: Summary of energetic processes occurring in *Synechocystis* to generate an proton motive force. Arrows indicate electron flow, which is either unidirectional or can be bidirectional in case of SDH. Lightning bolts indicate charge separation in both photosystems induced by light. *Abbreviations*: *PS II*, photosystem II; *PQ*, plastoquinol; *SDH*, succinate dehydrogenase; *NDH-1*, NADPH dehydrogenase; *cytb*$_6$*f*, cytochrome b_6f; *PS I*, photosystem I; *PC*, plastocyanine; *Ox*, terminal oxidase; Fd_{ox}, oxidized ferredoxin; Fd_{red}, reduced ferredoxin

3.3 Carbon metabolism of *Synechocystis* sp. PCC 6803

3.3.1 CO_2 fixation

ATP and reducing equivalents generated through photosynthetic reactions are utilized in the Calvin-Benson-Bessham cycle to fix atmospheric carbon dioxide. The key enzyme for carbon fixation is Ribulose-1,5-bisphosphate carboxylase/oxygenase (RubisCO). The enzyme uses ribulose-1,5-bisphosphate and CO_2 as substrates to catalyze the formation 3-keto-2-carboxyarabinitol-1,5-bisphosphate, an unstable intermediate, which decays very quickly into two molecules of 3-phosphoglycerate a key intermediate of primary carbon metabolism. RubisCO is not highly specific towards CO_2 and is able to utilize molecular oxygen as substrate. This leads to the formation of one molecule 3-phosphoglycerate and one molecule 2-phosphoglycolate which is toxic and has to be recycled in a process called photorespiration (Bauwe et al., 2010). To reduce the formation of 2-phosphoglycolate cyanobacteria have evolved a protein organelle the carboxysome (Yeates et al., 2008). The carboxysome shell proteins build up the ikosahedral carboxysome shell and from a diffusion barrier. Whilst RubisCO and carbonic anhydrase are trapped within the carboxysome through carboxysome shell proteins, small molecules like bicarbonate, 3-phosphoglycerate and ribulose-1,5-bisphosphate can diffuse through small pores formed by carboxysome shell proteins. Inside the carboxysome carbonic anhydrase strips away water from bicarbonate leading to a locally increased concentration of CO_2, thereby indirectly reducing the oxygenation reaction. This requires a high intracellular bicarbonate concentration achieved through several transport systems shown in figure 3.2.

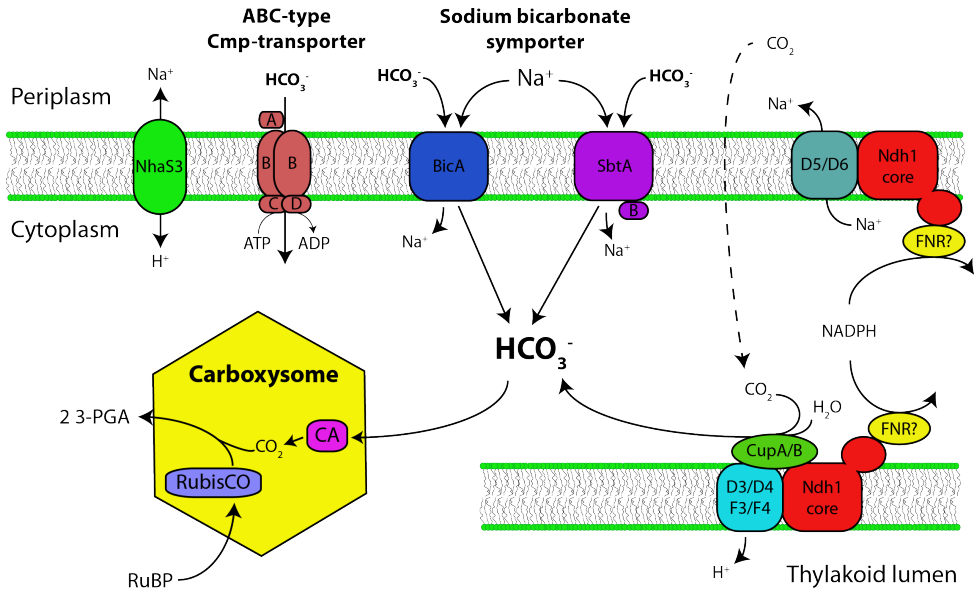

Fig. 3.2: Summary of all known CO_2 and HCO_3^- uptake systems of *Synechocystis* adopted from (Burnap et al., 2015). Abbreviations: 3-PGA: *3-phosphoglycerate*; RuBP: *Ribulose-1,5-bisphosphate*; CA: *Carbonic Anhydrase*; RubisCO: *Ribulose-1,5-bisphosphate carboxylase/oxygenase*; D3: *NdhD3*; D4: *NdhD4*; D5: *NdhD5*; D6: *NdhD6*; F3: *NdhF3*; F4: *NdhF4*

The transport systems differ in their affinity towards bicarbonate and the source of energy

used for transport. The high affinity Cmp system is a typical ABC type transport system and uses ATP to drive transport into the cytoplasm. Two sodium dependent bicarbonate symporters are known; the high affinity SbtAB system and the low affinity high velocity BicA system. Both systems require a sodium motive force, which is generated through the sodium-proton anti-porter NhaS3 and possibly the Ndh1 system in complex I with subunits NdhD5 and NdhD6. A third set of proteins is located at the thylakoid membrane and is considered to be a CO_2 uptake system. It catalyzes the hydration of CO_2 that can enter the cytoplasm through aquaporins or passively through diffusion (Ding et al., 2013). Once again a high and low affinity system is present and both of them require the core Ndh1 complex. The high affinity uptake system requires the CupA, NdhF3 and NdhD3 proteins, which are upregulated under conditions of low CO_2 levels. The low affinity system is composed of CupB, NdhF4 and NdhD4 and is expressed constitutively (Burnap et al., 2015).

3.3.2 Other carbon sources

Instead of fixing carbon dioxide *Synechocystis* can utilize various carbon sources for growth. Some laboratory strains have evolved the ability to utilize glucose for growth. Glucose is degraded though several pathways including glycolysis, oxidative pentose pathway and the Entner–Doudoroff pathway (Chen et al., 2016). One other organic compound known to be utilized during photoheterotrophic growth is acetate. Acetate is thought to be metabolized through the action of two pathways shown in figure 3.3.

Acetate utilization is though to directly supply the acetyl-CoA pool through acetyl-coenzyme A synthetase (Acs), with a net hydrolysis of 2 energy rich phosphoanhydrid bonds. The energetically more efficient pathway uses acetate kinase (AckA) to synthesize acetyl phosphate consuming one ATP molecule. Acetyl phosphate is then converted to acetyl-CoA through phosphotransacetylase (Pta). Specific environmental conditions could reverse this pathway in order to generate ATP. Fermentation of internal carbon storage compounds would then lead to acetate excretion, which does not occur during photoautotrophic growth (Chen et al., 2016). Acetyl-CoA generated through glycolysis could be converted to acetyl phosphate by Pta and used to generate ATP through AckA. Alternatively Xylulose-5-phosphate/fructose-6-phosphate phosphoketolase (XFPK) or xylulose 5-phosphate phosphoketolase (XPK) which directly convert sugars to acetyl phosphate, could be used to generate ATP through AckA.

3.3.3 Carbon storage

Fixed CO_2 is either directly utilized during metabolism for anabolic reactions or is stored intracellularly in form of carbon polymers. The three known storage polymers of *Synechocystis* are glycogen, polyhydroxybutyric acid (PHB) and cyanophycin. As cyanophycin is both a carbon and nitrogen storage compound it will not be covered here.

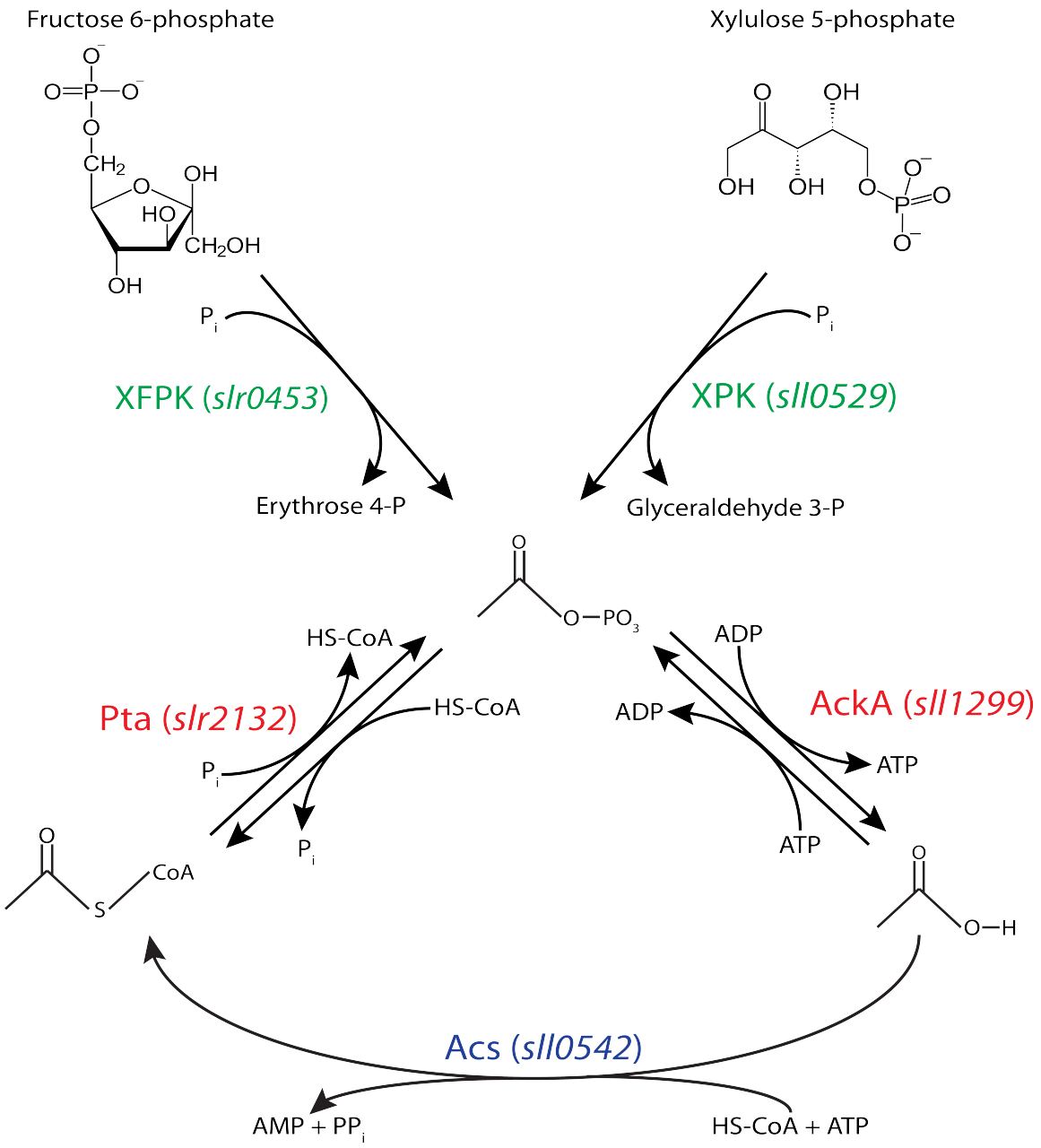

Fig. 3.3: Conversion of acetate to acetyl-CoA through acetyl phosphate. Acetyl phosphate formation is maintained through conversion of C5 and C6 sugars through phosphoketolases. Acs: *acetyl-coenzyme A synthetase*, Pta: *phosphotransacetylase*, AckA *acetate kinase*, XFPK: *xylulose-5-phosphate/fructose-6-phosphate phosphoketolase*, XPK: *xylulose 5-phosphate phosphoketolase*

3.3.3.1 Glycogen accumulation

Glycogen is thought to be the universal carbon storage compound in cyanobacteria and is required for survival under stress conditions (Suzuki et al., 2010; Gründel et al., 2012; De Philippis et al., 1992b). It is synthesized from glucose 1-phosphate by the action of two enzymes. ADP-glucose phosphorylase uses ATP and glucose 1-phosphate to synthesize the activated sugar ADP-glucose. ADP-glucose is used by glycogen synthase to transfer the sugar moiety to an existing α1,4 glucan or a maltodextrin primer (Preiss, 1984). ADP-glucose phosphorylase is stimulated through 3-phosphoglycerate (Levi and Preiss, 1976; Charng et al., 1992) and is sensitive to changes in the redox pool (Díaz-Troya et al., 2014). Glycogen is degraded by the action of glycogen phosphorylases and debranching enzymes to yield glucose 1-phosphate, which can be utilized in primary carbon metabolism. Transcript abundance of glycogen metabolic genes fluctuates during the day and night cycle (Pattanayak et al., 2014; Diamond et al., 2015; Saha et al., 2016) and nitrogen starvation induces transcription of glycogen catabolic and anabolic genes (Krasikov et al., 2012). Based on these data and physiological measurements of glycogen levels, glycogen was established to be the primary energy source to maintain survival during growth limiting conditions. Once the environmental conditions favor growth glycogen is degraded through various pathways to provide energy and carbon for growth (Xiong et al., 2015; Chen et al., 2016).

3.3.3.2 PHB accumulation

Environmental conditions triggering PHB accumulation are well understood, whilst the molecular mechanisms which trigger PHB accumulation are not. PHB is thought to accumulate during a metabolic imbalance when the supply of key macro-nutrients like nitrogen, potassium or phosphate is limited (Panda et al., 2006; Panda and Mallick, 2007). Nitrogen starvation triggers expression of PHB biosynthetic genes (Schlebusch and Forchhammer, 2010; Krasikov et al., 2012), so does cultivation using a day and night cycle (Saha et al., 2016). Up to 20 % of cell dry mass are accumulating as PHB during nitrogen starvation but only 5 % are accumulated during the day night cycle (Panda et al., 2006). Even though transcriptional responses are similar between both conditions the extent of PHB accumulating is very different and the cellular signals favoring PHB accumulation are unknown.

PHB biosynthesis requires the catalytic activity of only three enzymes. In a first step acetyl-CoA is condensed through β-ketothiolase (PhaA) to acetoacetyl-CoA, which is then reduced by acetoacetyl-CoA reductase (PhaB) to 3-hydroxybutyryl-CoA (Taroncher-Oldenburg et al., 2000). In the last step of PHB biosynthesis, PHB synthase catalyzes the polymerisation of 3-hydroxybutyryl-CoA to polyhydroxybutyric acid (PHB) (Hein et al., 1998). The biosynthesis of PHB and putative PHB granule structure is depicted in figure 3.4. The biochemical properties of two PhaA enzymes have been characterized and Michaleis-Menten constants of 0.4-0.7 mM have been reported for the condensation reaction, while free HS-CoA inhibits the reaction (Oeding and Schlegel, 1973; Oh et al., 1997). The reverse reaction (thioclastic cleavage) has a K_M of 0.12 mM. Due to the biochemical properties of this enzyme formation of acetoacetyl-CoA is very inefficient.

Consequently PhaB has a K_M value in the low μmolar range (2-10) and has an extremely high catalytic efficiency ($1.8 * 10^8 M^{-1} s^{-1}$), comparable to enzymes like carbonic anhydrase, in order to facilitate 3-hydroxybutyryl-CoA syntesis (Colby and Chen, 1992; Ploux et al., 1988).

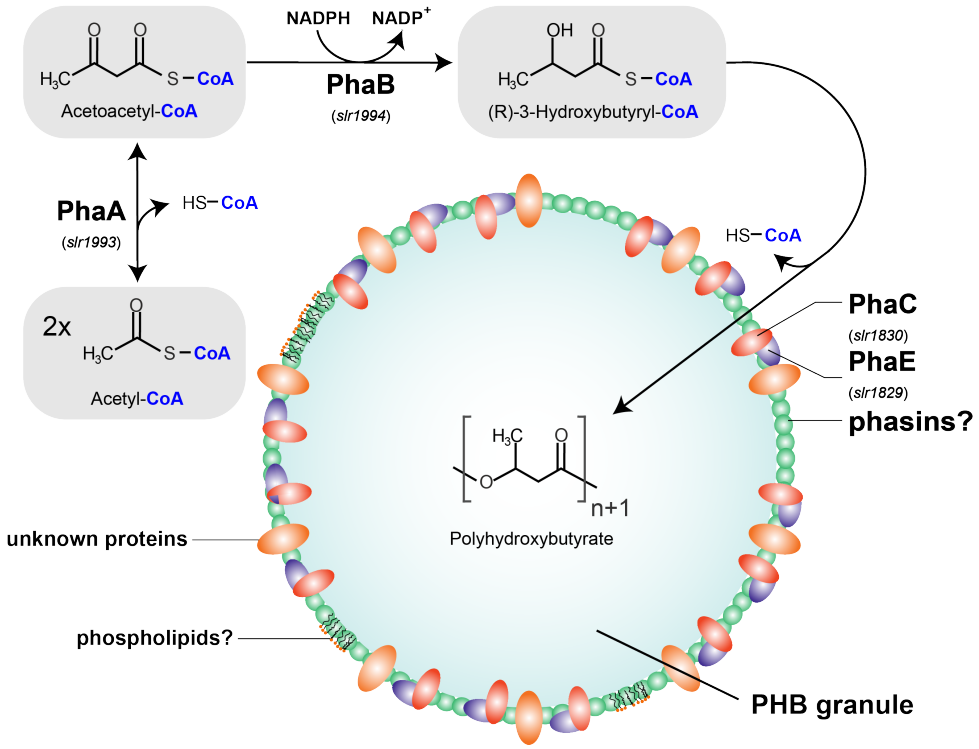

Fig. 3.4: Summary of reactions leading to the accumulation of PHB through PhaA, PhaB and the heterodimeric PHB synthase PhaEC. The PHB granule surface is potentially covered by phasin proteins, phospholipids and so far unknown proteins.

PHB synthases can be classified into four subgroups which share distinct characteristics (Rehm, 2006). Class I PHB synthases are 60-73 kDa in size, form homodimers and use short chain hydroxyalkanoic acids (C3-C5) as substrate. Class II enzymes are very similar to class I enzymes in dimerization and molecular weight but utilize longer chain hydroxyalkanoic acids (longer than C5) as substrate. Class III enzymes are heterodimers of PhaE (~40 kDa) and PhaC (~40 kDa) with the heterodimers dimerizing to form a tetramer. Like class I enzymes class III enzymes utilize short chain hydroxyalkanoic acids as substrate (C3-C5). Class IV enzymes are formed by heterodimers between PhaC (~40 kDa) and PhaR (~20 kDa) and use short chain hydroxyalkanoic acids as substrate (C3-C5).

Synechocystis possesses a type III PHB synthase. Both PhaC and PhaE are required *in vivo* to catalyze PHB formation and PhaC carries the catalytic triade (C149, D302 and H331) (Hein et al., 1998). The catalytic mechanism involves the formation of a covalently bound intermediate at C149. The covelently bound intermediate is attacked by the 3-hydroxyl group of a 3-hydroxybutyryl-CoA forming a non-covalently bound intermediate. The intermediate subsequently forms a covalent bond with C149 releasing the CoA moiety (Chen et al., 2015). It is so far unknown which role PhaE plays in catalysis. It could potentially transduce the redox state on PHB synthase activity

through glutathionylation (Chardonnet et al., 2015). PHB synthase is inhibited by NAD^+ and $NADP^+$ enabling the cell to adjust biosynthesis based on the intracellular red-ox balance (Jossek et al., 1998). *In vitro* studies with cyanobacterial PHB synthase have reported activation by acetyl phosphate (Miyake et al., 1997; Sharma et al., 2006). Genetic engineering to increase acetyl phosphate levels, in order to activate PHB synthase, could be a suitable approach to increase PHB production in cyanobacteria.

PHB associated proteins later named phasins, have initially been identified on the PHB granule surface of *Rhodococcus ruber* (Pieper-Fürst et al., 1994). Follow up studies have shown that deletion of a phasin protein leads to few big PHB granules (Wieczorek et al., 1995), while strong phasin expression results in many small PHB granules (Wahl et al., 2012). This led to the conclusion that phasin proteins regulate the surface to volume ratio of PHB granules. The biological function of phasins are manifold. Some phasin proteins alter the processivity of PHB synthase, whereas others can act as activators of PHB synthase (Jossek et al., 1998; Ushimaru et al., 2014; Pfeiffer and Jendrossek, 2014). A more specialized biological function is performed by the phasin PhaM in *Ralstonia eutropha* and PhaF in *Pseudomonas putida*. These proteins attach PHB granules to the nucleoid and thereby ensure equal distribution of PHB granules to daughter cells (Wahl et al., 2012; Galan et al., 2011). Hein et al. (1998) have reported the protein encoded by ORF *ssl2501* in *Synechocystis* to be associated to the PHB granule surface, which might be a phasin but *in vitro* evidence for this is missing. Next to phasin proteins PHB depolymerases, which degrade the polymer to hydroxybutyric acid and channel it back into primary metabolism, have to be associated. So far no PHB depolymerase has been identified in *Synechocystis*.

The PHB granule surface is a complex assembly of several types of proteins like phasins, PHB synthase, PHB depolymerase and others (Jendrossek and Pfeiffer, 2014). This led to the description of the PHB granule as bacterial organelle like microcompartment the Carbonosome (Jendrossek, 2009). Another vividly discussed aspect in the literature is whether phospholipids associate to the PHB granule *in vivo*. Whereas early reports indicated that phospholipids are associated to the surface of isolated PHB granules(Griebel et al., 1968; Mayer et al., 1996), other studies couldn't find conclusive evidence that this is also true for living cells (Beeby et al., 2012; Jendrossek et al., 2007).

3.4 Nitrogen metabolism of *Synechocystis* sp. PCC 6803

3.4.1 Transport and Assimilation of Nitrogen

Synechocystis is unable to fix atmospheric nitrogen and requires fixed nitrogen in form of nitrate, ammonium, urea or amino acids as nitrogen source for growth (Herrero et al., 2008). Nitrate and urea uptake is facilitated by ABC type transporters (Ohashi et al., 2011; Valladares et al., 2002). While ammonium transport across the membrane is facilitated through *amtB* homologs (Montesinos et al., 1998). *Synechocystis* posses three *amtB* genes of which *amt1* is thought to be the primary ammonium transporter (Montesinos et al., 1998). Several amino acid uptake systems

are known, which are either classic ABC-type transporters or sodium dependent symporters (Quintero et al., 2001). Amino acids can be directly used for metabolism, but nitrate has to be reduced through nitrate reductase and nitrite reductase to ammonia in order to be available for metabolism (Ohashi et al., 2011). Ammonia undergoes spontaneous protonation in aqueous solution forming ammonium, which can be used by glutamine synthetase (GS) for glutamine synthesis. In conjunction with GOGAT (glutamine oxoglutarate aminotransferase) GS forms the GS-GOGAT cycle to assimilate inorganic nitrogen for primary metabolism(Wolk et al., 1976).

3.4.2 Response to nitrogen starvation

Removal of a nitrogen source from the growth medium has a significant impact on the physiology of *Synechocystis*. It leads to strong morphological and metabolic changes termed chlorosis. As a first quick response to nitrogen starvation the transcription factor NtcA induces the expression of *nblA* (Sauer et al., 1999; Baier et al., 2001). NblA is an adapter protein that marks the light harvesting complexes (consisting of phycobiliproteins) for protein degradation (Sendersky et al., 2014; Baier et al., 2014). Consequently degradation of light harvesting complexes leads to a reduced phosynthetic activity of both photosystems, followed by a gradual degradation of thylakoid membranes. Nevertheless cells remain viable (Görl et al., 1998; Sauer et al., 2001). Increased protein turnover is used to adapt metabolism towards survival and prolonged starvation reduces metabolic activity. Adaptation towards nitrogen starvation coincides with carbon polymer synthesis. Glycogen content rises quickly, whereas the PHB content increases more gradually (Schlebusch and Forchhammer, 2010).

3.4.3 Regulation of nitrogen metabolism through the P_{II} (GlnB) protein

3.4.3.1 Structure function relationship of GlnB

P_{II} proteins are a highly conserved group of trimeric proteins with three loop regions (B-, C- and T-loop) extending from the protein (figure 3.5 A). This family of proteins is involved in the regulation of various nitrogen metabolism related processes through interaction with partner proteins (Forchhammer and Lüddecke, 2016).

P_{II} proteins are able to bind adenyl nucleotides most often ATP or ADP in the cleft formed between individual subunits. In case of *Synechococcus elongatus* and *Synechocystis* sp. PCC 6803, GlnB is also able to bind the TCA cycle intermediate 2-oxoglutarate (2-OG). For 2-OG binding, ATP has to be bound by P_{II} as it chelates a Mg^{2+} ion that is required to coordinate 2-OG (figure 3.5 B) (Fokina et al., 2010a). ATP and ADP compete for the nucleotide binding site (Fokina et al., 2011) and are bound in a concentration dependent manner. Affinity of the nucleotide binding site for either ATP or ADP is influenced through interaction with partner proteins, which can enforce a T-loop conformation favoring ADP binding instead of ATP (Zeth et al., 2014). Since bound ATP is required for 2-OG binding, P_{II} proteins are considered intracellular sensors of the cellular energy and carbon supply (Ninfa and Jiang, 2005). As shown in figure 3.5 the adopted secondary structure changes upon ligand binding dramatically. Upon 2-OG binding the C-terminus folds back and extends in the horizontal plane, whereas it is extended

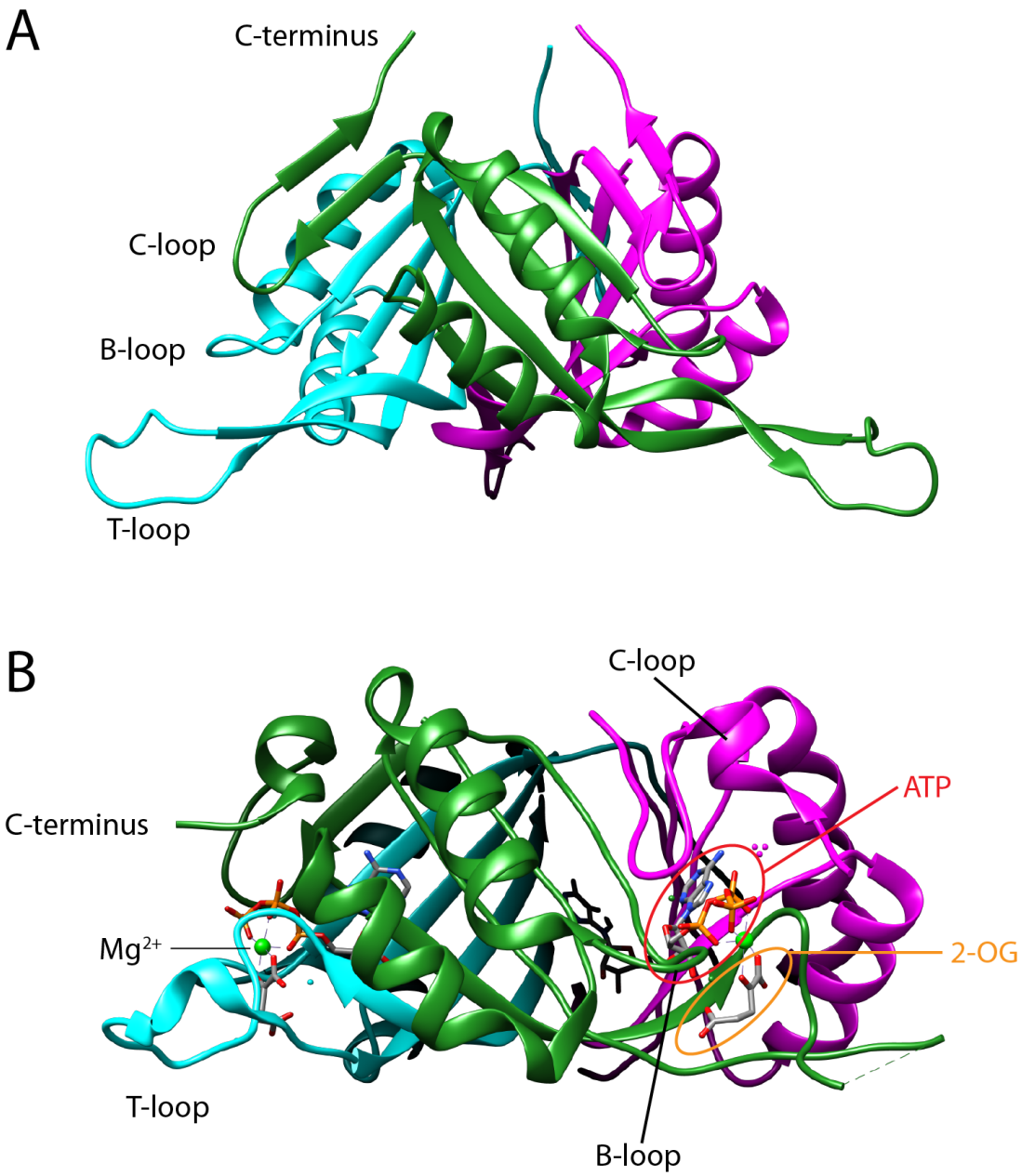

Fig. 3.5: A: Crystal structure of the P_{II} from *Synechococcus elongatus* PCC7942 without ligands (PDBID:1QY7). B:Crystal structure of the P_{II} from *Synechococcus elongatus* PCC7942 with bound ATP (highlighted in red) and 2-oxoglutarate (highlighted in orange) and the Mg^{2+} ion coordinating 2-OG binding (PDBID:2XUN). Binding of ATP and 2-OG alters the secondary structure of the T-loop, which becomes more organized and the C-terminus is rearranged.

in the vertical plane without ligands. The T-loop conformation changes notably and becomes more ordered, altering the surface of the protein. This in turn affects the affinity of P_{II} to its target proteins, resulting in a different regulatory outcome (Forchhammer and Lüddecke, 2016). Covalent modification at the T-loop (phosphorylation at Ser49 in unicellular cyanobacteria) adds an additional level of complexity and can prevent protein-protein interactions (Heinrich et al., 2004). Hence, the P_{II} regulatory system is a highly sophisticated sensory system tuning the regulatory output based on the adenylate charge, carbon supply and covalent modification.

3.4.3.2 The P_{II} interaction network

The P_{II} interaction network in unicellular cyanobacteria is best characterized for two target proteins. The enzyme catalyzing the committed step of arginine biosynthesis N-acetyl glutamate kinase (NAGK) (Heinrich et al., 2004; Maheswaran et al., 2004) and the transcriptional co-activator PipX (Espinosa et al., 2006; Llacer et al., 2010). The P_{II} interaction network with its known targets is summarized in figure 3.6.

NAG kinase (NAGK) catalyzes the phosphorylation of N-acetyl glutamate to N-acetyl glutamyl phosphate a committed step in arginine biosyntesis. The catalytic activity of the enzyme is regulated through a feedback loop and high arginine levels inhibit catalysis. If the enzyme is in complex with P_{II} much higher arginine levels are required to inhibit the enzymatic activity (Maheswaran et al., 2004). The interaction is highly sensitive towards 2-OG, which dissociates the complex. A negative charge at Ser49 of the T-loop prevents complex formation, making NAGK much more sensitive towards feedback inhibition (Lüddecke and Forchhammer, 2013; Heinrich et al., 2004). This regulatory principle has been utilized to boost cellular arginine levels. Using a P_{II} variant that is unable to sense 2-OG and therefore constantly reliefs NAGK from arginine feed back inhibition (Fokina et al., 2010b), high cyanophycin accumulation could be achieved (Watzer et al., 2015).

PipX is a transcriptional co-activator of the key transcription factor of nitrogen starvation NtcA (Herrero et al., 2001). While NtcA is able to bind to DNA by itself, 2-OG and PipX increase the affinity of NtcA towards DNA and stabilize the complex (Herrero et al., 2001; Llacer et al., 2010). The role of P_{II} in the regulatory network is to prevent the premature activation of NtcA by sequestering PipX from NtcA during exponential growth (Espinosa et al., 2006). Tuning down NtcA mediated expression during exponential growth appears to be crucial, as mutants of P_{II} in *Synechococcus elongatus* PCC7942 spontaneously accumulate mutations in PipX (Espinosa et al., 2009; Laichoubi et al., 2012). PipX-GlnB interaction is insensitive to a negative charge at the T-loop but 2-OG dissociates the complex (Llacer et al., 2010).

Nitrogen transport across the cytoplasmic membrane appears to be regulated by P_{II}, as *glnB* mutants were affected in nitrate transport (Lee et al., 2000; Kobayashi et al., 2005). The wild type was able to quickly cease nitrate transport across the membrane upon ammonium shock, whereas a P_{II} mutant continued nitrate uptake under these conditions. The regulation of this process

appears to be insensitive to P_{II} phosphorylation at S49. Kobayashi et al. (2005) have suggested that P_{II} regulates nitrate uptake through NrtC, a subunit of the nitrate ABC-type transporter, based on the observation that a C-terminal deletion of NrtC showed a P_{II} mutant phenotype and was unable to abrogate nitrogen import upon ammonia shock. However no biochemical evidence for the proposed regulation is present. Ammonium transport across the cytoplasmic membrane is facilitated by the AmtB channel, but can be blocked by GlnK (a P_{II} protein family member absent in cyanobacteria) in Enterobacteria. This is achieved by insertion of the T-loop in the pore formed by AmtB and can be prevented by covalent modification at the T-loop (Conroy et al., 2007). The interaction is also affected by the ligands ATP/ADP and 2-OG with the latter dissociating the complex, enabling ammonium influx into the cell (Radchenko et al., 2010). Even though experimental evidence confirming this regulation in cyanobacteria (through GlnB) is absent, this regulation is highly conserved among bacteria and archea and likely present in cyanobacteria.

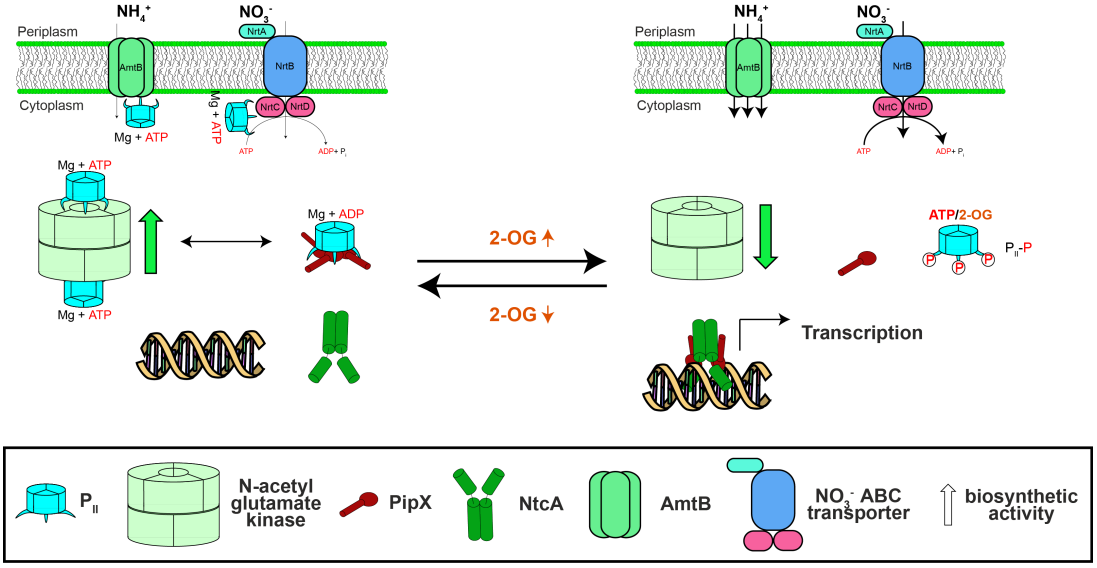

Fig. 3.6: Overview of the P_{II} interaction network in unicellular cyanobacteria. The effect of P_{II} interaction affects transport across the cytoplasmic membrane, biosynthetic activity or interaction with other proteins.

3.5 Research objective

In recent years cyanobacteria have attracted attention due to their potential use as biocatalysts. One of the best studied cyanobacterial species is the unicellular bacterium *Synechocystis* sp. PCC6803. *Synechocystis* produces the biopolymer polyhydroxybutyric acid (PHB) which has potential medical application in tissue engineering. However production rates are incredibly low with about 2.5 mg/(l d) in wild type. In order to increase production rates this works attempts to define the basic metabolic and regulatory principles favoring PHB synthesis. Therefore metabolic changes upon nitrogen starvation were investigated. Increases in acetyl phosphate levels were implied to increase PHB synthase activity upon nitrogen starvation. This was tested biochemically. In addition a detailed analysis was performed whether genetic alterations could potentially increase cellular acetyl phosphate levels leading to increased PHB production. The central regulatory protein GlnB emerged as a central regulator of acetyl-CoA metabolism. Hence, the impact of *glnB* mutation was investigated with regard to PHB accumulation. A second topic of the thesis was dedicated to the biogenesis of PHB granules. Several models were proposed in the literature. One model favors the formation of PHB granules at the membrane, consequently PHB grnaules should be engulfed by a phospholipid monolayer. Another model implicates that PHB granule formation occurs at the chromosome, due to the fact that a phasin protein that activates PHB synthase is associated to DNA. No phasins are known in *Synechocystis* sp. PCC 6803 therefore potential proteins associated to the PHB granule surface were identified and characterized.

4 Publication 1

Contributions of the candidate for the publication.
I have created strains expressing fluorescently labeled PHB synthase subunits and performed the microscopic analysis of those strains. The manuscript was written by me under the supervision of Prof. Forchhammer and I have taken part in the revision process.

4.1 Metabolic Changes in *Synechocystis* PCC6803 upon Nitrogen-Starvation: Excess NADPH Sustains Polyhydroxybutyrate Accumulation

Metabolites **2013**, *3*, 101-118; doi:10.3390/metabo3010101

OPEN ACCESS

metabolites

ISSN 2218-1989

www.mdpi.com/journal/metabolites/

Article

Metabolic Changes in *Synechocystis* PCC6803 upon Nitrogen-Starvation: Excess NADPH Sustains Polyhydroxybutyrate Accumulation

Waldemar Hauf [1], Maximilian Schlebusch [1], Jan Hüge [2], Joachim Kopka [2], Martin Hagemann [3] and Karl Forchhammer [1,*]

1. Interfakultäres Institut für Mikrobiologie und Infektionsmedizin Tübingen, Eberhard-Karls-Universität Tübingen, Auf der Morgenstelle 28, Tübingen, 72070, Germany; E-Mails: waldemar.hauf@gmail.com (W.H.); maximilian.schlebusch@googlemail.com (M.S.);
2. Max-Planck-Institut für Molekulare Pflanzenphysiologie, Am Mühlenberg 1, Golm, 14476, Germany; E-Mails: huege@ipk-gatersleben.de (J.H.); kopka@mpimp-golm.mpg.de (J.K.)
3. Universität Rostock, Institut Biowissenschaften, Pflanzenphysiologie, Albert-Einstein-Str. 3, Rostock, D-18059, Germany; E-Mail: martin.hagemann@uni-rostock.de

* Author to whom correspondence should be addressed; E-Mail: karl.forchhammer@uni-tuebingen.de; Tel.: +49-7071-2972096; Fax: +49-7071-295843.

Received: 20 December 2012; in revised form: 28 January 2013 / Accepted: 30 January 2013 / Published: 6 February 2013

Abstract: Polyhydroxybutyrate (PHB) is a common carbon storage polymer among heterotrophic bacteria. It is also accumulated in some photoautotrophic cyanobacteria; however, the knowledge of how PHB accumulation is regulated in this group is limited. PHB synthesis in *Synechocystis* sp. PCC 6803 is initiated once macronutrients like phosphorus or nitrogen are limiting. We have previously reported a mutation in the gene *sll0783* that impairs PHB accumulation in this cyanobacterium upon nitrogen starvation. In this study we present data which explain the observed phenotype. We investigated differences in intracellular localization of PHB synthase, metabolism, and the NADPH pool between wild type and mutant. Localization of PHB synthase was not impaired in the *sll0783* mutant; however, metabolome analysis revealed a difference in sorbitol levels, indicating a more oxidizing intracellular environment than in the wild type. We confirmed this by directly measuring the NADPH/NADP ratio and by altering the intracellular redox state of wild type and *sll0783* mutant. We were able to physiologically complement the mutant phenotype of diminished PHB synthase activity by making the intracellular environment more reducing. Our data illustrate that the NADPH pool is an important factor

for regulation of PHB biosynthesis and metabolism, which is also of interest for potential biotechnological applications.

Keywords: cyanobacteria; metabolome; nitrogen starvation; sorbitol; NADPH/NADP ratio; redox balance; Polyhydroxybutyrate; PHB synthase

1. Introduction

Cyanobacteria are Gram-negative prokaryotes capable to perform oxygenic photosynthesis [1]. They thrive in almost all illuminated ecosystems and contribute to the global carbon-cycle of the biosphere. In many natural environments, the availability of phosphorus and combined nitrogen is growth-limiting and, therefore, microorganisms have evolved various mechanisms to cope with this constraint [2]. Unicellular non-diazotrophic cyanobacteria respond to nitrogen limitation by a process termed chlorosis [3]. In this process, the light harvesting complexes are degraded and photosynthetic activity declines concomitant with degradation of thylakoid membranes [4]. The response towards changing levels of combined nitrogen in the environment and physiological adaptation to these conditions is mediated by the NtcA- and PII-system which induces alteration of gene expression as well as metabolic adaptation to altered nutrient availability [5–7].

During nitrogen starvation, carbon polymers like glycogen [4] and in some species PHB are accumulated [8]. The genes coding for precursor biosynthesis of PHB in *Synechocystis* sp. PCC 6803 are known; β-ketothiolase PhaA (*slr1993*), which condenses two acetyl-CoA to acetoacetyl-CoA, and acetoacetyl-CoA reductase PhaB (*slr1994*), which is responsible for reducing acetoacetyl-CoA with NADPH to hydroxybutyryl-CoA, are organized in one operon [9]. PHB synthase, the enzyme catalyzing the polymerization reaction to polyhydroxybutyrate, is encoded in a second operon and forms a heterodimer of PhaE (*slr1829*) and PhaC (*slr1830*) [10]. Expression of both operons is up-regulated upon nitrogen starvation [11] but biosynthetic activation of PHB synthase is independent of protein biosynthesis [12]. Hence, a complex regulatory network, which integrates different input signals, controls PHB biosynthetic activity and PHB granule formation.

How PHB granules form is still a matter of debate and several hypothesis have been proposed to explain experimental observations [13,14]. One of them is the budding model, which claims that PHB synthase associates with the cytoplasmic membrane and synthesizes PHB in the hydrophobic part of the membrane. This model requires PHB synthase to be spatially regulated within a cell. Thus, a mechanism that controls intracellular localization has to be present.

We have previously reported that inactivation of *sll0783*, a highly induced gene upon nitrogen starvation [15], results in a phenotype with highly reduced PHB accumulation. After induction of nitrogen starvation, PHB synthase was initially activated but decayed rapidly during prolonged nitrogen starvation [11]. Since the expression of the *pha*-genes was not strongly affected in the mutant, and the level of acetyl-CoA was not decreased, we suspected that impaired PHB synthase activity is due to a posttranscriptional process, in which the product of *sll0783* is involved. In this work we further investigated the cause of ceasing PHB synthase activity in the *sll0783* mutant by assessing the

intracellular localization of PHB synthase and globally analyzing changes in metabolism upon nitrogen starvation.

2. Results and Discussion

As shown previously, impaired PHB accumulation in an insertion knock out of *sll0783* in *Synechocystis* sp. PCC 6803 is due to a decay of transiently induced PHB synthase activity [11]. In the enzymatic assays of PHB synthase activity, we observed that the activity of the enzyme was mostly present in the insoluble fraction and only a minor activity could be detected in the soluble fraction after onset of nitrogen starvation. With prolonged nitrogen starvation, the biosynthetic activity of PHB synthase in the insoluble fraction of the *sll0783* mutant had almost vanished. Since the budding model for PHB granule biogenesis requires the PHB synthase to change its intracellular localization from a soluble to a membrane localized state, we asked the question whether the impaired activity of PHB synthase in the *sll0783* mutant is related to impaired localization of the enzyme as compared to the wild type.

2.1. Intracellular Localization of PHB Synthase

To resolve PHB localization in wild type and *sll0783* mutant cells, recombinant reporter strains were constructed with translational fusions of both PHB synthase subunits to eGfp to study accumulation and localization of PHB synthase upon nitrogen starvation. The genes *phaE* (*slr1829*) and *phaC* (*slr1830*) together with each 100 bp promoter upstream region were amplified by PCR with genomic DNA from *Synechocystis*. The gene encoding eGfp was amplified from plasmid pCESL19 [16] by PCR. Translational fusions of PhaE- and PhaC-eGfp were generated by performing a long flanking homology PCR and cloning the resulting PCR products in the broad host range vector pVZ322 [17]. The construct integrity was verified by sequencing and the vectors pVZ322-1829 (encoding PhaE-eGfp) and pVZ322-1830 (encoding PhaC-eGfp) were transformed in the wildtype and *sll0783* mutant background by triparental mating [18].

Additionally, we determined whether the translational fusion of eGfp at the C-terminus of either subunit of PHB synthase impaired localization and biosynthetic activity. We transformed both constructs in a mutant background in which either PhaE or both PhaE and PhaC were deleted by insertion of a kanamycin resistance cassette in their coding sequences. In both cases, the eGfp-tagged versions of PhaE and PhaC were able to complement the knock out, demonstrating that the fusion proteins were functional. PHB accumulation was observed once cells were starved for nitrogen and visualized using nile red. The eGfp signal co-localized with the nile red signal (as indicated by the orange color in the overlay) demonstrating that the tag did not alter the intracellular localization of PHB synthase to PHB granules (supplementary Figure S2). PHB granule numbers per cell and granule diameters were not affected.

Since the C-terminal fusion did not alter PHB biosynthetic activity and intracellular localization, positioning of PHB synthase was monitored in wild type and *sll0783* mutant background after cells had been transferred to BG11-medium lacking a combined nitrogen source. Cells were sampled 24 h, 48 h and 120 h after nitrogen starvation was induced. PHB granules were mostly observed in the periphery (white arrowheads) of the cell and granule number increased throughout nitrogen starvation

in the wild type. As seen previously, the *sll0783* mutant accumulated less PHB [11] and PHB granules were small even after 120 h of nitrogen starvation as seen in Figure 1. Nevertheless, both PHB synthase subunits co-localized with the residual PHB granules ruling out the possibility that impaired localization of PHB synthase could be the cause of deficient PHB synthase activity in the *sll0783* mutant. These results were confirmed by western blot analysis showing similar accumulation and distribution of PhaE between soluble and insoluble fraction in wild-type and *sll0783* mutant prior and during nitrogen starvation (supplementary Figure S3).

Figure 1. Intracellular localization of PhaC-eGfp and PhaE-eGfp in wild type and the *sll0783* mutant. Polyhydroxybutyrate (PHB) granules were stained with nile red and co-localization of both proteins to PHB granules was monitored. Co-localization between eGfp and nile red is seen as orange in the overly of all three channels. White arrowheads point to PHB granules which are localized to the cell periphery close to the cytoplasmic membrane as visualized by Bright field microscopy.

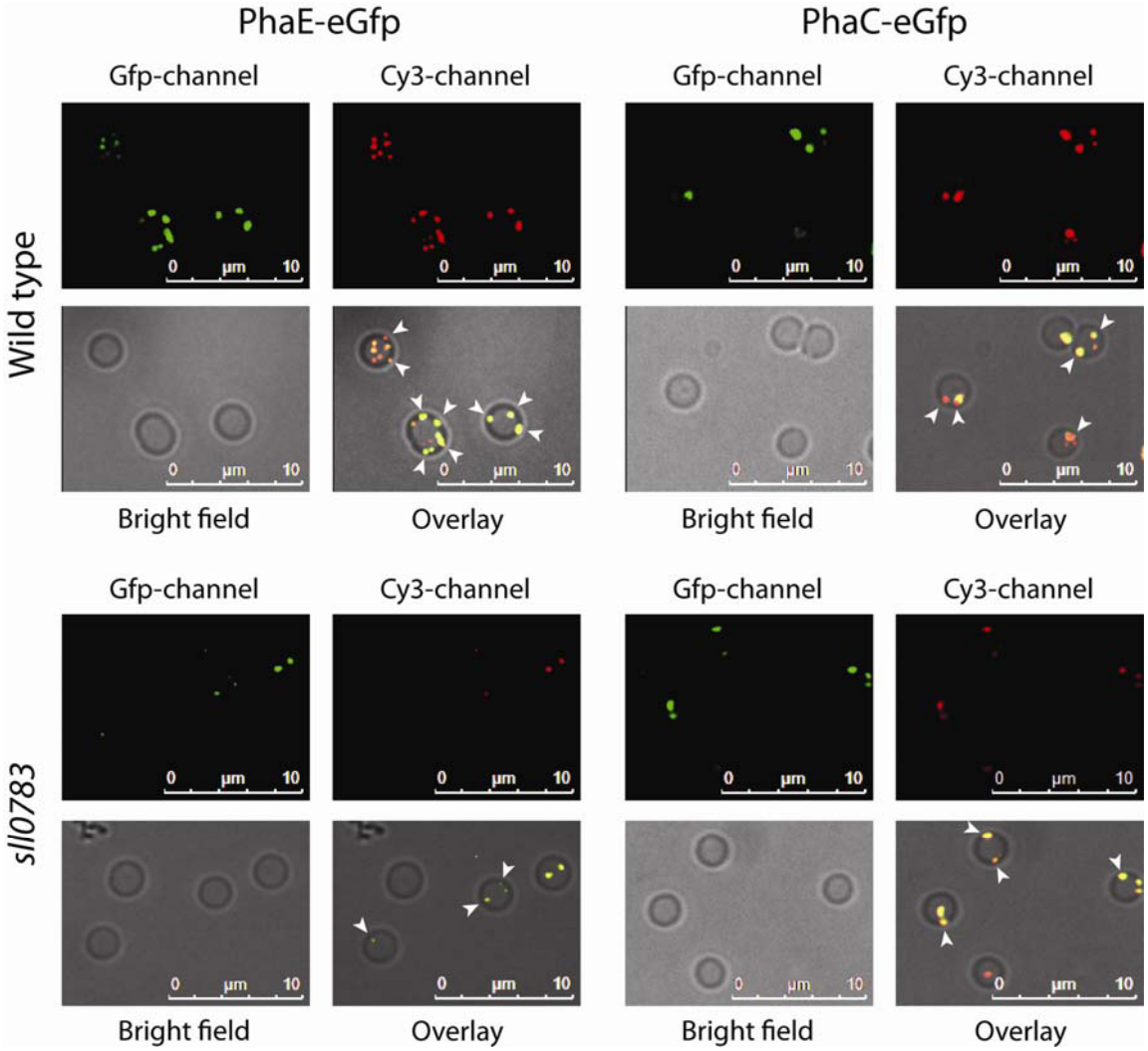

2.2. Metabolome Analysis of Wild Type Synechocystis sp. PCC 6803 and sll0783 Mutant

Since intracellular localization of PHB synthase was not altered in the *sll0783* mutant, we focused on the metabolic aspect of PHB biosynthesis to elucidate the cause for the observed phenotype. Our

previous results showed that acetyl-CoA levels were elevated in the mutant compared to the wild type. Hence, we investigated the metabolic profiles of 39 metabolites by a non-targeted GC-MS based metabolic profiling of wild type *Synechocystis* and *sll0783* mutant upon nitrogen starvation. Time points were chosen to monitor rapid acclimation towards nitrogen starvation within 24 h and long term adaptation was covered by the last time point, when cells have experienced 1 week of nitrogen starvation. Prior to sampling for metabolite extraction, cells were transferred in medium lacking a nitrogen source and were harvested by rapid filtration at different time points during nitrogen starvation. Harvested cells were immediately frozen in liquid nitrogen to stop all biochemical reactions and metabolites were extracted as previously described [19]. All data presented is the average of three independent biological samples. The metabolic profiling covered the central C and N metabolism, which is dominated by the Calvin-Benson cycle and the associated 2-phosphoglycolate metabolism as well as glycolysis, OPP, and the TCA cycle [20]. The TCA cycle is the interface between carbon and nitrogen metabolism since its intermediate 2-oxoglutarate provides carbon backbones for amino acid biosynthesis via the GS-GOGAT cycle [21].

2.2.1. Amino Acids

Within the first 24 h of nitrogen starvation, *Synechocystis* undergoes a dramatic change in metabolism [3]. In the first 6 h of nitrogen starvation, intracellular amino acid concentrations increase above levels detected prior to nitrogen starvation as seen in Figure 2. Within 24 h, the intracellular concentration of each amino acid drops and is similar to values obtained prior to the onset of nitrogen starvation. With prolonged nitrogen deprivation intracellular levels of amino acids decrease dramatically, for example, up to 10 times less lysine or phenylalanine is available compared to conditions when biologically available nitrogen is abundant. Glutamine and glutamate are an exception to this behavior. The intracellular levels of both amino acids decrease steadily throughout nitrogen starvation and do not peak at 6 h as observed for other amino acids. The amino acid pools of wild type and the *sll0783* mutant differ only slightly prior to nitrogen starvation and show similar tendencies after cells were deprived of nitrogen. However, the amino acid pools in the mutant responded less dynamic to the altered nutritional status than in the wild type. The observed phenomenon of increasing intracellular amino acids within the first 6 h of nitrogen starvation is explained by the fact that the light harvesting phycobiliproteins are degraded within the first hours of nitrogen starvation, due to the action of activated NblA [22,23]. Prolonged nitrogen starvation decreases the intracellular amino acid pools significantly, since no nitrogen source is present in the growth medium and biosynthetic activity of glutamine synthetase cannot be sustained, therefore biosynthesis of amino acids is halted. The steady decrease of glutamate and glutamine throughout nitrogen starvation is caused by the increased activity of the GS-GOGAT cycle and lack of a nitrogen source. In this process the supply of the cycle with ammonia is interrupted however glutamine and glutamate are still consumed for protein biosynthesis, causing the steady intracellular decline of both amino acids.

Thus, amino acid levels in wild type and *sll0783* mutant behave similarly. These observations confirm our previous results that the mutant is not impaired in acclimation towards nitrogen starvation [11]. Since carbon and nitrogen metabolism are interconnected through the GS-GOGAT cycle we investigated the metabolic changes of the TCA cycle.

Figure 2. Amino acid levels of the wild type and the *sll0783* mutant throughout nitrogen starvation. Black bars represent the metabolites levels prior to nitrogen starvation (0 h), cyan bars represent values obtained 6 h, red bars 24 h and green bars 168 h after nitrogen starvation has been induced. All bars represent x-fold changes in metabolite levels compared to the level in wild type at time point 0 h. The red lines mark the values 2 and 0.5. Values above or below these lines represent statistically significant changes of metabolite levels when compared to wild type at time point 0 h.

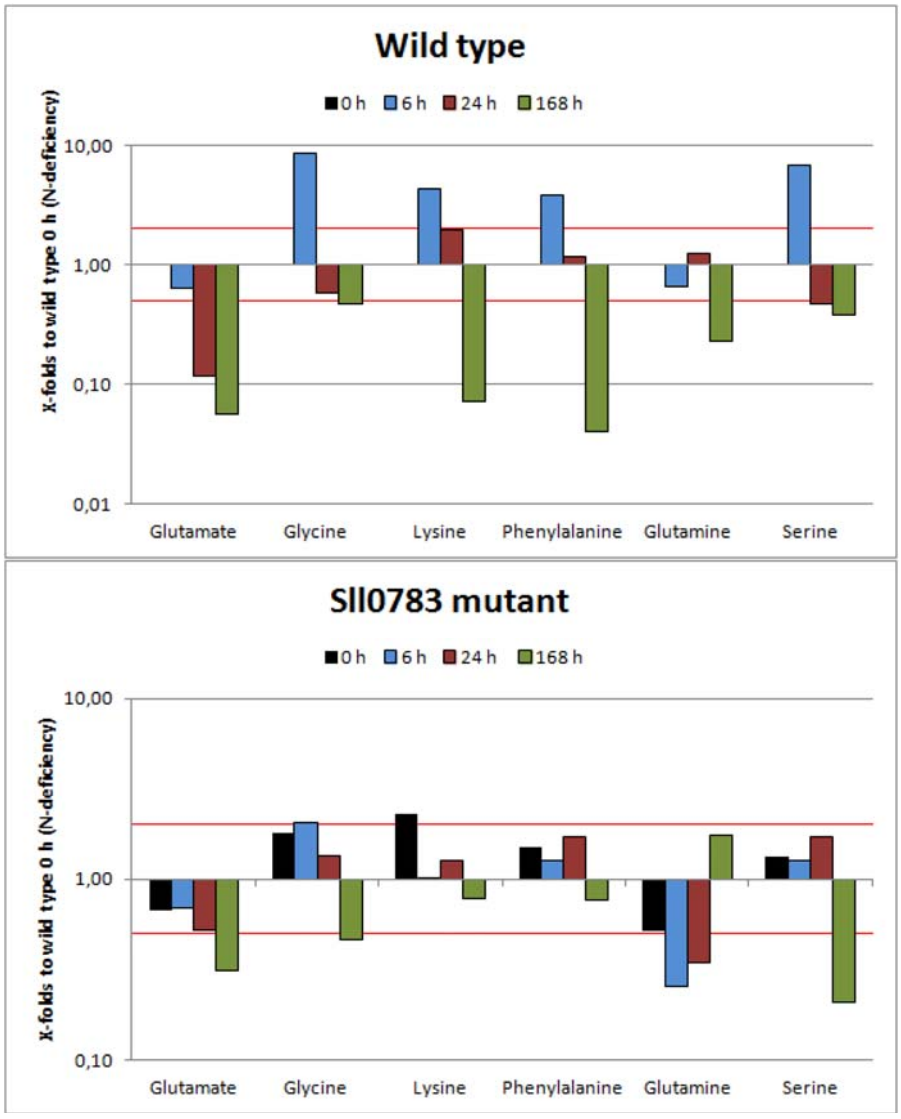

2.2.2. TCA-Cycle

Figure 3 shows that TCA cycle intermediates accumulated throughout nitrogen starvation in wild type cells. All metabolites with exception of succinic and oxalic acid, which can be derived from the TCA cycle, accumulated in the wild type. Succinic acid levels remained relatively stable and the levels of oxalic acid decreased slightly, which can be derived from oxaloacetic acid. In contrast, however, intracellular concentrations of the other four detected TCA intermediates increased. Levels of citric acid were 9 times higher 168 h after onset of nitrogen starvation compared to levels before nitrogen starvation. This accumulation could be explained by increased NADPH levels, which act as feedback

inhibitors of isocitrate dehydrogenase [24], leading to an accumulation of isocitrate. The chemical equilibrium catalyzed by aconitase is strongly on the side of citrate [25], hence citrate accumulates. Fumaric acid levels peaked 24 h after nitrogen starvation was induced. At this time point almost 10 times more fumaric acid was present than prior to nitrogen starvation. However, the intracellular amount of fumaric acid decreased once nitrogen starvation progressed. Similar tendencies were also observed for malic acid. Levels increased throughout nitrogen starvation and peaked 24 h after shift to nitrogen limiting conditions followed by a decrease at 168 h, which was not as profound as seen for fumaric acid. Levels of 2-oxoglutaric acid increased as well but not as dramatically as seen for the other three metabolites described previously.

Figure 3. Levels of tri- and dicarboxylic acid intermediates in wild type and the *sll0783* mutant throughout nitrogen starvation. Black bars represent the metabolites levels prior to nitrogen starvation (0 h), cyan bars represent values obtained 6 h, red bars 24 h and green bars 168 h after nitrogen starvation has been induced. All bars represent x-fold changes in metabolite levels compared to the level in wild type at time point 0 h. The red lines mark the values 2 and 0.5. Values above or below these lines represent statistically significant changes of metabolite levels when compared to wild type at time point 0 h.

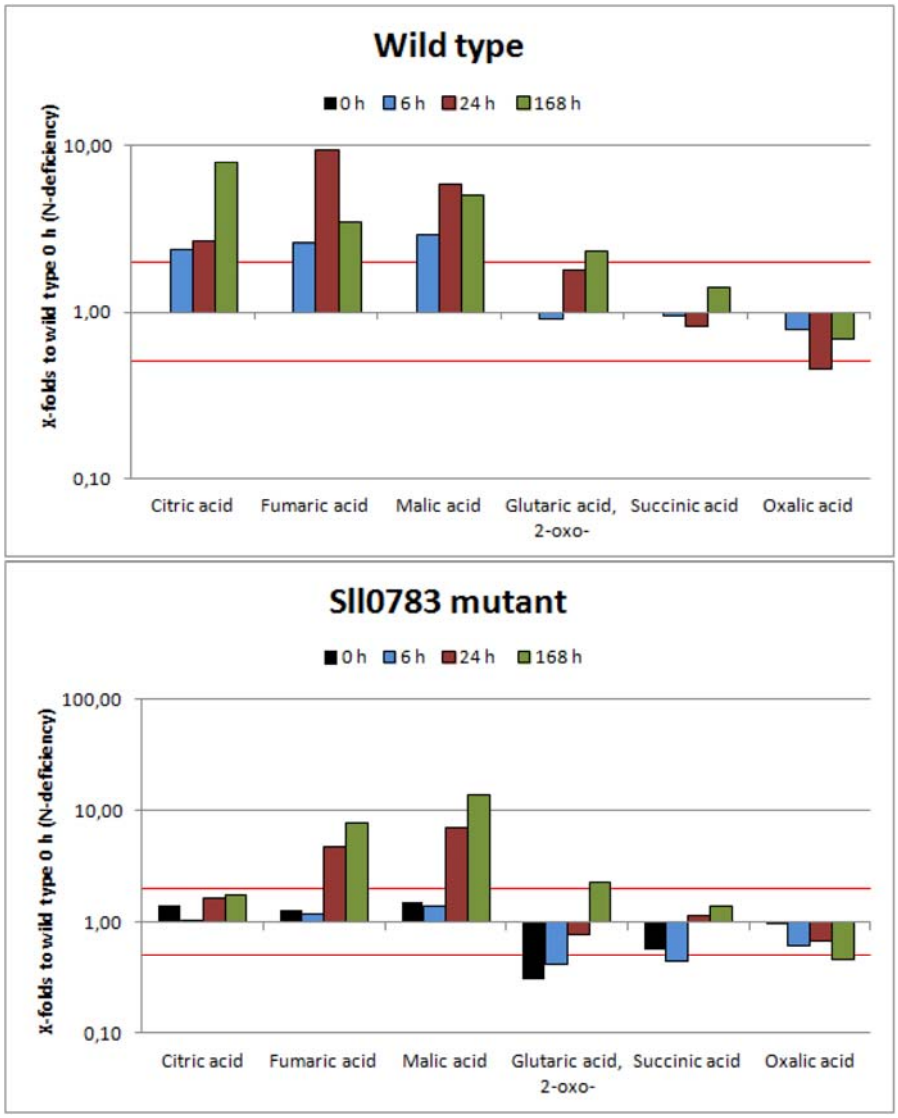

Compared to wild type, the levels of the TCA cycle intermediates were slightly different in cells of the *sll0783* mutant. Citric acid never accumulated as seen in the wild type and considering the somewhat increased levels prior to nitrogen starvation intracellular levels of citric acid remained almost unchanged throughout the period metabolites were monitored. Initially, levels of 2-oxoglutaric acid and succinic acid were lower than in the wild type but steadily increased throughout nitrogen starvation reaching intracellular concentrations similar to wild type. Intracellular concentrations of oxalic acid behaved similarly to the wild type and only minor differences could be observed. Levels of malic acid and fumaric acid rose in the mutant to levels even higher than seen in the wild type and remained high; however the rise was delayed and observed 24 h and not 6 h after nitrogen depletion. Since precursors for the TCA cycle are generated through glycolysis we also investigated some selected metabolites of this pathway.

2.2.3. Sugar Metabolism

Intermediates of sugar metabolism increased within the first 24 h of nitrogen starvation in cells of the wild type, followed by a decrease as nitrogen starvation progressed (Figure 4). Glucose, fructose 6-phosphate and 3-phosphoglycerate levels increased significantly 24 h after depletion of a nitrogen source, however decreased again with prolonged nitrogen starvation. Especially fructose 6-phosphate levels increased up to 100-fold compared to the control. Glucose 6-phosphate levels and phosphoenolperuvic acid levels increased as well, but not as strongly as for the three metabolites mentioned above. The burst of fructose 6-phosphate and 3-phosphoglycerate levels (Figure 4) seems to be an immediate consequence of nitrogen starvation. The latter metabolite is the first stable product of carbon fixation and precursor of most organic carbon in *Synechocystis* [26]. While under nitrogen sufficient conditions, fixed carbon is rapidly converted into PEP to drive amino acid biosynthesis, this can't happen under nitrogen limitation. Instead, 3-phosphoglycerate accumulates and fixed carbon is used for glycogen synthesis through gluconeogenesis [27], explaining the increased glucose and fructose 6-phosphate levels. This interpretation is supported by expression analysis of *Synechocystis* upon nitrogen starvation, which shows that expression of *gap2* (glyceraldehydes-3-phosphate dehydrogenase), an enzyme required for gluconeogenesis [28], and glycogen biosynthetic genes *glgA* and *glgB* are upregulated within 6 h of nitrogen starvation [15], resulting in accumulation of glycogen. A similar tendency in the response of these sugar and glycolysis metabolites was observed for these metabolites in the *sll0783* mutant, however initial metabolite levels differed from wild type. This could be due to the fact that Sll0783 is already expressed prior to nitrogen starvation (see immunoblot analysis of Sll0783 protein in supplementary Figure S4) and a knock out could alter metabolism under nitrogen sufficient growth conditions which cannot be seen phenotypically [11]. A striking difference between wild type and mutant was observed for the change in the intracellular level of sorbitol. In the wild-type, sorbitol levels increased strongly in the first 6 h of nitrogen-starvation (30-fold accumulation) and then remained high throughout nitrogen starvation. In the *sll0783* mutant, sorbitol levels almost did not increase in response to nitrogen-starvation. By contrast, after 24 h sorbitol levels decreased below the initial level. Sorbitol biosynthesis is dependent on a reduction step by which a hexose is reduced by NADPH leading to sorbitol. Obviously, the mutant is not capable of catalyzing this reaction efficiently. This finding was taken as a first hint that the redox balance could be disturbed

in the mutant. Probably, mutant cells are less capable of providing sufficient NADPH to drive the sorbitol biosynthesis. A full list of metabolites detected is provided in the supplementary section.

Figure 4. Accumulation of sugar metabolites in wild type and the *sll0783* mutant throughout nitrogen starvation. Black bars represent the metabolites levels prior to nitrogen starvation (0 h), cyan bars represent values obtained 6 h, red bars 24 h and green bars 168 h after nitrogen starvation has been induced. All bars represent x-fold changes in metabolite levels compared to the level in wild type at time point 0 h. The red lines mark the values 2 and 0.5. Values above or below these lines represent statistically significant changes of metabolite levels when compared to wild type at time point 0 h.

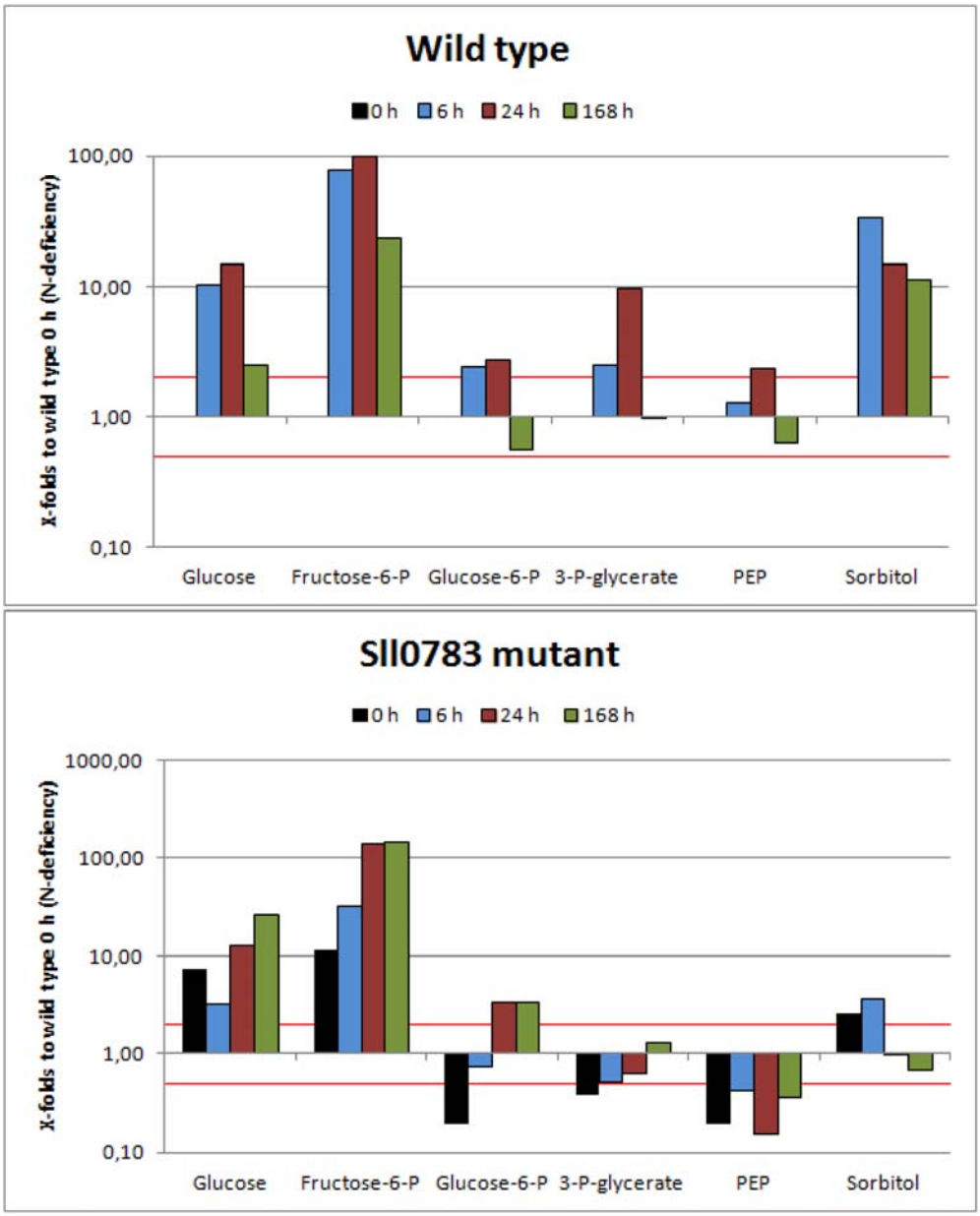

2.3. Nitrogen Starvation Shifts the Intracellular Redox Balance towards a More Reduced State

The results from metabolome analysis indicated the observed phenotype of diminished PHB synthase activity and impaired PHB accumulation might be caused by a change in the intracellular

redox pool, which has been previously suggested to play a role in regulating PHB biosynthesis [24]. Hence, we determined the ratio between NADPH and NADP throughout nitrogen starvation in wild type and *sll0783* mutant. To do so, cells were transferred to medium lacking a nitrogen source, harvested and lysed in order to determine the NADPH/NADP ratio by a colorimetric test. With prolonged nitrogen starvation, the balance between NADPH and NADP is shifted in the wild type towards NADPH, whereas the ratio remains stable in the *sll0783* mutant (Figure 5a). This result corresponds with the observation that sorbitol doesn't accumulate in the mutant as seen in wild type, which was assumed to be due to a lack of reducing equivalents. This observation raised the question whether the deficient PHB synthase activity of the mutant can be restored by manipulating the intracellular redox balance by applying defined inhibitors such as DCMU, DCCD and CCCP, which alter the turnover of redox equivalents. DCMU inhibits photosystem II by blocking the QB binding site thereby diminishing the linear photosynthetic electron flow, which in turn lowers the intracellular NADPH concentration [29]. CCCP uncouples ADP phosphorylation from the membrane potential thereby generating a lack of ATP for biosynthetic reactions. DCCD specifically inhibits ATP synthase without inhibiting photosynthetic electron flow, which in turn leads to decreased intracellular ATP levels [30]. Low levels of ATP lead to a reduced carbon flow through the Calvin-Benson cycle, which is a major sink for NADPH and ATP in photosynthetic organisms thereby creating a more reducing intracellular environment. All three inhibitors of energy metabolism were added to the cultures after they have been shifted to medium lacking nitrogen and cells were harvested as described in the methods section to determine the NADPH/NADP ratio. DCMU treatment shifted the redox balance slightly towards NADP, whereas DCCD and CCCP strongly shifted the balance towards NADPH, both in wild type and *sll0783* mutant as shown in Figure 5b, c. The shift towards more NADPH than NADP became more profound as nitrogen starvation progressed and was highest after 72 h.

Figure 5. (**a**) The intracellular redox state in wild type (black bars) and the *sll0783* (white bars) changes upon nitrogen starvation. (**b**) Intracellular redox state during nitrogen starvation of the wild type without inhibitor (circle), incubated with DCMU (squares), incubated with CCCP (triangle) and DCCD (inverted triangle). (**c**) Intracellular redox state during nitrogen starvation of the *sll0783* mutant without inhibitor (circle), incubated with DCMU (squares), incubated with CCCP (triangle) and DCCD (inverted triangle). Errors between individual measurements were below 5%; therefore, error bars are left out.

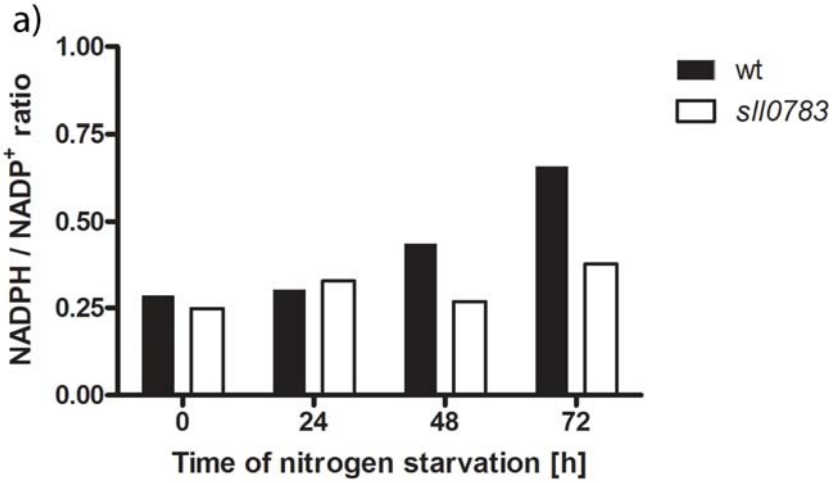

Figure 5 . *Cont.*

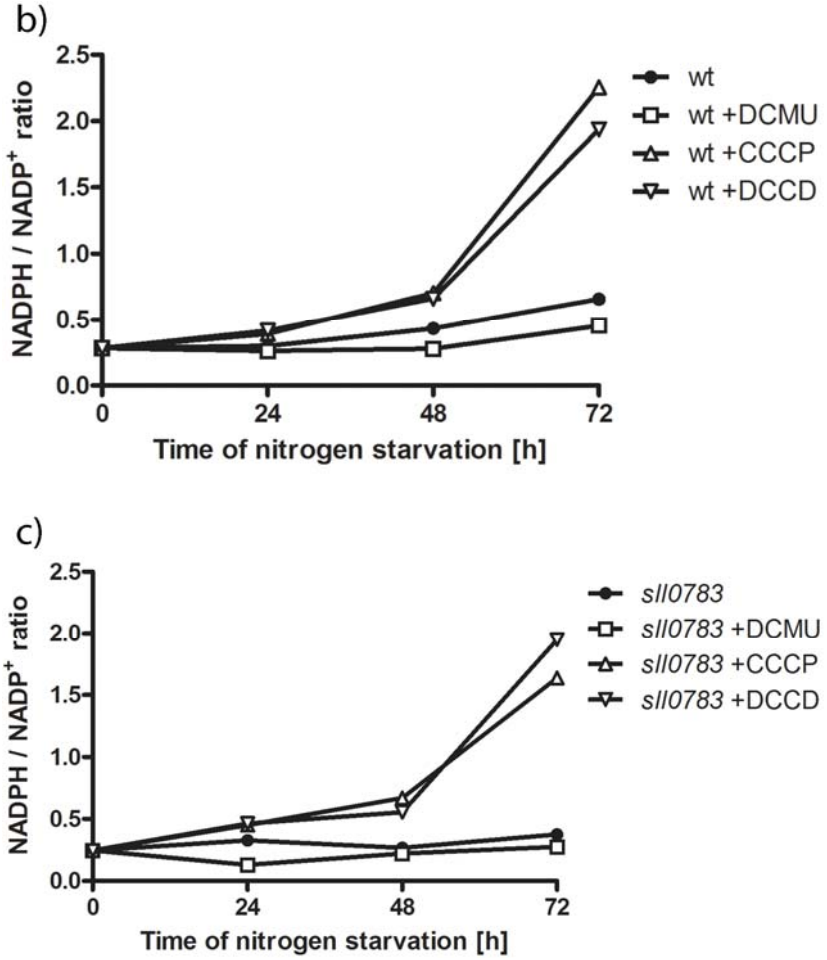

Even though all three inhibitors act immediately on their targets, a time period of 48 h was required to see a profound difference in NADPH between treated and non-treated cells. The delayed response could be explained by the special physiological state the cell enter upon nitrogen starvation. The activity of PSII is down-regulated [3], the phycobiliproteins are degraded and in general, cells tune down metabolic activity [31]. The free amino acids obtained by phycobiliprotein degradation can be catabolized to sustain the redox balance or supply cells with ATP by substrate chain phosphorylation. On the other hand, the cells accumulate the reduced polymers glycogen and PHB, which now act as a sink for reduction equivalents. Altogether, the intracellular redox state appears to be highly regulated and severe metabolic perturbation is required to bring it out of balance [27].

In summary, these measurements confirmed that the used substances were suited to alter the intracellular redox state and gave us the opportunity to test our hypothesis that the observed phenotype of diminished PHB synthase activity and impaired PHB accumulation is caused by the disturbed redox balance in the *sll0783* mutant.

2.4. PHB Synthase in the sll0783 Mutant is Impaired Due to an Altered Redox Balance

Addition of DCMU, CCCP or DCCD was previously reported to influence PHB accumulation in the cyanobacterium *Nostoc muscorum* [32] and treatment of *Spirulina maxima* with CCCP resulted in PHB accumulation during nitrogen sufficient conditions [33]. Our measurements showed that these

inhibitors affect the intracellular NADPH/NADP ratio (Figure 5). This led to the hypothesis that PHB biosynthetic activity can be recovered in the *sll0783* mutant by altering the intracellular redox balance using these inhibitors. This possibility was tested by shifting the cells into nitrogen-free medium and adding the inhibitors to the cell culture. PHB synthase activity was determined as described in the methods section 24 h, 48 h and 72 h after cells had been shifted to nitrogen free medium. The influence of DCMU, CCCP and DCCD on biosynthetic activity of PHB synthase was significant. Inhibition of the linear photosynthetic electron flow by DCMU markedly decreased PHB synthase activity in wild type and *sll0783* mutant, whereas both inhibitors affecting ATP biosynthesis had the opposite effect as seen in Figure 6a, b. CCCP and DCCD strongly increased biosynthetic activity of PHB synthase in the wild type and *sll0783* mutant to levels which were higher than without inhibitors. Both CCCP and DCCD were able to suppress the phenotype of diminished biosynthetic activity of PHB synthase in the *sll0783* mutant during nitrogen starvation. Biosynthetic activity of PHB synthase was strongly increased and the mutant reached activity values similar to the wild type without any inhibitor. The physiological complementation of the *sll0783* mutant using uncouplers of ATP synthesis, which results in a more reduced intracellular environment, confirms the proposal that the disturbed NADPH pool in the mutant is responsible for impaired PHB synthase activity. Once the redox balance is restored, PHB synthase activity rises to values similar to wild type and thereby physiologically complements the mutant phenotype. Our measurements of the NADPH/NADP ratio (Figure 5) and the PHB synthase activity (Figure 6) also explain why [32] were able to increase PHB accumulation by utilizing these metabolic inhibitors. This highlights the importance of the redox balance to sustain the biosynthetic activity of PHB synthase.

Figure 6. (**a**) PHB synthase activity in crude cell-extracts in wild type cells without inhibitors (circle), incubated with DCMU (squares), incubated with CCCP (triangle) and DCCD (inverted triangle) throughout nitrogen starvation. (**b**) PHB synthase activity in crude cell extracts of *sll0783* mutant cells without inhibitors (circle), incubated with DCMU (squares), incubated with CCCP (triangle) and DCCD (inverted triangle) throughout nitrogen starvation. Values are the mean of three independent measurements.

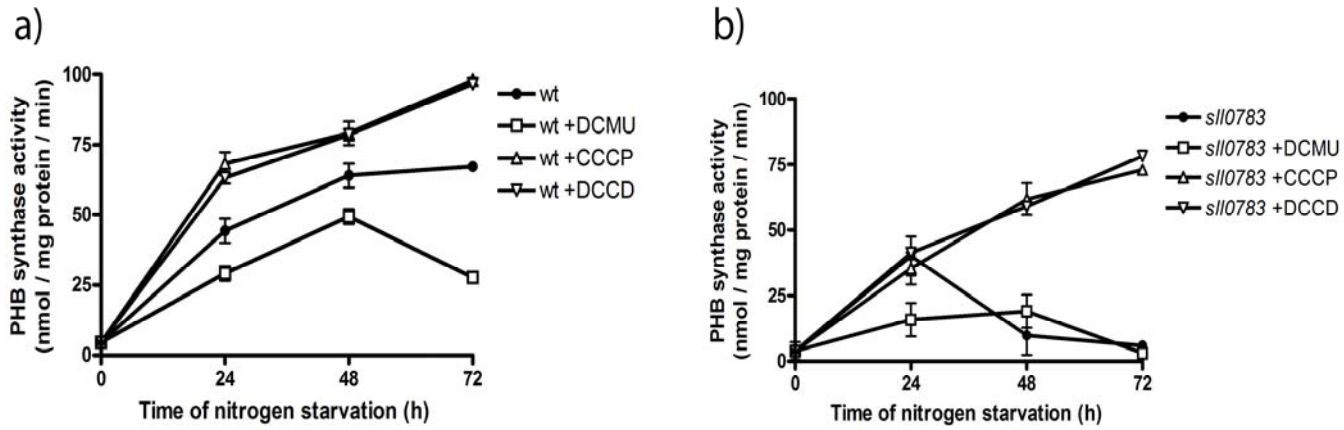

3. Experimental Section

3.1. Culture Conditions

Wild type *Synechocystis* sp. strain PCC 6803, the *sll0783* mutant and the corresponding reporter strains (harboring pVZ322-1829 or pVZ322-1830) were grown photoautotrophically in BG11 medium [34] supplemented with 5 mM $NaHCO_3$ in flasks shaken at 150 rpm at a continuous photon flux density of 50 µmol photons m^{-2} s^{-1} at 28 °C. For initiation of nitrogen deprivation, 50 ml of exponentially growing cells was harvested by centrifugation (8 min, 4,000 rpm) and the pellet was resuspended in $NaNO_3$ -free BG11 medium (BG11-N) and centrifuged again. Finally, the washed cells were resuspended again in BG11-N to an optical density at 750 nm (OD_{750}) of 0.4 and incubated as described above. To alter the intracellular redox state DCMU, CCCP and DCCD were added to a final concentration of 10 µM in the growth medium. To ensure sufficient carbon supply for PHB biosynthesis, 10 mM acetate was added to the growth medium when PHB biosynthetic assays and the NADPH/NADP ratio were determined.

3.2. Metabolite Extraction

Samples of 5 to 10 ml cells, equivalent to approximately 10^9 cells/ml, were separated from the medium by quick filtration (0.45-mm nitrocellulose filters, Schleicher and Schuell) in the light. Cells on filters were placed in 2-ml Eppendorf tubes and immediately frozen in liquid nitrogen. The metabolomics profiling via GC-EI-TOF-MS, compound identification and data processing were done according to [19].

3.3. Measurements of the NADPH Pool

Colorimetric assays were performed using commercial kit $NADP^+$/NADPH Quantification Kit (Biovision, USA). Biochemical reactions were stopped by adding equal volumes of ice to the cell culture and cells were pelleted. The cell pellet was suspended in 200 µL $NADP^+$/NADPH extraction buffer and disrupted in a Fast-Prep24 apparatus (MP Biomedicals, USA) for 3 × 20 sec with an intensity setting of 6.5 M/s. Cell debris was removed by centrifugation at 1,000 g for 1 min. The supernatant was centrifuged again at 25,000 g for 30 min. Afterwards the supernatants were normalised to protein level before they were passed through a Microcon YM-10 filter (Millipore, USA) to remove NADPH consuming enzymes. The flow-through was used for the detection of both, NADPH and total $NADP^+$/NADPH level according to the manual. All samples were processed in a single multiwell experiment run to aid quantification and comparability. Colorimetric measurements were made at 25 °C using optical density measurements at 450nm (OD_{450}) in a microplate reader EL808 (BioTek, USA). OD_{450} measurements were converted to ng/mg protein using a standard curve for NADPH.

3.4. PHB Synthase Assay

All steps for preparing cell extracts were performed at 4°C or on ice. Cells of *Synechocystis* sp. PCC 6803 and corresponding mutants were harvested from nitrogen-*limited* or nitrogen-sufficient

cultures by centrifugation for 8 min at 4,000 g. Then, they were suspended in lysis buffer (25 mM Tris/HCl, pH 7.4, 50 mM KCl, 5 mM $MgCl_2$ and 0.5 mM EDTA) and disrupted in a Fast-Prep24 apparatus (MP Biotechnology, Germany) for 3 × 20 sec with an intensity setting of 6.5 M/s. Cell debris was removed by centrifugation at 1,000 g for 1 min to obtain the crude extract. For further analysis, crude extract was separated into a soluble and insoluble fraction by centrifugation at 20,000 g for 15 min. The insoluble fraction was suspended in 0.5 ml Tris/HCl, pH 7.4.

Assay of PHB synthase activity was carried out as described previously [35]. The assay mixtures (200 µL) contained 20 µg of protein, 100 µM DL-3-hydroxybutyryl-CoA, and 1 mM 5,5'-dithiobis (2-nitrobenzoic acid) (DTNB) in 25 mM Tris/HCl, pH 7.4, buffer with 20 mM $MgCl_2$. The reaction mixtures were transferred to microplate wells, and the reaction was started by addition of the substrate DL-3-hydroxybutyryl-CoA. The reaction was recorded in an EL808 microplate reader (BioTek) at a temperature setting of 30 °C and the time course of the change in A409 (due to the reaction of the released CoA with DTNB) was monitored for 5 min.

3.5. Microscopy

PHB granules in *Synechocystis* sp. PCC 6803 cells were visualized by staining with the fluorescent dye Nile red. To 20 µL of cell culture, 6.6 µL Nile red solution (1 µg mL^{-1} in ethanol) was added. Of this mixture, 10 µL were dropped on glass slides, which had been covered with 1 mL 2% agarose in H_2O and dried. The cells were analyzed by fluorescence microscopy using a Leica DM5500B microscope with a 100x/1.3 oil objective lens (Leica Microsystems, Germany) and a filter cube with 545/50 nm excitation and 610/75 nm suppression. Pictures were taken with a Leica DFC360FX camera. Fluorescence of eGfp fusion proteins was monitored using a filter cube with 470/40 nm excitation and 525/50 nm suppression.Z-Stacks of 0.1-0.2 µm were recorded and processed with the deconvolution software Leica LAS AF. Standard deconvolution procedure was done by using blind method and 10 iterations.

4. Conclusions

Our study is the first to investigate global metabolic changes upon nitrogen starvation covering most metabolites of glycolysis, calvin cycle, TCA cycle and amino acid pools in *Synechocystis* sp. PCC 6803. Our data demonstrate that profound changes happen at the metabolic level once nitrogen starvation is applied (Figures 2–4). The spiking levels of amino acids 6 h after nitrogen starvation correlates with the degradation of the phycobilisomes [3], a reaction that delivers free amino acids (Figure 2). The following dramatic decrease of intracellular amino acids is in agreement to previous studies, reporting that intracellular C:N ratio changes upon nitrogen starvation from 5:1 to 10:1 [15].

Whereas some TCA cycle intermediates accumulated within the first 24 h followed by a decrease throughout nitrogen starvation (citrate, fumarate and malic acid) or others remained almost unchanged (succinate), citric acid was an exception. Its levels remained high in the wild-type even 168 h after nitrogen starvation was induced. This accumulation can be explained by increased NADPH levels in the wild-type (see above), whereas in the *sll0783* mutant, NADPH levels and hence citrate does not accumulate to that extent. In the absence of combined nitrogen, the oxo acids cannot be converted to amino acids. Instead, the flux of newly fixed carbon is immediately redirected towards

gluconeogenesis and the synthesis of reduced carbon products. This metabolic shift is clearly visible regarding the sorbitol levels, which strongly increase in the wild-type. Biosynthesis of sorbitol requires NADPH and the inability of the mutant to accumulate sorbitol agrees with its impaired redox-response. Sorbitol is known from plant metabolism and has only been considered as osmoprotectant in *Synechocystis* sp. PCC 6803 [36], but has so far not been characterized as metabolite in cyanobacteria. The present investigation suggests that rapid sorbitol accumulation after nitrogen-deprivation might function as redox-buffering reaction.

Whereas the synthesis of glycogen and sorbitol appears to be the first response of carbon metabolism upon nitrogen starvation, the activity of PHB synthase increases steadily and reaches its maximum only after 2 days of nitrogen starvation in the wild-type. During this time, the intracellular milieu of *Synechocystis* wild type becomes increasingly reduced, whereas this is not the case in the *sll0783* mutant. This correlates with the activity of PHB synthase during ongoing nitrogen starvation. The initial activation of PHB synthase immediately after nitrogen-starvation is most likely mediated by acetyl phosphate [12] whereas the reducing environment is required to sustain this metabolic reaction. Altering the intracellular redox balance towards a more reducing environment with CCCP and DCCD (Figure 5b, c) increased biosynthetic activity of PHB synthase in wild type beyond the untreated control and restored activity in the mutant (Figure 6). These data imply that PHB synthesis is redox-controlled and the present investigation corroborates previous suggestions [24], that PHB serves as a redox-sink to store excess NADPH during imbalanced metabolic situations.

Altogether we show that the observed phenotype of impaired PHB accumulation in the *sll0783* mutant is caused by the lack of reducing equivalents and is independent of intracellular localization of both PHB synthase subunits. As Sll0783 is homologous to DsrE family proteins which are involved in regulation of intracellular sulfur redox reactions our results support the role of Sll0783 in the regulation of the intracellular redox balance. Unfortunately we are still not able to pin point the function of this protein; however, upregulation upon nitrogen starvation [15] and high abundance of this protein in nitrogen starved cells [6] (see also supplementrary Figure 4) emphasizes its importance. Based on the operon structure and the transcriptional regulation of *sll0783* and its neighboring genes, which encode a nitrile hydrolase (*sll0784*), a protein with homologies to radical SAM superfamily (*sll0785*) and an acyltransferase (*sll0786*), we presume that these proteins might be involved in degradation and utilization of "unusual" nitriles occurring in nature [37]. The specific deletion of *sll0783* might deregulate a redox-chain reaction catalyzed by these proteins, leading to an uncontrolled consumption of NADPH altering the intracellular redox balance and causing the observed phenotype of decreased PHB accumulation.

Acknowledgments

This project was supported by the DFG-funded GRK 1708 "Molecular principles of bacterial survival strategies". We thank Johanna Weirich for technical assistance.

Conflict of Interest

The authors declare no conflict of interest.

References

1. Stanier, R.Y.; Cohen-Bazire, G. Phototrophic prokaryotes: the cyanobacteria. *Annu. Rev. Microbiol.* **1977**, *31*, 225–274.
2. Harder, W.; Dijkhuizen, L. Physiological responses to nutrient limitation. *Annu. Rev. Microbiol.* **1983**, *37*, 1–23.
3. Gorl, M.; Sauer, J.; Baier, T.; Forchhammer, K. Nitrogen-starvation-induced chlorosis in Synechococcus PCC 7942: Adaptation to long-term survival. *Microbiology* **1998**, *144*, 2449–2458.
4. Schwarz, R.; Forchhammer, K. Acclimation of unicellular cyanobacteria to macronutrient deficiency: Emergence of a complex network of cellular responses. *Microbiology* **2005**, *151*, 2503–2514.
5. Herrero, A.; Muro-Pastor, A.M.; Flores, E. Nitrogen control in cyanobacteria. *J. Bacteriol.* **2001**, *183*, 411–425.
6. Fadi Aldehni, M.; Sauer, J.; Spielhaupter, C.; Schmid, R.; Forchhammer, K. Signal transduction protein P (II) is required for NtcA-regulated gene expression during nitrogen deprivation in the cyanobacterium Synechococcus elongatus strain PCC 7942. *J. Bacteriol.* **2003**, *185*, 2582–2591.
7. Llacer, J.L.; Espinosa, J.; Castells, M.A.; Contreras, A.; Forchhammer, K.; Rubio, V. Structural basis for the regulation of NtcA-dependent transcription by proteins PipX and PII. *Proc. Natl. Acad. Sci. USA* **2010**, *107*, 15397–15402.
8. Panda, B.; Jain, P.; Sharma, L.; Mallick, N. Optimization of cultural and nutritional conditions for accumulation of poly-beta-hydroxybutyrate in *Synechocystis* sp. PCC 6803. *Bioresource Technol.* **2006**, *97*, 1296–1301.
9. Taroncher-Oldenburg, G.; Nishina, K.; Stephanopoulos, G. Identification and analysis of the polyhydroxyalkanoate-specific beta-ketothiolase and acetoacetyl coenzyme A reductase genes in the cyanobacterium Synechocystis sp. strain PCC6803. *Appl. Environ. Microbiol.* **2000**, *66*, 4440–4448.
10. Hein, S.; Tran, H.; Steinbuchel, A. Synechocystis sp. PCC6803 possesses a two-component polyhydroxyalkanoic acid synthase similar to that of anoxygenic purple sulfur bacteria. *Arch. Microbiol.* **1998**, *170*, 162–170.
11. Schlebusch, M.; Forchhammer, K. Requirement of the nitrogen starvation-induced protein Sll0783 for polyhydroxybutyrate accumulation in Synechocystis sp. strain PCC 6803. *Appl. Environ. Microbiol.* **2010**, *76*, 6101–6107.
12. Miyake, M.; Kataoka, K.; Shirai, M.; Asada, Y. Control of poly-beta-hydroxybutyrate synthase mediated by acetyl phosphate in cyanobacteria. *J. Bacteriol.* **1997**, *179*, 5009–5013.
13. Cho, M.; Brigham, C.J.; Sinskey, A.J.; Stubbe, J. Purification of polyhydroxybutyrate synthase from its native organism, Ralstonia eutropha: implications for the initiation and elongation of polymer formation *in vivo*. *Biochemistry* **2012**, *51*, 2276–2288.
14. Jendrossek, D. Polyhydroxyalkanoate granules are complex subcellular organelles (carbonosomes). *J. Bacteriol.* **2009**, *191*, 3195–3202.
15. Krasikov, V.; Aguirre von Wobeser, E.; Dekker, H.L.; Huisman, J.; Matthijs, H.C. Time-series resolution of gradual nitrogen starvation and its impact on photosynthesis in the cyanobacterium Synechocystis PCC 6803. *Physiol. Plantarum* **2012**, *145*, 426–439.

16. Muro-Pastor, A.M.; Olmedo-Verd, E.; Flores, E. All4312, an NtcA-regulated two-component response regulator in Anabaena sp. strain PCC 7120. *FEMS Microbiol. Lett.* **2006**, *256*, 171–177.
17. Zinchenko, V.V.; Piven, I.V.; Melnik, V.A.; Shestakov, S.V. Vectors for the complementation analysis of cyanobacterial mutants. *Russ. J. Genet.* **1999**, *35*, 228–232.
18. Wolk, C.P.; Vonshak, A.; Kehoe, P.; Elhai, J. Construction of shuttle vectors capable of conjugative transfer from Escherichia coli to nitrogen-fixing filamentous cyanobacteria. *Proc. Natl. Acad. Sci. USA* **1984**, *81*, 1561–1565.
19. Eisenhut, M.; Huege, J.; Schwarz, D.; Bauwe, H.; Kopka, J.; Hagemann, M. Metabolome phenotyping of inorganic carbon limitation in cells of the wild type and photorespiratory mutants of the cyanobacterium Synechocystis sp. strain PCC 6803. *Plant. Physiol.* **2008**, *148*, 2109–2120.
20. Zhang, S.; Bryant, D.A. The tricarboxylic acid cycle in cyanobacteria. *Science* **2011**, *334*, 1551–1553.
21. Wolk, C.P.; Thomas, J.; Shaffer, P.W.; Austin, S.M.; Galonsky, A. Pathway of nitrogen metabolism after fixation of 13N-labeled nitrogen gas by the cyanobacterium, *Anabaena cylindrica*. *J. Biol. Chem.* **1976**, *251*, 5027–5034.
22. Collier, J.L.; Grossman, A.R. A small polypeptide triggers complete degradation of light-harvesting phycobiliproteins in nutrient-deprived cyanobacteria. *EMBO J.* **1994**, *13*, 1039–1047.
23. Sauer, J.; Gorl, M.; Forchhammer, K. Nitrogen starvation in *synechococcus* PCC 7942: involvement of glutamine synthetase and NtcA in phycobiliprotein degradation and survival. *Arch. Microbiol.* **1999**, *172*, 247–255.
24. Senior, P.J.; Dawes, E.A. Poly-β-hydroxybutyrate biosynthesis and the regulation of glucose metabolism in Azotobacter beijerinckii. *Biochem. J.* **1971**, *125*, 55–66.
25. England, P.J.; Denton, R.M.; Randle, P.J. The influence of magnesium ions and other bivalent metal ions on the aconitase equilibrium and its bearing on the binding of magnesium ions by citrate in rat heart. *Biochem. J.* **1967**, *105*, 32C–33C.
26. Huege, J.; Goetze, J.; Schwarz, D.; Bauwe, H.; Hagemann, M.; Kopka, J. Modulation of the major paths of carbon in photorespiratory mutants of synechocystis. *PloS One* **2011**, *6*, e16278.
27. Grundel, M.; Scheunemann, R.; Lockau, W.; Zilliges, Y. Impaired glycogen synthesis causes metabolic overflow reactions and affects stress responses in the cyanobacterium *Synechocystis* sp. PCC 6803. *Microbiology* **2012**, *158*, 3032–3043.
28. Koksharova, O.; Schubert, M.; Shestakov, S.; Cerff, R. Genetic and biochemical evidence for distinct key functions of two highly divergent GAPDH genes in catabolic and anabolic carbon flow of the cyanobacterium *Synechocystis* sp. PCC 6803. *Plant. Mol. Biol.* **1998**, *36*, 183–194.
29. Metz, J.G.; Pakrasi, H.B.; Seibert, M.; Arntzen, C.J. Evidence for a Dual Function of the Herbicide-Binding D1-Protein in Photosystem-Ii. *FEBS Lett.* **1986**, *205*, 269–274.
30. Zürrer, H.; Snozzi, M.; Bachofen, R. Specific binding of DCCD to reaction centers of the photosynthetic bacterium Rhodospirillum rubrum and its effect of certain photosynthetic reactions. *FEBS Lett.* **1983**, *153*, 151–155.
31. Sauer, J.; Schreiber, U.; Schmid, R.; Volker, U.; Forchhammer, K. Nitrogen starvation-induced chlorosis in Synechococcus PCC 7942. Low-level photosynthesis as a mechanism of long-term survival. *Plant. Physiol.* **2001**, *126*, 233–243.
32. Mallick, N.; Sharma, L.; Singh, A.K. Poly-beta-hydroxybutyrate accumulation in Nostoc muscorum: Effects of metabolic inhibitors. *J. Plant. Physiol.* **2007**, *164*, 312–317.

33. Dephilippis, R.; Ena, A.; Guastini, M.; Sili, C.; Vincenzini, M. Factors Affecting Poly-Beta-Hydroxybutyrate Accumulation in Cyanobacteria and in Purple Nonsulfur Bacteria. *FEMS Microbiol. Rev.* **1992**, *9*, 187–194.
34. Rippka, R. Isolation and Purification of Cyanobacteria. *Method Enzymol.* **1988**, *167*, 3–27.
35. Valentin, H.; Steinbüchel, A. Application of enzymatically synthesized short-chain-length hydroxy fatty acid coenzyme A thioesters for assay of polyhydroxyalkanoic acid synthases. *Appl. Microbiol. Biotechnol.* **1994**, *40*, 699–709.
36. Marin, K.; Stirnberg, M.; Eisenhut, M.; Kramer, R.; Hagemann, M. Osmotic stress in Synechocystis sp. PCC 6803: Low tolerance towards nonionic osmotic stress results from lacking activation of glucosylglycerol accumulation. *Microbiology* **2006**, *152*, 2023–2030.
37. Estepa, J.; Luque-Almagro, V.M.; Manso, I.; Escribano, M.P.; Martinez-Luque, M.; Castillo, F.; Moreno-Vivian, C.; Roldan, M.D. The nit1C gene cluster of Pseudomonas pseudoalcaligenes CECT5344 involved in assimilation of nitriles is essential for growth on cyanide. *Env. Microbiol. Rep.* **2012**, *4*, 326–334.

4.2 Supplementary information

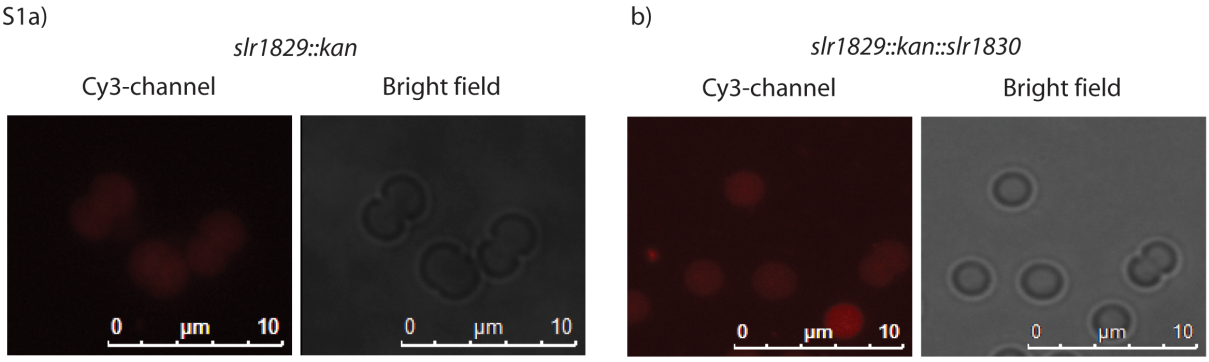

Figure 1. (**a**) Fluorescence microscopic image of a strain with the genomic deletion of *slr1829* (PhaE), that were stained with nile red to visiualize PHB. (**b**) Fluorescence microscopic image of a strain with the genomic deletion of *slr1829* (PhaE) and *slr1830* (PhaC) stained with nile red. In both images no PHB granules are visible due to the deletion of PhaE or PhaE and PhaC.

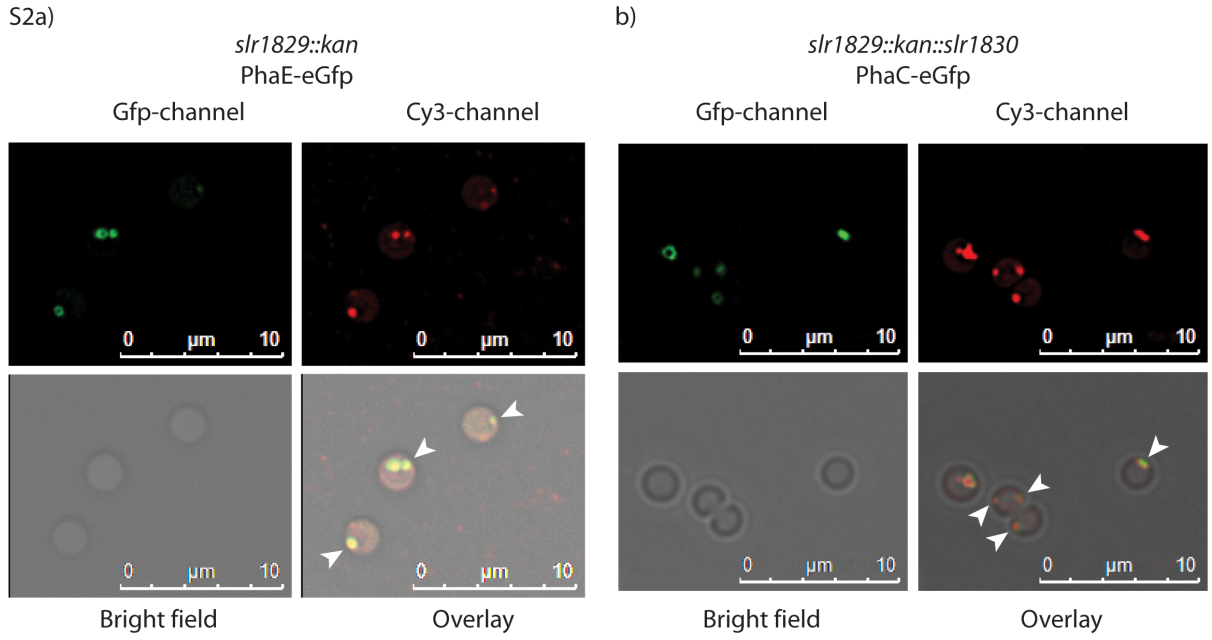

Figure 2. (**a**) Fluorescence microscopic image of the *slr1829* deletion strain complemented with PhaE-eGfp. (**b**) Fluorescence microscopic image of the *slr1829* and *slr1830* deletion strain complemented with PhaC-eGfp. Samples were stained with nile red dto visualize PHB. Both eGfp tagged PHB synthase subunits remain functional after addition of the fluorescence tag. White arrowheads show PHB granules in close proximity to the cytoplasmic membrane.

S3

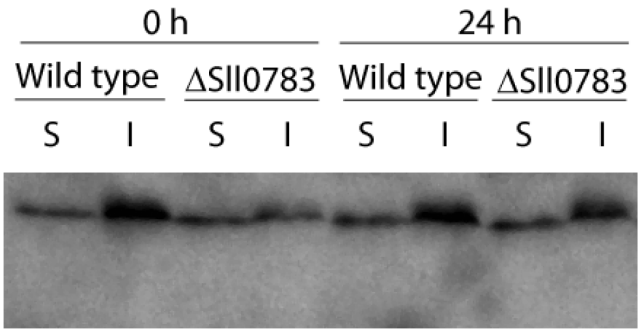

Western blot with an antibody against PhaE shows protein levels between wild type and the *sll0783* mutant, before nitrogen starvation has been applied and 24 h troughout nitrogen starvation. Soluble (S) and insoluble (I) fraction were monitored for PhaE content.

S4

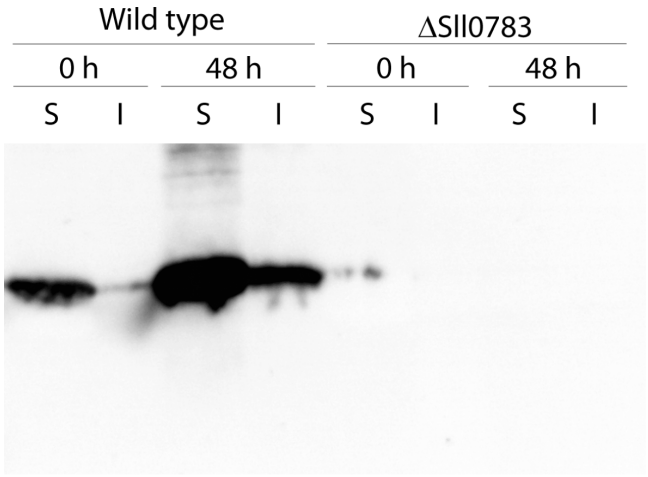

Western blot against Sll0783 in the wild type and *sll0783* mutant, before nitrogen starvation and 48 after nitrogen starvation was induced. Sll0783 is already present before nitrogen starvation has been induced and is highly upregulated during nitrogen starvation.

Experimental section

Cells were harvested and treated as described in 3.4 *PHB synthase assay*. Protein concentration was determined using the Bradford assay. 20 µg of total protein of the soluble and insoluble fraction was applied on the SDS-PAGE. SDS-PAGE and Western blot were performed using standard procedures. PhaE was detected with an primary antibody raised against PhaE of *Synechocystis* sp. PCC 6803.

				Analyte	Normalized Response [IS-1 OD750-1 ml-1 (sample volume)]							
Metabolite	**Sum Formula**	**KEGG-ID**	**CAS-ID**	**MPIMP-ID**	**Average**							
					0 h	6 h	24 h	168 h	0 h	6 h	24 h	168 h
					wt 0h	wt 6h	wt 24h	wt 168h	sll0783 0h	sll0783 6h	sll0783 24h	sll0783 168h
					AV	AV	AV	AV	AV	AV	AV	AV
Acids												
Citric acid	C6H8O7	C00158	77-92-9	A182004-101	7,86E-03	1,86E-02	2,06E-02	6,18E-02	1,13E-02	8,33E-03	1,29E-02	1,39E-02
Fumaric acid	C4H4O4	C00122	110-17-8	A137001-101	1,73E-04	4,51E-04	1,62E-03	5,89E-04	2,26E-04	2,08E-04	8,22E-04	1,36E-03
Malic acid	C4H6O5	C00149	97-67-6	A149001-101	4,40E-04	1,28E-03	2,54E-03	2,17E-03	6,59E-04	6,08E-04	3,07E-03	6,17E-03
Glutaric acid, 2-oxo-	C5H6O5	C00026	328-50-7	A158004-101	7,82E-03	7,19E-03	1,40E-02	1,82E-02	2,34E-03	3,29E-03	6,14E-03	1,77E-02
Succinic acid	C4H6O4	C00042	110-15-6	A134001-101	8,54E-04	8,13E-04	6,93E-04	1,21E-03	4,87E-04	3,84E-04	9,84E-04	1,18E-03
Oxalic acid	C2H2O4	C00209	144-62-7	A113002-101	2,52E-03	1,97E-03	1,15E-03	1,73E-03	2,44E-03	1,54E-03	1,71E-03	1,16E-03
Glycolic acid	C2H4O3	C00160	79-14-1	A106002-101	5,38E-04	3,21E-04	2,19E-04	2,82E-04	4,46E-04	2,81E-04	4,15E-04	1,69E-04
Amino Acids												
Aspartic acid	C4H7NO4	C00049	56-84-8	A144003-101	4,06E-04	1,53E-03	1,43E-03	7,93E-05	1,20E-03	7,67E-04	1,39E-03	4,70E-04
Glutamate	C5H9NO4	C00025	56-86-0	A154002-101	2,53E-02	1,62E-02	2,93E-03	1,42E-03	1,71E-02	1,75E-02	1,33E-02	7,79E-03
Glycine	C2H5NO2	C00037	56-40-6	A133001-101	9,01E-04	7,62E-03	5,19E-04	4,25E-04	1,62E-03	1,85E-03	1,20E-03	4,13E-04
Isoleucine	C6H13NO2	C00407	73-32-5	A132002-101	3,35E-05	2,63E-04	2,88E-05	2,25E-05	1,29E-04	3,22E-05	8,99E-05	1,35E-04
Lysine	C6H14N2O2	C00047	56-87-1	A192003-101	2,57E-04	1,09E-03	5,04E-04	1,85E-05	3,09E-03	2,59E-04	1,56E-03	3,24E-03
Phenylalanine	C9H11NO2	C00079	63-91-2	A164001-101	3,51E-04	1,35E-03	4,13E-04	1,43E-05	5,30E-04	4,42E-04	5,96E-04	2,71E-04
Glutamine	C5H7NO3	C02238		A153002-101	1,50E-02	9,78E-03	1,82E-02	3,39E-03	7,75E-03	3,76E-03	5,09E-03	2,61E-02
Serine	C3H7NO3	C00065	56-45-1	A128001-101	1,11E-03	7,43E-03	5,25E-04	4,20E-04	1,48E-03	1,39E-03	1,90E-03	2,27E-04
Threonine	C4H9NO3	C00188	72-19-5	A140001-101	8,28E-05	5,28E-04	1,57E-04	6,87E-05	1,64E-04	9,26E-05	1,73E-04	3,33E-04
Valine	C5H11NO2	C00183	72-18-4	A122001-101	1,85E-05	1,20E-04	0,00E+00	2,67E-05	7,27E-05	5,25E-05	2,76E-05	0,00E+00
N- Compounds												
Adenosine	C10H13N5O4	C00212	58-61-7	A265001-101	2,32E-03	2,40E-03	6,70E-03	1,95E-03	9,25E-04	1,31E-03	3,79E-03	6,66E-03
Ethanolamine	C2H7NO	C00189		A128002-101	2,59E-02	4,25E-02	3,16E-02	3,43E-02	3,12E-02	3,71E-02	4,58E-02	3,51E-02
Uracil	C4H4N2O2	C00106	66-22-8	A136001-101	8,96E-05	5,81E-05	2,90E-05	5,94E-05	7,58E-05	2,31E-05	1,72E-05	1,09E-04
Phenolic Compounds												
Benzoic acid**	C7H6O2	C00180	65-85-0	A128003-101	1,62E-03	2,73E-03	1,48E-03	1,72E-03	2,05E-03	2,23E-03	5,34E-03	9,41E-04
Phosphates												
Adenosine-5'-monophosphat	C10H14N5O7P	C00020	61-19-8	A307003-101	0,00E+00	0,00E+00	1,95E-05	0,00E+00	0,00E+00	0,00E+00	1,41E-05	2,10E-05
Fructose	C6H12O6	C00095	57-48-7	A187002-101	3,26E-04	2,47E-03	2,96E-03	1,37E-03	1,26E-03	2,06E-03	1,95E-03	3,71E-03
Glucose	C6H12O6	C00031	50-99-7	A189002-101	2,24E-04	2,29E-03	3,27E-03	5,52E-04	1,67E-03	7,16E-04	2,89E-03	5,86E-03
Fructose-6-P	C6H13O9P	C00085	643-13-0	A232002-101	4,10E-05	3,16E-03	4,09E-03	9,39E-04	4,69E-04	1,30E-03	5,80E-03	6,02E-03
Glucose-6-P	C6H13O9P	C00092	56-73-5	A235002-101	3,92E-03	9,45E-03	1,05E-02	2,22E-03	7,58E-04	2,89E-03	1,34E-02	1,35E-02
3-P-glycerate	C3H7O7P	C00197	820-11-1	A181003-101	3,34E-03	8,27E-03	3,21E-02	3,26E-03	1,28E-03	1,69E-03	2,05E-03	4,32E-03
PEP	C3H5O6P	C00074	138-08-9	A159005-101	1,97E-04	2,52E-04	4,63E-04	1,25E-04	3,72E-05	8,41E-05	2,99E-05	6,91E-05
Sorbitol	C6H14O6	C00794	50-70-4	A193001-101	1,32E-03	4,34E-02	5,74E-03	5,50E-03	3,38E-03	4,81E-03	1,27E-03	9,05E-04
Polyhydroxy Acids												
Galactonic acid	C6H12O7	C00880	576-36-3	A199002-101	1,12E-04	2,44E-04	3,17E-04	5,98E-05	1,84E-04	1,85E-04	5,78E-04	3,01E-04
Gluconic acid	C6H12O7	C00257	526-95-4	A200001-101	8,55E-06	2,60E-05	2,40E-04	1,73E-05	2,97E-05	0,00E+00	8,79E-05	2,29E-04
Glyceric acid	C3H6O4	C00258	473-81-4	A135003-101	6,67E-03	4,03E-03	8,03E-03	2,46E-03	3,96E-03	1,38E-03	4,39E-03	5,02E-03
Threonic acid	C4H8O5	C01620	7306-96-9	A156001-101	3,98E-02	3,83E-02	4,85E-02	1,80E-02	5,30E-02	2,66E-02	5,30E-02	3,89E-02
Polyols												
Inositol, myo-	C6H12O6	C00137	87-89-8	A209002-101	2,86E-03	4,39E-03	1,08E-02	0,00E+00	1,83E-03	2,75E-03	5,22E-03	0,00E+00
Monosaccharides												
Disaccharides												
Sucrose	C12H22O11	C00089	57-50-1	A264001-101	1,02E-03	3,29E-02	6,21E-03	2,67E-02	1,28E-03	1,08E-03	1,09E-02	8,63E-02
Trehalose, alpha,alpha'-	C12H22O11	C01083	99-20-7	A274002-101	3,56E-05	8,52E-05	1,14E-04	5,49E-05	9,19E-05	3,52E-05	8,12E-05	1,01E-04
Trisaccharides												
Kestose, 1-	C18H32O16	C03661		A340003-101	0,00E+00	0,00E+00	0,00E+00	0,00E+00	0,00E+00	0,00E+00	0,00E+00	0,00E+00
Raffinose	C18H32O16	C00492	512-69-6	A337002-101	0,00E+00	0,00E+00	0,00E+00	0,00E+00	0,00E+00	0,00E+00	0,00E+00	0,00E+00
Inositol-1-phosphate, myo-	C6H13O9P	C01177		A243001-101	4,13E-05	5,91E-05	0,00E+00	9,47E-06	1,60E-05	1,07E-05	6,89E-05	9,69E-05
Pyroglutamic acid	C5H7NO3	C02238		A153002-101	4,03E-02	2,59E-02	2,12E-02	4,80E-03	2,48E-02	1,37E-02	1,84E-02	3,39E-02
Glutamic acid	C5H9NO4	C00025	56-86-0	A154002-101	2,53E-02	1,62E-02	2,93E-03	1,42E-03	1,71E-02	1,75E-02	1,33E-02	7,79E-03
Glutamine	C5H7NO3	C02238		A153002-101	1,50E-02	9,78E-03	1,82E-02	3,39E-03	7,75E-03	-3,76E-03	5,09E-03	2,61E-02
Glutaric acid, 2-oxo-	C5H6O5	C00026	328-50-7	A158004-101	7,82E-03	7,19E-03	1,40E-02	1,82E-02	2,34E-03	3,29E-03	6,14E-03	1,77E-02

				Analyte	X-fold change to wt 0h (N-deficiency)								
Metabolite	**Sum Formula**	**KEGG-ID**	**CAS-ID**	**MPIMP-ID**	**wild type**				***sll0783***				
					0 h	6 h	24 h	168 h	0 h	6 h	24 h	168 h	
Acids													
Citric acid	C6H8O7	C00158	77-92-9	A182004-101	1,00	2,36	2,62	7,86	1,44	1,06	1,63	1,77	0,06
Fumaric acid	C4H4O4	C00122	110-17-8	A137001-101	1,00	2,61	9,37	3,41	1,31	1,20	4,76	7,89	0,14
Malic acid	C4H6O5	C00149	97-67-6	A149001-101	1,00	2,90	5,77	4,93	1,50	1,38	6,98	14,03	0,00
Glutaric acid, 2-oxo-	C5H6O5	C00026	328-50-7	A158004-101	1,00	0,92	1,79	2,33	0,30	0,42	0,79	2,26	0,00
Succinic acid	C4H6O4	C00042	110-15-6	A134001-101	1,00	0,95	0,81	1,41	0,57	0,45	1,15	1,38	0,03
Oxalic acid	C2H2O4	C00209	144-62-7	A113002-101	1,00	0,78	0,46	0,69	0,97	0,61	0,68	0,46	1,98
Glycolic acid	C2H4O3	C00160	79-14-1	A106002-101	1,00	0,60	0,41	0,52	0,83	0,52	0,77	0,31	0,88
Amino Acids													
Aspartic acid	C4H7NO4	C00049	56-84-8	A144003-101	1,00	3,77	3,53	0,20	2,96	1,89	3,43	1,16	0,19
Glutamate	C5H9NO4	C00025	56-86-0	A154002-101	1,00	0,64	0,12	0,06	0,67	0,69	0,53	0,31	0,00
Glycine	C2H5NO2	C00037	56-40-6	A133001-101	1,00	8,46	0,58	0,47	1,80	2,06	1,34	0,46	0,66
Isoleucine	C6H13NO2	C00407	73-32-5	A132002-101	1,00	7,84	0,86	0,67	3,85	0,96	2,68	4,03	0,00
Lysine	C6H14N2O2	C00047	56-87-1	A192003-101	1,00	4,23	1,96	0,07	2,26	1,01	1,26	0,78	0,33
Phenylalanine	C9H11NO2	C00079	63-91-2	A164001-101	1,00	3,84	1,18	0,04	1,51	1,26	1,70	0,77	0,00
Glutamine	C5H7NO3	C02238		A153002-101	1,00	0,65	1,22	0,23	0,52	0,25	0,34	1,74	0,03
Serine	C3H7NO3	C00065	56-45-1	A128001-101	1,00	6,71	0,47	0,38	1,33	1,26	1,71	0,21	0,07
Threonine	C4H9NO3	C00188	72-19-5	A140001-101	1,00	6,38	1,90	0,83	1,98	1,12	2,09	4,02	0,00
Valine	C5H11NO2	C00183	72-18-4	A122001-101	1,00	6,49	1,00	1,44	3,93	2,84	1,49	1,00	6,38
N- Compounds													
Adenosine	C10H13N5O4	C00212	58-61-7	A265001-101	1,00	1,03	2,88	0,84	0,40	0,56	1,63	2,87	0,00
Ethanolamine	C2H7NO	C00189		A128002-101	1,00	1,64	1,22	1,32	1,20	1,43	1,77	1,36	9,46
Uracil	C4H4N2O2	C00106	66-22-8	A136001-101	1,00	0,65	0,32	0,66	0,85	0,26	0,19	1,22	0,00
Phenolic Compounds													
Benzoic acid**	C7H6O2	C00180	65-85-0	A128003-101	1,00	1,69	0,91	1,06	1,27	1,38	3,31	0,58	9,60
Phosphates													
Adenosine-5'-monophosphat	C10H14N5O7P	C00020	61-19-8	A307003-101									
Fructose	C6H12O6	C00095	57-48-7	A187002-101	1,00	7,57	9,07	4,20	3,86	6,31	5,98	11,36	12,33
Glucose	C6H12O6	C00031	50-99-7	A189002-101	1,00	10,21	14,57	2,46	7,44	3,19	12,91	26,13	25,30
Fructose-6-P	C6H13O9P	C00085	643-13-0	A232002-101	1,00	77,09	99,80	22,93	11,44	31,80	141,59	146,89	0,00
Glucose-6-P	C6H13O9P	C00092	56-73-5	A235002-101	1,00	2,41	2,67	0,57	0,19	0,74	3,41	3,43	0,00
3-P-glycerate	C3H7O7P	C00197	820-11-1	A181003-101	1,00	2,48	9,61	0,97	0,38	0,51	0,61	1,29	0,02
PEP	C3H5O6P	C00074	138-08-9	A159005-101	1,00	1,28	2,34	0,63	0,19	0,43	0,15	0,35	0,00
Sorbitol	C6H14O6	C00794	50-70-4	A193001-101	1,00	32,93	14,56	11,13	2,57	3,66	0,97	0,69	0,11
Polyhydroxy Acids													
Galactonic acid	C6H12O7	C00880	576-36-3	A199002-101	1,00	2,17	2,82	0,53	1,64	1,65	5,15	2,68	2,99
Gluconic acid	C6H12O7	C00257	526-95-4	A200001-101	1,00	3,04	28,07	2,03	3,47	1,00	10,27	26,80	0,00
Glyceric acid	C3H6O4	C00258	473-81-4	A135003-101	1,00	0,60	1,20	0,37	0,59	0,21	0,66	0,75	0,08
Threonic acid	C4H8O5	C01620	7306-96-9	A156001-101	1,00	0,96	1,22	0,45	1,33	0,67	1,33	0,98	0,52
Polyols													
Inositol, myo-	C6H12O6	C00137	87-89-8	A209002-101	1,00	1,53	3,77	1,00	0,64	0,96	1,82	1,00	0,00
Monosaccharides													
Disaccharides													
Sucrose	C12H22O11	C00089	57-50-1	A264001-101	1,00	32,29	6,10	26,23	1,26	1,06	10,66	84,73	0,33
Trehalose, alpha,alpha'-	C12H22O11	C01083	99-20-7	A274002-101	1,00	2,39	3,20	1,54	2,58	0,99	2,28	2,85	2,61
Trisaccharides													
Kestose, 1-	C18H32O16	C03661		A340003-101									
Raffinose	C18H32O16	C00492	512-69-6	A337002-101									
Inositol-1-phosphate, myo-	C6H13O9P	C01177		A243001-101	1,00	1,43	1,00	0,23	0,39	0,26	1,67	2,35	0,00
Pyroglutamic acid	C5H7NO3	C02238		A153002-101	1,00	0,64	0,52	0,12	0,62	0,34	0,46	0,84	0,03
Glutamic acid	C5H9NO4	C00025	56-86-0	A154002-101	1,00	0,64	0,12	0,06	0,67	0,69	0,53	0,31	0,00
Glutamine	C5H7NO3	C02238		A153002-101	1,00	0,65	1,22	0,23	0,52	0,25	0,34	1,74	1,21
Glutaric acid, 2-oxo-	C5H6O5	C00026	328-50-7	A158004-101	1,00	0,92	1,79	2,33	0,30	0,42	0,79	2,26	0,00

				Analyte	X-fold changeto wt 0h (N-deficiency)								
Metabolite	**Sum Formula**	**KEGG-ID**	**CAS-ID**	**MPIMP-ID**	**wild type**				***sll0783***				
					0 h	6 h	24 h	168 h	0 h	6 h	24 h	168 h	blank
Acids													
Citric acid	C6H8O7	C00158	77-92-9	A182004-101	1,00	2,36	2,62	7,86	1,44	1,06	1,63	1,77	0,06
Fumaric acid	C4H4O4	C00122	110-17-8	A137001-101	1,00	2,61	9,37	3,41	1,31	1,20	4,76	7,89	0,14
Malic acid	C4H6O5	C00149	97-67-6	A149001-101	1,00	2,90	5,77	4,93	1,50	1,38	6,98	14,03	0,00
Glutaric acid, 2-oxo-	C5H6O5	C00026	328-50-7	A158004-101	1,00	0,92	1,79	2,33	0,30	0,42	0,79	2,26	0,00
Succinic acid	C4H6O4	C00042	110-15-6	A134001-101	1,00	0,95	0,81	1,41	0,57	0,45	1,15	1,38	0,03
Oxalic acid	C2H2O4	C00209	144-62-7	A113002-101	1,00	0,78	0,46	0,69	0,97	0,61	0,68	0,46	1,98
Glycolic acid	C2H4O3	C00160	79-14-1	A106002-101	1,00	0,60	0,41	0,52	0,83	0,52	0,77	0,31	0,88
Amino Acids													
Aspartic acid	C4H7NO4	C00049	56-84-8	A144003-101	1,00	3,77	3,53	0,20	2,96	1,89	3,43	1,16	0,19
Glutamate	C5H9NO4	C00025	56-86-0	A154002-101	1,00	0,64	0,12	0,06	0,67	0,69	0,53	0,31	0,00
Glycine	C2H5NO2	C00037	56-40-6	A133001-101	1,00	8,46	0,58	0,47	1,80	2,06	1,34	0,46	0,66
Isoleucine	C6H13NO2	C00407	73-32-5	A132002-101	1,00	7,84	0,86	0,67	3,85	0,96	2,68	4,03	0,00
Lysine	C6H14N2O2	C00047	56-87-1	A192003-101	1,00	4,23	1,96	0,07	2,26	1,01	1,26	0,78	0,33
Phenylalanine	C9H11NO2	C00079	63-91-2	A164001-101	1,00	3,84	1,18	0,04	1,51	1,26	1,70	0,77	0,00
Glutamine	C5H7NO3	C02238		A153002-101	1,00	0,65	1,22	0,23	0,52	0,25	0,34	1,74	0,03
Serine	C3H7NO3	C00065	56-45-1	A128001-101	1,00	6,71	0,47	0,38	1,33	1,26	1,71	0,21	0,07
Threonine	C4H9NO3	C00188	72-19-5	A140001-101	1,00	6,38	1,90	0,83	1,98	1,12	2,09	4,02	0,00
Valine	C5H11NO2	C00183	72-18-4	A122001-101	1,00	6,49	1,00	1,44	3,93	2,84	1,49	1,00	6,38
N- Compounds													
Adenosine	C10H13N5O4	C00212	58-61-7	A265001-101	1,00	1,03	2,88	0,84	0,40	0,56	1,63	2,87	0,00
Ethanolamine	C2H7NO	C00189		A128002-101	1,00	1,64	1,22	1,32	1,20	1,43	1,77	1,36	9,46
Uracil	C4H4N2O2	C00106	66-22-8	A136001-101	1,00	0,65	0,32	0,66	0,85	0,26	0,19	1,22	0,00
Phenolic Compounds													
Benzoic acid**	C7H6O2	C00180	65-85-0	A128003-101	1,00	1,69	0,91	1,06	1,27	1,38	3,31	0,58	9,60
Phosphates													
Adenosine-5'-monophosphat	C10H14N5O7P	C00020	61-19-8	A307003-101									
Fructose	C6H12O6	C00095	57-48-7	A187002-101	1,00	7,57	9,07	4,20	3,86	6,31	5,98	11,36	12,33
Glucose	C6H12O6	C00031	50-99-7	A189002-101	1,00	10,21	14,57	2,46	7,44	3,19	12,91	26,13	25,30
Fructose-6-P	C6H13O9P	C00085	643-13-0	A232002-101	1,00	77,09	99,80	22,93	11,44	31,80	141,59	146,89	0,00
Glucose-6-P	C6H13O9P	C00092	56-73-5	A235002-101	1,00	2,41	2,67	0,57	0,19	0,74	3,41	3,43	0,00
3-P-glycerate	C3H7O7P	C00197	820-11-1	A181003-101	1,00	2,48	9,61	0,97	0,38	0,51	0,61	1,29	0,02
PEP	C3H5O6P	C00074	138-08-9	A159005-101	1,00	1,28	2,34	0,63	0,19	0,43	0,15	0,35	0,00
Sorbitol	C6H14O6	C00794	50-70-4	A193001-101	1,00	32,93	14,56	11,13	2,57	3,66	0,97	0,69	0,11
Polyhydroxy Acids													
Galactonic acid	C6H12O7	C00880	576-36-3	A199002-101	1,00	2,17	2,82	0,53	1,64	1,65	5,15	2,68	2,99
Gluconic acid	C6H12O7	C00257	526-95-4	A200001-101	1,00	3,04	28,07	2,03	3,47	1,00	10,27	26,80	0,00
Glyceric acid	C3H6O4	C00258	473-81-4	A135003-101	1,00	0,60	1,20	0,37	0,59	0,21	0,66	0,75	0,08
Threonic acid	C4H8O5	C01620	7306-96-9	A156001-101	1,00	0,96	1,22	0,45	1,33	0,67	1,33	0,98	0,52
Polyols													
Inositol, myo-	C6H12O6	C00137	87-89-8	A209002-101	1,00	1,53	3,77	1,00	0,64	0,96	1,82	1,00	0,00
Monosaccharides													
Disaccharides													
Sucrose	C12H22O11	C00089	57-50-1	A264001-101	1,00	32,29	6,10	26,23	1,26	1,06	10,66	84,73	0,33
Trehalose, alpha,alpha'-	C12H22O11	C01083	99-20-7	A274002-101	1,00	2,39	3,20	1,54	2,58	0,99	2,28	2,85	2,61
Trisaccharides													
Kestose, 1-	C18H32O16	C03661		A340003-101									
Raffinose	C18H32O16	C00492	512-69-6	A337002-101									
Inositol-1-phosphate, myo-	C6H13O9P	C01177		A243001-101	1,00	1,43	1,00	0,23	0,39	0,26	1,67	2,35	0,00
Pyroglutamic acid	C5H7NO3	C02238		A153002-101	1,00	0,64	0,52	0,12	0,62	0,34	0,46	0,84	0,03
Glutamic acid	C5H9NO4	C00025	56-86-0	A154002-101	1,00	0,64	0,12	0,06	0,67	0,69	0,53	0,31	0,00
Glutamine	C5H7NO3	C02238		A153002-101	1,00	0,65	1,22	0,23	0,52	0,25	0,34	1,74	1,21
Glutaric acid, 2-oxo-	C5H6O5	C00026	328-50-7	A158004-101	1,00	0,92	1,79	2,33	0,30	0,42	0,79	2,26	0,00

5 Publication 2

Contributions of the candidate for the publication.
All strains used in this study were either created by me or under my supervision. I have performed all fluorescence microscopy with fluorescently tagged proteins and performed detection of fluorescently tagged proteins by western blot. Biosynthetic activity of PHB synthase and oligomerization status of the phasin protein was performed by me. The manuscript was written by me under the supervision of Prof. Forchhammer and I have taken part in the revision process.

5.1 Photoautotrophic Polyhydroxybutyrate Granule Formation Is Regulated by Cyanobacterial Phasin PhaP in *Synechocystis* sp. Strain PCC 6803

AEM
Journals.ASM.org

Photoautotrophic Polyhydroxybutyrate Granule Formation Is Regulated by Cyanobacterial Phasin PhaP in *Synechocystis* sp. Strain PCC 6803

Waldemar Hauf, Björn Watzer, Nora Roos, Alexander Klotz, Karl Forchhammer

Interfaculty Institute of Microbiology and Infection Medicine Tübingen, Eberhard-Karls-Universität Tübingen, Tübingen, Germany

Cyanobacteria are photoautotrophic microorganisms which fix atmospheric carbon dioxide via the Calvin-Benson cycle to produce carbon backbones for primary metabolism. Fixed carbon can also be stored as intracellular glycogen, and in some cyanobacterial species like *Synechocystis* sp. strain PCC 6803, polyhydroxybutyrate (PHB) accumulates when major nutrients like phosphorus or nitrogen are absent. So far only three enzymes which participate in PHB metabolism have been identified in this organism, namely, PhaA, PhaB, and the heterodimeric PHB synthase PhaEC. In this work, we describe the cyanobacterial PHA surface-coating protein (phasin), which we term PhaP, encoded by *ssl2501*. Translational fusion of Ssl2501 with enhanced green fluorescent protein (eGFP) showed a clear colocalization to PHB granules. A deletion of *ssl2501* reduced the number of PHB granules per cell, whereas the mean PHB granule size increased as expected for a typical phasin. Although deletion of *ssl2501* had almost no effect on the amount of PHB, the biosynthetic activity of PHB synthase was negatively affected. Secondary-structure prediction and circular dichroism (CD) spectroscopy of PhaP revealed that the protein consists of two α-helices, both of them associating with PHB granules. Purified PhaP forms oligomeric structures in solution, and both α-helices of PhaP contribute to oligomerization. Together, these results support the idea that Ssl2501 encodes a cyanobacterial phasin, PhaP, which regulates the surface-to-volume ratio of PHB granules.

Cyanobacteria are photosynthetic microorganisms capable of oxygenic photosynthesis. ATP and reduction equivalents derived from photosynthetic electron flow are utilized to fix carbon dioxide and generate 3-phosphoglycerate (1). This metabolite can be utilized for either gluconeogenesis or glycolysis, providing the necessary carbon skeletons for biosynthesis of amino acids and other metabolites required for cell growth (2), when growth conditions are suitable and nutrients are abundant. In fact, carbon flux is greatly affected by the availability of macronutrients like nitrogen (3–5) and phosphorus, which may limit growth (6). Under nutrient-limiting conditions, cyanobacteria undergo a stress adaptation process termed chlorosis (7). This process leads to the degradation of light-harvesting complexes, causing reduced photosynthetic activity and thereby reduced metabolic activity (8). Furthermore, carbon flux is redirected toward glycogen synthesis upon macronutrient starvation (5). In addition, some cyanobacterial strains like *Synechocystis* sp. strain PCC 6803 (referred to here as *Synechocystis*) accumulate polyhydroxybutyrate (PHB) as a carbon and redox storage compound (9). PHB is synthesized in three biosynthetic steps, and all three enzymes catalyzing the reactions are known (10, 11). The first step involves a condensation of two acetyl coenzyme A (acetyl-CoA) groups to acetoacetyl-CoA by PhaA (*slr1993*). In the second step, PhaB (*slr1994*) reduces acetoacetyl-CoA to hydroxybutyryl-CoA, utilizing NADPH as the electron donor (10). In the last step of biosynthesis, hydroxybutyryl-CoA is polymerized to polyhydroxybutyrate by a class III PHB synthase, which is a heterodimer of PhaE (*slr1829*) and PhaC (*slr1830*) that builds the catalytically active enzyme in cyanobacteria (11). The PhaEC heterodimer (12) (or tetramer [13]) synthesizes PHB, thereby building up PHB granules, to which it is attached (4). This marks the boundaries of our understanding of PHB accumulation in cyanobacteria on a molecular level. However, the PHB granule surface is more complex and is coated by various different proteins, as observed with *Ralstonia eutropha* H16 (currently named *Cupriavidus necator*; referred to here as *R. eutropha*) (14). Some of these proteins are transcriptional regulators (PhaR) which modulate the transcriptional response upon biosynthesis of PHB (15); others are responsible for degradation and utilization of the intracellular stored PHB and are termed PHB depolymerases (PhaZ) (16). In addition to these functionally defined PHB-associated proteins, *R. eutropha* possesses at least 8 additional proteins, termed phasins, covering a large portion of the PHB granules (17, 18). These proteins have a variety of functions. Originally, phasins were identified as regulators of PHB granule size and number within a cell (19). More recently, specific phasins were identified as mediating the attachment of PHB granules to the nucleoid, as in the case of PhaM (20) in *R. eutropha* or PhaF from *Pseudomonas putida* KT2442 (21), thereby providing a mechanism for equal distribution of PHA granules to daughter cells. A phasin from *Azotobacter* sp. strain FA-8 ($PhaP_{Az}$) was described as promoting stress resistance in *Escherichia coli* (22),

Received 20 February 2015 **Accepted** 16 April 2015

Accepted manuscript posted online 24 April 2015

Citation Hauf W, Watzer B, Roos N, Klotz A, Forchhammer K. 2015. Photoautotrophic polyhydroxybutyrate granule formation is regulated by cyanobacterial phasin PhaP in *Synechocystis* sp. strain PCC 6803. Appl Environ Microbiol 81:4411–4422. doi:10.1128/AEM.00604-15.

Editor: M. J. Pettinari

Address correspondence to Karl Forchhammer, karl.forchhammer@uni-tuebingen.de.

Supplemental material for this article may be found at http://dx.doi.org/10.1128/AEM.00604-15.

doi:10.1128/AEM.00604-15

TABLE 1 Strains used in the study

Strain	Relevant feature	Source or reference
E. coli XL1-Blue	Cloning strain	Stratagene
E. coli RP4	Conjugation strain	34
E. coli BL21	Protein overexpression strain	57
Synechocystis sp. strain PCC 6803	Wild-type strain	Pasteur culture collection
Δ*ssl2501* mutant	Chromosomal deletion of *ssl2501*	This study
ssl2501	Δ*ssl2501* mutant complemented with pVZ322-2501	This study
ssl2501gfp	Δ*ssl2501* mutant complemented with pVZ322-2501gfp	This study
wt ssl2501Venus	Wild-type strain transformed with pVZ322-ssl2501Venus	This study
wt H1 Venus	Wild-type strain transformed with pVZ322-helix1Venus	This study
Δ*ssl2501* H1 Venus	Δ*ssl2501* mutant complemented with pVZ322-helix1Venus	This study
wt H2 Venus	Wild-type strain transformed with pVZ322-helix2Venus	This study
Δ*ssl2501* H2 Venus	Δ*ssl2501* mutant complemented with pVZ322-helix2Venus	This study

which is most likely associated with its chaperon-like activity (23). Even though many phasin proteins were identified, so far only a few have been studied biochemically in more detail (24). Genes encoding proteins homologous to phasins from *R. eutropha* or *P. putida* are absent in the genome of *Synechocystis*; however, Hein et al. (11) isolated PHB granules from *Synechocystis* and were able to detect many proteins of different molecular masses by SDS-PAGE. Of these, only one protein could be identified, the product of the open reading frame (ORF) *ssl2501*. However, subsequent studies found this protein repeatedly associated with thylakoid membranes (25, 26); therefore, the subcellular localization and consequently the biological function of this protein remain unclear. Homologs of Ssl2501 are present in several cyanobacterial strains, and the homologous protein in *Arthrospira platensis* NIES-39 (NIES39_Q00050) is predicted to have a so-called phasin 2 motif, based on the KEGG sequence similarity database (SSDB) (27). This prompted us to clarify whether the Ssl2501 protein may be a functional phasin in *Synechocystis*.

MATERIALS AND METHODS

Cultivation conditions. Standard cloning procedures were done in *E. coli* XL1 Blue (Stratagene) grown in LB medium at 37°C. Cyanobacterial strains were grown in BG11 medium (28) as described previously, with 40 to 50 μmol photons m^{-2} s^{-1} at 27°C and supplemented with 5 mM $NaHCO_3$ (28, 29). Growth was monitored by measuring the optical density at 750 nm (OD_{750}). Nitrogen starvation was induced by washing exponentially growing cells once with BG11 medium lacking sodium nitrate ($BG11_0$) and transferring them into $BG11_0$ at an OD_{750} of 0.4 as described previously (29). Antibiotics were added to the growth medium when required.

Strains, oligonucleotides, and plasmids used in this study. The strains used in this study are listed in Table 1. Oligonucleotides used for molecular biology techniques are listed in Table 2. Plasmids used in the study are listed in Table 3.

Construction of the *ssl2501* mutant and other strains. PCR fragments were generated using a high-fidelity polymerase (Q5; NEB) to amplify genes from genomic DNA or plasmids. Primers used to generate the constructs described in this study are listed in Table 3. A *ssl2501* mutant

TABLE 2 Oligonucleotides used for molecular biology techniques

Primer	Sequence
Kana-for	CCTCGTGAAGAAGGTGTTGCTGAC
Kana-rev	CAACCAATTAACCAATTCTGATT
Ssl2501 upfor	CGACGGTCTTGATGAAAC
Ssl2501 uprev	GTCAGCAACACCTTCTTCACGAGGAGGGCTAAAACCGCTAATAT
Ssl2501 dofor	TAATCAGAATTGGTTAATTGGTTGCTGATGTAAGCCTATTAACC
Ssl2501 dorev	TAATGGTAATGGCACTGATG
ssl2501for	GATCGTCGACTAATGGAGACGTGCGATACC
ssl2501rev	AGTTCTTCTCCTTTACTCATGTTAGCCGATACGGGCTCTT
Gfpfor	ATGAGTAAAGGAGAAGAACT
Gfprev	GATCCTGCAGTTATTTGTATAGTTCATCCA
ssl2502rev	AGTTCTTCTCCTTTACTCATTCGTTGGCGGTAGTTCCTTG
IBASsl2501for	TATACAAATGGCTAGCTGGAGCCACCCGCAGTTCGAAAAAGGCGCCATGAACACCCAGTTTTTTGAAGAATACC
IBASsl2501rev	GGATCCCCGGGTACCGAGCTCGAATTCGGGACCGCGGTCTCGGCTAGTTA GGCCGATCGGGCTCTTG
Venrev	ACACTGATGAATGTTCCGTTGCGCTGCCCGGATTACAGATCCTCTAGATTACTTGTACAGCTCGTCCATG CCG
promotorfor	ACACTGATGAATGTTCCGTTGCGCTGCCCGGATTACAGATCCTCTAGATTACTTGTACAGCTCGTCCATGCCG
hel1rev	TCCTCGCCCTTGCTCACGCTACCGCTGCCACTTCCTGATCCGCTACCTTTGGGCAGGCTTTCCATCCAAG
Venfor	GGTAGCGGATCAGGAAGTGGCAGCGGTAGCGTGAGCAAGGGCGAGGAGCTGTTC
revssl2501	CGCCCTTGCTCACGCTACCGCTGCCACTTCCTGATCCGCTACCGTTAGCCGATACGGGCT CTTGC
Venforhel2	GCAAGAGCCCGTATCGGCTGGTAGCGGATCAGGAAGTGGCAGCGGTAGCGTGAGCAAGGGCGAGGAGCTGTTC
Ssl2501for	TATACAAATGGCTAGCTGGAGCCACCCGCAGTTCGAAAAAGGCGCCATGAACACCCAGTTTTTTGAAGAATACC
Ssl2501rev	GGATCCCCGGGTACCGAGCTCGAATTCGGGACCGCGGTCTCGGCTAGTTAGCCGATACGGGCTCTTG
pET15b for	TCTAGAAATAATTTTGTTTAACTTTAAGAAGGAGATATACATGAACACCCAGTTTTTTGAAGAATACCAAAC
pET15b rev	CCAGGCCGCTGCTGTGATGATGATGATGATGGCTGCTGCCCGAGCTCGAATTCGGGACCC

TABLE 3 Plasmids used in the study

Plasmid	Relevant feature	Source or reference
pJet1.2	Cloning vector	Thermo Fisher
pJetΔ2501	Suicide vector for *ssl2501* deletion derived from pJet1.2	This study
pVZ322	Broad-host-range vector	32
pVZ322-2501gfp	eGFP fused to the C terminus of Ssl2501	This study
pVZ322-2501	*ssl2501* with native promoter	This study
pVZ322-2501Venus	Venus fused to the C terminus of Ssl2501 connected by a 10-amino-acid linker sequence	This study
pVZ322-helix1Venus	Venus fused to the C terminus of Ssl2501 helix 1, connected by a 10-amino-acid linker sequence	This study
pVZ322-helix2Venus	Venus fused to the C terminus of Ssl2501 helix 2, connected by a 10-amino-acid linker sequence	This study
pET15b*ssl2501*	Vector expressing *ssl2501* upon IPTG addition	This study
pET15bHelix2	Vector expressing helix 2 of *ssl2501* upon IPTG addition	This study

was constructed by amplifying up- and downstream genomic regions by PCR from genomic DNA with primers Ssl2501upfor, Ssl2501uprev, Ssl2501dofor, and Ssl2501dorev. A kanamycin resistance cassette was amplified from pVZ322 using primers Kana-for and Kana-rev. The flanking regions were fused at the 5′ and 3′ ends of a kanamycin resistance cassette by long flanking homology PCR (30) and cloned in pJet1.2 (Fermentas), resulting in pJetΔ2501. *Synechocystis* was transformed with plasmid pJetΔ2501 using its natural competence. The ORF *ssl2501* was amplified by PCR from genomic DNA with primers ssl2501for and ssl2501rev and fused to the coding sequence of enhanced green fluorescent protein (eGFP) derived from plasmid pCESL19 (31) by PCR with primers gfpfor and gfprev. The PCR fragment was inserted in pVZ322 (32) linearized with SalI and PstI, producing plasmid pVZ322-2501gfp. Plasmid pVZ322-2501 was constructed the same way. ORF *ssl2502* (CyanoBase) was amplified with ssl2501for and ssl2502rev and fused to eGFP in this plasmid, and it expresses native *ssl2501*, which is upstream of *ssl2502*. Venus was amplified with primers Venfor and Venrev and translationally fused to the C terminus of *ssl2501* (amplified with promotorfor and revssl2501), or the coding sequences of the first (amplified with promotorfor hel1rev) and second (gBlocks [IDT]) α-helices were assembled (33) in pVZ322 at the XbaI site. A Strep-tag was added to the N terminus of *ssl2501* (PCR amplified with Ssl2501for and Ssl2501rev) by inserting it in pASK-IBA5+ at the EheI site using Gibson assembly. The coding region of *ssl2501*in pASKIBA5+ (including the streptavidin tag) was amplified by PCR (primers pET15bfor and pET15brev) and inserted in pET15b at the unique NcoI site using Gibson assembly. Plasmids were propagated in *E. coli* XL1-Blue and isolated using the Peqlab miniprep kit. Sequence integrity of the plasmids was verified by sequencing. Plasmids able to replicate autonomously in *Synechocystis* were transferred by triparental mating as described previously (34).

Microscopy and staining procedures. Microscopy was performed with a Leica DM5500B fluorescence microscope using the 100×, 1.3 numerical aperture oil objective lens. Fluorescence microscopy was performed with three filter cubes. In order to detect eGFP, a BP470 40-nm excitation filter and a BP525 50-nm emission filter were used; this is referred to as the GFP channel. Venus fluorescence was detected using an ET500/20x excitation filter and an ET535/30m emission filter; this is referred to as the yellow fluorescent protein (YFP) channel. To detect Nile red fluorescence, a filter cube with BP535 50-nm excitation filters and a BP610 75-nm emission filter was used; this is referred to as the Cy3 channel. Image acquisition was done with a Leica DFC360FX black-and-white camera. Bright-field images were exposed for 5 ms and 80 to 200 ms in the fluorescence channels. Images were routinely taken as Z-stacks with 0.25 μm distance between images. Z-stacks were used to perform three-dimensional (3D) deconvolution using the built-in function of the Leica ASF software. Images were recolored by the Leica ASF software based on the filter used, and intensity levels were adjusted using AdobePhotoshopCS5. To visualize PHB granules under nitrogen starvation, 12 μl of cell culture was mixed with 6 μl Nile red solution (1 μg/ml in ethanol) and subsequently analyzed under the microscope.

Purification of recombinant proteins from *E. coli* BL21. For purification of recombinant proteins, the corresponding plasmids were transformed in *E. coli* BL21 and plated on LB agar with appropriate antibiotics. Single clones were picked to start an overnight culture, which was then used to inoculate the production culture. The production culture was grown at 37°C to an OD_{595} of 0.8, and recombinant-protein production was induced by addition of 2 mM isopropyl-β-D-thiogalactopyranoside (IPTG). Cultivation was continued at 20°C overnight. Then, the cells were harvested at 4,000 × *g* for 10 min, suspended in lysis buffer (50 mM Tris-HCl [pH 7.4], 50 mM KCl, 5 mM $MgCl_2$, 2 mM EDTA, 2 mM DL-dithiothreitol, 1 mM benzamidine, and 0.2 mM phenylmethylsulfonyl fluoride [PMSF]), and lysed using a Branson Sonifier. The cell lysate was cleared by centrifugation at 50,000 × *g* for 30 min, and the supernatant was loaded on a Strep-Tactin column using a peristaltic pump. The column was washed with five column volumes of washing buffer (100 mM Tris-HCl [pH 7.8], 150 mM NaCl, 5 mM $MgCl_2$, 1 mM EDTA, 2 mM DL-dithiothreitol, 1 mM benzamidine, and 0.2 mM PMSF), and proteins were eluted through the addition of desthiobiotin to a final concentration of 2.5 mM to the washing buffer. Desthiobiotin was removed by dialyzing the protein solution against 500 ml storage buffer (50 mM Tris-HCl [pH 7.4], 100 mM KCl, 5 mM $MgCl_2$, 0,5 mM EDTA, 50% [vol/vol] glycerol, 2 mM DL-dithiothreitol, 1 mM benzamidine).

SDS-PAGE and Western blotting. For electrophoretic separation of proteins, SDS-PAGE was performed with 12% polyacrylamide resolving gels as described previously (35, 36). Twenty micrograms of total protein was used for SDS-PAGE with nitrogen-starved cells, and 40 μg was used for exponentially growing cells. For Western blot analysis, proteins were blotted on a methanol-activated polyvinylidene difluoride (PVDF) membrane as described previously (37). Membranes were blocked with 10% (wt/vol) milk powder in TBS buffer (20 mM Tris-HCl [pH 7.4], 0.5% [wt/vol] NaCl) for 30 min. Afterwards the membrane was transferred to 1% (wt/vol) milk powder in TBS buffer containing 0.25 μg/ml primary antibody (anti-GFP polyclonal rabbit antibody; Santa Cruz Biotechnology, Inc.) and incubated in this solution overnight at 4°C. Nonbound primary antibody was removed by washing and secondary antibody (anti-rabbit polyclonal goat antibody–horseradish peroxidase conjugate; Sigma-Aldrich), diluted 1:10,000 in 1% (wt/vol) milk powder in TBS, was applied. Immunoreactive bands on the membrane were visualized using the LumiLight detection system (Roche Diagnostics) and the Gel Logic 1500 imaging system (Kodak) with the associated software.

Size exclusion chromatography and cross-linking of proteins. Prior to size exclusion chromatography or cross-linking, proteins were dialyzed in 100 mM potassium phosphate buffer (pH 7.8) overnight. Ten microliters of dialyzed protein was injected onto a Superdex 200 PC 3.2/30 equilibrated with running buffer (50 mM potassium phosphate buffer [pH 7.8]). Protein elution was detected at 280 nm. Proteins dialyzed in phosphate buffer were cross-linked by addition of 0.1% (wt/vol) glutaraldehyde for 10 min at room temperature. The cross-linking reaction was stopped by addition of Tris-HCl (pH 7.8) to a final concentration of 100

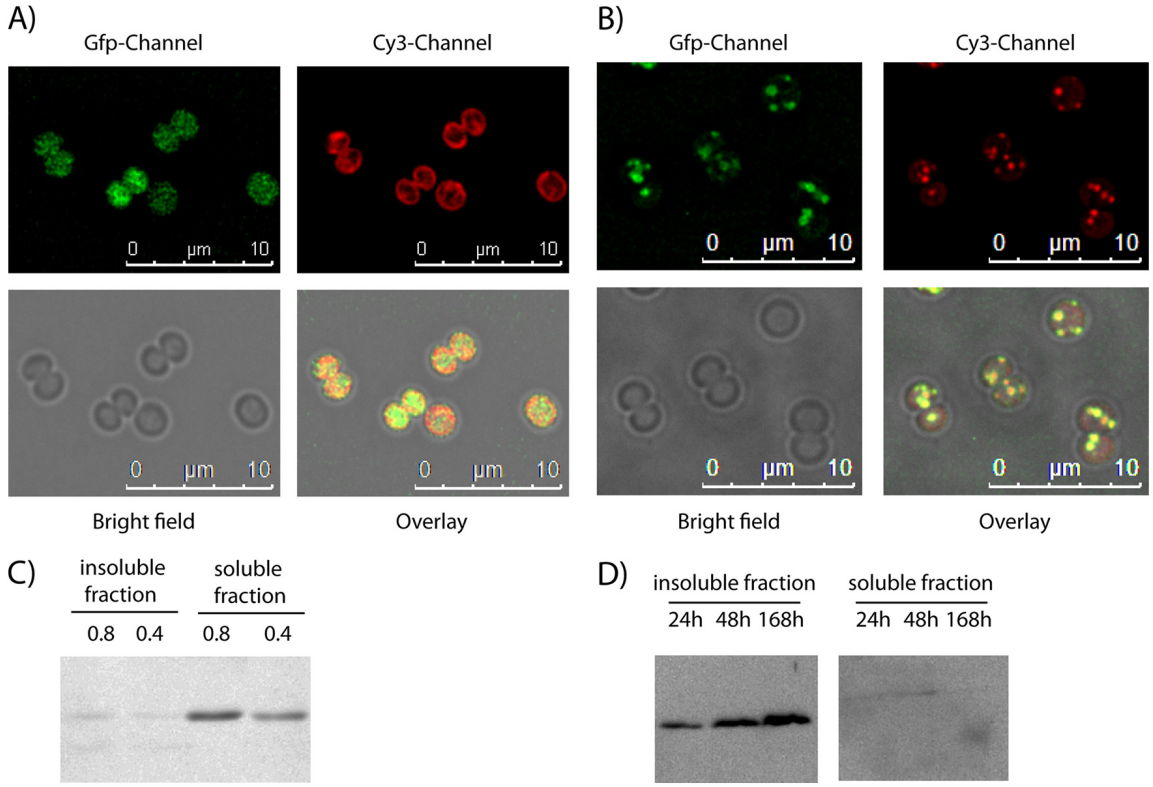

FIG 1 (A) Localization of Ssl2501-eGFP (GFP channel) in *Synechocystis* during exponential growth at an OD_{750} of 0.8 and the autofluorescence of thylakoid membranes (Cy3 channel). (B) *Synechocystis* cells that had been nitrogen starved for 5 days and expressed Ssl2501-eGFP (GFP channel) were stained with Nile red (Cy3 channel) to visualize PHB. The yellow color in the overlay indicates a colocalization between Ssl2501-GFP and the Nile red-stained PHB granule. (C) Western blot detection of Ssl2501-eGFP during exponential growth at OD_{750} of 0.8 and 0.4 using an anti-GFP primary antibody. (D) Western blot detection of Ssl2501-eGFP in nitrogen-starved cells using an anti-GFP primary antibody. Cell fracturing and separation in soluble and insoluble fractions were performed as described in Materials and Methods for the PHB synthase assay.

mM. Ten micrograms of protein was used to separate cross-linked proteins on Tricine-PAGE (36).

PHB synthase activity assay. PHB synthase assays were performed as previously described by Valentin et al. (38), with some modifications. Briefly, 30 ml cells was harvested by centrifugation at 4,000 × *g* and suspended in lysis buffer (25 mM Tris-HCl [pH 7.4], 50 mM KCl, 5 mM $MgCl_2$, 0,5 mM EDTA, and 1 mM benzamidine). Cells were lysed using FastPrep-24 (MP Biomedical) using 0.1-mm glass beads, and cell debris was removed by centrifugation for 5 s up to 10,000 × *g*. The resulting cell lysate was separated into a soluble and insoluble fraction by centrifugation at 25,000 × *g* for 30 min at 4°C. The insoluble material was suspended in lysis buffer, and protein concentrations in the fractions were determined as described by Bradford (39). PHB-biosynthetic activity was monitored by recording the change in absorbance at 412 nm for at last 30 min in the reaction buffer (25 mM Tris-HCl [pH 7.4], 1 mM DTNB [5,5′-dithiobis(2-nitrobenzoic acid)], 20 mM $MgCl_2$, and 100 μM hydroxybutyryl-CoA [Sigma-Aldrich]) after addition of 5 μg protein of the suspended insoluble fraction. The reaction temperature was held constant at 30°C.

PHB quantification. Intracellular PHB content was measured in principle as described previously (10). Cells were harvested at the dedicated time points by centrifugation (10 min, 4,000 × *g*, 25°C), washed once with distilled water, and dried for 3 h at 60°C. Dried pellets were boiled for 1 h in 1 ml concentrated H_2SO_4 diluted with 1 ml 0.014 M H_2SO_4. Cell debris was removed by centrifugation (10 min at 10,000 × *g*), and the supernatant was diluted 10-fold in 0.014 M H_2SO_4. Processed samples were analyzed by high-performance liquid chromatography (HPLC) using a Nucleosil 100 C_{18} column (125 by 3 mm) and 20 mM phosphate buffer (pH 2.5) as the liquid phase. Crotonic acid was detected at 210 nm, and commercially available PHB processed in parallel was used as a standard.

RESULTS AND DISCUSSION

Ssl2501-eGFP localizes to PHB granules. As previous studies identified the Ssl2501 protein at thylakoid membranes and PHB granules, Ssl2501 was translationally fused to eGFP and the recombinant gene was cloned into the *Synechocystis* shuttle vector pVZ322 in order to study the intracellular localization of this protein in more detail. The resulting plasmid, pVZ322-2501gfp, thus encodes a translational fusion of Ssl2501 with eGFP at its C terminus, which is transcriptionally controlled by the native *ssl2501* promoter. By using triparental mating (34), the plasmid was transferred in *Synechocystis* to study the intracellular localization of Ssl2501. To determine a potential localization of Ssl2501-GFP to thylakoid membranes, cells were grown under photoautotrophic growth conditions in BG11 medium to an OD_{750} of 0.8 and were then analyzed by fluorescence microscopy (Fig. 1A). After deconvolution of Z-stacked images, no apparent colocalization between thylakoid membranes and Ssl2501-eGFP could be observed. The eGFP signal was distributed in the cytoplasmic space, whereas the fluorescence of thylakoid membranes localized near the cell periphery. To study a possible colocalization with PHB granules, exponentially growing cells were transferred into BG11 medium lacking a nitrogen source ($BG11_0$). The nitrogen-free medium induces chlorosis in *Synechocystis*, leading to the degradation of the photosynthetic apparatus and concomitant accumulation of PHB (9). Cells were nitrogen starved for 5 days before a portion was stained with Nile red to visualize the PHB granules

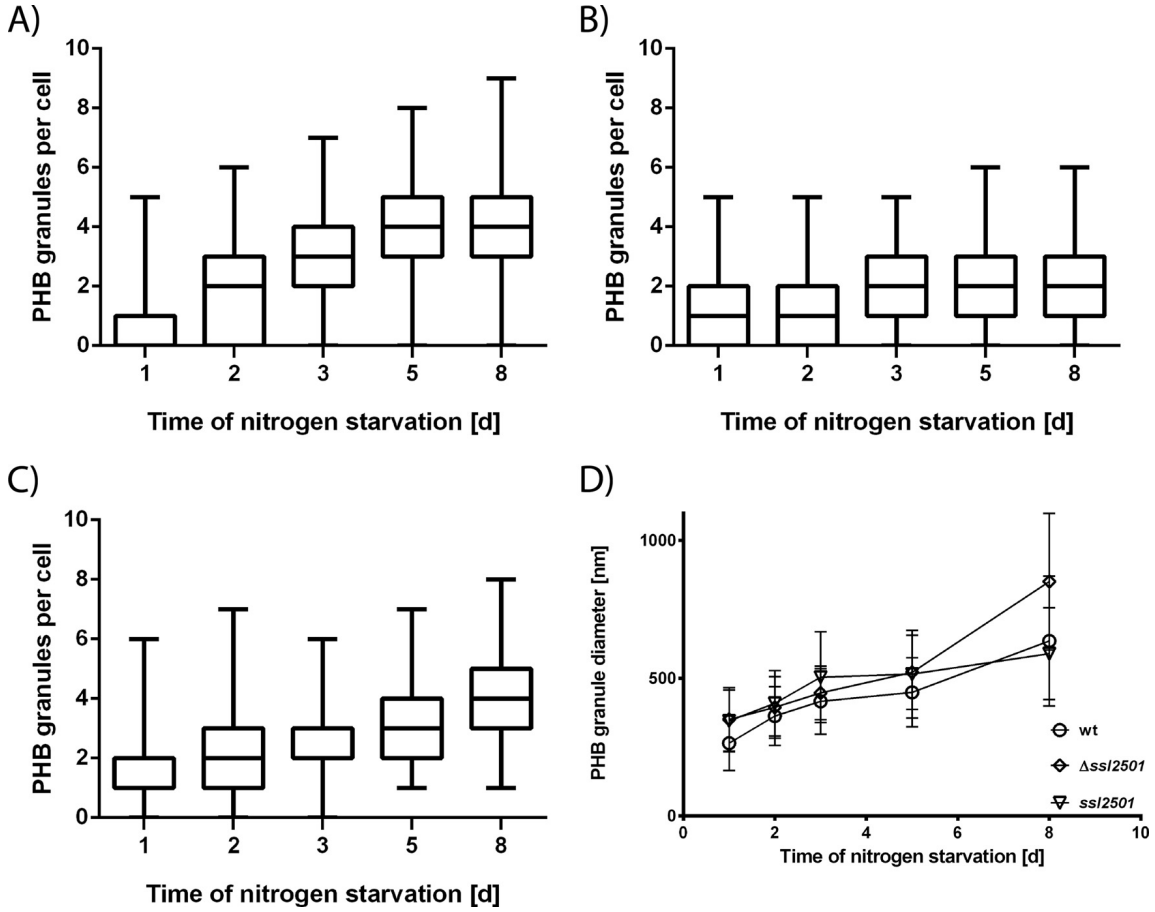

FIG 2 (A to C) Number of PHB granules per cell during nitrogen starvation in the wild type (A), the *ssl2501* mutant (B), and the *ssl2501* mutant complemented with plasmid pVZ322-2501 (C). Measurements represent the distribution of PHB granules in at least 150 cells at a given point. (D) Mean PHB granule diameter during nitrogen starvation in the wild type (open circles), the *ssl2501* mutant (diamonds), and the *ssl2501* mutant complemented with plasmid pVZ322-2501(inverted triangles). Difference in PHB granule diameters is statistically significant from day 6 on ($P < 0.0001$). Each data point represents the mean of at least 170 individual measurements of the PHB granule diameter.

by fluorescence microscopy (Fig. 1B). Under these conditions, the GFP channel showed that Ssl2501-eGFP aggregated in clusters. Pictures from the Cy3 channel visualize Nile red-stained PHB granules. Superimposition of images taken in the GFP channel, the Cy3 channel, and the bright field (to localize the entire cell shape) shows colocalization by yellow color in the overlay. As shown in Fig. 1B, Nile red-stained PHB granules colocalize with Ssl2501-GFP. These data supported the idea that Ssl2501 is a PHB granule-associated protein, as is the case for phasins. To determine whether Ssl2501-GFP remains granule associated in cell lysates, immunoblot analysis was performed with eGFP-specific antibodies. Extracts were prepared from exponentially growing and from nitrogen-starved cells, and the cell lysate was fractionated into soluble and insoluble fractions as described in Materials and Methods. Since PHB synthase activity is located in the insoluble fraction (29), the putative phasin Ssl2501-eGFP should localize in this fraction under conditions of PHB granule formation (nitrogen starvation). In exponentially growing cells devoid of PHB granules, Ssl2501-GFP was primarily localized in the soluble fraction (Fig. 1C), and only traces could be detected in the insoluble fraction, whereas under nitrogen-limiting conditions, the putative phasin was present only in the insoluble fraction, and only trace amounts of Ssl2501-GFP could be detected in the soluble fraction (Fig. 1D). This supports the microscopic data showing that during exponential growth, Ssl2501 is soluble in the cytoplasm, but once PHB permissive conditions appear, the protein is sequestered to PHB granules, rendering it insoluble.

Deletion of *ssl2501* alters PHB granule number and diameter. As one function of phasins is thought to be the regulation of PHB granule surface-to-volume ratio and the number of PHB granules within the cell (40), a genomic deletion of *ssl2501* could affect the size and amount of PHB granules within a cell. To assess this question, we constructed an *ssl2501* mutant in which the *ssl2501* open reading frame is replaced with a kanamycin resistance cassette. The complete segregation of the mutant was confirmed by PCR, as shown in Fig. S1 in the supplemental material. Wild-type *Synechocystis* and the *ssl2501* mutant were grown to an OD_{750} of 0.6 and transferred to nitrogen-depleted medium to induce PHB accumulation. In the course of nitrogen starvation, PHB granules were stained with Nile red, and the number of granules per cell was determined using fluorescence microscopy. Figure 2A and B show the distribution of PHB granules within a cell population at given time points during nitrogen starvation in the wild type and the *ssl2501* mutant, respectively. After 24 h of nitrogen starvation, up to five PHB granules could be seen in a wild-type cell, whereas 75% of the cells had no more than two granules.

With progression of nitrogen starvation, the number of PHB granules per cell increased and with it the number of cells which had more than two PHB granules. The median increased from one PHB granule per cell at day 1 of nitrogen starvation to four granules after 5 days of nitrogen starvation. The mutant behaved similarly in the beginning of nitrogen starvation, as it induced PHB granule formation, and the distribution of granules in the cell population was similar to that in the wild type. However, prolonged nitrogen starvation revealed a distinct mutant phenotype: The majority of cells accumulated only a few PHB granules. The median increased from one to two PHB granules per cell but not further, in contrast to the wild type. In addition, the heterogeneity in PHB granule numbers was reduced in the mutant, especially at the later time points of nitrogen starvation. Cells lacking *ssl2501* had a maximum of five PHB granules, whereas wild-type cells could have up to nine PHB granules. Representative images of the mutant and wild-type strain are shown in Fig. S2 in the supplemental material. This supported the idea that Ssl2501 is a phasin and is involved in PHB granule formation. To exclude the possibility that the observed phenotype is caused by a secondary effect and not the mutation introduced in *ssl2501*, the mutant was complemented with plasmid pVZ322-2501, which expresses native *ssl2501* controlled by the native promoter. The complemented strain was transferred in nitrogen-depleted $BG11_0$ and PHB granules were counted during nitrogen starvation (Fig. 2C). The PHB granule distribution in the complemented strain resembled the wild-type situation. The majority of cells had up to two PHB granules after 1 day of nitrogen starvation, and the number of PHB granules within a cell gradually increased throughout nitrogen starvation. This is also evident from the median, which increased gradually from one to four PHB granules per cell, as in the wild type.

Another possible function of phasins is to regulate the surface-to-volume ratio of a PHB granule. Hence, the mutant might have bigger PHB granules than the wild type. This hypothesis was tested by measuring PHB granule diameter at given time points using fluorescence microscopy (Fig. 2D). Since PHB had to be stained with Nile red, the measurement relies on fluorescence microscopy (with its own limitations) and a single measurement is only a rough estimation of one PHB granule diameter. Nevertheless, this analysis results in a quite accurate determination of average PHB granule diameter due to the relatively large size of *Synechocystis* cells and acquisition of Z-stack images with in average 25 layers. From each single cell, the different layers of the Z-stack were analyzed to find the largest diameter of an individual granule. In this way, approximately 200 PHB granules were measured (for statistical details, see Table S1 and Fig. S3 in the supplemental material). Similar to other phasin deletion mutants (19, 40), PHB granules in the *ssl2501* mutant were in fact apparently larger in diameter than those in the wild type, and the difference in granule size increased with prolonged nitrogen starvation. The mean PHB granule diameter of the wild type after 8 days of nitrogen starvation was estimated to be 640 nm (standard deviation [SD], 240 nm), whereas the mean PHB granule diameter of the mutant was 850 nm (SD, 250 nm). It should be noted that the large standard deviation reflects the natural variation of PHB granule size. The difference in granule size was statistically analyzed by a two-way unpaired *t* test, and the difference in size was statistically significant from day 6 on, with a *P* value smaller than 0.0001. This disparity disappeared upon complementation of the mutant strain with pVZ322-2501. The mean PHB granule diameter of the complemented strain was very similar to that of the wild type, and the mean PHB granule diameter after 8 days of nitrogen starvation was estimated to be 620 nm (SD, 190 nm), resembling the value obtained for the wild type. This further supports the hypothesis that *ssl2501* encodes a cyanobacterial phasin and that its product is a regulatory protein that modulates PHB granules *in vivo*. As the observed phenotypes of the *ssl2501* deletion and the *in vivo* colocalization of Ssl2501 with PHB fulfill the criteria for classical phasins (19, 40), the protein is referred to as PhaP. However, it should be noted that in most PHB-producing bacteria, typically more than one type of phasin protein is present (41). It is, therefore, possible that in *Synechocystis*, further phasin-like proteins might be present, which could influence PHB biogenesis.

PHB synthase activity but not PHB quantity is affected by *ssl2501* deletion. A recent study showed that the phasin PhaM from *R. eutropha* drastically reduces the lag time of PHB synthase *in vitro* (42). Therefore, deletion of the phasin *ssl2501* might change the biosynthetic activity or amount of PHB that accumulates in cells. Thus, both parameters were determined during nitrogen starvation, as shown in Fig. 3. PHB-biosynthetic assays were performed as described previously (29, 38), by lysing the cells and separating the raw cell extract into soluble and insoluble fractions, followed by measuring the biosynthetic activity in the insoluble fraction, where PHB granules accumulate due to their high density. PHB synthase activity increased during nitrogen starvation, with peak activity at the second day of nitrogen starvation, and then gradually decreased with prolonged nitrogen starvation, as seen in Fig. 3A. This tendency toward an activity peak at day 2 of nitrogen starvation was also seen in the *ssl2501* mutant; however, the absolute activity of PHB synthase was lower throughout nitrogen starvation than in the wild type. A typical reaction of a PHB synthase assay is shown in Fig. S4 in the supplemental material. To examine whether the reduced enzyme activity in the *ssl2501* mutant was due to decreased levels of PHB synthase, we compared the levels of one subunit of PHB synthase, PhaE, in wild-type and mutant cells by Western blotting (see Fig. S5 in the supplemental material). The levels of PhaE protein in both strains were similar, and no major differences could be observed. Therefore, the effect of decreased PHB synthase activity is not caused by altered enzyme levels but by the absence of PhaP on the PHB granule surface, which might act as a regulator of PHB synthase activity *in vivo*. The phasin GA24 of *Chromatium vinosum* was shown to alter the average polymer length synthesized by PHB synthase in *in vitro* assays, concluding that phasins alter the processivity of PHB synthase (43). The influence of phasins on PHB properties was also observed in the heterologous host *E. coli* (44). This work demonstrated that phasins regulate the PHB synthase activity *in vitro*, but the outcome of regulation depends on the individual PHB synthase. While PhaC proteins from *Ralstonia eutropha* and *Delftia acidovorans* were inhibited by the presence of phasins, PhaC from *Aeromonas caviae* was activated by the same phasins (44). The impact of phasins on PHB synthase activity highlights a possible biological function of phasin proteins: protecting the active conformation of PHB synthase and maybe other proteins, according to the recently reported chaperon activity of phasins (23). This function might be important, as PHB is synthesized during periods of imbalanced metabolism or stress, when protein stability is of great importance as protein turnover is reduced. The reduced activity of PHB synthase in the *Synechocystis ssl2501* mutant had

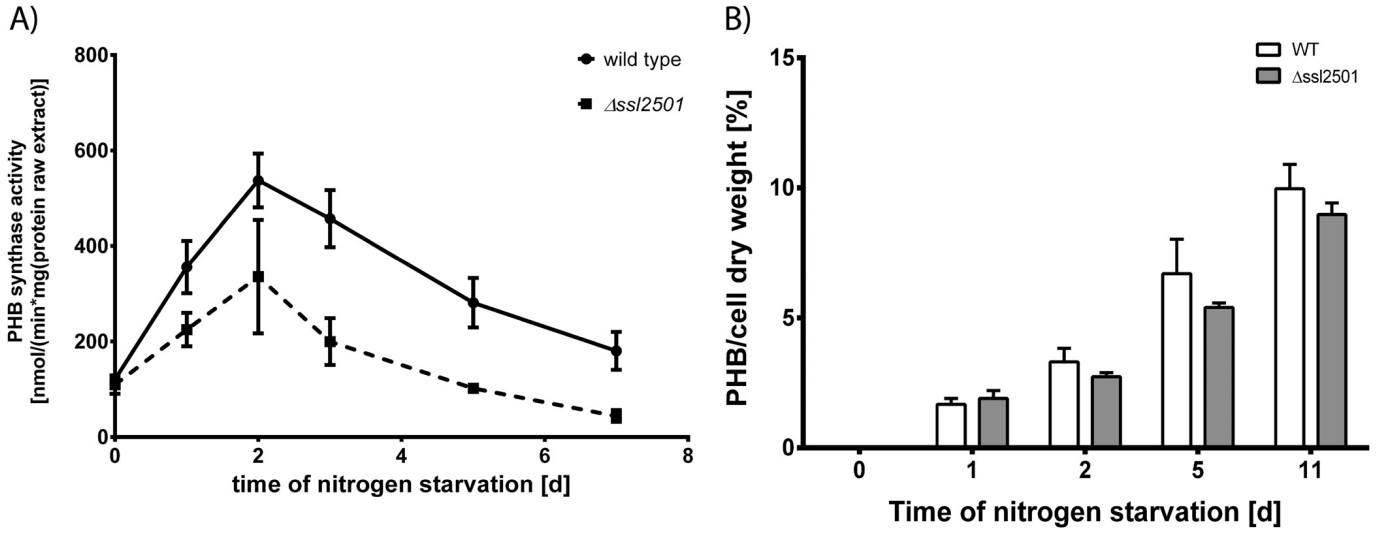

FIG 3 (A) PHB synthase activity of the wild type and mutant strain during nitrogen starvation; (B) intracellular accumulation of PHB in both strains. Measurements are means for three biological replicates. The PHB synthase activity in the *ssl2501* deletion strain is lower than in the wild type; nevertheless, the difference of accumulated PHB in both strains is minor and slightly lower in the *ssl2501*mutant.

only a minor influence on the total amount of intracellular PHB, as seen in Fig. 3B. PHB accumulated gradually during nitrogen starvation in both the wild type and the *ssl2501* mutant, with only minor differences in PHB quantity being detectable. Since PHB synthase activity in the PhaP mutant was significantly lower than that in the wild type, this result was unexpected. We conclude that in *Synechocystis*, the quantity of produced PHB is limited not by the activity of the PHB synthase but presumably by the supply of its substrate 3-hydroxybutyrate, which is provided by primary metabolism. This result sets a starting point for further metabolic engineering approaches to divert more carbon from primary metabolism toward this pathway for increased synthesis of PHB, 3-hydroxybutyrate, or 1-butanol as a precursor for fine chemicals (45–47).

Secondary-structure prediction of PhaP. Next, we tried complementation of the *ssl2501* mutant with PhaP-GFP. After induction of PHB synthesis by nitrogen starvation, PhaP-GFP associated with PHB granules and localized to the insoluble fraction. However, PhaP-GFP was not able to complement the mutant phenotype, namely, reduce granule diameter and increase PHB granule number per cell, as shown in Fig. S6 and S7 in the supplemental material. This implied that the large GFP might present a steric hindrance that affects the biological function of PhaP. To test this hypothesis, Ssl2501 was linked to Venus (a YFP variant with improved photochemical properties) (48) by a 10-amino-acid Gly-Ser flexible linker and inserted in pVZ322 yielding pVZ322-2501Venus. After transformation into the *ssl2501* mutant, association of PhaP with PHB granules as well as PHB granule size was determined microscopically (see Fig. S8 in the supplemental material). Importantly, the mutant phenotype could now be complemented, supporting the suggestion that the bulky GFP sterically impaired PhaP function, which can be overcome by a flexible linker. Whole-genome yeast two-hybrid assays suggested that PhaP interacts with itself, suggesting oligomerization (49). Oligomerization of other phasins has been described previously (24, 50–52), and these proteins can form dimers (PhaP5 from *R. eutropha*), trimers (PhaP1 from *R. eutropha*), tetramers ($PhaP_{Az}$ from *Azotobacter* sp. strain FA8 and PhaF from *Pseudomonas putida* KT2440), or dodecamers (PhaM from *R. eutropha*). Even though the purpose of oligomerization is not understood, it seems to be a conserved feature among phasin proteins and might stabilize the interaction between the proteins and the PHB surface. In order to identify possible structural features responsible for PHB association and self oligomerization, the secondary structure of PhaP was predicted using the PSIPRED server (53, 54). According to this prediction, the protein folds into two α-helices (see Fig. S9 in the supplemental material) and contains no coiled-coil regions as seen in other phasins (24, 51). The first helix starts at Thr_3 and ends at Glu_{26}, and the second α-helix starts at Asp_{39} and is predicted to end at Gln_{83}. Both helices are connected by an unstructured linker. In order to identify possible amphipathic regions responsible for binding to the PHB granule surface, a helix wheel projection was applied to both α-helices. Only the first α-helix is predicted to have amphipathic character (see Fig. S10 in the supplemental material), and six amino acids (Phe_5, Phe_6, Tyr_9, Leu_{13}, Trp_{16}, and Phe_{20}) make up the highly hydrophobic interface of the helix. The second α-helix does not have a distinct hydrophobic region but possesses a highly charged interface, which might be involved in oligomerization or protein-protein interactions (see Fig. S10 in the supplemental material).

Helix 1 and helix 2 of PhaP localize to PHB granules *in vivo*. To test whether α-helix 1 or 2 of PhaP is able to localize to PHB granules, both helices were translationally fused to Venus with a 10-amino-acid flexible linker, and the plasmids were transformed into the *ssl2501* mutant and wild-type backgrounds. PHB synthesis was induced by nitrogen starvation, and after 3 days, PHB granules in the cells were analyzed by fluorescence microscopy (Fig. 4A and B). The first α-helix is able to bind to PHB granules independently of the genetic background, as indicated by the orange color in the overlay of the Cy3 channel (Nile red) and the YFP channel (Venus). This is also shown in Fig. 4C and D, where an intensity profile of the Cy3 channel and YFP channel of a single PHB granule is plotted. The peak intensities of both channels overlap at the same position, meaning that the first α-helix of PhaP is able to localize to the PHB granule. However, not every

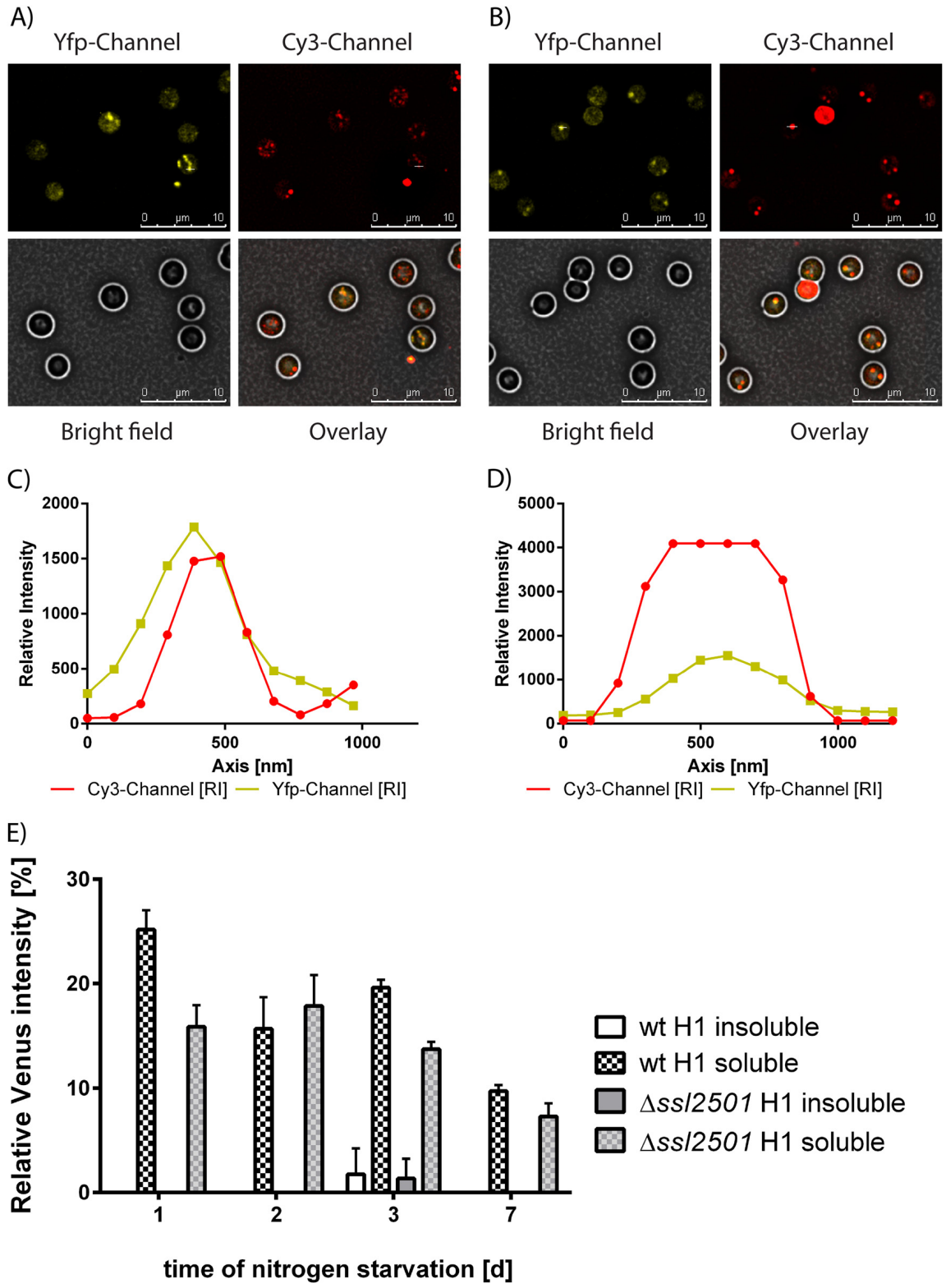

FIG 4 (A and B) Localization of PhaP helix 1-Venus in the wild type (A) and *ssl2501* mutant (B). (C and D) Signal intensities in the YFP and Cy3 channels of PhaP helix 1-Venus in the wild type (C) and *ssl2501* mutant (D). PhaP helix 1-Venus localization was quantified by Western blotting against GFP in the wild type and *ssl2501* mutant (E).

PHB granule stained by Nile red has a corresponding signal in the YFP channel. Furthermore, the signal in the YFP channel appears blurred, suggesting a lower affinity of helix 1 for PHB than for the full-length phasin. To independently confirm this observation, extracts were prepared from nitrogen-starved PHB-producing wild-type cells expressing full-length PhaP-Venus and from wild-type and *ssl2501* mutant cells carrying helix 1-Venus. The presence of Venus in soluble and insoluble fractions was determined by Western blotting. Band intensities were determined densitometrically and normalized to the Venus intensity in the insoluble fraction of the wild-type strain expressing PhaP-Venus after 1 day of nitrogen starvation (Fig. 4E). Surprisingly, we were not able to detect helix 1-Venus in the insoluble fraction (independent of the genotype) as we would have expected based on microscopic images. Helix 1-Venus was predominantly found in the soluble fraction with decreasing signal intensities as nitrogen starvation proceeded, suggesting that the affinity of the first α-helix for PHB is very low. The same types of experiments were then performed with the wild type and the *ssl2501* mutant expressing helix 2-Venus (Fig. 5A and B). The second α-helix of PhaP is able to bind to PHB granules, as can be seen by the orange color of the PHB granules in the overlay image. The association of the helix to PHB is independent of the genetic background, as confirmed by intensity plots of the Cy3 and YFP channel (Fig. 5C and D). The intensities simultaneously rise and fall, thereby confirming PHB granule localization of helix 2. As we have seen with helix 1, localization *in vivo* does not necessarily correlate with localization *in vitro*. Hence the localization of helix 2-Venus was tested by Western blotting as described above. The α-helix was found to localize in the soluble and insoluble fraction in the wild type, whereas it localized primarily in the insoluble fraction in the *ssl2501* mutant. This suggests that helix 2 competes with native PhaP for occupation of the PHB surface. PHB association of helix 2 seems stable, as it resists cell lysis. Taken together, these data indicate that helix 2 has a higher affinity for PHB than helix 1. Furthermore, the amount of helix 2-Venus in the wild-type background seemed to be higher than in the *ssl2501* mutant, suggesting that the presence of full-length PhaP protects helix 2 from degradation, in agreement with the suggested chaperon function of phasins (see above). Taken together, these observations demonstrate that the information to associate with PHB granules is present in both the first and second α-helix of PhaP, as both peptides associate with PHB granules *in vivo*, but helix 2 seems to be the primary anchor for PHB association.

Oligomerization of PhaP and helix 2 of PhaP. The localization experiments disproved the assumption that the first α-helix would be responsible for PHB binding and the second α-helix for oligomerization. Therefore, we next addressed the question of PhaP oligomerization by *in vitro* studies using recombinant proteins with an N-terminal Strep-tag II for purification. The full-length phasin and helix 2 of PhaP could be successfully purified to electrophoretic homogeneity, whereas helix 1 seemed to be unstable in *E. coli*. To confirm the structural prediction of PhaP, CD spectra of PhaP and helix 2 were taken. As shown in Fig. S11 in the supplemental material, the spectra of both proteins revealed characteristic minima at 208 and 222 nm, typical of α-helices. To test whether PhaP is able to interact with itself, as has been proposed (49), the protein was cross-linked using glutaraldehyde and analyzed using Tricine-SDS-PAGE (Fig. 6A). Four distinct bands were visible at the apparent molecular weights of a monomer, a dimer, a trimer and a tetramer, having calculated masses of 12 kDa, 24 kDa, 34 kDa, and 48 kDa, respectively. This result implies that PhaP forms a tetramer in solution. The same experiment was performed with helix 2 with a monomer size of 8.7 kDa. Surprisingly, six distinct bands with all intermediate oligomeric states were visible, suggesting the formation of a hexamer. As the *in silico* results suggested that helix 2 mediates PhaP oligomerization, we mixed equal amounts of both proteins and cross-linked them with glutaraldehyde. Following electrophoretic separation, mixed hetero-oligomers could be detected. Monomers and dimers of both proteins could be clearly identified as well as the trimeric form of helix 2; in addition, a third band with an apparent molecular mass of 32 kDa was visible, which could correspond to either the trimer of PhaP or a tetramer of the second α-helix, as these are indistinguishable on the gel. A top band was also present which was spread roughly between 44 and 54 kDa and could consist of several hetero-oligomers. Oligomerization was also investigated using size exclusion chromatography, allowing us to observe the interaction in a more dynamic mode (Fig. 6B). PhaP eluted as a single peak with an elution volume of 1.62 ml, corresponding to a molecular mass of approximately 44 kDa. As the calculated mass of a PhaP monomer is 12.3 kDa, a 44-kDa complex fits best with a tetramer, in agreement with the cross-linking experiments. The second α-helix eluted at 1.56 ml, corresponding to a size of approximately 58 kDa. As the monomer of α-helix 2 has a theoretical molecular mass of 8.7 kDa, this corresponds to a hexa- or heptamer forming a complex. In a 1:1 mixture of both proteins, the mixture eluted as a single peak at 1.60 ml, corresponding to a molecular mass of 48 kDa. In contrast to the single proteins, the elution peak of the protein mixture was slightly broader, suggesting that it consists of several mixed oligomers. If oligomerization of PhaP specifically occurred via α-helix 2, we would have expected constant tetramer formation also for isolated helix 2 and for the mixture. However, the preferential formation of hetero-oligomeric forms indicates that this corresponds to the most favorable thermodynamic state of complex formation. The fact that in the absence of helix 1 oligomers of different stoichiometry are formed indicates that helix 1 is involved in oligomerization of PhaP. This highlights the fact that the mode of oligomerization of PhaP is different than that described for other phasins, such as PhaF and $PhaP_{Az}$, which are thought to oligomerize through coiled-coil regions (24, 51). As PhaP requires both α-helices for correct oligomerization, the tertiary structure most likely resembles a doughnut formed by the eight α-helices. For thermodynamic reasons, partially hydrophobic surfaces are often involved in the formation of tertiary structures, aiding oligomerization (55, 56). As a consequence several modes of interaction of tetrameric PhaP with the PHB granule are conceivable. The exposed coiled region connecting the aligned helices might bind to the PHB granule surface; alternatively, the tertiary structure of PhaP could open its conformation to expose its hydrophobic residues for interaction with the PHB surface, or the hydrophobic core of the PhaP tetramer could accommodate a surface-exposed PHB strand.

Conclusion. This work demonstrates that the ORF *ssl2501* of *Synechocystis* encodes a cyanobacterial phasin, PhaP. PhaP attaches to the PHB granule surface and regulates the number and size of PHB granules within a cell. In addition, PhaP acts as a regulator affecting the biosynthetic activity of PHB synthase *in vivo*. It is predicted to fold into two α-helices, which contribute to the binding of the phasin to PHB. The second α-helix retains the

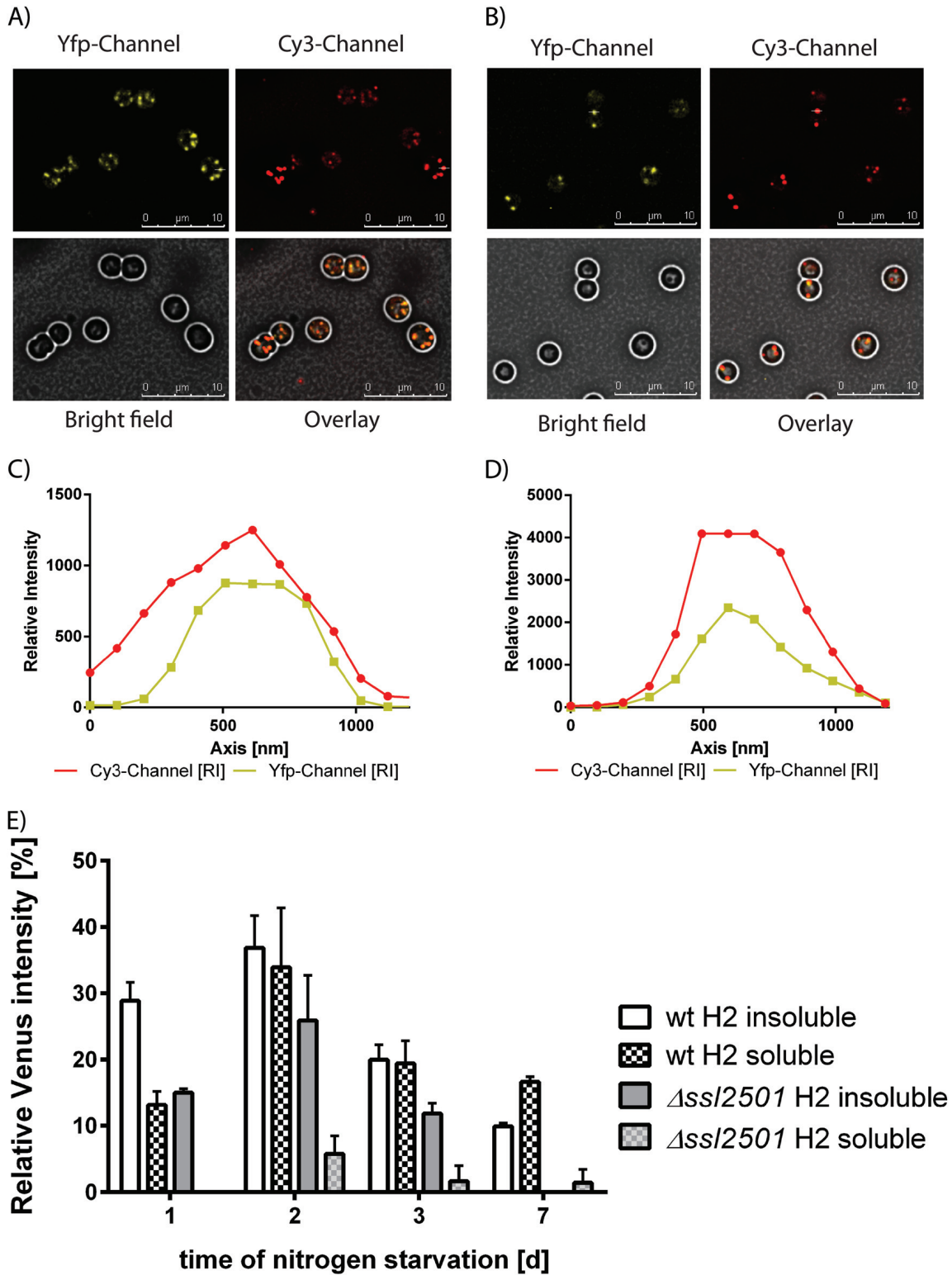

FIG 5 (A and B) Localization of PhaP helix 2-Venus in the wild type (A) and *ssl2501* mutant (B). (C and D) Signal intensities in the YFP and Cy3 channels of PhaP helix 2-Venus in the wild type (C) and *ssl2501* mutant (D). PhaP helix 2-Venus localization was quantified by Western blotting against GFP in the wild type and *ssl2501* mutant (E).

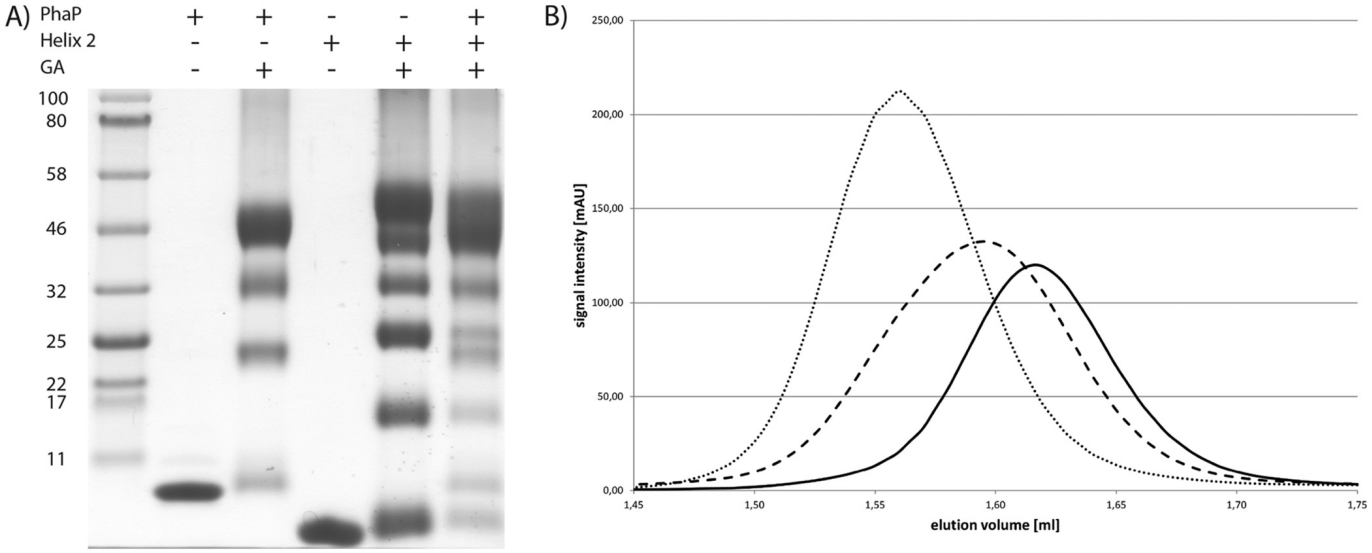

FIG 6 (A) Tricine-PAGE of PhaP, helix 2 of PhaP, and a mixture of both proteins cross-linked by glutaraldehyde. (B) Size exclusion chromatography of PhaP (solid line), helix 2 of PhaP (dotted line), and a mixture of both proteins (dashed line). PhaP elutes at 1.62 ml (44 kDa), helix 2 of PhaP at 1.56 ml (58 kDa), and the mixture at 1.6 ml (48 kDa).

ability to oligomerize but is not solely responsible for oligomerization.

ACKNOWLEDGMENTS

This work was supported by the DFG-funded GRK 1708 "Molecular principles of bacterial survival strategies."

We thank Marcus Hartmann and Albrecht Reinhard for help with CD spectroscopy and Johanna Weirich and Jan Lennings for technical assistance.

REFERENCES

1. **Stanier RY, Cohen-Bazire G.** 1977. Phototrophic prokaryotes: the cyanobacteria. Annu Rev Microbiol **31:**225–274. http://dx.doi.org/10.1146/annurev.mi.31.100177.001301.
2. **Knoop H, Gründel M, Zilliges Y, Lehmann R, Hoffmann S, Lockau W, Steuer R.** 2013. Flux balance analysis of cyanobacterial metabolism: the metabolic network of *Synechocystis* sp. PCC 6803. PLoS Comput Biol **9:**e1003081. http://dx.doi.org/10.1371/journal.pcbi.1003081.
3. **Osanai T, Oikawa A, Shirai T, Kuwahara A, Iijima H, Tanaka K, Ikeuchi M, Kondo A, Saito K, Hirai MY.** 2013. Capillary electrophoresis-mass spectrometry reveals the distribution of carbon metabolites during nitrogen starvation in *Synechocystis* sp. PCC 6803. Environ Microbiol **16:**512–524. http://dx.doi.org/10.1111/1462-2920.12170.
4. **Hauf W, Schlebusch M, Hüge J, Kopka J, Hagemann M, Forchhammer K.** 2013. Metabolic changes in *Synechocystis* sp. PCC6803 upon nitrogen-starvation: excess NADPH sustains polyhydroxybutyrate accumulation. Metabolites **3:**101–118. http://dx.doi.org/10.3390/metabo3010101.
5. **Hasunuma T, Kikuyama F, Matsuda M, Aikawa S, Izumi Y, Kondo A.** 2013. Dynamic metabolic profiling of cyanobacterial glycogen biosynthesis under conditions of nitrate depletion. J Exp Bot **64:**2943–2954. http://dx.doi.org/10.1093/jxb/ert134.
6. **Markou G, Chatzipavlidis I, Georgakakis D.** 2012. Effects of phosphorus concentration and light intensity on the biomass composition of *Arthrospira* (*Spirulina*) *platensis*. World J Microbiol Biotechnol **28:**2661–2670. http://dx.doi.org/10.1007/s11274-012-1076-4.
7. **Schwarz R, Forchhammer K.** 2005. Acclimation of unicellular cyanobacteria to macronutrient deficiency: emergence of a complex network of cellular responses. Microbiology **151:**2503–2514. http://dx.doi.org/10.1099/mic.0.27883-0.
8. **Görl M, Sauer J, Baier T, Forchhammer K.** 1998. Nitrogen-starvation-induced chlorosis in *Synechococcus* PCC 7942: adaptation to long-term survival. Microbiology **144:**2449–2458. http://dx.doi.org/10.1099/00221287-144-9-2449.
9. **Panda B, Jain P, Sharma L, Mallick N.** 2006. Optimization of cultural and nutritional conditions for accumulation of poly-beta-hydroxybutyrate in *Synechocystis* sp. PCC 6803. Bioresour Technol **97:**1296–1301. http://dx.doi.org/10.1016/j.biortech.2005.05.013.
10. **Taroncher-Oldenburg G, Nishina K, Stephanopoulos G.** 2000. Identification and analysis of the polyhydroxyalkanoate-specific beta-ketothiolase and acetoacetyl coenzyme A reductase genes in the cyanobacterium *Synechocystis* sp. strain PCC6803. Appl Environ Microbiol **66:**4440–4448. http://dx.doi.org/10.1128/AEM.66.10.4440-4448.2000.
11. **Hein S, Tran H, Steinbüchel A.** 1998. *Synechocystis* sp. PCC6803 possesses a two-component polyhydroxyalkanoic acid synthase similar to that of anoxygenic purple sulfur bacteria. Arch Microbiol **170:**162–170.
12. **Numata K, Motoda Y, Watanabe S, Osanai T, Kigawa T.** 2015. Co-expression of two polyhydroxyalkanoate synthase subunits from Synechocystis sp. PCC 6803 by cell-free synthesis and their specific activity for polymerization of 3-hydroxybutyryl-coenzyme A. Biochemistry **54:**1401–1407. http://dx.doi.org/10.1021/bi501560b.
13. **Müh U, Sinskey AJ, Kirby DP, Lane WS, Stubbe J.** 1999. PHA synthase from Chromatium vinosum: cysteine 149 is involved in covalent catalysis. Biochemistry **38:**826–837. http://dx.doi.org/10.1021/bi9818319.
14. **Jendrossek D.** 2009. Polyhydroxyalkanoate granules are complex subcellular organelles (carbonosomes). J Bacteriol **191:**3195–3202. http://dx.doi.org/10.1128/JB.01723-08.
15. **York GM, Stubbe J, Sinskey AJ.** 2002. The *Ralstonia eutropha* PhaR protein couples synthesis of the PhaP phasin to the presence of polyhydroxybutyrate in cells and promotes polyhydroxybutyrate production. J Bacteriol **184:**59–66. http://dx.doi.org/10.1128/JB.184.1.59-66.2002.
16. **Handrick R, Reinhardt S, Jendrossek D.** 2000. Mobilization of poly(3-hydroxybutyrate) in *Ralstonia eutropha*. J Bacteriol **182:**5916–5918. http://dx.doi.org/10.1128/JB.182.20.5916-5918.2000.
17. **Pötter M, Müller H, Reinecke F, Wieczorek R, Fricke F, Bowien B, Friedrich B, Steinbüchel A.** 2004. The complex structure of polyhydroxybutyrate (PHB) granules: four orthologous and paralogous phasins occur in *Ralstonia eutropha*. Microbiology **150:**2301–2311. http://dx.doi.org/10.1099/mic.0.26970-0.
18. **Sznajder A, Pfeiffer D, Jendrossek D.** 2015. Comparative proteome analysis reveals four novel polyhydroxybutyrate (PHB) granule-associated proteins in Ralstonia eutropha H16. Appl Environ Microbiol **81:**1847–1858. http://dx.doi.org/10.1128/AEM.03791-14.
19. **Wieczorek R, Pries A, Steinbüchel A, Mayer F.** 1995. Analysis of a 24-kilodalton protein associated with the polyhydroxyalkanoic acid granules in Alcaligenes eutrophus. J Bacteriol **177:**2425–2435.
20. **Pfeiffer D, Wahl A, Jendrossek D.** 2011. Identification of a multifunctional protein, PhaM, that determines number, surface to volume ratio, subcellular localization and distribution to daughter cells of poly(3-

hydroxybutyrate), PHB, granules in *Ralstonia eutropha* H16. Mol Microbiol **82:**936–951. http://dx.doi.org/10.1111/j.1365-2958.2011.07869.x.
21. **Galán B, Dinjaski N, Maestro B, de Eugenio LI, Escapa IF, Sanz JM, García JL, Prieto MA.** 2011. Nucleoid-associated PhaF phasin drives intracellular location and segregation of polyhydroxyalkanoate granules in Pseudomonas putida KT2442. Mol Microbiol **79:**402–418. http://dx.doi.org/10.1111/j.1365-2958.2010.07450.x.
22. **de Almeida A, Catone MV, Rhodius VA, Gross CA, Pettinari MJ.** 2011. Unexpected stress-reducing effect of PhaP, a poly(3-hydroxybutyrate) granule-associated protein, in Escherichia coli. Appl Environ Microbiol **77:**6622–6629. http://dx.doi.org/10.1128/AEM.05469-11.
23. **Mezzina MP, Wetzler DE, de Almeida A, Dinjaski N, Prieto MA, Pettinari MJ.** 8 October 2014. A phasin with extra talents: a polyhydroxyalkanoate granule-associated protein has chaperone activity. Environ Microbiol. http://dx.doi.org/10.1111/1462-2920.12636.
24. **Mezzina MP, Wetzler DE, Catone MV, Bucci H, Di Paola M, Pettinari MJ.** 2014. A phasin with many faces: structural insights on PhaP from *Azotobacter* sp. FA8. PLoS One **9:**e103012. http://dx.doi.org/10.1371/journal.pone.0103012.
25. **Srivastava R, Pisareva T, Norling B.** 2005. Proteomic studies of the thylakoid membrane of *Synechocystis* sp. PCC 6803. Proteomics **5:**4905–4916. http://dx.doi.org/10.1002/pmic.200500111.
26. **Wang Y, Sun J, Chitnis PR.** 2000. Proteomic study of the peripheral proteins from thylakoid membranes of the cyanobacterium *Synechocystis* sp. PCC 6803. Electrophoresis **21:**1746–1754.
27. **Pfeiffer D, Jendrossek D.** 2012. Localization of poly(3-hydroxybutyrate) (PHB) granule-associated proteins during PHB granule formation and identification of two new phasins, PhaP6 and PhaP7, in Ralstonia eutropha H16. J Bacteriol **194:**5909–5921. http://dx.doi.org/10.1128/JB.00779-12.
28. **Rippka R, Deruelles J, Waterbury JB, Herdman M, Stanier RY.** 1979. Generic assignments, strain histories and properties of pure cultures of cyanobacteria. J Gen Microbiol **111:**1–61. http://dx.doi.org/10.1099/00221287-111-1-1.
29. **Schlebusch M, Forchhammer K.** 2010. Requirement of the nitrogen starvation-induced protein Sll0783 for polyhydroxybutyrate accumulation in *Synechocystis* sp. strain PCC 6803. Appl Environ Microbiol **76:**6101–6107. http://dx.doi.org/10.1128/AEM.00484-10.
30. **Wach A.** 1996. PCR-synthesis of marker cassettes with long flanking homology regions for gene disruptions in *S. cerevisiae*. Yeast **12:**259–265. http://dx.doi.org/10.1002/(SICI)1097-0061(19960315)12:3<259::AID-YEA901>3.0.CO;2-C.
31. **Muro-Pastor AM, Olmedo-Verd E, Flores E.** 2006. All4312, an NtcA-regulated two-component response regulator in *Anabaena* sp strain PCC 7120. FEMS Microbiol Lett **256:**171–177. http://dx.doi.org/10.1111/j.1574-6968.2006.00136.x.
32. **Grigorieva G, Shestakov S.** 1982. Transformation in the cyanobacterium *Synechocystis* sp. 6803. FEMS Microbiol Lett **13:**367–370. http://dx.doi.org/10.1111/j.1574-6968.1982.tb08289.x.
33. **Gibson DG, Young L, Chuang RY, Venter JC, Hutchison CA, III, Smith HO.** 2009. Enzymatic assembly of DNA molecules up to several hundred kilobases. Nature Methods **6:**343–345. http://dx.doi.org/10.1038/nmeth.1318.
34. **Wolk CP, Vonshak A, Kehoe P, Elhai J.** 1984. Construction of shuttle vectors capable of conjugative transfer from *Escherichia coli* to nitrogen-fixing filamentous cyanobacteria. Proc Natl Acad Sci U S A **81:**1561–1565. http://dx.doi.org/10.1073/pnas.81.5.1561.
35. **Sambrook J, Russell DW.** 2001. Molecular cloning: a laboratory manual. Cold Spring Harbor Laboratory Press, Cold Spring Harbor, NY.
36. **Schagger H.** 2006. Tricine-SDS-PAGE. Nat Protoc **1:**16–22. http://dx.doi.org/10.1038/nprot.2006.4.
37. **Towbin H, Staehelin T, Gordon J.** 1979. Electrophoretic transfer of proteins from polyacrylamide gels to nitrocellulose sheets: procedure and some applications. Proc Natl Acad Sci U S A **76:**4350–4354. http://dx.doi.org/10.1073/pnas.76.9.4350.
38. **Valentin HE, Lee EY, Choi CY, Steinbüchel A.** 1994. Identification of 4-hydroxyhexanoic acid as a new constituent of biosynthetic polyhydroxyalcanoic acids from bacteria. Appl Microbiol Biotechnol **40:**710–716. http://dx.doi.org/10.1007/BF00173333.
39. **Bradford MM.** 1976. Rapid and sensitive method for quantitation of microgram quantities of protein utilizing principle of protein-dye binding. Anal Biochem **72:**248–254. http://dx.doi.org/10.1016/0003-2697(76)90527-3.
40. **Pieper-Fürst U, Madkour MH, Mayer F, Steinbüchel A.** 1994. Purification and characterization of a 14-kilodalton protein that is bound to the surface of polyhydroxyalkanoic acid granules in Rhodococcus ruber. J Bacteriol **176:**4328–4337.
41. **Jendrossek D, Pfeiffer D.** 2014. New insights in the formation of polyhydroxyalkanoate granules (carbonosomes) and novel functions of poly(3-hydroxybutyrate). Environ Microbiol **16:**2357–2373. http://dx.doi.org/10.1111/1462-2920.12356.
42. **Pfeiffer D, Jendrossek D.** 2014. PhaM is the physiological activator of PHB synthase (PhaC1) in *Ralstonia eutropha*. Appl Environ Microbiol **80:**555–563. http://dx.doi.org/10.1128/AEM.02935-13.
43. **Jossek R, Reichelt R, Steinbüchel A.** 1998. In vitro biosynthesis of poly(3-hydroxybutyric acid) by using purified poly(hydroxyalkanoic acid) synthase of *Chromatium vinosum*. Appl Microbiol Biotechnol **49:**258–266. http://dx.doi.org/10.1007/s002530051166.
44. **Ushimaru K, Motoda Y, Numata K, Tsuge T.** 2014. Phasin proteins activate *Aeromonas caviae* polyhydroxyalkanoate (PHA) synthase but not *Ralstonia eutropha* PHA synthase. Appl Environ Microbiol **80:**2867–2873. http://dx.doi.org/10.1128/AEM.04179-13.
45. **Wang B, Pugh S, Nielsen DR, Zhang W, Meldrum DR.** 2013. Engineering cyanobacteria for photosynthetic production of 3-hydroxybutyrate directly from CO2. Metab Eng **16:**68–77. http://dx.doi.org/10.1016/j.ymben.2013.01.001.
46. **Lan EI, Liao JC.** 2012. ATP drives direct photosynthetic production of 1-butanol in cyanobacteria. Proc Natl Acad Sci U S A **109:**6018–6023. http://dx.doi.org/10.1073/pnas.1200074109.
47. **Osanai T, Numata K, Oikawa A, Kuwahara A, Iijima H, Doi Y, Tanaka K, Saito K, Hirai MY.** 2013. Increased bioplastic production with an RNA polymerase sigma factor SigE during nitrogen starvation in *Synechocystis* sp. PCC 6803. DNA Res **20:**525–535. http://dx.doi.org/10.1093/dnares/dst028.
48. **Nagai T, Ibata K, Park ES, Kubota M, Mikoshiba K, Miyawaki A.** 2002. A variant of yellow fluorescent protein with fast and efficient maturation for cell-biological applications. Nat Biotechnol **20:**87–90. http://dx.doi.org/10.1038/nbt0102-87.
49. **Sato S, Shimoda Y, Muraki A, Kohara M, Nakamura Y, Tabata S.** 2007. A large-scale protein protein interaction analysis in *Synechocystis* sp. PCC6803 DNA Res **14:**207–216. http://dx.doi.org/10.1093/dnares/dsm021.
50. **Pfeiffer D, Jendrossek D.** 2013. Development of a transferable bimolecular fluorescence complementation system for the investigation of interactions between poly(3-hydroxybutyrate) granule-associated proteins in Gram-negative bacteria. Appl Environ Microbiol **79:**2989–2999. http://dx.doi.org/10.1128/AEM.03965-12.
51. **Maestro B, Galan B, Alfonso C, Rivas G, Prieto MA, Sanz JM.** 2013. A new family of intrinsically disordered proteins: structural characterization of the major phasin PhaF from Pseudomonas putida KT2440. PLoS One **8:**e56904. http://dx.doi.org/10.1371/journal.pone.0056904.
52. **Neumann L, Spinozzi F, Sinibaldi R, Rustichelli F, Potter M, Steinbüchel A.** 2008. Binding of the major phasin, PhaP1, from Ralstonia eutropha H16 to poly(3-hydroxybutyrate) granules. J Bacteriol **190:**2911–2919. http://dx.doi.org/10.1128/JB.01486-07.
53. **Buchan DW, Minneci F, Nugent TC, Bryson K, Jones DT.** 2013. Scalable web services for the PSIPRED protein analysis workbench. Nucleic Acids Res **41:**W349–W357. http://dx.doi.org/10.1093/nar/gkt381.
54. **Jones DT.** 1999. Protein secondary structure prediction based on position-specific scoring matrices. J Mol Biol **292:**195–202. http://dx.doi.org/10.1006/jmbi.1999.3091.
55. **Tsai C-J, Lin SL, Wolfson HJ, Nussinov R.** 1997. Studies of protein-protein interfaces: a statistical analysis of the hydrophobic effect. Protein Sci **6:**53–64.
56. **Ali MH, Imperiali B.** 2005. Protein oligomerization: how and why. Bioorg Med Chem **13:**5013–5020. http://dx.doi.org/10.1016/j.bmc.2005.05.037.
57. **Studier FW, Moffatt BA.** 1986. Use of bacteriophage T7 RNA polymerase to direct selective high-level expression of cloned genes. J Mol Biol **189:**113–130. http://dx.doi.org/10.1016/0022-2836(86)90385-2.

5.2 Supplementary information

Tab.S 1: Statistical analysis of the PHB granule diameter with a two tailed t-test. A F-test reveals that variance between wild type and mutant are similar strengthening the validity of the statistical analysis.

	wt 8 vs KO 8	wt 6 vs KO 6
P value	< 0.0001	< 0.0001
P value summary	****	****
Significantly different? ($P < 0.05$)	Yes	Yes
One- or two-tailed P value?	Two-tailed	Two-tailed
t, df	t=9.129 df=398	t=10.85 df=390
How big is the difference?		
Mean ± SEM	864.7 ± 20.28 N=170	825.4 ± 16.58 N=183
Mean ± SEM	635.2 ± 15.57 N=230	588.3 ± 14.40 N=209
Difference between means	-229.5 ± 25.14	-237.1 ± 21.85
95 % confidence interval	-278.9 to -180.1	-280.1 to -194.2
R square	0,1732	0,2319
F test to compare variances		
F,DFn, Dfd	1.254, 169, 229	1.161, 182, 208
P value	0.1123	0,2960
P value summary	ns	ns
Significantly different? ($P < 0.05$)	No	No

1. **Wiedemann C, Bellstedt P, Görlach M. 2013.** CAPITO–a web server-based analysis and plotting tool for circular dichroism data. Bioinformatics 14:1750-1757.

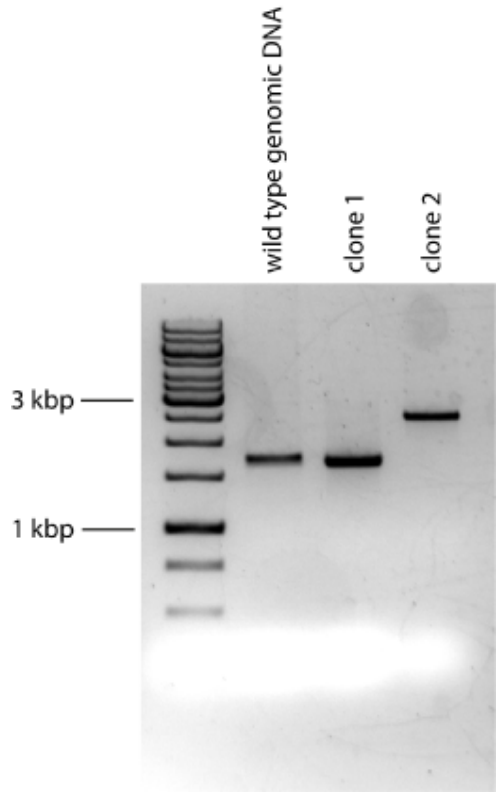

Fig.S 1: Screen for the replacement of all genomic copies of *ssl2501* by PCR with isolated genomic DNA as template. The wild type genetic background produces a PCR fragment with roughly 1.7 kbp in size whereas the mutant genetic background produces a PCR fragment with 2.5 kbp length.

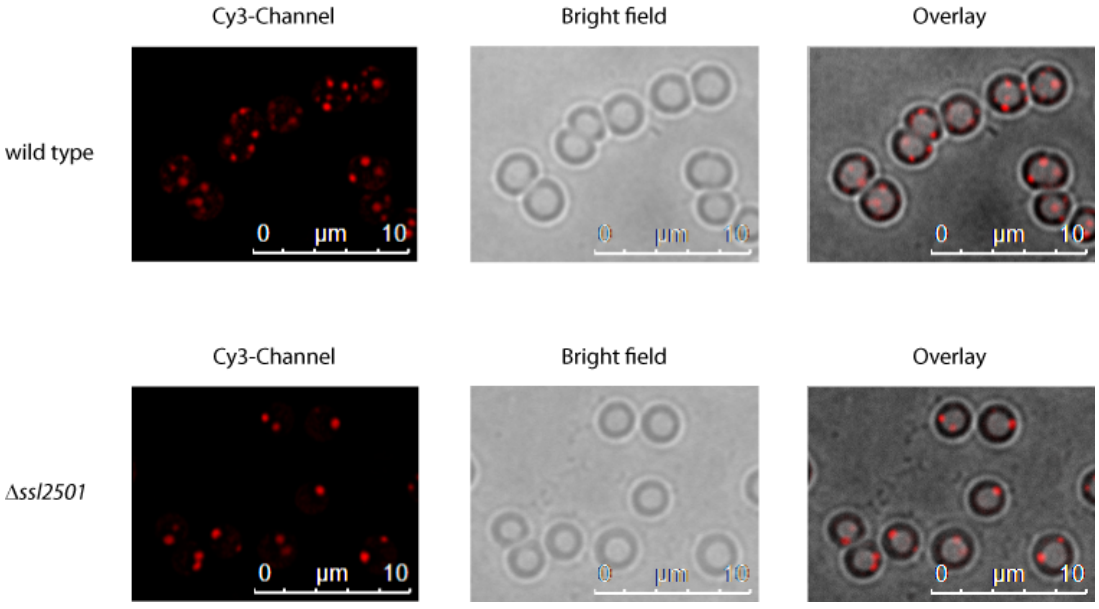

Fig.S 2: Microscopic observation of the wild type and Δ*ssl2501* strain after 7d of nitrogen starvation. PHB was stained with Nile Red and fluorescence of Nile Red incorporated into PHB was monitored in the Cy3 channel. The wild type has several medium size PHB granules whereas the *ssl2501* mutant has only up to three large PHB granules.

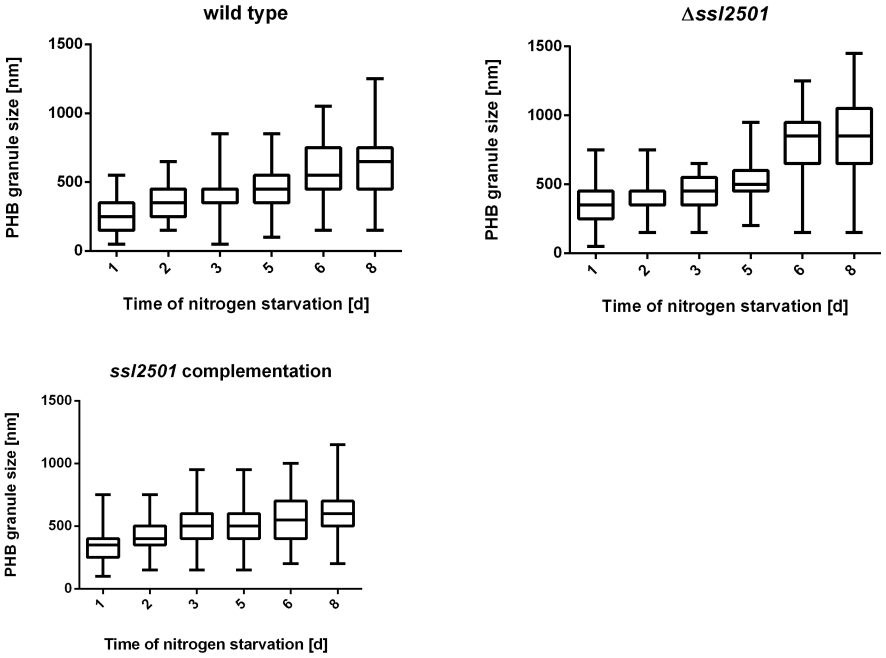

Fig.S 3: Distribution of PHB granules size during nitrogen starvation. PHB granules in the Δ*ssl2501* mutant are larger in diameter when compared to the wild type. The difference is significant after 6 days of nitrogen starvation with a p value smaller than 0.0001.

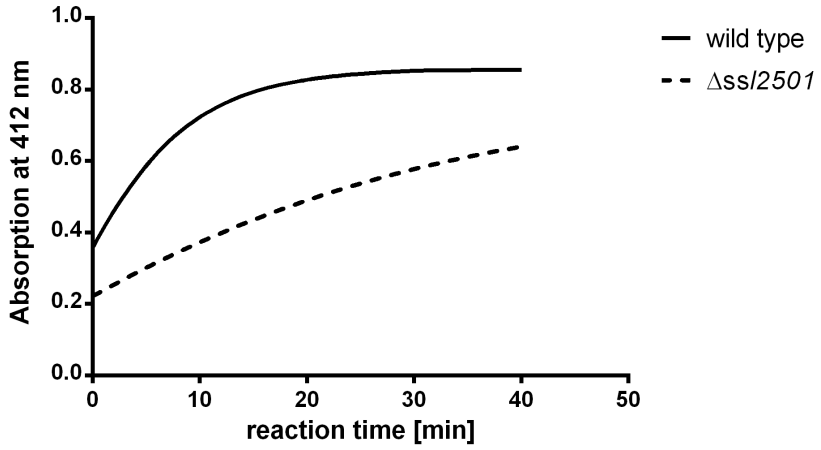

Fig.S 4: Typical photometric recording of a PHB-synthase assay of the wild type and the *ssl2501* mutant.

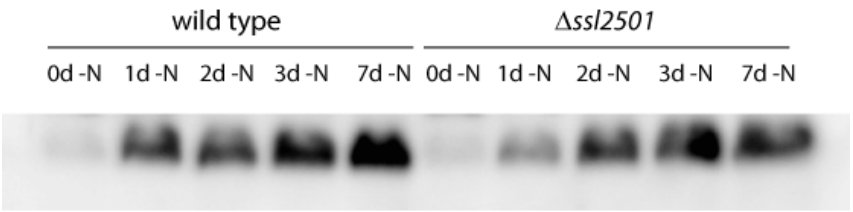

Fig.S 5: Western blot detection of PhaE in wild type and *ssl2501* mutant insoluble fraction, blotted on PVDF membrane after SDS-PAGE.

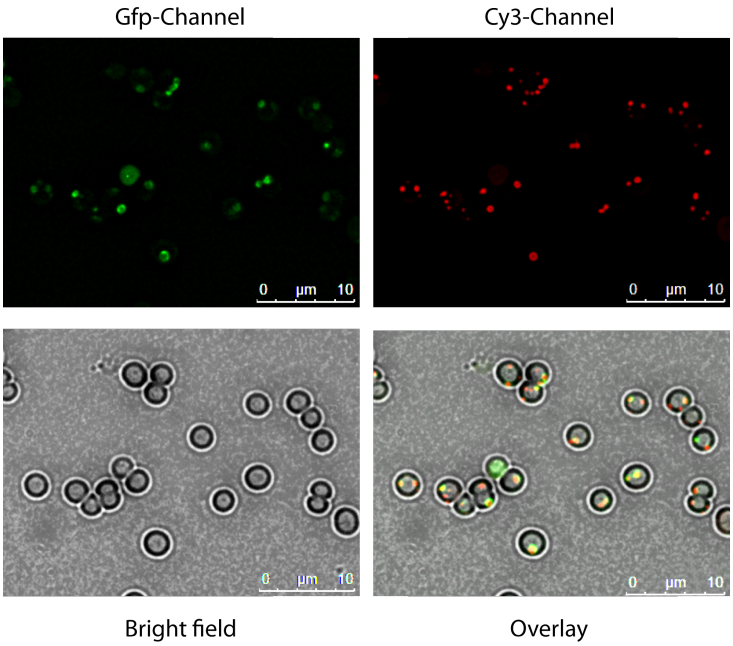

Fig.S 6: Complementation of the *ssl2501* mutant with Ssl2501-Gfp after six days of nitrogen starvation.

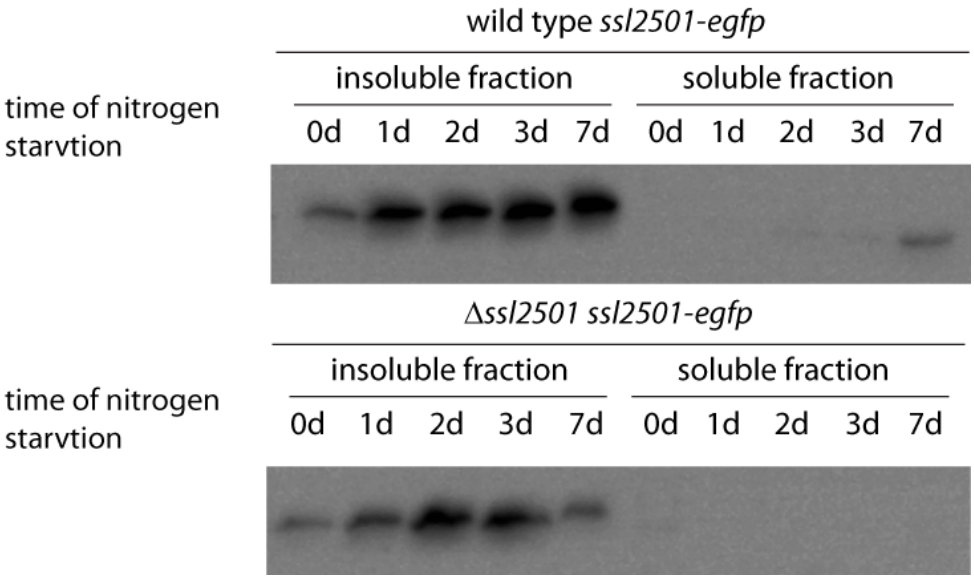

Fig.S 7: Western blot against Gfp of soluble and insoluble fractions of *Synechocystis* wild type and *ssl2501* cell extracts during nitrogen starvation.

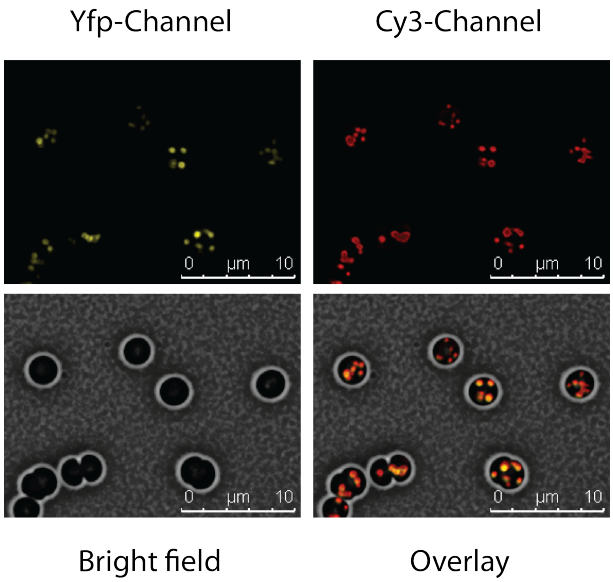

Fig.S 8: Microscopic investigation of the *ssl2501* mutant complemented with plasmid pVZ322-2501Venus. PhaP-Venus localizes to the PHB granules, which have the same size as in the wild type.

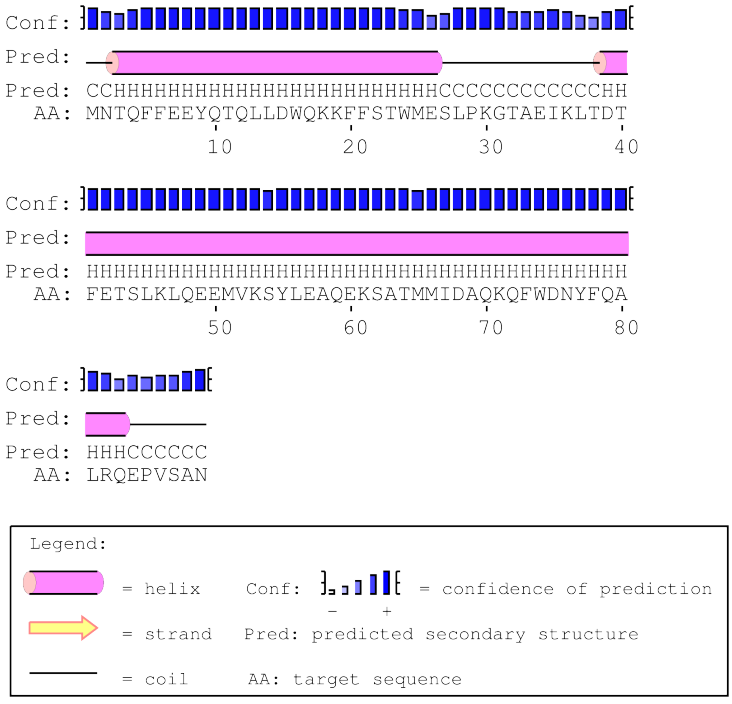

Fig.S 9: Secondary structure prediction of the phasin PhaP (Ssl2501) with PSIPRED. Based on the prediction PhaP fold in two a-helices. The first helix is 24 amino acids long. The second helix is 44 amino acids long. Both helices are connected by a 12 amino acid long unstructured region.

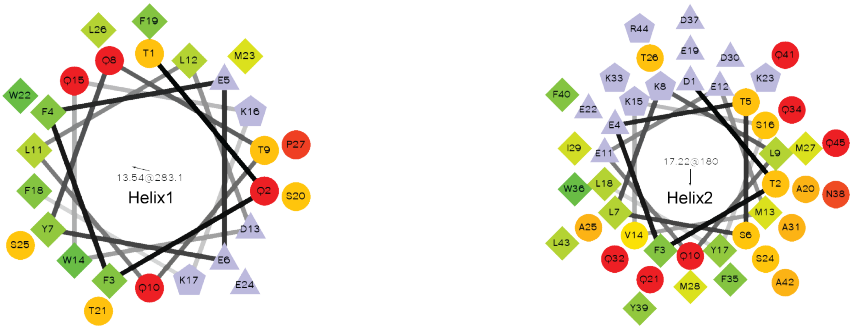

Fig.S 10: The derived helix wheel projections of both α-helices. The first α-helix has a highly hydrophobic side, which is formed by residues F3, F4, Y7, L11, W14, F18 of the helix. This helix might be responsible for the interaction with the hydrophobic PHB granule surface. No clear hydrophobic region is evident from the projection of the second α-helix, however a highly charged region is present. The charged region is made up of four posiively charged amino acids (K8, K15, K33 and R44) and five negatively charged residues (D1, E12, E19, D30 and D37) of this helix, which might aid in protein protein interactions and self oligomerization. Helix wheel projections were performed using a script provided by http://rzlab.ucr.edu/. Hydrophilic residues are shown as circles, hydrophobic residues as diamonds, potentially negatively charged as triangles, and potentially positively charged as pentagons. Hydrophobicity is color coded as well: the most hydrophobic residue is green, and the amount of green is decreasing proportionally to the hydrophobicity, with zero hydrophobicity coded as yellow. Hydrophilic residues are coded red with pure red being the most hydrophilic (uncharged) residue, and the amount of red decreasing proportionally to the hydrophilicity. The potentially charged residues are light blue.

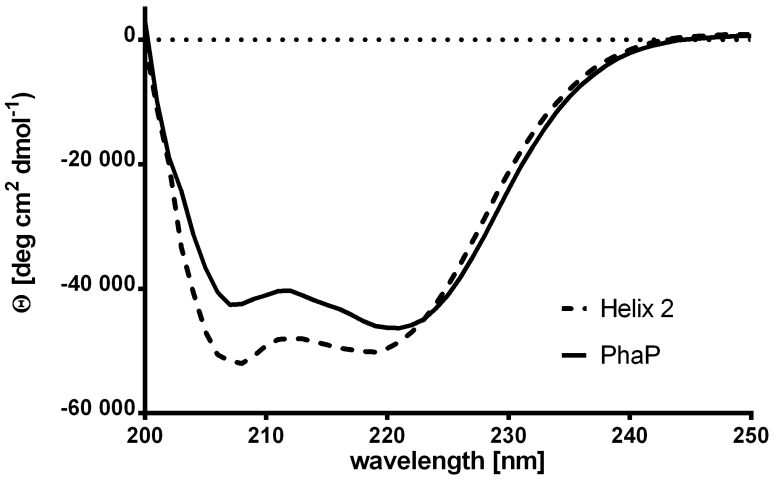

Fig.S 11: Circular dichroism spectra of recombinant PhaP and Helix2 of PhaP. Both proteins show predominantly α-helical features with characteristic minima around 208 and 222 nm. CD-Spectra were determined using a Jasco J-810 Spectropolarimeter. CD spectra were processed using the CAPITO webtool (5).

6 Publication 3

Contributions of the candidate for the publication.
LactC2 constructs with Venus-, sfGfp- and mTurq2-Lact were created by me and I have analyzed the heterologus PHB production in *Escherichia coli*. I was involved in writing the manuscript.

6.1 Polyhydroxyalkanoate (PHA) Granules Have no Phospholipids

SCIENTIFIC REPORTS

OPEN

Polyhydroxyalkanoate (PHA) Granules Have no Phospholipids

Stephanie Bresan[1,*], Anna Sznajder[1,*], Waldemar Hauf[2,*], Karl Forchhammer[2], Daniel Pfeiffer[3] & Dieter Jendrossek[1]

Received: 16 March 2016
Accepted: 05 May 2016
Published: 25 May 2016

Polyhydroxybutyrate (PHB) granules, also designated as carbonosomes, are supra-molecular complexes in prokaryotes consisting of a PHB polymer core and a surface layer of structural and functional proteins. The presence of suspected phospholipids in the surface layer is based on *in vitro* data of isolated PHB granules and is often shown in cartoons of the PHB granule structure in reviews on PHB metabolism. However, the *in vivo* presence of a phospholipid layer has never been demonstrated. We addressed this topic by the expression of fusion proteins of DsRed2EC and other fluorescent proteins with the phospholipid-binding domain (LactC2) of lactadherin in three model organisms. The fusion proteins specifically localized at the cell membrane of *Ralstonia eutropha* but did not co-localize with PHB granules. The same result was obtained for *Pseudomonas putida*, a species that accumulates another type of polyhydroxyalkanoate (PHA) granules related to PHB. Notably, DsRed2EC-LactC2 expressed in *Magnetospirillum gryphiswaldense* was detected at the position of membrane-enclosed magnetosome chains and at the cytoplasmic membrane but not at PHB granules. In conclusion, the carbonosomes of representatives of α-*proteobacteria*, β-*proteobacteria* and γ-*proteobacteria* have no phospholipids *in vivo* and we postulate that the PHB/PHA granule surface layers in natural producers generally are free of phospholipids and consist of proteins only.

Polyhydroxybutyrate (PHB) and related polyhydroxyalkanoates (PHAs) are important storage compounds of carbon and energy in *Eubacteria* and *Archaea*. PHB and PHAs are accumulated when cells are living in an environment with a surplus of a suitable carbon source and/or when growth and cell division are impaired due to a limitation by a nutrient other than the carbon source. Research of the last decades in many laboratories has led to a detailed understanding of the biochemical pathways leading to the formation of PHB or PHA granules[1–8]. A large number of proteins/genes has been described that are necessary for and are involved in the formation of such storage PHB/PHA inclusion bodies. Detailed descriptions of key enzymes such as PHA synthases, PHA depolymerases and phasins (structural PHA granule associated proteins) are given in numerous publications[9–18]. Although only three genes are essential to provide the information for the biochemical pathway from the central metabolite acetyl-CoA to the PHB polymer, much more genes with putative functions in PHB metabolism have been identified in *Ralstonia eutropha* H16 (alternative designation *Cupriavidus necator* H16), the model organism of PHB research. The products of these genes comprise the key enzymes of polymerisation (PHB synthases)[19–21], depolymerisation (PHB depolymerases)[22–26], polymer surface displayed proteins, so-called phasins[27–33], and other proteins that are necessary for the regulation and the subcellular localization of the granules[34–36]. Most of these proteins are specifically localized on the surface of PHB granules as was shown by immuno-gold-labelling and transmission electron microscopy[27,35,37] or by fluorescence microscopy using fusions of green fluorescent protein variants and the target proteins[26,32,33,38–41]. The finding of so many proteins on the PHB granule surface with different functions has led to the classification of PHB granules as multifunctional units and the designation as carbonosomes[42] has been proposed for these organelle-like structures[43–45]. A similar variety of surface-displayed proteins was detected in PHA granules of the model organism of PHA accumulating species, *P. putida*[17,46–50] and in other well-studied PHA accumulating species; for a selection see[51–54].

However, the exact molecular composition of the PHB/PHA granule surface layer is still not known. While it is generally accepted that several proteins are part of the PHB/PHA granule surface layer *in vivo*, the presence or absence of phospholipids on the PHB/PHA granule surface is controversially discussed[4,5,8,50,55–57]. The basis for the assumption that phospholipids are present in the surface layer of PHB granules is the identification of

[1]Institute of Microbiology, University Stuttgart, Germany. [2]Department of Organismic Interactions, Eberhard Karls Universität Tübingen, Germany. [3]Lehrstuhl für Mikrobiologie, Universität Bayreuth, Germany. *These authors contributed equally to this work. Correspondence and requests for materials should be addressed to D.J. (email: dieter.jendrossek@imb.uni-stuttgart.de)

phosphatidic acid and at least one other lipid-like (acetone extractable) compound in purified PHB granules of *Bacillus megaterium* almost 50 years ago[55] and the detection of phosphatidyl-ethanolamine, phosphatidyl-glycerol, diphosphatidyl-glycerol and a fourth not-identified compound (possibly phosphatidyl-serine) in isolated native PHB granules of *R. eutropha* (at that time designated as *Alcaligenes eutrophus*)[58]. However, it is possible that phospholipids bind artificially to the hydrophobic polymer after disrupture of the cells during the PHB granule isolation process. As a consequence, the identification of phospholipids in isolated PHB granules is not a proof for the *in vivo* presence of phospholipids in the PHB surface layer. Electron microscopy could be a suitable tool to image the surface layer of PHB granules. Indeed, electron micrographs of thin sections of PHB accumulating bacteria were frequently published in the past but the resolution of those images in most cases was of insufficient quality. One example of high technical quality in electron microscopy is the publication of Boatman in 1964 who investigated the inclusions of *Rhodospirillum rubrum* and showed that PHB granules were covered by a surface layer of 4 nm thickness[59]. This value corresponded to approximately half of the size of a cytoplasmic membrane and would be indicative for a (phospholipid) monolayer. If the PHB surface layer was composed of phospholipids, a single unit membrane (half of a double layer) with the polar groups facing to the cytoplasm and the hydrophobic tails pointing to the hydrophobic PHB polymer core would make sense. Similar determinations of the thickness of the PHB granule surface layer were made for *R. eutropha (A. eutrophus)* and other PHA accumulating bacteria by co-workers of Frank Mayer's lab: they determined a value of about 2.9 to 3.8 nm[60] and concluded that PHB granules in *R. eutropha* most likely are covered by a monolayer. However, the nature of the monolayer, proteins, phospholipids or a mixture of both, could not be resolved.

Recently, high resolution images of PHB accumulating *R. eutropha* cells were published but the nature of the PHB granule surface layer could not be determined[61]. Evidence for a discontinuous surface layer was provided that would not be in agreement with a continuous phospholipid layer. In another PHB accumulating species, *Caryophanon latum*, a relatively thick PHB granule boundary layer of 14 nm was detected in electron micrographs of thin sections. Globular shaped molecules were present in negatively stained samples of PHB granules liberated from *C. latum* and suggested that the surface layer could consist of proteins only[62]. In summary, none of the above-mentioned contributions was able to prove or disprove the *in vivo* presence of phospholipids in the surface layer of PHB granules.

In this study, we addressed this question by the expression of a set of fusion proteins of fluorescent proteins and the LactC2-domain of lactadherin in *R. eutropha*. Lactadherin is a protein of milk fat that specifically binds to phospholipids *in vivo* via its C2 domain[63,64]. Fluorescence microscopical analyses of the cells expressing the fusion proteins revealed that only the cytoplasmic membrane contained phospholipids but not the PHA granules of three model organisms. This finding excluded the presence of phospholipids in PHB/PHA granules *in vivo.*

Results

Construction of fluorescent fusion proteins and expression in *E. coli*. Fusions of the fluorescent protein DsRed2EC (or related fluorescent proteins as indicated in Table 1) with the phospholipid-binding domain of bovine lactadherin (LactC2) were constructed and ligated under control of the constitutively expressed promoter of the *R. eutropha phaCAB* operon into the broad host range plasmid pCM62. The expression of fluorescent proteins in *E. coli* (no producer of PHB granules) alone generally resulted in uniform fluorescence and confirmed that the proteins were soluble in the cytoplasm (Fig. 1A). In contrast to this, the cytoplasmic membrane and occasionally the cell periphery near the cell poles were fluorescent when the DsRed2EC-LactC2 fusion was expressed in *E. coli* and only a minor fluorescence signal was detected in the cytoplasm (Fig. 1B). Similar results (localization at the cell membrane) were obtained when fusions of super-folder GFP (sfGFP)[65] or mTurquoise2[66] were fused to the LactC2 domain and expressed in *E. coli* (Fig. 1C,D). These results showed that the LactC2 fusion protein was functionally expressed and specifically bound to phospholipid molecules of the cytoplasmic membrane in *E. coli*.

Expression of DsRed2EC and DsRed2EC-LactC2 in *R. eutropha*. Next, we transferred the LactC2 fusion constructs to *R. eutropha*. As shown in Fig. 2A, expression of DsRed2EC alone resulted in more or less uniform fluorescence of the cytoplasm and confirmed that DsRed2EC is a soluble protein in *R. eutropha* as in *E. coli*. *R. eutropha* accumulated PHB granules during growth on NB medium. PHB granules can be seen in the phase contrast image of Fig. 2A as dark stained globular structures. Remarkably, no fluorescence was visible in the red channel at the position of the PHB granule. This indicated that DsRed2EC alone is not able to bind to PHB granules.

When we expressed the DsRed2EC-LactC2 fusion first in a Δ*phaC* background (Fig. 2B), in which the cells cannot accumulate PHB granules because of the absence of the key enzyme of PHB biosynthesis (PHB synthase PhaC), a uniform fluorescence of the cytoplasmic membrane was achieved. We conclude that the DsRed2EC-LactC2 fusion specifically binds to the phospholipids of the cell membrane. Next, the DsRed2EC-LactC2 fusion was expressed in *R. eutropha* wild type cells (Fig. 2C). The same uniform fluorescence of the cytoplasmic membrane was observed as found for the Δ*phaC R. eutropha* mutant. However, PHB granules were present and could be detected in the corresponding phase contrast images. The PHB granules appeared as dark regions (in phase contrast) but DsRed2EC-LactC2-specific fluorescence was absent from the suspected positions of PHB granules. As an alternative to identification by phase contrast, PHB granules can be visualized by staining with Nile red but in this case, a differentiation between Nile red and DsRed2EC-LactC2 fluorescence is not possible. To provide a phase contrast-independent proof for the presence of PHB granules in the wild type, PHB granules were labelled by the expression of a fusion of the enhanced yellow fluorescent protein (eYFP) with an inactive PHB synthase (PhaC with C319A mutation) that specifically localizes at the surface of PHB granules. This construct was transferred to *R. eutropha* and expressed together with the DsRed2EC-LactC2 fusion (Fig. 2D). It has been shown previously that the inactive PHB synthase fusion (eYFP-PhaC) was specifically attached to PHB granules in *R. eutropha* without changing the PHB content of *R. eutropha*[33]. It is evident from

Strain/plasmid	Relevant characteristic	Source/reference
Escherichia coli JM109	cloning strain	
E. coli HMS174		82
E. coli S17-1	conjugation strain	83
E. coli WM3064	conjugation strain	William Metcalf
E. coli BL21(DE3)	Heterologous expression of pET Duet vector	84
Ralstonia eutropha H16	Wild type	DSMZ 428
R. eutropha H16 Δ*phaP1*	Chromosomal deletion of *phaP1*	31
R. eutropha H16 Δ(*phaP1-phaP4)*	Chromosomal deletions of *phaP1-phaP4*	31
R. eutropha H16 Δ(*phaP1-phaP5)*	Additional deletion of *phaP5* in Δ*phaP1-phaP4* background	32
Pseudomonas putida GPO1	*Pseudomonas putida* wild type strain	85
M. gryphiswaldense MSR-1 R/S	Wild type	86
M. gryphiswaldense mamC-egfp	*mamC-egfp* chromosomal fusion	67
M. gryphiswaldense Δ*mamAB*	deletion of *mamAB* operon	87
M. gryphiswaldense Δ*phbCAB*	deletion of *phbCAB* operon	67
pJM9238	expression of *phaCAB*	82
pBBR1MCS2	broad host range vector, Km^r	88
pBBR1MCS2-P_{phaC}-*eyfp-c1*	universal vector for construction of fusions C-terminal to eYFP under the P_{phaC} promoter	32
pBBR1MCS2-P_{phaC}-*eyfp*-c1-*psd*	N-terminal fusion of Psd of *R. eutropha* to eYFP	this study
pBBR1MCS-2-P_{phaC}-*DsRed2EC-c1*	universal vector for construction of fusions C-terminal to DsRed2EC under control of the P_{phaC} promoter of *R. eutropha*	this study
pCM62	broad host range vector, Tc^r	89
pCM62-P_{phaC}-*DsRed2EC*-c1	universal vector for construction of fusions C-terminal to DsRed2EC under control of the P_{phaC} promoter of *R. eutropha*	this study
p416	source of LactC2	76
pETDuet-*phaCerulean-phaAB-venus-lactC2*	Co-expression of *phaC*-Cerulean-*phaAB* and Venus-LactC2	this study
pCM62-P_{phaC}-*DsRed2EC*-c1-*lactC2*	plasmid for expression of DsRed2EC-LactC2	this study
pCM62-P_{phaC}-*mTurquoise2*-c1-*lactC2*	plasmid for expression of *mTurquoise2*-LactC2	this study
pCM62-P_{phaC}-*sfgfp*-c1-*lactC2*	plasmid for expression of *sfGFP*-LactC2	this study
pBBR1MCS2-P_{phaC}-*eyfp*-c1-*phaC1*(C319A)	N-terminal fusion of inactive PhaC1(C319A) to eYFP	33
pBAM-P_{mamDC}-*dsRed2EC*-c1-*lactC2*	plasmid for expression of DsRed2EC-LactC2	this study
pBAM-P_{tet}-*dsRed2EC*-c1-*lactC2*	plasmid for expression of DsRed2EC-LactC2	this study

Table 1. Strains, plasmids used in this study. Resistance against kanamycin (Km^r), tetracycline (Tc^r).

the overlay images in Fig. 2D that the DsRed2EC-LactC2 fusion did not co-localize with the PhaC-eYFP-labelled PHB granules. The same results were obtained when the mTurquoise2-LactC2 or the sfGFP-LactC2 fusions were expressed in *R. eutropha* wild type in which PHB was stained with the lipophilic dye Nile red (Suppl. Fig. S1). mTurquoise2 and sfGFP have higher fluorescence intensities and shorter folding times, respectively, than DsRed2EC. These results are in line with the presence of phospholipids in the cytoplasmic membrane but contradict the presence of phospholipids on the surface of PHB granules.

Expression of DsRed2EC-LactC2 in *R. eutropha* phasin mutants. Phasin proteins, in particular PhaP1, constitute the major fraction of PHB granule associated proteins in *R. eutropha*[26]. To investigate whether the presence of phasin proteins protects the surface layer of PHB granules from interaction with the cytoplasmic membrane and from binding of phospholipids we expressed the DsRed2EC-LactC2 fusion in a Δ*phaP1* background (Fig. 3A), in a Δ*phaP1*-Δ*phaP4* background (Fig. 3B) and in a Δ*phaP1*-Δ*phaP5* (Fig. 3C) background (in case of the Δ*phaP1* strain with the additional presence of the inactive eYFP-PhaC (C319A) fusion (Fig. 3A)). Essentially, the same results as for the wild type were obtained. A DsRed2EC-LactC2-specific fluorescence could not be detected at the location of the PHB granules in any of the phasin mutant strains; only the cytoplasmic

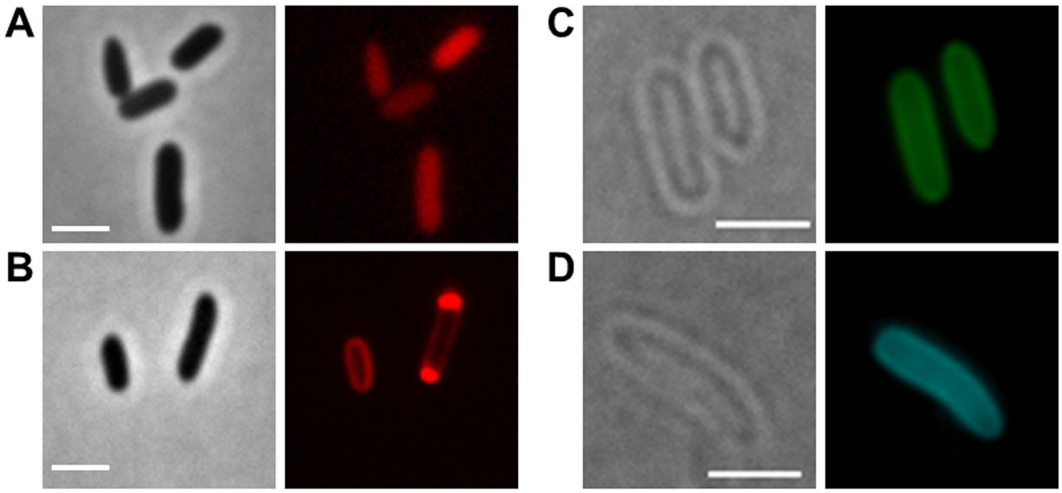

Figure 1. Expression of fluorescent proteins in *E. coli*. (**A**) expression of DsRed2EC alone (phase contrast/red channel), fluorescence visible in the cytoplasm, (**B**) Expression of DsRed2EC-LactC2 fusion (phase contrast/red channel), note, uniform fluorescence of the cell membrane and additional fluorescent foci at the cell poles in some cells, (**C**) Expression of sfGFP-LactC2 fusion (bright field/green channel), (**D**) Expression of mTurquoise2-LactC2 (bright filed/blue channel). Scale bars correspond to 2 μm. Since *E. coli* is not able to synthesize PHB no granules are visible.

membrane was fluorescent in all cases. These results show that the absence of the major phasin PhaP1 or of any of the phasin proteins PhaP1 to PhaP5 did not enable DsRed2EC-LactC2 to bind to PHB granules. Our data suggest that phospholipids-even in the absence of phasin proteins-apparently do not bind to PHB granules.

DsRed2EC-LactC2 binds to magnetosome chains but not to PHB granules in *M. gryphiswaldense*. The attachment of phospholipid-binding proteins to membranes could depend on membrane curvature. Since PHB granules are much smaller than whole cells, the curvature of a potential phospholipid membrane of PHB granules would be substantially higher and potentially could prevent binding of LactC2. Moreover, the inner side of the cell membrane has a negative curvature while a potentially existing PHB granule membrane would have a positive curvature. To exclude that binding of the LactC2 domain of lactadherin is specific for a negative membrane curvature we looked for an appropriate positive control of LactC2-binding to membranes with positive curvature. Unfortunately, most inclusions of prokaryotes, as far as known, are not enclosed by phospholipid membranes. Magnetosomes of magnetotactic bacteria, however, are an exception and it is well known that magnetosomes are membrane-surrounded prokaryotic organelles with positive membrane curvature. Notably, magnetosome membranes have a similar composition as the cytoplasmic membrane[43,45]. Binding of dsRed-LactC2 to the magnetosome chains of magnetotactic bacteria would be therefore a suited positive control to test the ability of the dsRed-LactC2 fusion to detect membrane-enclosed organelles with a positive membrane curvature. Due to the small size of magnetosomes (≈35 nm in diameter in *M. gryphiswaldense)* in comparison to PHB granules (200–400 nm in diameter) individual magnetosomes cannot be resolved by light microscopy. However, magnetosomes of most magnetotactic bacteria form chains of many magnetosomes aligned on a cytoskeleton-like filament[43]. Therefore, the detection of a filament-like fluorescence signal of DsRed2EC-LactC2 expressed in a magnetotactic species would indicate the binding of the DsRed2EC-LactC2 fusion to the membranes of magnetosomes. We expressed the DsRed2EC-LactC2 fusion in *M. gryphiswaldense* and cultivated the recombinant bacteria under conditions at which they readily form magnetosome chains. The presence of magnetic particles in the recombinant strain was verified by the use of a magnet positioned near the microscope. As shown in Fig. 4A1,A2, chain-like fluorescence signals of recombinant DsRed2EC-LactC2 were visible. These signals resembled images of *M. gryphiswaldense* cells in which the magnetosome-specific MamC protein was fused to eGFP (Fig. 4C1). A non-magnetic *M. gryphiswaldense* mutant strain, in which the 16.4 kbp *mamAB* operon was deleted, did not form any chain-like fluorescent signals when DsRed2EC-LactC2 was expressed (Suppl. Fig. S2). However, DsRed2EC-LactC2 was bound to the cell membrane of *M. gryphiswaldense* cells (for image with focus to cell membrane, see Fig. 4B1). Occasionally, fluorescent foci were detected in the region of the cell membrane or within the cells (Suppl. Fig. S2B1,B2). Since *M. gryphiswaldense* is also able to synthesize PHB and since magnetosomes-containing *M. gryphiswaldense* cells usually harbour one to several PHB granules[67] it could be that the observed fluorescent foci of DsRed2EC-LactC2 might represent PHB granules to which the fusion protein was attached. However, by comparing the cells shown in Suppl. Fig. S2B1,B2 in bright field and in fluorescence mode it is evident that the dark globular structures (representing PHB granules) did not co-localize with the foci of DsRed2EC-LactC2 that were found in some cells. Examination of other cells with fluorescent DsRed2EC foci never resulted in a co-localization with globular structures visible in bright field. This result corroborated the inability of the DsRed2EC-LactC2 fusion to bind to PHB granules in *M. gryphiswaldense*. Our finding was further verified by the expression of DsRed2EC-LactC2 in a PHB-negative background of *M. gryphiswaldense (ΔphaCAB)* (Suppl. Fig. S3). Again, chain-like fluorescent signals corresponding to a magnetosome chain were

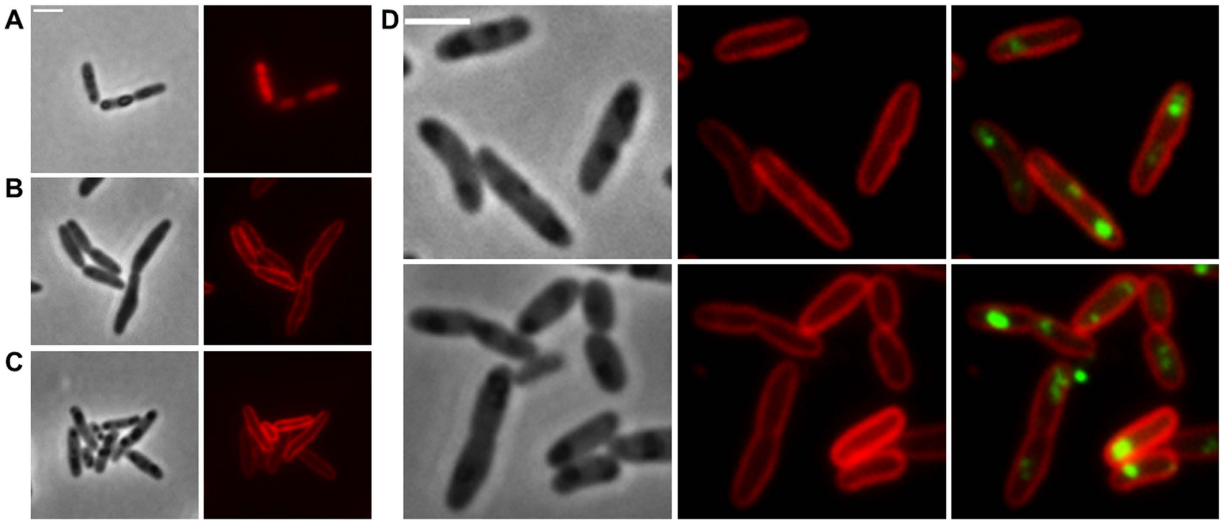

Figure 2. Expression of DsRed2EC and DsRed2EC-LactC2 in *R. eutropha* H16. Expression of DsRed2EC alone in wild type (**A**). Expression of DsRed2EC-LactC2 in Δ*phaC* mutant (**B**) and in wild type (**C**). Phase contrast (left) and red channel (right) in (**A–C**). In (**D**), DsRed2EC-LactC2 was co-expressed with eYFP-PhaC (C319A) in *R. eutropha* wild type (from left to right: phase contrast, red channel, merge of red and green channels). Scale bars correspond to 2 μm.

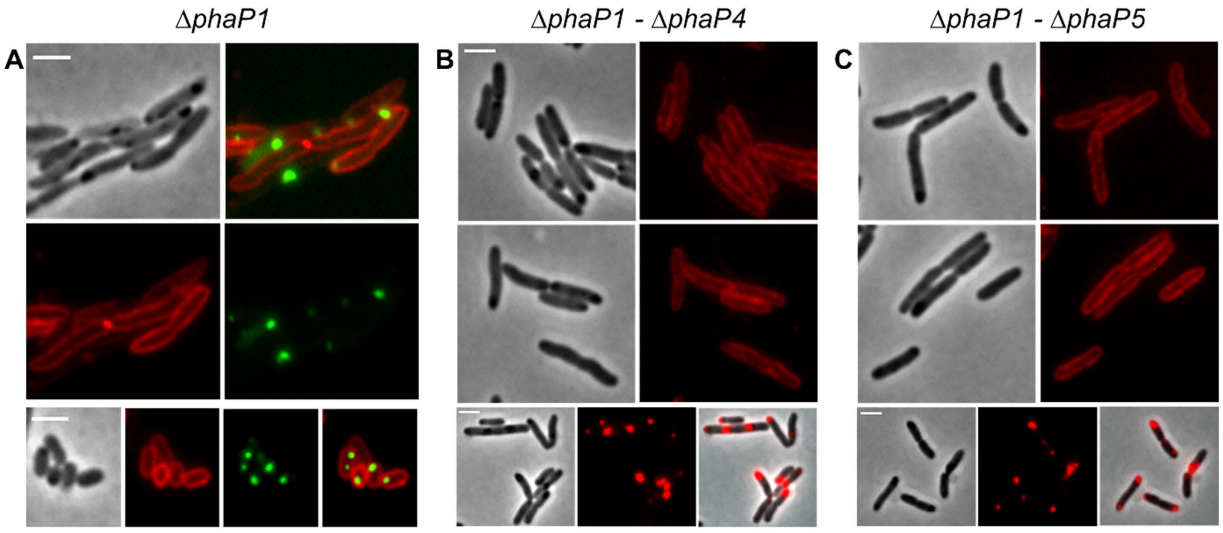

Figure 3. Expression of DsRed2EC-LactC2 in *R. eutropha* phasin mutants. Co-expression of DsRed2EC-LactC2 and eYFP-PhaC in Δ*phaP1* mutant (**A**). Expression of DsRed2EC-LactC2 in Δ*phaP1*-Δ*phaP4* mutant (**B**) and in Δ*phaP1*-Δ*phaP5* mutant (**C**). Phase contrast and fluorescent images are shown. In the bottom rows of (**B**,**C**) cells were additionally stained with Nile red to indicate the position of PHB granules more clearly than in phase contrast images (phase contrast, red channel, merge). Scale bars correspond to 2 μm.

identified in the cells (see Suppl. Fig. S3A1–A4 for cells with focus to chain-like structures). Furthermore, occasionally some cells harboured fluorescent foci (Suppl. Fig. S3B1). Since the Δ*phaCAB* mutant does not produce PHB, the occasionally formed fluorescent foci cannot represent PHB granules. In summary, our data with the *M. gryphiswaldense* strains demonstrate that the DsRed2EC-LactC2 fusion protein was specifically bound to the cell membrane and the membrane-enclosed magnetosome chains but not to the surface layer of PHB granules. These finding are in agreement with the presence of phospholipids in the cell membrane and in the magnetosome membrane but with the absence of such phospholipids in the PHB granule surface layer.

Expression of LactC2 in PHB accumulating *E. coli*. Previous fluorescence microscopical analysis of recombinant *E. coli* cells that harbour the PHB biosynthetic genes (*phaCAB*) of *R. eutropha* have shown that the first synthesized PHB granules were always located at the cell poles and in the area of the future septum (see Fig. 7 of[68]). Although the resolution of light microscopy did not allow an unambiguous detection it seemed

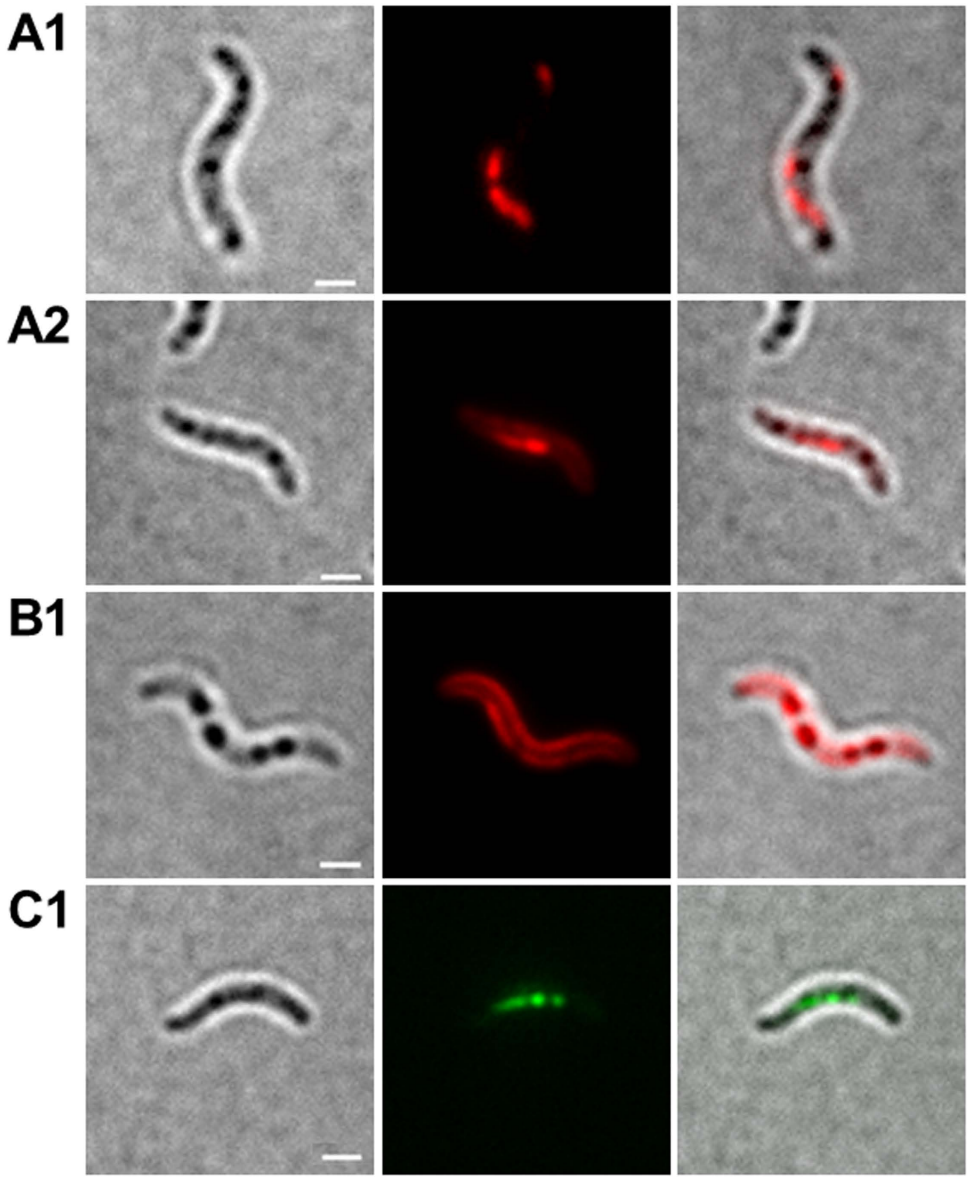

Figure 4. Expression fusion proteins in *M. gryphiswaldense*. Cells expressing DsRed2EC-LactC2 focussed to filament-like fluorescence representing magnetosome-filaments (**A1 and A2**). Cell expressing DsRed2EC-LactC2 focussed to cell membrane fluorescence (**B1**). Cell expressing MamC-GFP (**C1**). Note, presence of several globular inclusions in all images (PHB granules) that do not co-localize with DsRed2EC-LactC2 or with MamC-eGFP. Individual magnetosomes are too small (≈35 nm) to be visible in bright field. From left to right: bright field, fluorescence channel, merge. Scale bars correspond to 2 μm.

possible that the PHB granules could come into physical contact with the cytoplasmic membrane in a recombinant PHB producing organism. To test if the proximity of the PHB granules to the cytoplasmic membrane in a recombinant *E. coli* strain resulted in the uptake and presence of phospholipids in PHB granules we expressed the DsRed2EC-LactC2 fusion in recombinant PHB accumulating *E. coli* cells. As shown in Fig. 5A, partial co-localization of PHB granules (as localized by phase contrast images) and DsRed2EC-LactC2 fluorescence was indeed observed. However, not all PHB granules revealed a DsRed2EC-LactC2-specific fluorescence. To study the recombinant system in more detail, an *E. coli* strain was constructed in which LactC2 fused to the yellow fluorescent Venus protein and the PHB synthase (PhaC) fused to Cerulean (a brighter CFP variant) were co-expressed from a pETDuet-1 vector. As shown in Fig. 5B, PHB granules-identified by phase contrast and by Cerulean-PHB synthase fluorescence-were indeed preferentially located at the cell poles. Remarkably, we detected an apparent co-localization of some but again not of all PHB granules (PhaC-Cerulean) and Venus-LactC2 fluorescence. These results imply that some recombinant PHB granules in *E. coli* could be covered by lipids. This finding will be discussed below.

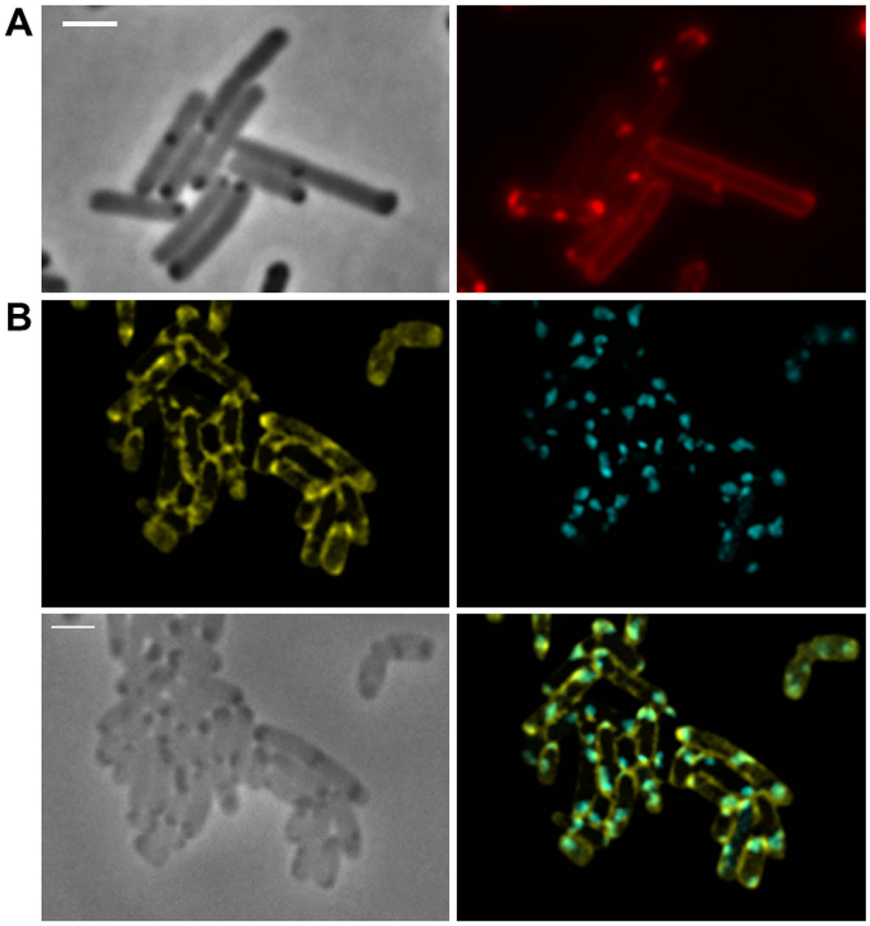

Figure 5. Expression of DsRed2EC-LactC2 and Venus-LactC2 in recombinant PHB accumulating *E. coli*. *E. coli* HMS174 cells co-expressing the *phaCAB* genes of *R. eutropha* (pJM9238) and DsRed2EC-LactC2 are shown in (**A**) phase contrast left, red channel right. Microscopic images of *E. coli* BL21(DE3) co-expressing the *phaC-Cerulean-phaAB* operon and Venus-LactC2 from the pETDuet-vector in (**B**) Venus channel middle left, Cerulean channel middle right, phase contrast bottom left, merge in bottom right. Scale bars correspond to 2 μm.

Expression of LactC2-fusions in *P. putida*. To determine whether carbonosomes of medium-chain length PHA accumulating bacteria contained phospholipids *in vivo* we transferred the constructs carrying the mTurquoise2- and the sfGFP-LactC2 fusions to *P. putida* and determined the positions of PHA granules and of the fusion proteins (Fig. 6). When the cells were cultivated under PHA permissive conditions (mineral salts medium with sodium octanoate as precursor of PHA building blocks) only the cytoplasmic membrane was fluorescent. PHA granules, that became visible in bright field or after staining with Nile red, showed no LactC2-fusion protein fluorescence. These findings confirmed that medium chain length PHA granules in *P. putida*-similar to short-chain length PHA (PHB) granules in *R. eutropha*-do not contain phospholipids *in vivo*.

Phosphatidyl-serine decarboxylase localizes at the cytoplasmic membrane and is absent from PHB granules *in vivo*. Phosphatidyl-ethanolamine is the main phospholipid in *R. eutropha* and is synthesized from phosphatidyl-serine by removal of the carboxylic acid group of the serine moiety. This decarboxylase step is catalysed by phosphatidyl-serine decarboxylase that is encoded by the *psd* (A1038) in *R. eutropha*. We constructed an eYFP-Psd fusion and expressed it in *R. eutropha*. Fluorescence microscopical analysis revealed that eYFP-Psd is associated to the cytoplasmic membrane. We assume that the decarboxylation of phosphatidyl-serine to phosphatidyl-ethanolamine is performed shortly before or after the insertion of phospholipids into the membrane. When the strain was cultivated under PHB permissive conditions only a cell membrane-localization of the eYFP-Psd protein was observed and no fluorescence was detected at the position of the PHB granules (Fig. 7). This result is in agreement with the absence of phospholipids in PHB granules.

Phospholipids bind to PHB granules *in vitro*. As shown above, in PHB accumulating *R. eutropha* cells, fluorescent proteins fused to the phospholipid-binding domain LactC2 of lactadherin were exclusively bound to the cytoplasmic membrane *in vivo*. No evidence for an *in vivo* attachment to the surface layer of PHB granules was obtained. To find an explanation for the *in vitro* detection of phospholipids in isolated PHB granules as described 50 years ago[55] we purified native PHB granules via two glycerol gradients from *R. eutropha* strains that either

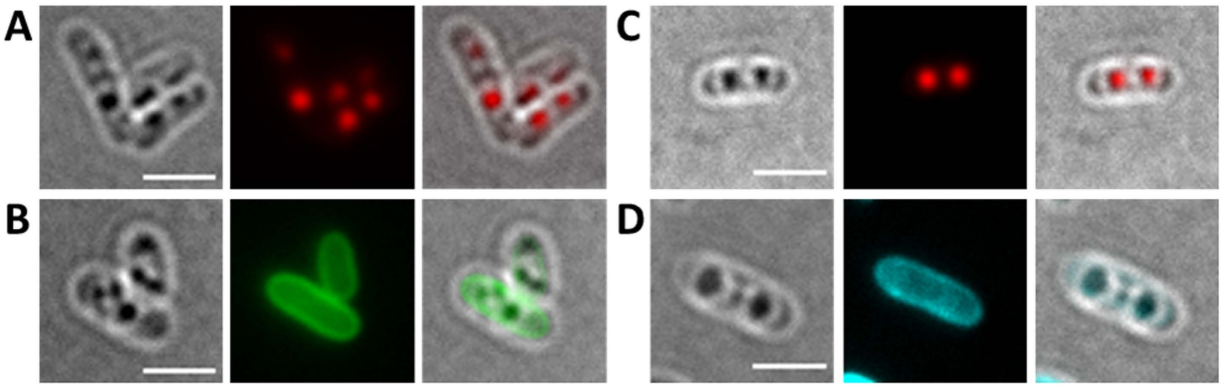

Figure 6. Expression of LactC2 fusion proteins in *P. putida*. Cells of *P. putida* expressing sfGFP-LactC2 (**A**,**B**) or mTurquoise-LactC2 (**C**,**D**) were grown in mineral salts medium with sodium octanoate to promote PHA granule formation. Cells were stained with Nile red in (**A**,**C**) to visualize PHA granules. From left to right: bright field, red (top row) or green/turquoise (bottom row) channel and overlay images. Note, formation of globular inclusions visible in bright field that are stained by Nile-red (PHA granules) but that show no sfGFP-LactC2 or mTurquoise-LactC2 fluorescence. Scale bars correspond to 2 μm.

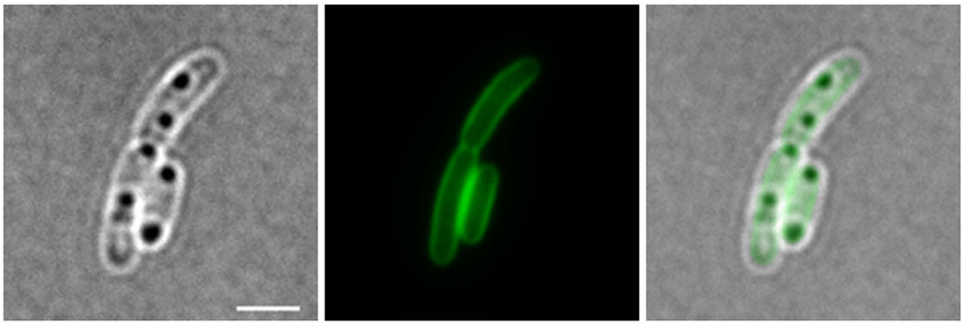

Figure 7. Expression of eYFP-Psd (phosphatidyl-serine decarboxylase) in *R. eutropha* H16. From left to right: bright field, green channel, merge). eYFP-Psd co-localizes with the cell membrane but not with globular structures (PHB granules) that are visible in bright field. Scale bar corresponds to 2 μm.

expressed DsRed2EC alone or the DsRed2EC-LactC2 fusion and examined the granules by fluorescence microscopy. The PHB granule band of both glycerol density gradients had a white to beige colour and no evidence for the presence of large amounts of DsRed2EC was obtained. When PHB granules isolated from the DsRed2EC expressing strain were examined by fluorescence microscopy, no red-fluorescent granules were detected. This result is consistent with the data of Fig. 1 and confirmed that DsRed2EC has no affinity to PHB granules either *in vivo* or *in vitro*. When PHB granules that had been isolated from the DsRed2EC-LactC2-expressing strain were examined, most PHB granules were also non-fluorescent and showed that the DsRed2EC-LactC2 fusion also has no binding affinity to PHB granules. However, occasionally we detected PHB granules (less than 1% of isolated PHB granules) that showed red fluorescence (Suppl. Fig. S4). This indicated that in some cases the DsRed2EC-LactC2 fusion apparently can bind to PHB granules. We assume that fragments of the cytoplasmic membrane were artificially bound to PHB granules in a minor fraction of PHB granules and that the DsRed2EC-LactC2 fusion was able to bind to these phospholipid-contaminated PHB granules *in vitro*. This finding can explain the detection of trace amounts of phospholipids in isolated native PHB granules half a century ago by Griebel and co-workers[55].

Discussion

A variety of phospholipid-binding proteins is known from literature (for overviews see[69,70]). Many of them depend on the presence of Ca^{2+} and/or are specific for phospholipids present in eukaryotes such as phosphatidyl-inositols and their mono- or multi-phosphorylated variants[70,71]. Blood clotting factor V and factor VIII as well as bovine lactadherin represent two Ca^{2+}-independent phospholipid-binding proteins[63,72]. These proteins specifically bind to phospholipids via C-terminal located phospholipid-binding domains (C-domains). In lactadherin, two of such binding domains are present (C1 and C2 domain). In particular, the C2-domain (LactC2) is responsible for the high binding affinity of lactadherin to phospholipids[64]. The crystal structure of lactadherin was solved and the membrane binding part has been identified[73]. In an early publication using an *in vitro* binding assay, a low specificity of lactadherin for a variety of phospholipids such as phosphatidyl-serine (PS), phosphatidyl-ethanolamine (PE), phosphatidyl-inositol (PI), phosphatidyl-glycerol (PG), phosphatidic acid and cardiolipine (CL) but not

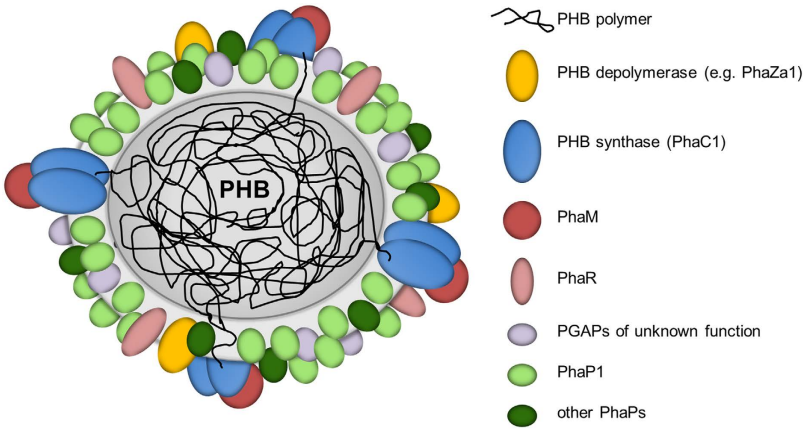

Figure 8. Model of an *in vivo* PHB granule in *R. eutropha* H16. The surface layer is free of phospholipids and consists of proteins only. The presently known PHB granule associated proteins (PGAPs) are symbolised by differentially coloured globules. All proteins in this model had been previously shown to be bound to PHB granules *in vivo* by expression of appropriate fusions with fluorescent proteins. For details and overview see references[8,26]. The dimension of the surface layer is enlarged relative to the polymer core for better visibility.

to phosphatidyl-choline (PC) was shown[63]. Later, it was suggested that the LactC2 domain apparently conferred high membrane binding ability in particular to PS-containing membranes *in vivo*[64,74]. The extent to which the LactC2 domain binds also to phospholipids other than PS *in vivo* is not exactly known. However, lactadherin binds to a phospholipid mixture with an excess of PE in comparison to the concentration of PS even if the PS content is only 0.03%. Another factor that stimulates binding of lactadherin to PS-containing phospholipids is a high degree of curvature[74] as it is present near the cell poles of rod-shaped bacteria and in small vesicles and PHB/PHA granules if such granules would contain phospholipids.

PE, PS and CL are the main components in eubacterial membranes. In *R. eutropha*, PG, PE, PS, and CL have been identified as membrane lipids[75] with PE as the major component. Since lactadherin is able to bind to phospholipids with only trace amounts of PS, the DsRed2EC-LactC2 and related fusion constructs of our study should be suitable tools to detect PS-containing phospholipids *in vivo*. Indeed, a fusion of the LactC2 domain of bovine lactadherin with a green fluorescent protein has been previously used to detect PS-containing membranes in mammalian cells[76]. In this study, the specific fluorescence of the cell membranes of *R. eutropha*, *E. coli*, *P. putida* and of *M. gryphiswaldense* upon expression of the DsRed2EC-LactC2 construct is in full agreement with the presence of phospholipids in cell membranes of these species and confirms the specificity of the fluorescent LactC2 construct for the detection of phospholipids in prokaryotes. The finding that DsRed2EC-LactC2 was able to bind to the magnetosome chains of *M. gryphiswaldense* illustrates that also membranes of prokaryotic organelles with a strong positive curvature can be detected. The nature of the DsRed2EC-LactC2 foci that were observed in a minor fraction of the cell population remains unclear and might indicate the presence of a rare, yet to be identified membrane-embedded structure.

We never observed a co-localization of LactC2 fused to DsRed2EC or of one of the other fluorescent fusion constructs with carbonosomes in *R. eutropha*, *P. putida. or M. gryphiswaldense*. The simultaneous binding of DsRed2EC-LactC2 to the cell membrane and to the magnetosome chain but its absence at PHB granules in *M. gryphiswaldense* strongly indicates that PHB granules apparently do not contain phospholipids in the surface layer *in vivo.* A consequence of our findings is that the surface layer of carbonosomes is a protein layer. A current model of the structure of a PHB granule with all proteins identified *in vivo* for *R. eutropha* is given in Fig. 8.

Only when PHB granules were synthesized in a recombinant *E. coli* background, a potential co-localization of LactC2 was detected for some PHB granules. The artificial *E. coli* system lacks the native surface of carbonosomes as it can be found in *R. eutropha* or *P. putida*[8,26,49,57]. Hence, the hydrophobic surface of the polymer in *E. coli* is at least partially exposed to the cytoplasm where it might come in contact with the cytoplasmic membrane, in particular because PHB granules in *E. coli* tend to localize close to the cell poles. In *R. eutropha* and in *P. putida,* carbonosomes (and possibly also in *M. gryphiswaldense*) are attached to a subcellular scaffold (most likely the bacterial nucleoid) via interaction with PhaM[36,77] and PhaF[50] and do not localize at the cell poles even in the absence of PhaP1. As a consequence of over-production and close localization to the cell periphery, PHB granules in recombinant *E. coli* might abstract phospholipids to the PHB granule surface. The same artificial binding of phospholipids to the PHB granule surface layer happens *in vitro* during the PHB granule isolation process and was confirmed in this study by the occasional detection of DsRed2EC-LactC2 fluorescence in an isolated PHB granule fraction. This finding well explains the detection of traces of phospholipids in isolated PHB granules by Merrick and co-workers almost 50 years ago[55]. Since no LactC2-conferred fluorescence was detected in PHB or PHA granules in *R. eutropha* (PHB accumulating representative of β-*proteobacteria)*, *P. putida (*PHA accumulating representative of γ-*proteobacteria)*, or *M. gryphiswaldense* (PHB accumulating representative of α-*proteobacteria)*, we conclude that membrane lipids are not present in the surface layer of native PHB/PHA granules *in vivo*. The fact that recombinant PHB granules in a foreign host can be covered by LactC2-reacting material demonstrates that the detection system is fairly sensitive and would detect phospholipids if present. In conclusion, we have

ruled out the presence of phospholipids *in vivo* in naturally formed PHB and PHA granules and this is in line with cryo-tomography data[61]. We assume that the finding of phospholipids in isolated PHB granules most likely is an *in vitro* artefact and reflects the potential of carbonosomes to accommodate lipids on its surface under non-physiological conditions. As a further observation of this study, the enrichment of DsRed2EC-LactC2 near the cell poles in some cells might indicate that prokaryotic membranes can have a non-random distribution of phospholipids similar to the presence of so-called lipid rafts.

Methods

Bacterial strains, plasmids and culture conditions. Bacterial strains and plasmids used in this study are shown in Table 1. *E. coli* strains were grown in Lysogeny broth (LB) medium supplemented with the appropriate antibiotics at 37 °C. In some cases 0.5% (wt/vol) of glucose was added to promote accumulation of PHB of recombinant *E. coli* strains harbouring the PHB biosynthetic genes. *R. eutropha* H16 strains were grown on nutrient broth (NB, 0.8%, (wt/vol)) with or without addition of 0.2% (wt/vol) of sodium gluconate at 30 °C. *Pseudomonas putida* GPO1 (previously *P. oleovorans*) was grown in mineral salts medium with addition of sodium octanoate (0.3%, wt/vol) at 30 °C. *M. gryphiswaldense* was grown in modified flask standard medium (FSM) at 28 °C in 15 ml polypropylene tubes with sealed screw caps and a culture volume of 10 ml at micro-oxic conditions with moderate shaking (120 rpm)[78].

Construction of fluorescent fusion proteins. Constructions of in frame fusion proteins generally were prepared via PCR. The DNA sequences of the used synthetic desoxyribo-oligonucleotides and the amino acid sequences of the resulting fusion proteins are shown in Suppl. Tables S5 and S6. All PCR constructs were ligated into appropriate vectors and transformed to *E. coli*. The DNA sequence of each construct was verified by commercial DNA sequencing of the entire length of the PCR-amplified region and only constructs with correct DNA sequence were used.

The plasmids were transformed to *E. coli* by standard transformation and were subsequently transferred via conjugation from recombinant *E. coli* S17-1 to *R. eutropha* H16. Selection was achieved by plating on mineral salts medium supplemented with 0.2% fructose and 15 μg ml^{-1} tetracycline or 350 μg ml^{-1} kanamycin, respectively. For *P. putida* GPO1, plasmids were transformed using electroporation as described elsewhere[79]. Selection was achieved by plating on NB medium and 15 μg ml^{-1} tetracycline. For *M. gryphiswaldense*, pBAM plasmids were transferred from *E. coli* WM3064 to *M. gryphiswaldense* MSR-1. Selection was achieved by addition of 5 μg/ml kanamycin.

Isolation of PHB granules. PHB granules were isolated from French press (twice) disrupted cells by two subsequent glycerol gradient centrifugations as described previously[80].

Microscopical methods. Formation of PHB granules was followed by fluorescence microscopy using Nile red as dye (1–10 μg/ml DMSO, Nile red solution at 5–40% [vol/vol]). Fluorescence microscopy and detection of fluorescent proteins (eYFP, DsRed2EC, Venus, Cerulean, sfGFP, or mTurquoise2) was performed on a Zeiss Axioplan, Leica DM5500 B microscope or Nikon Ti-E microscope (MEA53100) by using F41-007 Cy3 and F41-54 Cy2 filters for analysis of the PHB granules (Nile red stained) and DsRed2EC and for eYFP analysis, respectively. Venus fluorescence was detected using an excitation filter ET500/20x and an emission filter ET535/30m. Cerulean fluorescence was detected with excitation filter ET436/20x and an emission filter ET480/40m. A specific filter set (excitation, 415/20 nm; emission, 520/60) was used to visualize mTurquoise2 and sfGFP was detected with the aid of a standard filter set (excitation, 500/24 nm; emission, 542/27nm).

Pictures were taken with a digital camera (Hamamatsu Orca Flash 4.0 sCMOS camera and processed with Nikon imaging software. To avoid a potential cross-talk between fluorescence channels images were recorded with and without Nile red. PHB granules could be also visualized by phase contrast or bright field microscopy. To image fluorescent protein fusions 5 μl portions of the sample were immobilized on agarose pads (1% (wt/vol) in phosphate buffered saline) and covered with a coverslip. Images were processed with ImageJ Fiji v1.50c[81].

References

1. Anderson, A. J. & Dawes, E. A. Occurrence, metabolism, metabolic role, and industrial uses of bacterial polyhydroxyalkanoates. *Microbiol. Rev.* **54,** 450–472 (1990).
2. Madison, L. L. & Huisman, G. W. Metabolic engineering of poly(3-hydroxyalkanoates): from DNA to plastic. *Microbiol. Mol. Biol. Rev.* **63,** 21–53 (1999).
3. Stubbe, J. *et al.* Nontemplate-dependent polymerization processes: polyhydroxyalkanoate synthases as a paradigm. *Annu. Rev. Biochem.* **74,** 433–480 (2005).
4. Pötter, M. & Steinbüchel, A. Biogenesis and Structure of polyhydroxyalkanoate granules. *Microbiol. Monogr.* **1,** 110–136 (2006).
5. Grage, K. *et al.* Bacterial polyhydroxyalkanoate granules: biogenesis, structure, and potential use as nano-/micro-beads in biotechnological and biomedical applications. *Biomacromolecules* **10,** 660–669 (2009).
6. Rehm, B. H. A. Bacterial polymers: biosynthesis, modifications and applications. *Nat. Rev. Microbiol.* **8,** 578–592 (2010).
7. Chen, G.-Q. A microbial polyhydroxyalkanoates (PHA) based bio- and materials industry. *Chem Soc Rev* **38,** 2434–2446 (2009).
8. Jendrossek, D. & Pfeiffer, D. New insights in the formation of polyhydroxyalkanoate granules (carbonosomes) and novel functions of poly(3-hydroxybutyrate). *Environ Microbiol* **16,** 2357–2373 (2014).
9. Rehm, B. H. A. Polyester synthases: natural catalysts for plastics. *Biochem J* **376,** 15–33 (2003).
10. Stubbe, J. & Tian, J. Polyhydroxyalkanoate (PHA) hemeostasis: the role of PHA synthase. *Nat. Prod. Rep.* **20,** 445–457 (2003).
11. Wodzinska, J. *et al.* Polyhydroxybutyrate synthase: Evidence for covalent catalysis. *J. Am. Chem. Soc.* **118,** 6319–6320 (1996).
12. Cho, M., Brigham, C. J., Sinskey, A. J. & Stubbe, J. Purification of a polyhydroxybutyrate synthase from its native organism, *Ralstonia eutropha*: implications in the initiation and elongation of polymer formation *in vivo*. *Biochemistry* 2276–2288 (2012). doi: 10.1021/bi2013596.

13. Wieczorek, R., Steinbüchel, A. & Schmidt, B. Occurrence of polyhydroxyalkanoic acid granule-associated proteins related to the *Alcaligenes eutrophus* H16 GA24 protein in other bacteria. *FEMS Microbiol Lett* **135,** 23–30 (1996).
14. Jendrossek, D. & Handrick, R. Microbial degradation of polyhydroxyalkanoates. *Annu. Rev. Microbiol.* **56,** 403–432 (2002).
15. Martinez, V. *et al.* Identification and biochemical evidence of a medium-chain-length polyhydroxyalkanoate Depolymerase in the *Bdellovibrio bacteriovorus* predatory hydrolytic arsenal. *Applied and environmental microbiology* **78,** 6017–6026 (2012).
16. Eggers, J. & Steinbüchel, A. Poly (3-hydroxybutyrate) degradation in *Ralstonia eutropha* H16 is mediated stereoselectively to (S)-3-hydroxybutyryl-CoA via crotonyl-CoA. *J Bacteriol* **195,** 3213–3223 (2013).
17. Maestro, B. *et al.* A new family of intrinsically disordered proteins: structural characterization of the major phasin PhaF from Pseudomonas putida KT2440. *PLoS ONE* **8,** e56904 (2013).
18. Mezzina, M. P. *et al.* A phasin with many faces: Structural insights on PhaP from *Azotobacter* sp. FA8. *PLoS ONE* **9,** e103012 (2014).
19. Peoples, O. P. & Sinskey, A. J. Poly-beta-hydroxybutyrate (PHB) biosynthesis in *Alcaligenes eutrophus* H16. Identification and characterization of the PHB polymerase gene (*phbC*). *J Biol Chem* **264,** 15298–15303 (1989).
20. Schubert, P., Steinbüchel, A. & Schlegel, H. G. Cloning of the *Alcaligenes eutrophus* genes for synthesis of poly-beta-hydroxybutyric acid (PHB) and synthesis of PHB in *Escherichia coli*. *J Bacteriol* **170,** 5837–5847 (1988).
21. Slater, S. C., Voige, W. H. & Dennis, D. E. Cloning and expression in *Escherichia coli* of the *Alcaligenes eutrophus* H16 poly-beta-hydroxybutyrate biosynthetic pathway. *J Bacteriol* **170,** 4431–4436 (1988).
22. Handrick, R., Reinhardt, S. & Jendrossek, D. Mobilization of poly(3-hydroxybutyrate) in *Ralstonia eutropha*. *J Bacteriol* **182,** 5916–5918 (2000).
23. Saegusa, H., Shiraki, M., Kanai, C. & Saito, T. Cloning of an intracellular Poly[D(−)-3-Hydroxybutyrate] depolymerase gene from *Ralstonia eutropha* H16 and characterization of the gene product. *J Bacteriol* **183,** 94–100 (2001).
24. York, G. M. *et al. Ralstonia eutropha* H16 encodes two and possibly three intracellular poly[D-(−)-3-hydroxybutyrate] depolymerase genes. *J Bacteriol* **185,** 3788–3794 (2003).
25. Sznajder, A. & Jendrossek, D. To be or not to be a PHB depolymerase: PhaZd1 (PhaZ6) and PhaZd2 (PhaZ7) of *Ralstonia eutropha* are highly active PHB depolymerases but have no detectable role in mobilization of accumulated PHB. *Applied and environmental microbiology* **16,** 4936–4946 (2014).
26. Sznajder, A., Pfeiffer, D. & Jendrossek, D. Comparative proteome analysis reveals four novel polyhydroxybutyrate (PHB) granule-associated proteins in *Ralstonia eutropha* H16. *Applied and environmental microbiology* **81,** 1854–1858 (2015).
27. Wieczorek, R., Pries, A., Steinbüchel, A. & Mayer, F. Analysis of a 24-kilodalton protein associated with the polyhydroxyalkanoic acid granules in *Alcaligenes eutrophus*. *J Bacteriol* **177,** 2425–2435 (1995).
28. Steinbüchel, A. *et al.* Considerations on the structure and biochemistry of bacterial polyhydroxyalkanoic acid inclusions. *Can. J. Microbiol.* **41** Suppl 1, 94–105 (1995).
29. York, G. M., Junker, B. H., Stubbe, J. A. & Sinskey, A. J. Accumulation of the PhaP phasin of *Ralstonia eutropha* is dependent on production of polyhydroxybutyrate in cells. *J Bacteriol* **183,** 4217–4226 (2001).
30. York, G. M., Stubbe, J. & Sinskey, A. J. New insight into the role of the PhaP phasin of Ralstonia eutropha in promoting synthesis of polyhydroxybutyrate. *J Bacteriol* **183,** 2394–2397 (2001).
31. Pötter, M. *et al.* The complex structure of polyhydroxybutyrate (PHB) granules: four orthologous and paralogous phasins occur in *Ralstonia eutropha*. *Microbiology* (*Reading, Engl*) **150,** 2301–2311 (2004).
32. Pfeiffer, D. & Jendrossek, D. Interaction between poly(3-hydroxybutyrate) granule-associated proteins as revealed by two-hybrid analysis and identification of a new phasin in *Ralstonia eutropha* H16. *Microbiology* **157,** 2795–2807 (2011).
33. Pfeiffer, D. & Jendrossek, D. Localization of poly(3-hydroxybutyrate) (PHB) granule-associated proteins during PHB granule formation and identification of two new phasins, PhaP6 and PhaP7, in *Ralstonia eutropha* H16. *J Bacteriol* **194,** 5909–5921 (2012).
34. York, G. M., Stubbe, J. & Sinskey, A. J. The *Ralstonia eutropha* PhaR protein couples synthesis of the PhaP phasin to the presence of polyhydroxybutyrate in cells and promotes polyhydroxybutyrate production. *J Bacteriol* **184,** 59–66 (2002).
35. Pötter, M., Madkour, M. H., Mayer, F. & Steinbüchel, A. Regulation of phasin expression and polyhydroxyalkanoate (PHA) granule formation in *Ralstonia eutropha* H16. *Microbiology* (*Reading, Engl*) **148,** 2413–2426 (2002).
36. Pfeiffer, D., Wahl, A. & Jendrossek, D. Identification of a multifunctional protein, PhaM, that determines number, surface to volume ratio, subcellular localization and distribution to daughter cells of poly(3-hydroxybutyrate), PHB, granules in *Ralstonia eutropha* H16. *Mol Microbiol* **82,** 936–951 (2011).
37. Gerngross, T. U., Reilly, P., Stubbe, J., Sinskey, A. J. & Peoples, O. P. Immunocytochemical analysis of poly-beta-hydroxybutyrate (PHB) synthase in *Alcaligenes eutrophus* H16: localization of the synthase enzyme at the surface of PHB granules. *J Bacteriol* **175,** 5289–5293 (1993).
38. Barnard, G. C., McCool, J. D., Wood, D. W. & Gerngross, T. U. Integrated recombinant protein expression and purification platform based on *Ralstonia eutropha*. *Applied and environmental microbiology* **71,** 5735–5742 (2005).
39. Uchino, K., Saito, T., Gebauer, B. & Jendrossek, D. Isolated poly(3-hydroxybutyrate) (PHB) granules are complex bacterial organelles catalyzing formation of PHB from acetyl coenzyme A (CoA) and degradation of PHB to acetyl-CoA. *J Bacteriol* **189,** 8250–8256 (2007).
40. Neumann, L. *et al.* Binding of the major phasin, PhaP1, from *Ralstonia eutropha* H16 to poly(3-hydroxybutyrate) granules. *J Bacteriol* **190,** 2911–2919 (2008).
41. Hauf, W. *et al.* Metabolic Changes in Synechocystis PCC6803 upon Nitrogen-Starvation: Excess NADPH Sustains Polyhydroxybutyrate Accumulation. *Metabolites* **3,** 101–118 (2013).
42. Jendrossek, D. Polyhydroxyalkanoate granules are complex subcellular organelles (carbonosomes). *J Bacteriol* **191,** 3195–3202 (2009).
43. Scheffel, A. *et al.* An acidic protein aligns magnetosomes along a filamentous structure in magnetotactic bacteria. *Nature* **440,** 110–114 (2006).
44. Cornejo, E., Abreu, N. & Komeili, A. Compartmentalization and organelle formation in bacteria. *Curr. Opin. Cell Biol.* **26,** 132–138 (2014).
45. Komeili, A. Molecular mechanisms of compartmentalization and biomineralization in magnetotactic bacteria. *FEMS Microbiol. Rev.* **36,** 232–255 (2012).
46. Prieto, M. A., Bühler, B., Jung, K., Witholt, B. & Kessler, B. PhaF, a polyhydroxyalkanoate-granule-associated protein of *Pseudomonas oleovorans* GPo1 involved in the regulatory expression system for *pha* genes. *J Bacteriol* **181,** 858–868 (1999).
47. de Eugenio, L. I. *et al.* Biochemical evidence that *phaZ* gene encodes a specific intracellular medium chain length polyhydroxyalkanoate depolymerase in *Pseudomonas putida* KT2442: characterization of a paradigmatic enzyme. *J Biol Chem* **282,** 4951–4962 (2007).
48. de Eugenio, L. I. *et al.* The PhaD regulator controls the simultaneous expression of the *pha* genes involved in polyhydroxyalkanoate metabolism and turnover in *Pseudomonas putida* KT2442. *Environ Microbiol* **12,** 1591–1603 (2010).
49. Dinjaski, N. & Prieto, M. A. Swapping of phasin modules to optimize the *in vivo* immobilization of proteins to medium-chain-length polyhydroxyalkanoate granules in *Pseudomonas putida*. *Biomacromolecules* **14,** 3285–3293 (2013).
50. Galán, B. *et al.* Nucleoid-associated PhaF phasin drives intracellular location and segregation of polyhydroxyalkanoate granules in *Pseudomonas putida* KT2442. *Mol Microbiol* **79,** 402–418 (2011).
51. McCool, G. J. & Cannon, M. C. Polyhydroxyalkanoate inclusion body-associated proteins and coding region in Bacillus megaterium. *J Bacteriol* **181,** 585–592 (1999).
52. McCool, G. J. & Cannon, M. C. PhaC and PhaR are required for polyhydroxyalkanoic acid synthase activity in *Bacillus megaterium*. *J Bacteriol* **183,** 4235–4243 (2001).

53. Handrick, R. *et al.* Unraveling the function of the *Rhodospirillum rubrum* activator of polyhydroxybutyrate (PHB) degradation: the activator is a PHB-granule-bound protein (phasin). *J Bacteriol* **186,** 2466–2475 (2004).
54. Cai, S. *et al.* Identification of the haloarchaeal phasin (PhaP) that functions in polyhydroxyalkanoate accumulation and granule formation in *Haloferax mediterranei*. *Applied and environmental microbiology* **78,** 1946–1952 (2012).
55. Griebel, R., Smith, Z. & Merrick, J. M. Metabolism of poly-beta-hydroxybutyrate. I. Purification, composition, and properties of native poly-beta-hydroxybutyrate granules from *Bacillus megaterium*. *Biochemistry* **7,** 3676–3681 (1968).
56. Ruth, K., de Roo, G., Egli, T. & Ren, Q. Identification of two acyl-CoA synthetases from *Pseudomonas putida* GPo1: one is located at the surface of polyhydroxyalkanoates granules. *Biomacromolecules* **9,** 1652–1659 (2008).
57. Dinjaski, N. & Prieto, M. A. Smart polyhydroxyalkanoate nanobeads by protein based functionalization. *Nanomedicine* **11,** 885–899 (2015).
58. Horowitz, D. M. & Sanders, K. M. Amorphous, biomimetic granules of polyhydroxybutyrate: preparation, characterization, and biological implications. *J. Am. Chem. Soc.* **116,** 2695–2702 (1994).
59. Boatman, E. S. Observations on the fine structure of spheroplasts of *Rhodospirillum rubrum*. *J. Cell Biol.* **20,** 297–311 (1964).
60. Mayer, F. & Hoppert, M. Determination of the thickness of the boundary layer surrounding bacterial PHA inclusion bodies, and implications for models describing the molecular architecture of this layer. *J Basic Microbiol* **37,** 45–52 (1997).
61. Beeby, M., Cho, M., Stubbe, J. & Jensen, G. J. Growth and localization of polyhydroxybutyrate granules in *Ralstonia eutropha*. *J Bacteriol* **194,** 1092–1099 (2012).
62. Jendrossek, D., Selchow, O. & Hoppert, M. Poly (3-hydroxybutyrate) granules at the early stages of formation are localized close to the cytoplasmic membrane in *Caryophanon latum*. *Applied and environmental microbiology* **73,** 586–593 (2007).
63. Andersen, M. H., Berglund, L., Rasmussen, J. T. & Petersen, T. E. Bovine PAS-6/7 binds alpha v beta 5 integrins and anionic phospholipids through two domains. *Biochemistry* **36,** 5441–5446 (1997).
64. Andersen, M. H., Graversen, H., Fedosov, S. N., Petersen, T. E. & Rasmussen, J. T. Functional analyses of two cellular binding domains of bovine lactadherin. *Biochemistry* **39,** 6200–6206 (2000).
65. Pédelacq, J.-D., Cabantous, S., Tran, T., Terwilliger, T. C. & Waldo, G. S. Engineering and characterization of a superfolder green fluorescent protein. *Nat. Biotechnol.* **24,** 79–88 (2006).
66. Goedhart, J. *et al.* Structure-guided evolution of cyan fluorescent proteins towards a quantum yield of 93%. *Nat Commun* **3,** 751 (2012).
67. Raschdorf, O., Plitzko, J. M., Schüler, D. & Müller, F. D. A tailored *galK* counterselection system for efficient markerless gene deletion and chromosomal tagging in *Magnetospirillum gryphiswaldense*. *Applied and environmental microbiology* **80,** 4323–4330 (2014).
68. Jendrossek, D. Fluorescence microscopical investigation of poly(3-hydroxybutyrate) granule formation in bacteria. *Biomacromolecules* **6,** 598–603 (2005).
69. Stace, C. L. & Ktistakis, N. T. Phosphatidic acid- and phosphatidylserine-binding proteins. *Biochim. Biophys. Acta* **1761,** 913–926 (2006).
70. Lemmon, M. A. Membrane recognition by phospholipid-binding domains. *Nat. Rev. Mol. Cell Biol.* **9,** 99–111 (2008).
71. Várnai, P. & Balla, T. Live cell imaging of phosphoinositide dynamics with fluorescent protein domains. *Biochim. Biophys. Acta* **1761,** 957–967 (2006).
72. Gilbert, G. E. & Drinkwater, D. Specific membrane binding of factor VIII is mediated by O-phospho-L-serine, a moiety of phosphatidylserine. *Biochemistry* **32,** 9577–9585 (1993).
73. Shao, C., Novakovic, V. A., Head, J. F., Seaton, B. A. & Gilbert, G. E. Crystal structure of lactadherin C2 domain at 1.7A resolution with mutational and computational analyses of its membrane-binding motif. *J Biol Chem* **283,** 7230–7241 (2008).
74. Otzen, D. E., Blans, K., Wang, H., Gilbert, G. E. & Rasmussen, J. T. Lactadherin binds to phosphatidylserine-containing vesicles in a two-step mechanism sensitive to vesicle size and composition. *Biochim. Biophys. Acta* **1818,** 1019–1027 (2012).
75. Thiele, O. W., Dreysel, J. & Hermann, D. The 'free' lipids of two different strains of hydrogen-oxidizing bacteria in relation to their growth phases. *Eur J Biochem* **29,** 224–236 (1972).
76. Yeung, T. *et al.* Membrane phosphatidylserine regulates surface charge and protein localization. *Science* **319,** 210–213 (2008).
77. Wahl, A., Schuth, N., Pfeiffer, D., Nussberger, S. & Jendrossek, D. PHB granules are attached to the nucleoid via PhaM in *Ralstonia eutropha*. *BMC Microbiol.* **12,** 262 (2012).
78. Heyen, U. & Schüler, D. Growth and magnetosome formation by microaerophilic *Magnetospirillum* strains in an oxygen-controlled fermentor. *Applied microbiology and biotechnology* **61,** 536–544 (2003).
79. Wang, Q. *et al.* Quick and efficient method for genetic transformation of biopolymer-producing bacteria. *J. Chem. Technol. Biotechnol.* **85,** 775–778 (2009).
80. Handrick, R. *et al.* A new type of thermoalkalophilic hydrolase of *Paucimonas lemoignei* with high specificity for amorphous polyesters of short chain-length hydroxyalkanoic acids. *J Biol Chem* **276,** 36215–36224 (2001).
81. Schindelin, J. *et al.* Fiji: an open-source platform for biological-image analysis. *Nat. Methods* **9,** 676–682 (2012).
82. Kidwell, J., Valentin, H. E. & Dennis, D. Regulated expression of the *Alcaligenes eutrophus pha* biosynthesis genes in *Escherichia coli*. *Applied and environmental microbiology* **61,** 1391–1398 (1995).
83. Simon, R., Priefer, U. & Pühler, A. A broad host- range mobilization system for *in vivo* genetic engineering: trans- poson mutagenesis in Gram-negative bacteria. *Nat. Biotechnol.* **1,** 784–791 (1983).
84. Studier, F. W. & Moffatt, B. A. Use of bacteriophage T7 RNA polymerase to direct selective high-level expression of cloned genes. *J. Mol. Biol.* **189,** 113–130 (1986).
85. de Smet, M. J., Eggink, G., Witholt, B., Kingma, J. & Wynberg, H. Characterization of intracellular inclusions formed by *Pseudomonas oleovorans* during growth on octane. *J Bacteriol* **154,** 870–878 (1983).
86. Schultheiss, D., Kube, M. & Schüler, D. Inactivation of the flagellin gene *flaA* in *Magnetospirillum gryphiswaldense* results in nonmagnetotactic mutants lacking flagellar filaments. *Applied and environmental microbiology* **70,** 3624–3631 (2004).
87. Lohße, A. *et al.* Functional analysis of the magnetosome island in *Magnetospirillum gryphiswaldense*: the mamAB operon is sufficient for magnetite biomineralization. *PLoS ONE* **6,** e25561 (2011).
88. Kovach, M. E. *et al.* Four new derivatives of the broad-host-range cloning vector pBBR1MCS, carrying different antibiotic-resistance cassettes. *Gene* **166,** 175–176 (1995).
89. Marx, C. J. & Lidstrom, M. E. Development of improved versatile broad-host-range vectors for use in methylotrophs and other Gram-negative bacteria. *Microbiology* **147,** 2065–2075 (2001).

Acknowledgements

This work was supported by grants of the Deutsche Forschungsgemeinschaft to K.F. (GRK1708) and to D.J. (Je 152-17/1). We thank Anne-Claude Gavin for providing plasmid p416.

Author Contributions

S.B. and A.S. performed most fluorescence microscopical experiments with natural carbonosome producers; W.H. constructed most fusion proteins and conducted the experiments with recombinant *E. coli*. D.P. performed construction of universal DsRed2EC fusion plasmids and *M. gryphiswaldense* strains. K.F. and D.J. designed the study. D.J. wrote the manuscript. All authors read and approved the manuscript.

Additional Information

Supplementary information accompanies this paper at http://www.nature.com/srep

Competing financial interests: The authors declare no competing financial interests.

How to cite this article: Bresan, S. *et al.* Polyhydroxyalkanoate (PHA) Granules Have no Phospholipids. *Sci. Rep.* **6**, 26612; doi: 10.1038/srep26612 (2016).

6.2 Supplementary information

Suppl. Materials

Polyhydroxyalkanoate (PHA) Granules Have no Phospholipids

Stephanie Bresan[1], Anna Sznajder[1], Waldemar Hauf[2], Karl Forchhammer[2], Daniel Pfeiffer[3] and Dieter Jendrossek[1]

[1]*Institute of Microbiology, University Stuttgart, Germany*

[2]*Department of Organismic Interactions, Eberhard Karls Universität Tübingen, Germany*

[3]*Lehrstuhl für Mikrobiologie, Universität Bayreuth, Germany*

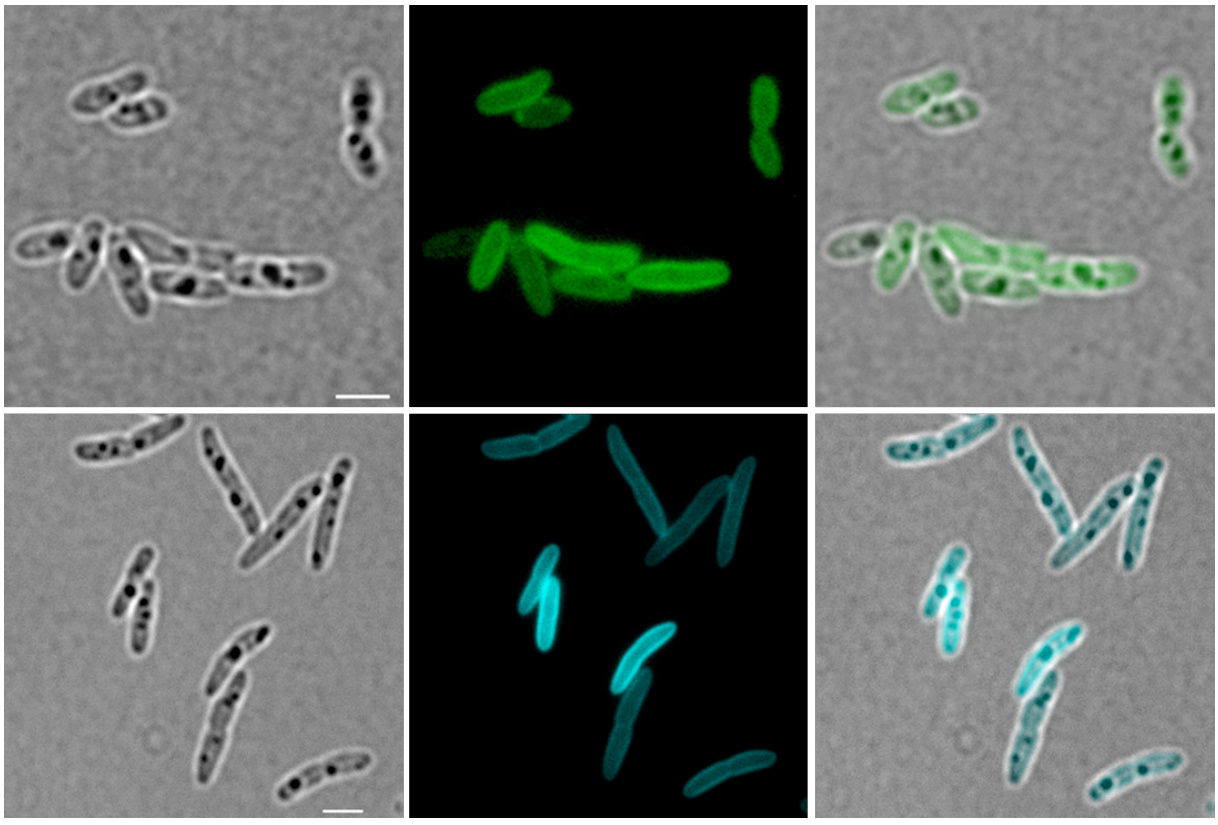

Suppl. Fig. S1: Expression of sfGFP-LactC2 and mTurquoise2-LactC2 in *R. eutropha*.

Cells were grown under PHB permissive conditions. From left to right: bright field, green (top middle) or turquoise (bottom middle) channel, merge. Scale bars correspond to 2 µm. No co-localization of sfGFP-LactC2 or mTurquoise2-LactC2 with PHB granules that are visible in bright field.

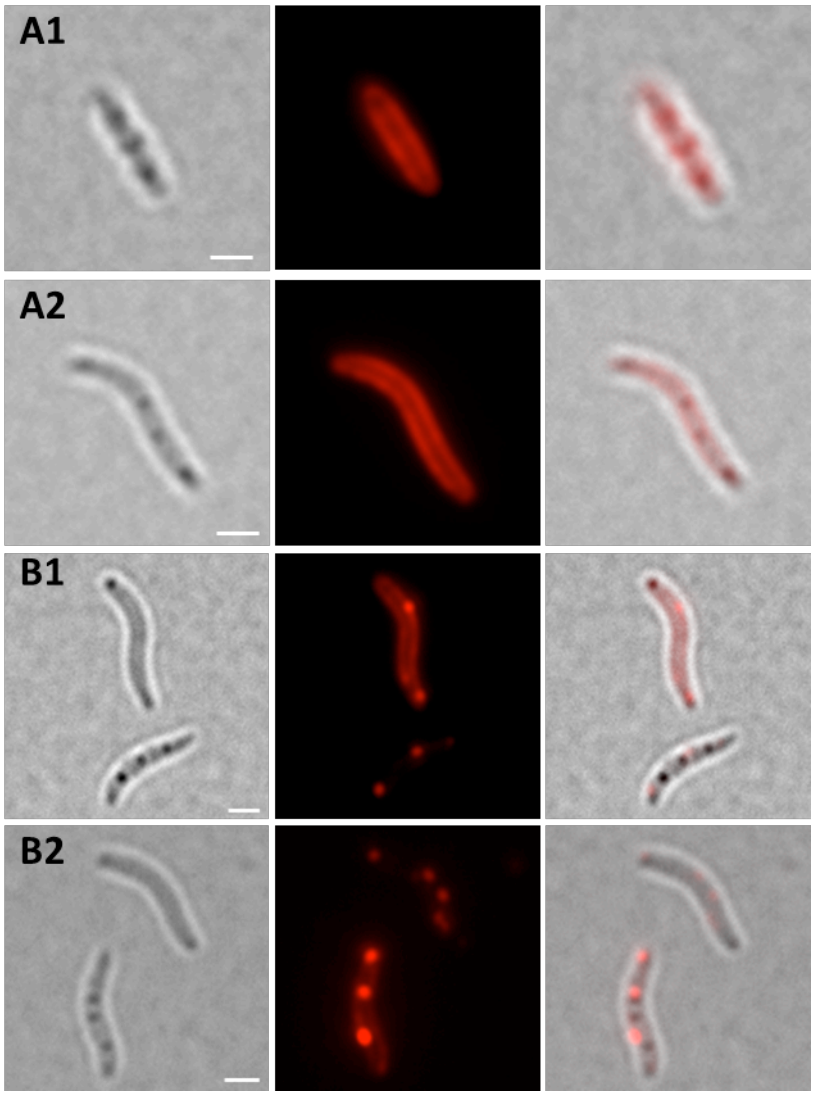

Suppl. Fig. S2: Expression of DsRed2EC-LactC2 in magnetosome-free *M. gryphiswaldense* Δ*mamAB* mutant. Cells showing membrane-bound DsRed2EC-LactC2 fluorescence but no filament-like fluorescence (**A1 and A2**). Cells focussed to foci of DsRed2EC-LactC2 fluorescence (**B1 and B2**). Note, presence of several globular inclusions in bright field (PHB granules) in all images that do not co-localize with DsRed2EC-LactC2 fluorescence. From left to right: bright field, fluorescence channel, merge. Scale bars correspond to 2 µm.

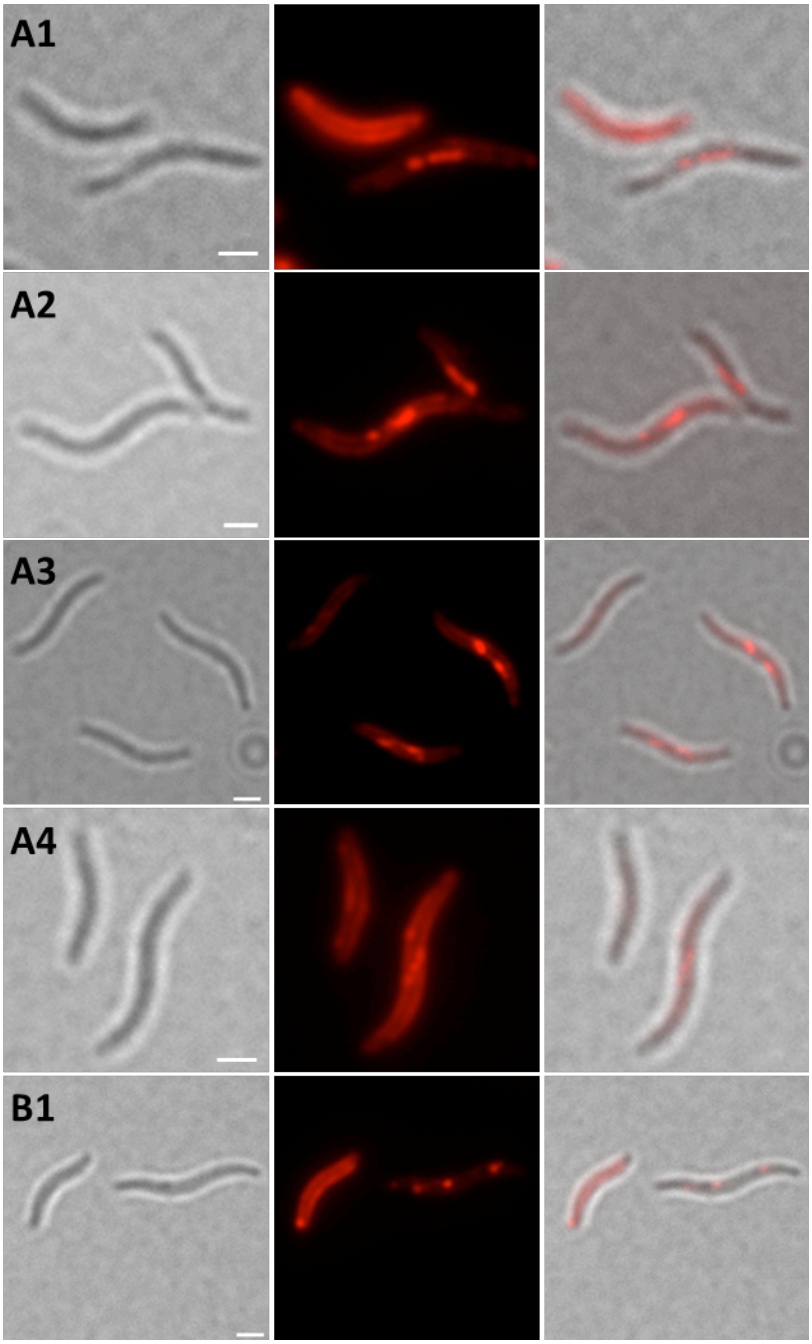

Suppl. Fig. S3: Expression of DsRed2EC-LactC2 in PHB granule-free *M. gryphiswaldense* ∆*phaCAB* mutant. Cells focussed to filament-like dsRed2EC-LactC2 fluorescence resembling magnetosome chains (**A1-A4**). **C**ell focussed to cell membrane-bound DsRed2EC-LactC2 fluorescence and foci of DsRed2EC-LactC2 fluorescence (**B1**). Note, absence of any globular inclusions in bright field (PHB granules). From left to right: bright field, fluorescence channel, merge. Scale bars correspond to 2 µm.

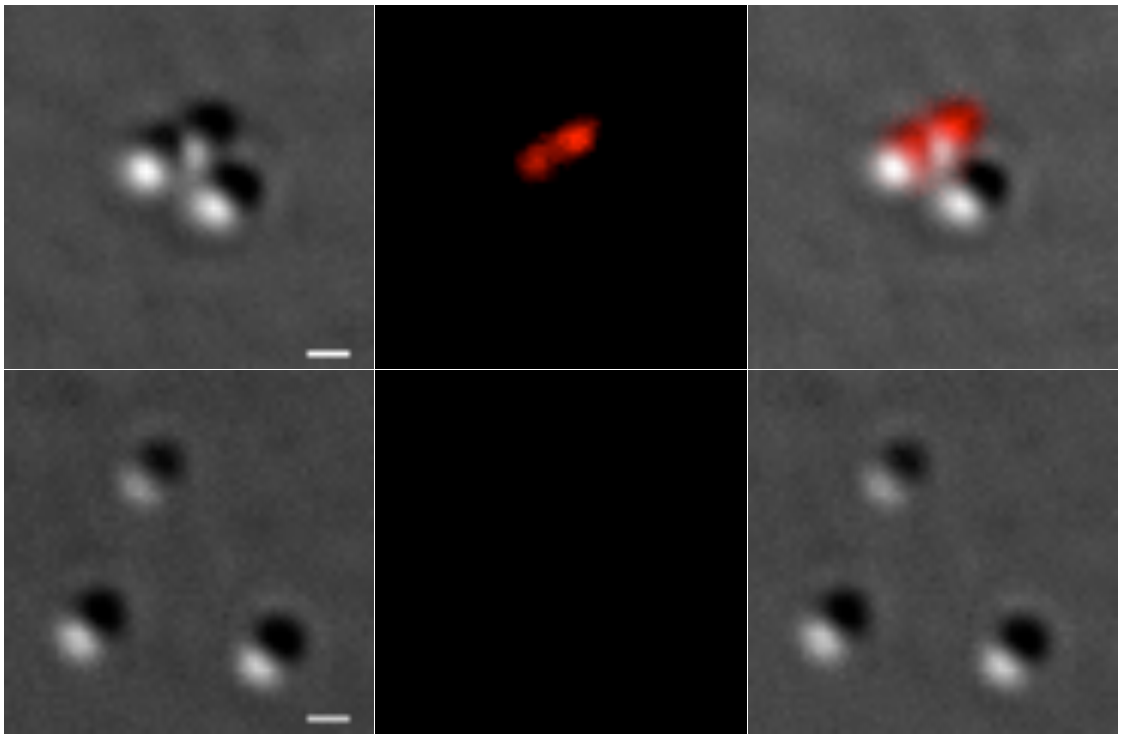

Suppl. Fig. S4: PHB granules isolated from *R. eutropha* H16 cells. PHB granules isolated from *R. eutropha* H16 cells expressing DsRed2EC-LactC2 are shown in the top row. In the bottom row, PHB granules isolated from *R. eutropha* H16 cells expressing DsRed2EC alone are shown. DIC (left), red channel (middle), overlay (right). Scale bars correspond to 0.5 µm.

Suppl. Table S5: Primers used for construction of gene fusions

plasmid	primer for amplification of inserts
pBBR1MCS-2-P_{phaC}-*eyfp*-c1-*psd*	**eYFP-Psd-for:** ccgctcgaggcatgaactatcctcatccgctgatcgcc **eYFP-Psd-rev:** cgggatcctcacttcacgtcgagttcggcgaggatg
pCM62-P_{phaC}-*dsRed2*-c1	**DsRed2EC-for:** gggaattccatatggcgagcagtgagaacatcatcacc **DsRed2EC-rev:** ggactagttgatcagttatctagatccggtggatcc
pCM62-P_{phaC}-*dsRed2EC*-c1-*lactC2*	**LactC2-for:** cccaagcttcatgcactgaaccctaggcc **LactC2-rev:** ggactagtttaacagcccagcagctcc
pETDuet-*phaCcrAB venlactC2*	**PhaA-for:** gggatcactctcggcatggacgagctgtacaagtgacgcttgcatgagtgccgg **PhaB-rev:** gaattcggatcctggctgtggtgatgatggtgatggctgctgcctcagcccatgtgcaggccg **PhaC- Cerulean-for:** cccctctagaaataattttgtttaactttaagaaggagatataccatggcgaccggcaaagg **PhaC- Cerulean-rev:** gctaccgctgccacttcctgatccgctacctgccttggctttgacgtatcgcc **Venus-Lact-for:** ccccatcttagtatattagttaagtataagaaggagatatacatatggtgagcaagggcgagg **Venus-Lact-rev:** cttcaggcctaggggttcagtgcacttgtacagctcgtccatgccgag **ReCr-for:** gtcaaagccaaggcaggtagcggatcaggaagtggcagcggtagcgtgagcaagggcgaggagctgttc **ReCr-rev:** ccggcactcatgcaagcgtcacttgtacagctcgtccatg **LactC2-for:** ctcggcatggacgagctgtacaagtgcactgaacccctaggcctgaag **LactC2-rev:** gtcagcgatcgcgtggccggccgatatccaattgagatctgcttaacagcccagcagctccac
pCM62-P_{phaC}-*mTurquoise2*-c1-*lactC2*	**mmTurq2-LactC2-for:** ccatgcaaagtgccggccagggcaatgcccggagccggttcgaatagtgacggcagagagacaa-tcaacatatgagcaagggcgaggagctg **mTurq2-LactC2-rev:** gggatggtattatccttcaggcctaggggttcagtgcatgaagcttgagctcgagatcttttatatagctcgtccatacccaag
pCM62-P_{phaC}-*sfgfp*-c1-*lactC2*	**sfGFP-LactC2-for:** ccatgcaaagtgccggccagggcaatgcccggagccggttcgaatagtgacggcagagagacaatcaacatatggcatcaaaaggtgaag aattatttac **sfGFP-LactC2-rev:** tggtattatccttcaggcctaggggttcagtgcatgaagcttgagctcgagatcttttatataattcatccataccatgtg
pBAM-P_{mamDC}-*dsRed2EC*-c1-*lactC2*	**DsRed2EC-LactC2-for:** gggaattccatatggcgagcagtgagaacatcatcacc **DsRed2EC-LactC2-rev:** gggaattcgctagcttaacagcccagcagctccactcg

Suppl. Table S6: Amino acid sequences of constructed fusion proteins

DsRed2EC-LactC2:
MASSENIITEFMRFKVRMEGTVNGHEFEIEGEGEGRPYEGHNTVKLKVTKGGPLPFAWDILSPQFQYGSK
VYVKHPADIPDYKKLSFPEGFKWERVMNFEDGGVATVTQDSSLQDGCFIYKVKFIGVNFPSDGPVMQKK
TMGWEASTERLYPRDGVLKGETHKALKLKDGGHYLVEFKSIYMAKKPVQLPGYYYVDAKLDITSHNEDYT
IVEQYERTEGRHHLFL*RSRAQAS*CTEPLGLKDNTIPNKQITASSYYKTWGLSAFSWFPYYARLDNQGKFNA
WTAQTNSASEWLQIDLGSQKRVTGIITQGARDFGHIQYVAAYRVAYGDDGVTWTEYKDPGASESKIFPG
NMDNNSHKKNIFETPFQARFVRIQPVAWHNRITLRVELLGC

sfGFP-LactC2:
MASKGEELFTGVVPILVELDGDVNGHKFSVRGEGEGDATNGKLTLKFICTTGKLPVPWPTLVTTLTYGVQ
CFSRYPDHMKRHDFFKSAMPEGYVQERTISFKDDGTYKTRAEVKFEGDTLVNRIELKGIDFKEDGNILGHK
LEYNFNSHNVYITADKQKNGIKANFKIRHNVEDGSVQLADHYQQNTPIGDGPVLLPDNHYLSTQSVLSKD
PNEKRDHMVLLEFVTAAGITHGMDELYK*RSRAQAS*CTEPLGLKDNTIPNKQITASSYYKTWGLSAFSWFP
YYARLDNQGKFNAWTAQTNSASEWLQIDLGSQKRVTGIITQGARDFGHIQYVAAYRVAYGDDGVTWTE
YKDPGASESKIFPGNMDNNSHKKNIFETPFQARFVRIQPVAWHNRITLRVELLGC

eYFP-Psd:
MVSKGEELFTGVVPILVELDGDVNGHKFSVSGEGEGDATYGKLTLKFICTTGKLPVPWPTLVTTFGYGLQC
FARYPDHMKQHDFFKSAMPEGYVQERTIFFKDDGNYKTRAEVKFEGDTLVNRIELKGIDFKEDGNILGHK
LEYNYNSHNVYIMADKQKNGIKVNFKIRHNIEDGSVQLADHYQQNTPIGDGPVLLPDNHYLSYQSALSKD
PNEKRDHMVLLEFVTAAGITLGMDELYK*SGLRSRG*MNYPHPLIAREGWPFLAGAFVISLLVHASAGFWW
ALPLWIITVFVLQFFRDPPRPIPSQPNAVLAPADGRIVVVEKTQDPYAGREALKISVFMNVFNVHSNRVSV
DGAVEKVEYFPGKFVNADMDKASVENERNAVLIRRAADGQLVTLVQVAGLVARRILCYTKVGDNLSRGQ
RYGFIRFGSRVDVYLPLDARPRVTIGEKVSASSTILAELDVK

PhaC-Cerulean-PhaAB (sequence of PhaA and PhaB not shown)**:**
MATGKGAAASTQEGKSQPFKVTPGPFDPATWLEWSRQWQGTEGNGHAAASGIPGLDALAGVKIAPA
QLGDIQQRYMKDFSALWQAMAEGKAEATGPLHDRRFAGDAWRTNLPYRFAAAFYLLNARALTELADA
VEADAKTRQRIRFAISQWVDAMSPANFLATNPEAQRLLIESGGESLRAGVRNMMEDLTRGKISQTDESA
FEVGRNVAVTEGAVVFENEYFQLLQYKPLTDKVHARPLLMVPPCINKYYILDLQPESSLVRHVVEQGHTVF
LVSWRNPDASMAGSTWDDYIEHAAIRAIEVARDISGQDKINVLGFCVGGTIVSTALAVLAARGEHPAASV
TLLTTLLDFADTGILDVFVDEGHVQLREATLGGGAGAPCALLRGLELANTFSFLRPNDLVWNYVVDNYLK
GNTPVPFDLLFWNGDATNLPGPWYCWYLRHTYLQNELKVPGKLTVCGVPVDLASIDVPTYIYGSREDHIV
PWTAAYASTALLANKLRFVLGASGHIAGVINPPAKNKRSHWTNDALPESPQQWLAGAIEHHGSWWPD
WTAWLAGQAGAKRAAPANYGNARYRAIEPAPGRYVKAKA*GSGSGSGSGS*VSKGEELFTGVVPILVELDG
DVNGHKFSVSGEGEGDATYGKLTLKFICTTGKLPVPWPTLVTTLTWGVQCFARYPDHMKQHDFFKSAM
PEGYVQERTIFFKDDGNYKTRAEVKFEGDTLVNRIELKGIDFKEDGNILGHKLEYNAISDNVYITADKQKNG
IKANFKIRHNIEDGSVQLADHYQQNTPIGDGPVLLPDNHYLSTQSKLSKDPNEKRDHMVLLEFVTAAGITL
GMDELYK

Venus-LactC2:
MVSKGEELFTGVVPILVELDGDVNGHKFSVSGEGEGDATYGKLTLKLICTTGKLPVPWPTLVTTLGYGLQC
FARYPDHMKQHDFFKSAMPEGYVQERTIFFKDDGNYKTRAEVKFEGDTLVNRIELKGIDFKEDGNILGHK
LEYNYNSHNVYITADKQKNGIKANFKIRHNIEDGGVQLADHYQQNTPIGDGPVLLPDNHYLSYQSKLSKD
PNEKRDHMVLLEFVTAAGITLGMDELYKCTEPLGLKDNTIPNKQITASSYYKTWGLSAFSWFPYYARLDN
QGKFNAWTAQTNSASEWLQIDLGSQKRVTGIITQGARDFGHIQYVAAYRVAYGDDGVTWTEYKDPGA
SESKIFPGNMDNNSHKKNIFETPFQARFVRIQPVAWHNRITLRVELLGC

mTurquoise2-LactC2:

MSKGEELFTGVVPILVELDGDVNGHKFSVSGEGEGDATYGKLTLKFICTTGKLPVPWPTLVTTLSWGVQC
FARYPDHMKQHDFFKSAMPEGYVQERTIFFKDDGNYKTRAEVKFEGDTLVNRIELKGIDFKEDGNILGHK
LEYNYFSDNVYITADKQKNGIKANFKIRHNIEDGGVQLADHYQQNTPIGDGPVLLPDNHYLSTQSKLSKDP
NEKRDHMVLLEFVTAAGITLGMDELYK*RSRAQAS*CTEPLGLKDNTIPNKQITASSYYKTWGLSAFSWFPY
YARLDNQGKFNAWTAQTNSASEWLQIDLGSQKRVTGIITQGARDFGHIQYVAAYRVAYGDDGVTWTEY
KDPGASESKIFPGNMDNNSHKKNIFETPFQARFVRIQPVAWHNRITLRVELLGC

Amino acids coding for the fluorescent protein are indicated by coloured letters, amino acids of the linker region are shown in italic letters and amino acids of the protein of interest are indicated by non-italic black letters

7 Publication 4

Contributions of the candidate for the publication.
Lipid analysis was performed by me. I designed and analyzed pull-down experiments, acetyl-CoA and total fatty acid quantifications. I have conceived and written the manuscript with the guidance of Prof. Forchhammer.

7.1 Interaction of the Nitrogen Regulatory Protein GlnB (PII) with Biotin Carboxyl Carrier Protein (BCCP) Controls Acetyl-CoA Levels in the Cyanobacterium *Synechocystis* sp. PCC 6803

frontiers in Microbiology

ORIGINAL RESEARCH
published: 26 October 2016
doi: 10.3389/fmicb.2016.01700

Interaction of the Nitrogen Regulatory Protein GlnB (P_{II}) with Biotin Carboxyl Carrier Protein (BCCP) Controls Acetyl-CoA Levels in the Cyanobacterium *Synechocystis* sp. PCC 6803

*Waldemar Hauf[1], Katharina Schmid[1], Edileusa C. M. Gerhardt[2], Luciano F. Huergo[2,3] and Karl Forchhammer[1]**

[1] Interfaculty Institute of Microbiology and Infection Medicine Tübingen, Eberhard-Karls-Universität Tübingen, Tübingen, Germany, [2] Departamento de Bioquímica e Biologia Molecular, Universidade Federal do Paraná, Curitiba, Brazil, [3] Setor Litoral, Universidade Federal do Paraná, Matinhos, Brazil

The family of P_{II} signal transduction proteins (members GlnB, GlnK, NifI) plays key roles in various cellular processes related to nitrogen metabolism at different functional levels. Recent studies implied that P_{II} proteins may also be involved in the regulation of fatty acid metabolism, since GlnB proteins from Proteobacteria and from *Arabidopsis thaliana* were shown to interact with biotin carboxyl carrier protein (BCCP) of acetyl-CoA carboxylase (ACC). In case of *Escherichia coli* ACCase, this interaction reduces the k_{cat} of acetyl-CoA carboxylation, which should have a marked impact on the acetyl-CoA metabolism. In this study we show that the P_{II} protein of a unicellular cyanobacterium inhibits the biosynthetic activity of *E. coli* ACC and also interacts with cyanobacterial BCCP in an ATP and 2-oxoglutarate dependent manner. In a P_{II} mutant strain of *Synechocystis* strain PCC 6803, the lacking control leads to reduced acetyl-CoA levels, slightly increased levels of fatty acids and formation of lipid bodies as well as an altered fatty acid composition.

Keywords: acetyl-CoA, GlnB (P_{II}), BCCP, cyanobacteria, *Synechocystis* sp. PCC 6803

OPEN ACCESS

Edited by:
Weiwen Zhang,
Tianjin University, China

Reviewed by:
Qiang Wang,
Institute of Hydrobiology (Chinese Academy of Sciences), China
Takashi Osanai,
Meiji University, Japan

***Correspondence:**
Karl Forchhammer
karl.forchhammer@uni-tuebingen.de

Specialty section:
This article was submitted to Microbial Physiology and Metabolism, a section of the journal Frontiers in Microbiology

Received: *20 June 2016*
Accepted: *12 October 2016*
Published: *26 October 2016*

Citation:
Hauf W, Schmid K, Gerhardt ECM, Huergo LF and Forchhammer K (2016) Interaction of the Nitrogen Regulatory Protein GlnB (P_{II}) with Biotin Carboxyl Carrier Protein (BCCP) Controls Acetyl-CoA Levels in the Cyanobacterium Synechocystis sp. PCC 6803. Front. Microbiol. 7:1700. doi: 10.3389/fmicb.2016.01700

INTRODUCTION

De novo fatty acid biosynthesis is an essential metabolic step for microbial growth as it provides fatty acids for phospholipid biosynthesis, which is crucial for the integrity of the cell membrane. The first and committed step in fatty acid biosynthesis is catalyzed by the enzyme acetyl-CoA carboxylase (ACC). In bacteria, the ACC enzyme complex consists of three functional units: i) the biotin carboxyl carrier protein (BCCP, *accB*) is covalently modified at a conserved lysine residue with biotin; ii) biotin carboxylase (BC, *accC*) carboxylates the biotin residue during the catalytic cycle in an ATP-dependent manner and iii) carboxyl transferase (CT, *accA* and *accD*) translocates the "activated" CO_2 in the active site from biotin to acetyl-CoA forming malonyl-CoA, the substrate for fatty acid elongation (Cronan and Waldrop, 2002). Biosynthetic activity of ACC is subjected to tight regulation by several mechanisms. The enzyme is feedback inhibited by acyl-ACP (Jiang and Cronan, 1994) and the catalytic activity of CT is decreased by its own transcript when acetyl-CoA levels are low. Evidence that the CT component additionally represses the translation of the

accA/accD mRNA (Meades et al., 2010) has been challenged lately (Smith and Cronan, 2014). Disturbance of ACC regulation has been shown to impact the acetyl-CoA pool (Davis et al., 2000; Zha et al., 2009). Recent findings showed that ACC in *Arabidopsis thaliana* and *Escherichia coli* is regulated additionally through interaction of BCCP with the P_{II} protein GlnB (Feria Bourrellier et al., 2010; Gerhardt et al., 2015).

P_{II} proteins are small homotrimeric signal transduction proteins with binding sites for ATP/ADP and 2-OG at the three intersubunit-clefts and large flexible T-loops emanating from these sites, with the T-loop conformation reflecting the ligand binding status (Forchhammer and Lüddecke, 2016). Furthermore, the T-loops may be covalently modified in their apical region, either by uridylylation or adenylylation at Tyr51 or by phosphorylation of Ser49 in cyanobacteria (Leigh and Dodsworth, 2007; Merrick, 2014; Forchhammer and Lüddecke, 2016). In most cases, covalent modification negatively affects interaction of P_{II} with its targets. In unicellular cyanobacteria, two P_{II} partners have been characterized; the transcriptional co-activator PipX and the key enzyme of arginine synthesis, N-acetyl glutamate kinase (NAGK). PipX interaction with P_{II} requires a conformation of the GlnB T-loop, which is stabilized by ADP, but is counteracted by joined ATP-Mg^{2+}-2-OG binding (Llácer et al., 2010; Zeth et al., 2014; Lüddecke and Forchhammer, 2015). However, P_{II}-PipX interaction is not affected by phosphorylation of P_{II} at S49 in the T-loop (Llácer et al., 2010). Formation of the P_{II}-PipX complex prevents PipX to function as co-activator of the global nitrogen-transcription factor NtcA (Espinosa et al., 2006; Llácer et al., 2010). The interaction of P_{II} with NAGK is thought to be mediated in a two-step process (Ma et al., 2014). First, an encounter complex is formed, which leads in the second step to bending of the T-loop (Fokina et al., 2010b), enabling T-loop residues to interact with and activate NAGK (Llácer et al., 2007). This P_{II}-NAGK interaction is highly sensitive to 2-OG, whose binding results in repulsion of the T-loop leading to the dissociation of the P_{II}-NAGK complex. Complex formation with P_{II} strongly diminishes allosteric feedback-inhibition of NAGK by arginine (Maheswaran et al., 2004; Fokina et al., 2010a). 2-oxoglutarate is thought to be the key metabolite in signaling the carbon/nitrogen balance in cyanobacteria (Muro-Pastor et al., 2001). Lack of a nitrogen source or excess CO_2 leads to an increase in the 2-OG pool (Muro-Pastor et al., 2001; Eisenhut et al., 2008; Hauf et al., 2013), which coincides with phosphorylation of GlnB (Forchhammer and Tandeau de Marsac, 1995a,b) The recent description of a highly conserved GlnB-BCCP interaction (Gerhardt et al., 2015) suggests that this interaction should also play a role in cyanobacteria. However, metabolic consequences of the GlnB-BCCP interaction have not yet been described and its physiological consequences remain unclear. A potential control of ACCase activity by P_{II} could link acetyl-CoA pools and synthesis of fatty acids to the nitrogen status of the cells. The levels of acetyl-CoA pools mirror its consumption through various acetyl-CoA dependent reactions and replenishment ultimately through CO_2-fixation. Several studies have been performed in *Synechocystis* using metabolic engineering to increase acetyl-CoA pools (Liu et al., 2011; Tan et al., 2011). Yet, our understanding of the acetyl-CoA metabolism in cyanobacteria is limited. A few studies, that have addressed the question how acetyl-CoA pools respond during nitrogen deprivation came to controversial results: in some studies, the acetyl-CoA pools increased (Joseph et al., 2014; Anfelt et al., 2015), or were almost unchanged (Schlebusch and Forchhammer, 2010) whereas other reported modest (Osanai et al., 2014) or strong decrease (Hondo et al., 2015) upon nitrogen deprivation. Different growth conditions, extraction procedures, or data normalization could account for the divergence. So far, no study has been performed in which the acetyl-CoA pools during different growth conditions and C/N regimes were systematically compared in *Synechocystis*. This work was performed to verify the putative interaction of GlnB with BCCP in cyanobacteria and to reveal its physiological impact by studying acetyl-CoA metabolism and fatty acid accumulation in P_{II} mutant of *Synechocystis* sp. PCC 6803.

MATERIALS AND METHODS

Strains and Plasmids

For all cloning procedures Q5 polymerase (NEB) was used. Constructs were assembled according to Gibson et al. (2009) from gBlocks® (IDT) or PCR products and the vector backbone. Sequence integrity was verified by DNA sequencing (GATC biotech). Bacterial strains and plasmids are listed in **Table 3**. Complementation of the P_{II} mutant was performed as described by Wolk et al. (1984) with plasmids pVZ322-P_{II}-Ven and pVZ322-P_{II}S49E-Ven.

Protein Expression

ACC of *E. coli* was extracted as described previously (Gerhardt et al., 2015). BirA was expressed in *E. coli* as described before (Gerhardt et al., 2015). P_{II} protein from *Synechocystis* and *Synechococcus* was purified as described previously (Heinrich et al., 2004). For expression of *Synechocystis* BCCP in *E. coli* BL21(DE3) was grown in 2YT medium at 37°C and expression was induced with IPTG at an OD_{600} of 0.8. Induced culture was cultivated at 25°C over night. Cells were harvested at 4000 × g for 10 min., cell pellets were combined with a cell suspension overexpressing BirA in biotinylation buffer (50 mM HEPES pH8, 10 mM KCl, 5% v/v glycerol, 5 mM $MgCl_2$, 1 mM Biotin, 10 mM ATP, and 1 mM Benzamidine). Cells were homogenized with a Branson Sonifier S-250A and the lysate was incubated for 1 h at 37°C, followed by 4°C over night to biotinylate BCCP. BCCP was extracted from the cleared cell lysate (centrifugation for 30 min. at 25,000 × g at 4°C) through Ni-NTA affinity chromatography. Cleared lysate was loaded on a wash buffer (50 mM TrisHCl pH7.5, 100 mM KCl, 20% v/v glycerol, and 50 mM imidazol) equilibrated Histrap FF Crude column (GE healthcare). The column was washed with 10 column volumes wash buffer and bound protein was eluted with elution buffer (50 mM TrisHCl pH7.5, 100 mM KCl, 20% v/v glycerol and 500 mM imidazol). The eluted protein was dialyzed against a storage buffer (50 mM HEPES pH 7.8 100 mM KCl, 50% v/v glycerol) over night at 4°C. Biotinylation of BCCP was verified using immunoblotting and subsequent detection of biotinylated proteins using streptavidin-HRP conjugate with chemiluminscence.

ACC Activity

ACC activity was measured by coupling ACC catalyzed ATP hydrolysis to the activities of pyruvate kinase (PK) and lactate dehydrogenase (LDH) as described (Beez et al., 2009; Broussard et al., 2013). The reaction buffer consisted of 50 mM imidazole, 50 mM KCl, 20 mM $MgCl_2$, 0.2 mM NADH, 1 mM phosphoenolpyruvate, 10 mM ATP, 0.5 mM DTT, 4.4 units of LDH, 6 units PK, and 10 mM $NaHCO_3$. The pH of the final reaction mixture was 7.5. Following concentrations of ACC subunits were used for the enzyme assay: 10 nM carboxyl transferase (tetramer), 20 nM biotin carboxylase (dimer) and 200 nM biotin carboxyl carrier protein (monomer). Different concentrations of P_{II} and 2-OG were used as indicated in the text. The reactions were pre-incubated for 15 min. and started by the addition of acetyl-CoA 400 μM. The oxidation of NADH to NAD^+ was recorded at 25°C over 20 min. in a SPECORD 200 photometer (Analytik Jena) at 340 nm. From the slope of decreasing absorption, reaction velocity was calculated with an extinction coefficient for NADH of 6220 M^{-1}. For the determination of catalytic constants, the data were fitted to Michaelis-Menten equation using GraphPad prism software

Protein Co-precipitation

Prior to protein co-precipitation experiments BCCP conformation was checked by size exclusion chromatography (20 mM potassium phosphate buffer pH 7.8 100 mM NaCl) ensuring properly folded BCCP was used for experiments. 30 μl Ni-NTA agarose coated magnetic beads (Quiagen) preequilibrated in binding buffer (50 mM TrisHCl pH 8.0, 100 mM NaCl, 0.1% w/v N,N-Dimethyldodecylamine N-oxide (LDAO), 10% v/v glycerol, and 20 mM imidazole) were used. Binding was performed in 700 μl binding buffer with magnetic beads, 30 μg BCCP, and 35 μg P_{II} for 20 min. at room temperature. Unbound protein was washed off, three times with 300 μl binding buffer and bound proteins were eluted in 20 μl elution buffer (50 mM TrisHCl pH 8.0, 100 mM NaCl, 0.1% w/v N,N-Dimethyldodecylamine N-oxide (LDAO), 10% v/v glycerol, and 500 mM imidazole). Various metabolites were added to the binding buffer with final concentrations as indicated. Eluted fractions were analyzed by Tricine-SDS PAGE (Schägger, 2006) and stained with InstantBlue (Expedeon). Stained gels were scanned and band intensities were analyzed densitometrically. Scanned images were gray scaled and inverted with Adobe PhotoshopCS6, mean pixel intensities were determined for the P_{II} protein band and used as a proxy for protein abundance for subsequent analysis.

Cyanobacterial Cultivation

Synechocystis sp. PCC 6803 was grown in BG11 medium (Rippka et al., 1979) at 27°C, supplemented with 5 mM $NaHCO_3$ on a rotary shaker at light intensities of 50–80 μmol photons $s^{-1}m^{-2}$. For imposing nitrogen-starvation conditions, cells were first grown in BG11 medium to an optical density (750 nm) of 0.4–0.6, harvested by centrifugation at 4000 × g for 10 min., then washed with BG11-N (BG11 lacking $NaNO_3$), pelleted again at 4000 × g for 10 min., and finally re-suspended in BG11–N (supplemented with 5 mM $NaHCO_3$) to an OD_{750} of 0.4. For growth with ammonium, cells were grown to OD_{750} of 0.6–0.8 and diluted in BG11-N medium to OD_{750} 0.1. The medium was buffered with TES pH8, supplemented with $NaHCO_3$ and NH_4Cl to a final concentration of 5 mM.

Estimation of Intracellular Acetyl-CoA

To estimate the intracellular acetyl-CoA levels 20 ml of growing culture was pelleted at 4000 × g for 10 min. and frozen at −80°C until measured. Cell pellets were suspended in 200 μl 1 M cold perchloric acid. Suspended cells were lysed using a FastPrepR-24 (MP Biomedicals) for 30 s and 6.5 m/s five times with glass beads (0.1–0.11 mm diameter). Cell debris and glass beads were pelleted at 13,000 × g at 4°C for 10 min. The supernatant was neutralized with 3 M $KHCO_3$ and excess $KHCO_3$ was removed through centrifugation at 13,000 × g for 2 min. at 4°C. The clear supernatant was used for acetyl-CoA measurements using the Acetyl-CoenzymeA kit (Sigma-Aldrich) according to the manufacturer's instruction. Fluorescence intensities were measured using a SpectraMax M2 microplate reader with $\lambda_{ex} = 535$ nm and $\lambda_{em} = 587$ nm.

Fatty Acid Quantification

Fatty acids were quantified as described previously (Wawrik and Harriman, 2010). Cell pellets of 2 ml culture were thawed in in 200 μl saponification reagent (25% methanol in 1N NaOH) and lysed with glass beads (0.1–0.11 mm diameter) in a FastPrepR-24 (MP Biomedicals) for 30 s and 6.5 m/s five times. Cell lysates were saponified for 30 min. at 95°C and vortexed every 5 min. Cell extracts were neutralized with 200 μl neutralization reagent (1N HCl, 100 mM Tris pH 8.0) and copper reagent (9 vol. aq. 1 M triethanolamine, 1 vol. N-acetic acid, 10 vol. 6.45% (w/v) Cu $(NO_3)_2 \cdot 3H_2O$). Samples were vortexed for 2 min. and 250 μl chloroform was added and vortexed for additional 2 min. Phase separation was achieved by centrifugation and 50 μl of the organic phase was transferred in two separate new tubes. In one tube 50 μl 2-butanol were added and used as blank. The second tube was mixed with 1% (w/v) sodium diethyldithiocarbamate in 2-butanol leading to color development in the sample. Absorption was measured at 440 nm in a SpectraMaxM2 microplate reader and the absorption of the blank was subtracted from the sample manually. Lipid concentration was estimated based on a standard curve with palmitic acid.

Fatty Acid Composition

Two hundred milliliters exponentially growing culture were harvested at 4000 × g at 25°C, the cell pellet was washed once with water, pelleted at 20,000 × g for 3 min., frozen in liquid nitrogen and stored at −80°C until used. Cell pellets were lyophilized for 16 h. Pentadeconoic acid was added to 20 mg CDW which was used for saponification with 1 ml 3,75 M NaOH in 50% methanol (v/v) for 35 min. at 100°C. Free fatty acids were methylated by addition of 2 ml methylation reagent (3.25 M HCl in 45% methanol (v/v) for 12 min. at 80°C. Fatty acid methyl esters (FAME) were extracted with 2 ml n-hexane through vortexing and 10 min. incubation on a revolving laboratory mixer. The organic phase was transferred in a new vial to which

3 ml 0.3 M NaOH were added and incubated for 10 min. on a revolving laboratory mixer. The organic phase was transferred in a GC vial and evaporated under nitrogen gas flow at 60°C. FAME were dissolved in 50 µl dichlormethane and analyzed by gas chromatography.

GC Analysis of Fatty Acid Methyl Esters

GC analysis was performed with a Shimadzu GC9A equipped with a FID detector and a DBWAX-30 W (30 m × 0.319 mm) column with nitrogen as carrier gas. 5 µl of sample was injected, the injector and detector temperature was set at 250°C. The Oven temperature increased from 160° to 200°C at a rate of 4°C per minute, and from 200 to 240°C at 8°C per minute and remained constant for 10 min. at 240°C. Fatty acid methyl esters were identified based on retention times determined with commercially available fatty acid methyl esters. FAME were quantified using response factors with pentadecanoic acid as internal standard.

Extraction of Lipids from Cellular Biomass

Two hundred milliliters exponentially growing culture was pelleted at 4000 × g for 10 min. at 25°C. The pellet was washed with deionized water, cells were pelleted at 20,000 × g for 3 min. and the pellet was frozen at −20°C until further use. Bacterial pellets were dried in a centrifugal evaporator for 16 h at 25°C. Dried cell matter (15–40 mg CDW) was used for lipid extraction as described before (Bligh and Dyer, 1959). Dried material was transferred in a glass vial with a PTFE lined screw cap lid, suspended in 3 ml Methanol:Chloroform (2:1), vortexed vigorously and incubated for 1 h on a revolving laboratory mixer. After incubation 1 ml chloroform and 1.8 ml deionized water were added, vortexed and phase separation was induced through centrifugation for 10 min. at 4000 × g. The organic phase was transferred in a fresh glass vial and the aqueous phase was extracted twice with 1 ml chloroform followed by 4 ml Isooctane:Ehtylacetate (3:1). All organic phases were combined and solvents were evaporated under nitrogen gas stream. Lipids were suspended in either 200 µl Chloroform: Methanol (1:1) or Hexane:Ether:Acetic acid (80:20:1).

Lipid Droplet Visualization in Synechocystis

To 100 µl *Synechocystis* cell suspension 1 µl Bodipy® 493/503 (10 mg/ml in DMSO) was added and incubated for 5 min. Cells were pelleted at 10,000 × g for 2 min. and cell pellets were suspended in PBS buffer pH 7.5. Two microliter were dropped on a poly lysine coated glass slide and examined using a Leica DM5500B microscope. Image acquisition was performed with a Leica DFC360FX black and white camera, fluorescence images were recolored using Leica application suite. Green fluorescence was detected using an excitation filter BP470/40 and an emission filter BP525/50. Fluorescence images were acquired with 100 ms exposure time. Bright field images were acquired with 6 ms exposure time. Intensity levels of images were adjusted using PhotoshopCS6.

TLC of Lipids

Lipid extracts were spotted on silica gel 60 (Merck Millipore) TLC plates. Phospholipids were resolved using Chloroform:Methanol:NH_4OH (70:30:5) as mobile phase (Merritt et al., 1991). Glycolipids were visualized spraying the plates with 2.4% (w/v) α-naphtol in 10% sulfuric acid 80% (v/v) ethanol and baking the plate at 120°C until purple spots were visible (Wang and Benning, 2011). Neutral lipids were resolved using a Hexane:Ether (90:10) mobile phase and stained with iodine vapor (Ruiz-Lopez et al., 2003). Individual spots were scraped of and lipids were extracted with Hexane:Ether:Acetic acid (80:20:1).

GC/MS Analysis

Solvent extracted lipids from silica gel were subjected to saponification and FAME were synthesized as described above. FAMEs were detected using a Shimadzu GC17A with a QP-5000MS (GC-MS) using an optima 5MS (15 m × 0.25 mm) column with Helium as carrier gas. 5 µl of sample was injected, the injector temperature was set at 320°C. The column was heated to 90°C and the temperature was hold for 5 min., heated up at a rate of 20°C/min. to 200°C, heated at a rate of 4°C/min. to 300°C and hold for 2 min. at 300°C. The MS detector voltage was set at 1.65 keV.

RESULTS

Cyanobacterial GlnB Affects the Activity of *E. coli* ACC

The *E. coli* acetyl-coenzyme A carboxylase (ACC) was used in a previous study as a model system to investigate the effect of GlnB/GlnZ from *Azospirillum brasilense* and GlnB/GlnK from *E. coli* on enzyme activity (Gerhardt et al., 2015). Here, we first investigated the effect of several characterized *Synechococcus elongatus* PCC7942 P_{II} protein variants (*Sc*P_{II}) on ACC activity. Initial assays were carried out at a fixed concentration of 10 mM ATP. *Synechococcus* GlnB (*Sc*GlnB) was able to efficiently inhibit the *E. coli* ACC activity and increasing concentrations of GlnB correlated with increased inhibition of ACC (**Figure 1A**). The maximum inhibition was calculated to be 93% (SE: 6.8%) with an EC_{50} for *Sc*GlnB of 0.31 µM (SE: 0.066 µM). As interaction of BCCP and *Azospirillum* GlnB was shown to be affected by 2-OG, ACC activity was measured in presence of 1 µM GlnB and various 2-OG concentrations (**Figure 1B**). Increasing concentrations of 2-OG were able to efficiently relief ACC from GlnB-dependent inhibition and the IC_{50} value for 2-oxoglutarate was calculated to be 4.8 µM (SE: 0.2 µM), which is almost exactly the K_d of the first 2-OG binding site (5.1 µM) of GlnB (Fokina et al., 2010b). To reveal, which positions in *Sc*P_{II} are important for ACCase regulation, various variants of *Sc*P_{II} were tested in their ability to inhibit ACC activity (**Figure 1C**). Point mutations in the T-loop of R45 and R47 to alanine and the phosphomimetic S49D/S49E variants were not as efficient in inhibiting ACC activity as wild type P_{II}. In contrast, mutations of S49G, Y51A, and E54A in the T-loop and E85A were not affected in inhibiting ACC activity. Two P_{II} variants (I86N and R103H) were, however, completely unable to inhibit ACC activity. Addition of 1 mM

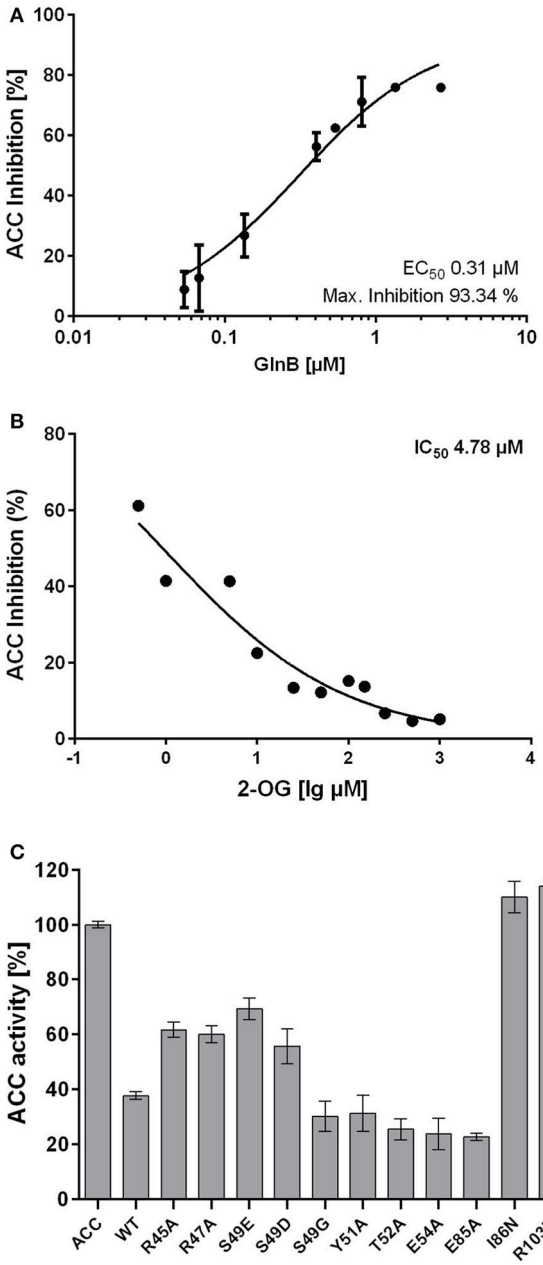

FIGURE 1 | (A) Inhibition of ACC activity in response to various GlnB concentrations. The EC_{50} value was calculated to be 0.31 µM (SE: 0.07 µM). **(B)** Inhibition of ACC with increasing 2-OG concentrations. The IC_{50} was calculated to be 4.8 µM (SE: 0.2 µM). **(C)** Activity of ACC with various GlnB point mutated proteins present in the reaction mixture.

2-OG to the reaction relieved ACC inhibition in all P_{II} variants. This confirms the previous assumption, that GlnB regulation of ACCase activity is highly conserved in bacteria.

SyGlnB-BCCP Interaction Depends on the Concentration of ATP and 2-OG

Since the aim of this study was to characterize the physiological effect of P_{II} on the acetyl-CoA metabolism, but the P_{II} mutant of *Synechococcus* accumulates second site mutations in *pipX* (Espinosa et al., 2009) we decided to study this effect in the P_{II} mutant of *Synechocystis*, in which *pipX* and *ntcA* are not affected. Even though *Sc*GlnB shares 95% sequence identity with GlnB of *Synechocystis* (*Sy*GlnB) we wanted to verify the interaction of *Sy*GlnB and *Synechocystis* BCCP proteins *in vitro*. To this end, recombinant proteins were expressed and purified from *E. coli.* His-tagged BCCP was used as bait protein using Ni-NTA coated magnetic beads. BCCP GlnB interaction was strictly dependent on the presence of Mg^{2+} ions and ATP. Like in *A. brasilense* and *E. coli,* 2-OG negatively affected the ATP-dependent P_{II} binding to BCCP (**Figure 2A**). No P_{II} protein could be recovered in the presence of ADP. An ATP titration experiment was performed and the amount of co-precipitated protein was plotted against the ATP concentration (**Figure 2B**). The apparent EC_{50} for ATP was determined to be 68 µM (SE 13.2 µM) through non-linear fitting and is in good agreement with the K_d of the third ATP binding site of cyanobacterial GlnB (47.4 µM), which exhibits three anticooperative sites (Fokina et al., 2010b). The same type of analysis was performed for 2-OG, titrated in the presence of a fixed concentration of 0.5 mM ATP (**Figure 2C**). The apparent IC_{50} value was calculated, assuming dose response dependent inhibition using a standard slope. The resulting IC_{50} for 2-oxoglutarate was determined to be 41.3 µM (SE 1.7 µM). This value is lower than the K_d of the third GlnB 2-OG binding site (106.7 µM) but well above the Kd of the second site (11.1 µM) (Fokina et al., 2011), which suggests that occupation of the third 2-OG binding determines dissociation of the *Sy*GlnB-*Sy*BCCP complex. GlnB is known to be phosphorylated *in vivo* at position Ser49 under nitrogen-poor conditions or high CO_2-supply to nitrate-grown cells. In the case of P_{II}-NAGK interaction, Ser49 phosphorylation prevents complex formation (Heinrich et al., 2004) and the phosphomimetic variant S49D was unable to interact with NAGK (Llácer et al., 2007). As shown above, the phosphomimetic variants of *Sc*GlnB (S49D and S49E) had reduced efficiency in inhibiting *E. coli* ACCase. To find out, how phosphomimetic variants *Sy*GlnB are affected in binding the cognate *Sy*BCCP protein, the affinity of *Sy*GlnB variants S49D, S49E, S49C, and the wild type protein were tested toward *Sy*BCCP through pull down experiments (**Figure 2D**). Instead of using the S49G variant we decided to use the S49C variant as mutation of S49 to glycine could have a negative impact on complex stability (Lüddecke and Forchhammer, 2013). The S49E variant was completely unable to bind BCCP. The other negatively charged variant S49D, weakly interacted with BCCP, showing only about 20% maximal binding as compared to wild-type GlnB. Likewise, the EC_{50} for GlnB increased 4-fold compared to wild type GlnB. By contrast, substitution of Ser49 to Cys had only a minor effect on GlnB-BCCP interaction (about 90% maximal binding), indicating that the negative charge at position 49 that impairs BCCP-GlnB interaction. As ATP binding influences the T-loop conformation, a titration of ATP with the two variants S49C and S49D was performed (**Figure 2E**). The S49C mutation increases the calculated EC_{50} value for ATP from 68 to 143 µM (SE 24 µM) and to 231 µM (SE 36 µM) for the S49D variant. Maximum binding of GlnB was calculated to be 88.2 mean pixel intensity (SE 3.8 mpi) for the S49C variant which

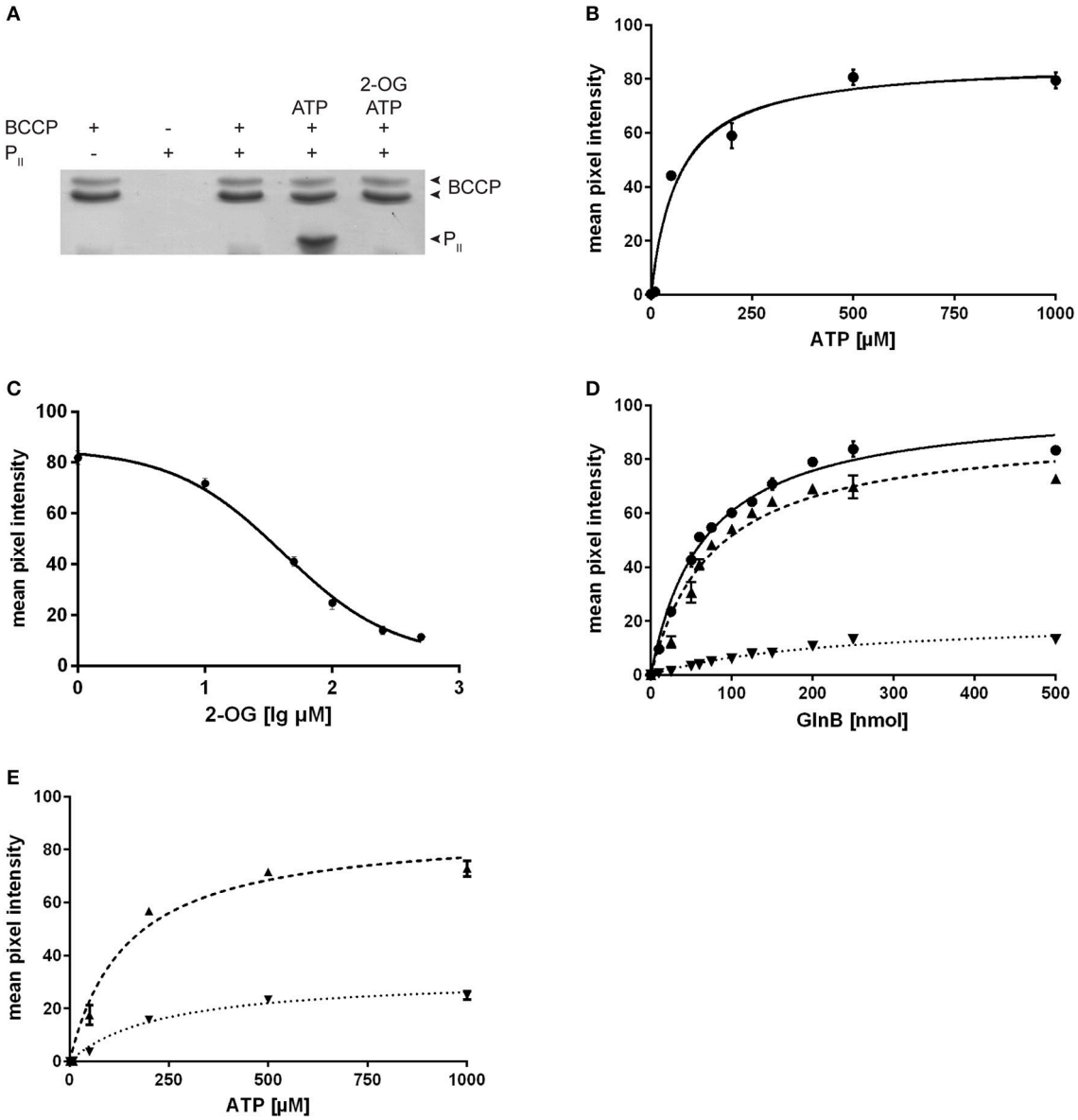

FIGURE 2 | (A) Pull down experiments of Synechocystis BCCP and GlnB using BCCP as bait. Experiments were performed using 0.5 mM Mg^{2+}, 0.5 mM ATP and 1 mM 2-OG where indicated. **(B)** ATP titration of the BCCP-GlnB interaction while the amount of GlnB used was held constant and a calculated EC_{50} value of 68.0 µM (SE 13.2 µM) for ATP. The maximum binding was calculated to be 86.6 mpi (SE 3.8 mpi). **(C)** Influence of 2-OG on the BCCP-GlnB interaction. The IC_{50} of 2-OG is 41.3 µM (SE 1.7 µM). **(D)** Increasing amounts of GlnB and its S49 variants were used with BCCP as bait with 0.5 mM Mg^{2+} and 0.5 mM ATP. The EC_{50} is 65.9 nmol (SE 4.2 nmol) for wild type (circles), 77.0 nmol (SE 8.6 nmol) for S49C (triangles) and 224 nmol (SE 32.1 nmol) for S49D (inverted triangles). Maximum binding was calculated to be 100.7 mpi (SE 2.2 mpi) for the wild type protein, 91.4 mpi (SE 3.7 mpi) for the S49C variant and 21.0 mpi (SE 1.6 mpi) for the S49D variant. **(E)** ATP titration of the BCCP-GlnB S49C and S49D variant (as in **B**). The calculated ATP EC_{50} value for S49C variant is 143 µM (SE 24 µM) and 231 µM (SE 36 µM) for the S49D variant. Maximum binding was calculated to be 88.2 mpi (SE 3.8 mpi) for the S49C variant and 32.2 mpi (SE 1.7 mpi) for the S49D variant.

was almost identical to the wild type protein (86.6 mpi; SE 3.8 mpi), but was much lower for the S49D variant with 32.2 mpi (SE 1.7 mpi) at saturating ATP concentrations. On the one hand, the doubling of the EC_{50} for ATP implies that substitution of serine 49 to cysteine (which is bulkier) requires increased ATP concentrations to fit the T-loop into a conformation that binds to BCCP. At excess ATP concentrations, the mutation had no influence on the total amount of GlnB that can be co-precipitated with BCCP, in agreement with the GlnB titration experiment above. On the other hand, when the T-loop carries the S49D mutation, more than three times higher ATP concentrations were required to enforce the appropriate conformation for complex formation with BCCP. Moreover, the stability of the complex was reduced to one third, as compared to the complex with

wild-type GlnB. Taken together, introduction of a negative charge at position 49 in the T-loop of P_{II} destabilizes the BCCP-GlnB complex. This, together with the fact, that the S49E *Sy*GlnB variant was completely unable to interact with BCCP, strongly indicates that phosphorylated P_{II} will not be able to interact with BCCP.

Deletion of *glnB* Alters Acetyl-CoA Metabolism

The *in vitro* experiments showed that GlnB directly binds BCCP and affects ACC activity, and furthermore, interaction is sensitive to Ser49 modification. From these findings, we hypothesized that phosphorylation of P_{II} should have an impact on either fatty acid or acetyl-CoA metabolism during varying carbon-nitrogen regimes, which correspond to different degrees of P_{II} phosphorylation in *Synechocystis* (Forchhammer and Tandeau de Marsac, 1995a). This regulation should be abolished in a *Synechocystis* P_{II} mutant. To examine this prediction, wild type and P_{II} mutant strains were grown with different nitrogen and carbon supply (nitrate or ammonia as nitrogen source, gently shaking without aeration, corresponding to the lowest CO_2 supply; or vigorous bubbling with either ambient air (0.04%) or 2% CO_2). The expected phosphorylation status of P_{II} was verified (Supplementary Figure 1) and cellular acetyl-CoA levels as well as total fatty acid concentrations were determined in exponentially growing cultures under these conditions. Regardless of the carbon or nitrogen regime, the acetyl-CoA level in the P_{II} mutant was always much lower than in the wild type (**Figure 3A**). Remarkably, the acetyl-CoA levels in the wild type differed with changing carbon and nitrogen regimes. In particular in nitrate grown cells, the acetyl-CoA levels decreased significantly in presence of 2% CO_2 supply. Under these conditions, P_{II} displays the highest degree of phosphorylation, and acetyl-CoA levels in wild-type and mutant cells are similar. However, under any condition that leads to a low degree of P_{II} phosphorylation (either nitrate grown with limiting CO_2-supply or ammonia grown cells), the acetyl-CoA levels were strongly increased, whereas it stayed low in the P_{II} deficient mutant. Total fatty acid levels did not differ as much as the acetyl-CoA levels, but slightly higher fatty acid levels in the P_{II} mutant were always visible. The differences were particularly significant in ammonia grown cells with low carbon supply, where P_{II} is always present in the non-phosphorylated state in the wild type (**Figure 3B**). The carbon regime had a marked impact on the fatty acid content, in both strains. Increased CO_2 supply favored a higher intracellular lipid content. This effect is probably due to improved CO_2-fixation, that will ultimately result in increased CO_2-fixation products than can flow into various anabolic pathways.

Nitrogen starvation represents the situation of maximal P_{II} phosphorylation (Forchhammer and Tandeau de Marsac, 1995a). If the assumption is correct, that P_{II} phosphorylation abrogates its inhibitory effect on ACCase, then the differences in acetyl-CoA levels between wild-type and P_{II} mutant should disappear under those conditions. Therefore, we analyzed acetyl-CoA and total fatty acid levels of cells subjected to 8 h nitrogen-starvation and compared it to conditions during exponential growth with nitrate as nitrogen source. In agreement with our expectation, in 8 h nitrogen-starved cells, the acetyl-CoA levels dropped in the wild-type to the low levels observed in the P_{II} mutant (**Table 1**). As acetyl-CoA levels in *E. coli* decrease during late exponential (Chohnan and Takamura, 1991) and stationary phase, the growth phase dependence of acetyl-CoA levels was measured in *Synechocystis* strains. In the wild-type, acetyl-CoA levels were high during exponential growth and decreased with increasing optical densities. As already shown above, strongly reduced levels of acetyl-CoA in the P_{II} mutant were visible over all time points (**Figure 4A**). Complementation of the P_{II} mutant with the wild-type *glnB* gene was able to complement the low acetyl-CoA level phenotype, but introduction of the gene encoding the P_{II} S49E variant, which was not able to interact with BCCP retained the mutant phenotype. Total fatty acid levels

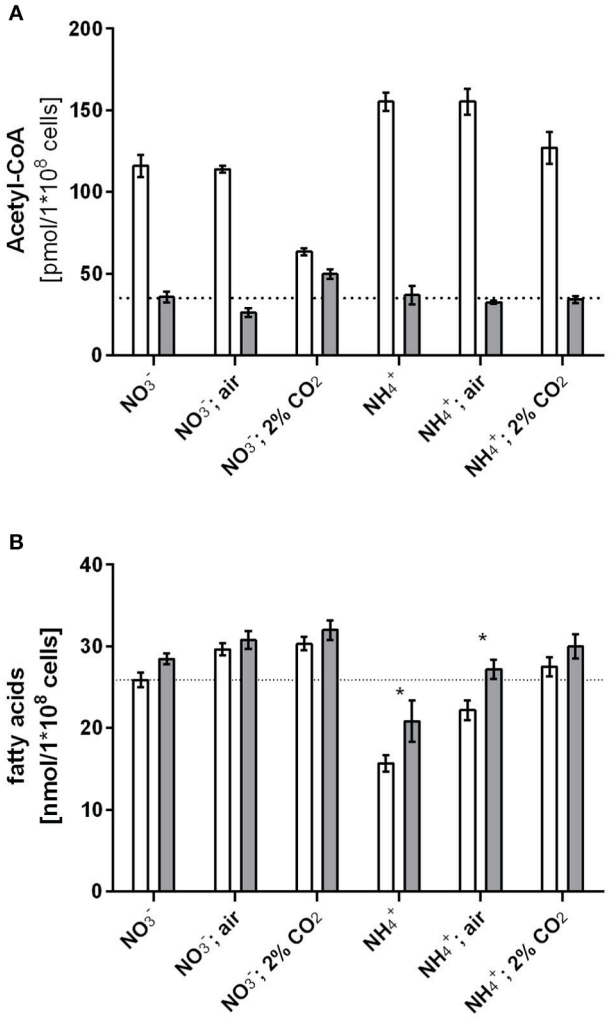

FIGURE 3 | Acetyl-CoA levels (A) and fatty acid levels (B) under different carbon nitrogen regimes during exponential growth in the wild type and the P_{II} mutant. Values represent the mean of three biological replicates. Differences in acetyl-CoA levels using the tested growth conditions are statistically significant ($p < 0.05$; unpaired *t*-test). Statistically significant values of fatty acid levels are marked with a star ($p < 0.05$; unpaired *t*-test).

TABLE 1 | Acetyl-CoA and total fatty acid levels of wild type and the P_{II} mutant during exponential growth and 8 h after nitrogen starvation.

	Wild type	ΔP_{II}	Wild type	ΔP_{II}
	Acetyl-CoA [pmol/1*10^8 cells]		Fatty acids [nmol/1*10^8 cells]	
0 h	127.45 ± 9.3	43.95 ± 3.4	22.37 ± 1.2	25.43 ± 1.7
8 h	47.74 ± 2.0	48.98 ± 1.5	18.92 ± 2.4	21.15 ± 1.0

generally increased during growth and the difference between wild type and P_{II} mutant got smaller at the later stages of growth but was significantly different in the first 48 h of growth (**Figure 4B**). The complemented strain had similar fatty acid levels as the wild type, but the S49E variant was not able to complement the P_{II} mutant phenotype. The difference between wild-type and P_{II} mutant in fatty acid levels during ammonia-supplemented growth was verified using GC analysis. GC results matched the values obtained with the colorimetric assay but additionally provided qualitative information, how fatty acid composition might be altered. As shown in **Table 2**, mutation of GlnB shifted the molar composition of fatty acids, which increased the amount of palmitic acid by about 15% at the same time decreasing the amount of linoleic acid to the same extent. The fatty acid profile of the P_{II} complemented strain was very similar to that of the wild type, whereas the S49E strain had a fatty acid composition reminiscent of the P_{II} mutant exemplifying that the S49E P_{II} variant is a loss-of function mutant with respect to regulation of fatty acid metabolism. Triple unsaturated fatty acids were increased in both complemented strains.

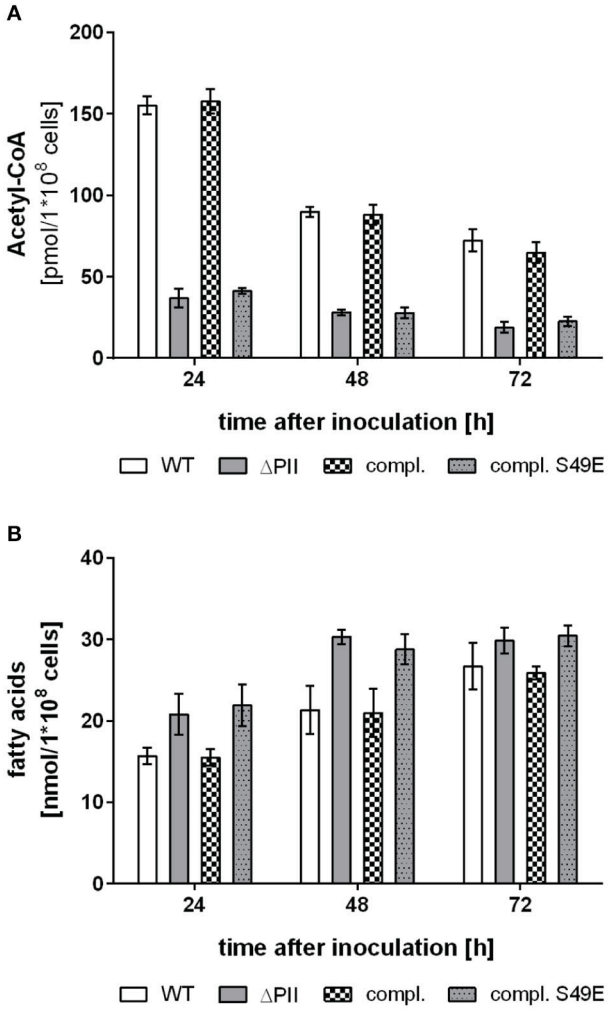

FIGURE 4 | Accumulation of acetyl-CoA (A) and fatty acids (B) during growth in standard BG11 with ammonia as nitrogen source in wild type (white bars), the P_{II} mutant (gray bars), the P_{II} complemented strain (checked bars) and the P_{II}-S49E complemented strain (gray dotted bars). Values represent the mean of three biological replicates. Differences in acetyl-CoA levels are statistically significant throughout growth between wild type and the P_{II} mutant ($p < 0.05$; unpaired *t*-test). Differences in fatty acid levels between wild type and the P_{II} mutant are statistically significant within the first 48 h of growth ($p < 0.05$; unpaired *t*-test).

Altered Acetyl-CoA Metabolism Promotes Intracellular Lipid Accumulation

Intracellular lipids can be visualized microscopically using the hydrophobic dye Bodipy® 493/503, which gives a green fluorescence and specifically stains neutral lipids (Gocze and Freeman, 1994). Therefore, we examined wild-type and P_{II} deficient mutant cells by fluorescence microscopy. A strong intracellular fluorescence signal could be detected in some wild type cells taken from early exponential phase of growth, as exemplarily shown in **Figure 5A**. The number of lipid bodies per cell was determined and is shown in **Figure 5B**. Cells of the P_{II} mutant have at least one or two lipid bodies (mean 1.6 lipid droplets per cell), whereas only few cells have lipid bodies in wild type (mean 0.39 lipid droplets per cell). Lipid droplets formed transiently in the early phase of growth and disappeared with increasing optical densities, possibly being converted to phospholipids. To gain further insights in this phenotype, total lipids were extracted from exponentially growing cultures and the phospholipid content was analyzed using thin layer chromatography. No significant difference in phospholipid content was apparent between wild type and the P_{II} mutant excluding the accumulation of phospholipids in the observed vesicles. Hence the extracts were subjected to thin layer chromatography using a system, which is able to resolve more hydrophobic lipids (**Figure 5C**). Staining with iodine vapor revealed spots occurring in both wild type and P_{II} mutant and an additional spot only present in the P_{II} mutant. These spots migrate similar to a triacylglycerol standard (composed of C12, C14 and C16 triacylglycerols) and sesame oil (a complex mixture of C16 and various C18 fatty acids containing triacylglycerols). Stained spots were scraped off, extracted and converted to fatty acid methyl esters for GC/MS analysis. The lower spot contained primarily palmitic and stearic acid and minor traces of pentadecaonic and heptadecanoic fatty acid. The upper spot present in the P_{II} mutant contained primarily palmitic and stearic fatty acids (with no pentadecaonic and heptadecanoic fatty acids present). No unsaturated C16 or C18 fatty acids could be detected in both spots.

TABLE 2 | Molar composition of fatty acids in %.

	C16	C16:1	C18	C18:1	C18:2	C18:3
Wild type	26.86 ± 0.05	10.36 ± 0.19	1.94 ± 0.8	1.01 ± 0.28	56.68 ± 0.52	3.15 ± 1.0
ΔP_{II}	42.46 ± 5.92	10.92 ± 0.78	1.26 ± 0.52	2.85 ± 0.37	41.37 ± 4.67	1.13 ± 0.4
compl.	26.82 ± 3.81	10.06 ± 1.12	3.24 ± 0.72	1.21 ± 0.17	46.52 ± 11.92	12.14± 7.34
compl. S49E	38.04 ± 7.27	8.96 ± 1.31	1.54 ± 0.25	1.74 ±0.29	37.73 ± 7.39	11.99 ± 9.32

Values represent mean values and SE of at least three biological replicates.

TABLE 3 | Bacterial strains and plasmids used in the study.

Strain/plasmid	Genotype/description	Source/reference
STRAINS		
E. coli Top10	General cloning strain	Invitrogen
E. coli BL21 (DE3)	Strain for protein expression	Invitrogen
E. coli J53 (RP4)	Helper strain for tri-parental mating	Wolk et al., 1984
Synechocystis sp. PCC6803	Wild type strain	Stanier et al., 1971
ΔP_{II}	*glnB*$^-$ strain of *Synechocystis* sp. PCC6803	Hisbergues et al., 1999
Complementation	ΔP_{II} strain complemented with P_{II}-Venus	This study
Complementation S49E	ΔP_{II} strain complemented with P_{II}S49E-Venus	This study
PLASMIDS		
pET15b	Expression vector for His-tagged proteins	Novagen
pET15*accB*	Expression of *Synechocystis* His-BCCP	This study
pCY216	Expression of *E. coli* BirA	Chapman-Smith et al., 1994
pET16b*accAD*	Expression of *E. coli* His-AccA and AccD	Soriano et al., 2006
pET16b*accC*	Expression of *E. coli* His-AccC	Soriano et al., 2006
pTRPETBCCPn	Expression of *E. coli* His-BCCP	Rodrigues et al., 2014
pASK-IBA3	Expression vector for Strep-taged proteins	IBA life sciences
pASK-IBA3*glnB*	Expression of C-terminally tagged GlnB from *Synechococcus elongatus*. PCC7942	Heinrich et al., 2004
pASK-IBA3*glnBS49D*	*Synechococcus* GlnB variant S49D	Espinosa et al., 2006
pASK-IBA3*glnBS49E*	*Synechococcus* GlnB variant S49E	Heinrich et al., 2004
pASK-IBA3*glnBR45A*	*Synechococcus* GlnB variant R45A	This study
pASK-IBA3*glnBR47A*	*Synechococcus* GlnB variant R47A	This study
pASK-IBA3*glnBS49G*	*Synechococcus* GlnB variant S49G	This study
pASK-IBA3*glnBY51A*	*Synechococcus* GlnB variant Y51A	This study
pASK-IBA3*glnBT52A*	*Synechococcus* GlnB variant T52A	This study
pASK-IBA3*glnBE54A*	*Synechococcus* GlnB variant E54A	This study
pASK-IBA3*glnBE85A*	*Synechococcus* GlnB variant E85A	This study
pASK-IBA3*glnBI86N*	*Synechococcus* GlnB variant I86N	Fokina et al., 2010b
pASK-IBA3*glnBR103H*	*Synechococcus* GlnB variant R103H	This study
pASK-IBA3*glnBSc*	Expression of C-terminally tagged GlnB from *Synechocystis* sp. PCC6803	This study
pASK-IBA3*glnBS49CSc*	*Synechocystis* GlnB variant S49C	This study
pASK-IBA3*glnBS49DSc*	*Synechocystis* GlnB variant S49D	This study
pASK-IBA3*glnBS49ESc*	*Synechocystis* GlnB variant S49E	This study
pVZ322	Broad host range expression vector	Grigorieva and Shestakov, 1982
pVZ322-P_{II}-Ven	Expression of wild type GlnB with the fluorophore Venus at the C-terminus	This study
pVZ322-P_{II}S49E-Ven	Expression of GlnB S49E variant with the fluorophore Venus at the C-terminus	This study

DISCUSSION

Previous work has demonstrated that the P_{II} protein GlnB from *A. thaliana*, as well as bacterial GlnB proteins from *Azospirillum brasilense* and *E. coli* interact with BCCP (Rodrigues et al., 2014) and change the biosynthetic activity of ACCase (Feria Bourrellier et al., 2010; Gerhardt et al., 2015). Here, the interaction of BCCP with GlnB could be confirmed for unicellular cyanobacteria, and for the first time, an implication of P_{II} signaling on acetyl-CoA metabolism could be demonstrated.

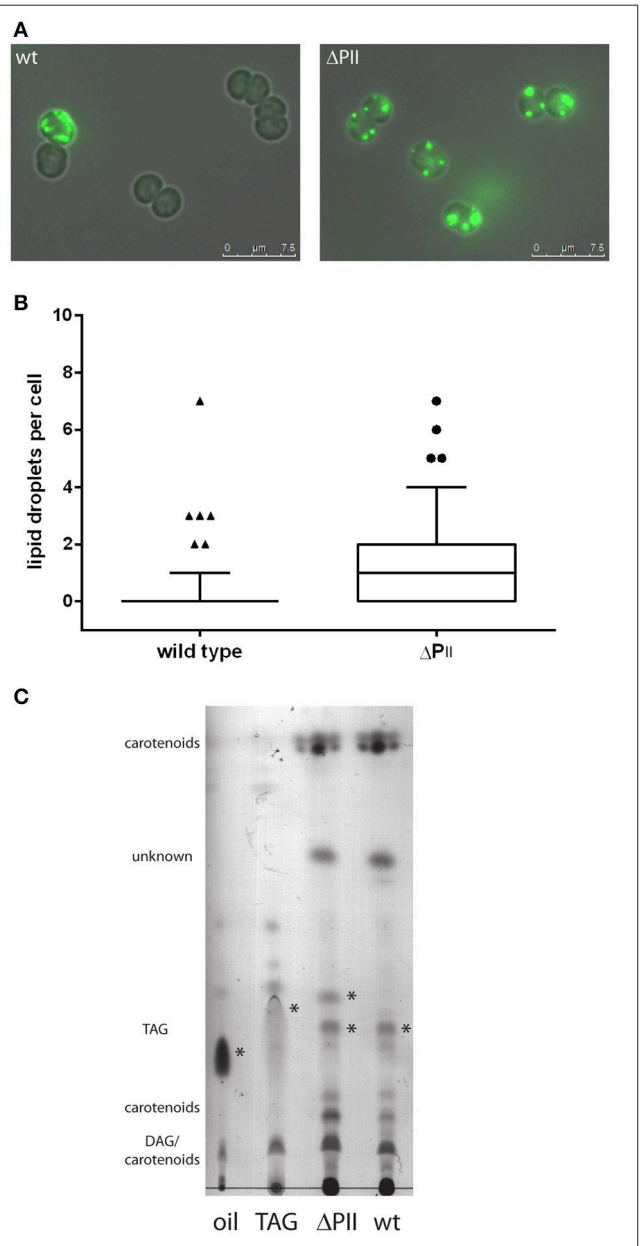

FIGURE 5 | (A) Microscopic image of wild type and P_{II} mutant stained with Bodipy 493/503 during exponential growth. Images are the superimposition of the fluorescence and bright field image. **(B)** Occurrence of lipid droplets per cell in the wild type (mean: 0.39 ± 0.12) and P_{II} mutant (mean: 1.65 ± 0.23) at an OD_{750} of 0.2. The box plot displays the 10–90 percentile. The result is statistically significant with a *p*-value smaller than 0.0001 determined by an unpaired two tailed *t*-test. **(C)** Thin layer chromatography of hydrophobic lipids. Possible triacylglycerols are marked with asterisk. *DAG: diacylglycerol TAG: triacylglycerol.*

The effect of *Synechococcus* P_{II} on the reconstituted *E. coli* ACCase activity qualitatively matches the results of protein-protein interaction determined for *Sy*P_{II}-BCCP interaction. This implies that wild-type P_{II} proteins from cyanobacteria tune down ACCase activity by binding to the BCCP subunit of ACCase, whilst a negative charge of the T-loop at position 49 (phosphomimetic mutants S49E and S49D) impairs ACCase regulation. Residue R103 of P_{II} is directly involved in salt bridge contact to the gamma-phosphate of ATP (Fokina et al., 2010a). Consequently, R103 mutants of P_{II} are affected in ATP binding and the inability of the R103 variant to regulate ACCase matches the strict ATP dependence of P_{II}-BCCP interaction. Binding of effector molecules by P_{II} tremendously alters the conformation of its T-loop (Fokina et al., 2010a; Truan et al., 2014; Zeth et al., 2014; Forchhammer and Lüddecke, 2016), suggesting that the ATP requirement for P_{II}-BCCP complex formation is due to the ATP-induced T-loop conformation of P_{II}. Occupation of all three ATP binding sites seem required in order to form a stable GlnB-BCCP complex. The complex is destabilized by 2-OG concentrations that are 4-fold higher than the affinity constant of the second binding site (Fokina et al., 2010b), suggesting that binding of 2-OG to the third binding site determines the stability of the complex. This implies that all three T-loops of GlnB, which communicate with the ligand binding sites, are involved in complex formation with BCCP. By contrast, using the reconstituted ACC from *E. coli* as assay system, GlnB mediated activity inhibition could be relieved low 2-OG concentrations (IC_{50} value of only 4.8 μM), which were well below the concentration required to inhibit formation of the BCCP-GlnB complex (42 μM). It is likely, that subtle conformational changes of the P_{II} T-loop in the GlnB-BCCP complex caused by 2-OG binding to the high affinity binding site 1 (K_d = 5.1 μM) cause this effect. A similar post-binding effect has been observed for the P_{II} target NtrB in *E. coli*, where P_{II} in complex with NtrB regulated the phosphatase activity in response to 2-OG, an effect that was termed post binding regulation (Jiang and Ninfa, 2009).

The importance of the T-loop for complex formation was clearly highlighted by the phosphomimetic variants of P_{II} where the negative charge at T-loop position 49 strongly impaired GlnB BCCP interaction. In case of the S49D variant, this could be partially overcome by applying excess ATP concentrations. Apparently, electrostatic repulsion hinders the T-loop to adopt the proper conformation for BCCP binding, which back couples to the ATP binding site. Interestingly, the charge neutral substitution S49C also had an effect on the interaction and required increased ATP concentrations (EC_{50} 143 μM) to enable GlnB BCCP interaction. This effect might be caused by sterical hindrance due to increased bulkiness of the T-loop and to compensate this distortion, increased ATP concentrations were required enforce the T–loop in the BCCP-accepting conformation. Interestingly the I86N variant, which is locked in a compact T-loop conformation (Fokina et al., 2010b) was completely unable to exhibit regulation on ACC activity, emphasizing that the T-loop conformation plays a critical role in ACC inhibition. Which specific T-loop conformation elicits inhibition of ACC remains to be elucidated from a structural biological perspective.

Gerhardt et al. (2015) demonstrated that the interaction of GlnB with ACCase tunes down the k_{cat} of the reaction 3.5 times but does not affect the K_M value of *E. coli* ACC toward acetyl-CoA, for which a K_M of 228 μM was determined. Assuming a cell volume of 0.5 μl for $1*10^8$ cells allows an estimation of the

intracellular acetyl-CoA concentration in the wild type and the P_{II} mutant. At growth conditions, where a low phosphorylation status of P_{II} is expected, and consequently, P_{II} complexed to BCCP, the acetyl-CoA concentrations of the wild type were in the range of 226–310 μM, which is close to the K_M for ACC. When conditions change toward increased P_{II} phosphorylation, dissociation of the P_{II} BCCP complex is expected and hence, acceleration of ACCase activity. This should lead to an immediate draining of the acetyl-CoA pool below the K_M for ACCase. The turn-over of the reaction will necessarily slow down and the acetyl-CoA pool will finally reach a new equilibrium. This is in fact observed during nitrogen starvation, growth with nitrate and CO_2, or the P_{II} mutant (52–74 μM). The total flux through the ACCase reaction is, however, not strongly affected in such a steady state. Solely the factor that limits the over-all reaction is different: either ACCase is limited by interaction with P_{II} (in presence of high acetyl-CoA levels) or by low acetyl-CoA levels (in the absence of P_{II} interaction). The regulatory impact of T-loop modification of P_{II} on ACCase control and acetyl-CoA levels was clearly revealed through complementation with P_{II} variants. The *in vivo* acetyl-CoA levels of the S49E complemented variant remained as low as in the P_{II} deficient mutant, but could be recovered by complementation with native P_{II}.

In line with these kinetic considerations above, the fatty acid levels in the wild type and the P_{II} mutant were quite similar under most tested conditions and only significantly different when cells were grown with ammonia (HCO_3^- or air bubbling as carbon source). Steady-state malonyl-CoA levels are 10 times lower than acetyl-CoA levels (Bennett et al., 2009). This is in agreement with the ACCase reaction being the rate-limiting step in fatty acid synthesis, whereas the condensation reaction is efficiently consuming malonyl-CoA. Therefore, the activity regulation of ACCase by P_{II} is unlikely to affect the hardly detectable cellular malonyl-CoA levels. Fatty acids are primarily present in phospholipids, which build up the outer, cytoplasmic and thylakoid membranes. Due to the abundant membrane system present in cyanobacteria, the corresponding fatty acid pool is big and less prone to fluctuations. Acetyl-CoA on the contrary is quickly turned over and used in various anabolic reactions, while the pool size is comparably low (see above) and prone to fluctuations based on the carbon or nitrogen supply. Hence, a tight regulation of ACCase is necessary to control the size of this important metabolite pool, without strongly affecting the pool of fatty acids. Interestingly the fatty acid distribution was slightly shifted toward C16 fatty acids, which were more abundant in the P_{II} mutant and the S49E complemented strain.

The two main metabolic routes which provide the cell with acetyl-CoA are CO_2 fixation through the Calvin-Benson-Bessham cycle (CBB) or degradation of glycogen through various pathways (Xiong et al., 2015; Chen et al., 2016). The biggest differences in acetyl-CoA pools were visible in the first 48 h of growth. Conversely, total fatty acid levels were slightly higher in the P_{II} mutant and the S49E complemented strain during this early period of growth. This growth period is characterized by degradation of internal carbon reserves to provide carbon and energy for growth. Furthermore, in the early growth phase, when the optical density of the culture is still low, photosynthetic activity is at its maximum. Since nitrogen is abundant in this growth phase, P_{II} should interact with ACC to keep the acetyl-CoA levels high, thereby slightly reducing the synthesis of fatty acids. The high acetyl-CoA levels could be beneficial for other anabolic reactions, which require acetyl-CoA, such as the synthesis of arginine (N-acetyl-glutamate) or leucine (synthesis of α-isopropylmalate). Furthermore, acetyl-CoA levels assure carbon flux into the citric acid cycle to maintain the GS-GOGAT cycle, which is constantly depleted through nitrogen assimilation. Moreover, high acetyl-CoA levels could play a role for protein acetylation, which was recently demonstrated to be abundant in *Synechocystis* (Mo et al., 2015), but it is so far unclear how acetylation influences the enzymatic activities of those enzymes.

Transition to the light-limited linear growth phase at higher optical densities correlated with reduced acetyl-CoA levels. In this phase of growth, light intensity decreases due to self-shading of the cells, which limits photosynthesis and slows down growth (Foster et al., 2007). This negatively affects CO_2 fixation, and consequently, the acetyl-CoA pools, replenished by CO_2 fixation products, decrease during the linear growth in the wild type and P_{II} complemented strain. As a consequence, the fatty acid levels became indistinguishable between wild-type the P_{II} deficient mutant.

The observation that throughout the growth phase, acetyl-CoA levels decreased has previously been reported also from *E. coli* (Chohnan and Takamura, 1991). These authors have argued that the carbon supply in form of glucose is key to high intracellular acetyl-CoA levels in *E. coli*. However, control by the P_{II} regulatory system might play an important role also in this case, an assumption, which requires further investigation. In contrast to the effect of P_{II} regulation in the early growth phase, other regulatory mechanisms so far known appear to inhibit ACC activity at later stages of growth (Jiang and Cronan, 1994; Meades et al., 2010).

Higher total fatty acid levels in the early exponential growth phase coincide with the transient appearance of lipid droplets, most prominently in the P_{II}-deficient mutant. Lipid droplets are best known in eukaryotes and a recent report established a connection between lipid body formation and GlnB (Zalutskaya et al., 2015). Reduced levels of GlnB protein in the eukaryotic green algae *Chlamydomonas reinhardtii* increased the amount and the size of lipid bodies. Even though lipid bodies have been previously described in *Synechocystis* using electron microscopy, they were suggested to play a role in thylakoid maintenance (van de Meene et al., 2006). Within the last decade lipid droplets have emerged as intracellular inclusions also present in heterotrophic bacteria (Kalscheuer et al., 2001; Yang et al., 2012) or the filamentous cyanobacterium *Nostoc punctiforme* (Peramuna and Summers, 2014; Perez et al., 2016), where they contain triacylglycerides, α-tocopherol and alkanes (Peramuna and Summers, 2014). Isolated lipids of *Synechocystis* migrated on TLC similar to sesame oil and a triacylglycerol mixture and GC/MS analysis revealed that they primarily contained C16 and C18 saturated fatty acids with traces of pentadecanoic and heptadecanoic acid as has been observed in exponentially grown *N. punctiforme* (Peramuna and Summers, 2014). These lipids must therefore be triacylglycerols as TLC and GC/MS analysis

suggest, even though diacylglycerol acyltransferase homologs are absent in the genome of *Synechocystis*. Lipid droplets disappeared in the later phases of growth and probably represent a dynamic reservoir for fatty acid storage (in form of TAG) and turnover (Yang et al., 2012). Although no triacylglycerol synthase has been identified in the genome of *Synechocystis*, the presence of a triacylglycerol lipase encoded by *sll1969* supports a functional triacyl-glycerol metabolism in this strain. This suggests a hitherto unknown triacylglycerol synthase in *Synechocystis* PCC 6803.

Taken together, this study showed that BCCP-GlnB interaction is present in the cyanobacterial linage and must have arose early in the evolution of P_{II} proteins, as it is present in distantly related bacterial lineages (Feria Bourrellier et al., 2010; Gerhardt et al., 2015). This regulation has later been transferred to the plant kingdom through cyanobacterial endosymbiosis, where it has been conserved in plant metabolism (Feria Bourrellier et al., 2010; Zalutskaya et al., 2015). The present study shows that interaction with BCCP allows P_{II} to control the cellular acetyl-CoA levels. P_{II} regulation of ACCase provides the opportunity for an intriguing regulatory feedback loop: low 2-OG levels promote P_{II}-ACCase interaction and cause an increase in acetyl-CoA levels through restriction of ACCase activity. In turn, this could promote the flux into the oxidative branch of the TCA cycle, leading to increased 2-OG levels. Such a feedback loop could help in maintaining and balancing the 2-OG levels under nitrogen-rich conditions, but requires further investigation and experimental verification. Once carbon supply is limited, this is sensed by P_{II} through low 2-OG levels and according to our data, this enables the cell to limit fatty acid synthesis more efficiently than in the absence of P_{II} regulation. The fact that this interaction is conserved from bacteria to plants indicates a considerable selective advantage in fine-tuning metabolic homeostasis.

AUTHOR CONTRIBUTIONS

EG: Performed and designed experiments with reconstituted *E. coli* ACC; KS: Performed and designed pull-down experiments, acetyl-CoA and total fatty acid quantifications; WH: Performed lipid analysis, designed and analyzed pull-down experiments, acetyl-CoA and total fatty acid quantifications; KF: Supervised the work and conceived and wrote the manuscript with LH and WH; All authors have read and approved the manuscript.

FUNDING

This work was supported by DFG grant Fo195/9-2 and RTG1708. EG and LH acknowledge CNPq, INCT, CAPES and Fundação Araucária for the financial support.

ACKNOWLEDGMENTS

We thank Thomas Härtner for technical support and fatty acid analysis.

SUPPLEMENTARY MATERIAL

The Supplementary Material for this article can be found online at: http://journal.frontiersin.org/article/10.3389/fmicb.2016.01700/full#supplementary-material

REFERENCES

Anfelt, J., Kaczmarzyk, D., Shabestary, K., Renberg, B., Rockberg, J., Nielsen, J., et al. (2015). Genetic and nutrient modulation of acetyl-CoA levels in Synechocystis for n-butanol production. *Microb. Cell Fact.* 14, 167. doi: 10.1186/s12934-015-0355-9

Beez, S., Fokina, O., Herrmann, C., and Forchhammer, K. (2009). N-Acetyl-L-Glutamate Kinase (NAGK) from oxygenic phototrophs: P-II signal transduction across domains of life reveals novel insights in NAGK control. *J. Mol. Biol.* 389, 748–758. doi: 10.1016/j.jmb.2009.04.053

Bennett, B. D., Kimball, E. H., Gao, M., Osterhout, R., Van Dien, S. J., and Rabinowitz, J. D. (2009). Absolute metabolite concentrations and implied enzyme active site occupancy in *Escherichia coli*. *Nat. Chem. Biol.* 5, 593–599. doi: 10.1038/nchembio.186

Bligh, E. G., and Dyer, W. J. (1959). A rapid method of total lipid extraction and purification. *Can. J. Biochem. Physiol.* 37, 911–917. doi: 10.1139/o59-099

Broussard, T. C., Price, A. E., Laborde, S. M., and Waldrop, G. L. (2013). Complex formation and regulation of *Escherichia coli* acetyl-CoA carboxylase. *Biochemistry* 52, 346–3357. doi: 10.1021/bi4000707

Chapman-Smith, A., Turner, D. L., Cronan, J. E. Jr., Morris, T. W., and Wallace, J. C. (1994). Expression, biotinylation and purification of a biotin-domain peptide from the biotin carboxy carrier protein of *Escherichia coli* acetyl-CoA carboxylase. *Biochem. J.* 302(Pt 3), 881–887. doi: 10.1042/bj3020881

Chen, X., Schreiber, K., Appel, J., Makowka, A., Fähnrich, B., Roettger, M., et al. (2016). The entner-doudoroff pathway is an overlooked glycolytic route in cyanobacteria and plants. *Proc. Natl. Acad. Sci. U.S.A.* 113, 5441–5446. doi: 10.1073/pnas.1521916113

Chohnan, S., and Takamura, Y. (1991). A Simple micromethod for measurement of CoASH and its use in measuring intracellular levels of CoASH and short chain Acyl-CoAs in *Escherichia coli* K12 cells. *Agric. Biol. Chem.* 55, 87–94. doi: 10.1271/bbb1961.55.87

Cronan, J. E. Jr., and Waldrop, G. L. (2002). Multi-subunit acetyl-CoA carboxylases. *Prog. Lipid Res.* 41, 407–435. doi: 10.1016/S0163-7827(02)00007-3

Davis, M. S., Solbiati, J., and Cronan, J. E. Jr. (2000). Overproduction of acetyl-CoA carboxylase activity increases the rate of fatty acid biosynthesis in *Escherichia coli*. *J. Biol. Chem.* 275, 28593–28598. doi: 10.1074/jbc.M004756200

Eisenhut, M., Huege, J., Schwarz, D., Bauwe, H., Kopka, J., and Hagemann, M. (2008). Metabolome phenotyping of inorganic carbon limitation in cells of the wild type and photorespiratory mutants of the cyanobacterium *Synechocystis* sp strain PCC 6803. *Plant Physiol.* 148, 2109–2120. doi: 10.1104/pp.108.129403

Espinosa, J., Castells, M. A., Laichoubi, K. B., and Contreras, A. (2009). Mutations at pipX suppress lethality of PII-deficient mutants of *Synechococcus elongatus* PCC 7942. *J. Bacteriol.* 191, 4863–4869. doi: 10.1128/JB.00557-09

Espinosa, J., Forchhammer, K., Burillo, S., and Contreras, A. (2006). Interaction network in cyanobacterial nitrogen regulation: PipX, a protein that interacts in a 2-oxoglutarate dependent manner with PII and NtcA. *Mol. Microbiol.* 61, 457–469. doi: 10.1111/j.1365-2958.2006.05231.x

Feria Bourrellier, A. B., Valot, B., Guillot, A., Ambard-Bretteville, F., Vidal, J., and Hodges, M. (2010). Chloroplast acetyl-CoA carboxylase activity is 2-oxoglutarate-regulated by interaction of PII with the biotin carboxyl carrier subunit. *Proc. Natl. Acad. Sci. U.S.A.* 107, 502–507. doi: 10.1073/pnas.0910097107

Fokina, O., Chellamuthu, V. R., Forchhammer, K., and Zeth, K. (2010a). Mechanism of 2-oxoglutarate signaling by the *Synechococcus elongatus* PII signal transduction protein. *Proc. Natl. Acad. Sci. U.S.A.* 107, 19760–19765. doi: 10.1073/pnas.1007653107

Fokina, O., Chellamuthu, V. R., Zeth, K., and Forchhammer, K. (2010b). A novel signal transduction protein P-II variant from *Synechococcus elongatus* PCC

7942 indicates a two-step process for NAGK-P-II complex formation. *J. Mol. Biol.* 399, 410–421. doi: 10.1016/j.jmb.2010.04.018

Fokina, O., Herrmann, C., and Forchhammer, K. (2011). Signal-transduction protein P-II from *Synechococcus elongatus* PCC 7942 senses low adenylate energy charge *in vitro*. *Biochem. J.* 440, 147–156. doi: 10.1042/BJ20110536

Forchhammer, K., and Lüddecke, J. (2016). Sensory properties of the PII signalling protein family. *FEBS J.* 283, 425–437. doi: 10.1111/febs.13584

Forchhammer, K., and Tandeau de Marsac, N. (1995a). Functional analysis of the phosphoprotein PII (glnB gene product) in the cyanobacterium *Synechococcus* sp. strain PCC 7942. *J. Bacteriol.* 177, 2033–2040.

Forchhammer, K., and Tandeau de Marsac, N. (1995b). Phosphorylation of the PII protein (glnB gene product) in the cyanobacterium *Synechococcus* sp. strain PCC 7942: analysis of *in vitro* kinase activity. *J. Bacteriol.* 177, 5812–5817.

Foster, J. S., Singh, A. K., Rothschild, L. J., and Sherman, L. A. (2007). Growth-phase dependent differential gene expression in *Synechocystis* sp. strain PCC 6803 and regulation by a group 2 sigma factor. *Arch. Microbiol.* 187, 265–279. doi: 10.1007/s00203-006-0193-6

Gerhardt, E. C., Rodrigues, T. E., Müller-Santos, M., Pedrosa, F. O., Souza, E. M., Forchhammer, K., et al. (2015). The bacterial signal transduction protein GlnB regulates the committed step in fatty acid biosynthesis by acting as a dissociable regulatory subunit of acetyl-CoA carboxylase. *Mol. Microbiol.* 95, 1025–1035. doi: 10.1111/mmi.12912

Gibson, D. G., Young, L., Chuang, R. Y., Venter, J. C., Hutchison, C. A., and Smith, H. O. (2009). Enzymatic assembly of DNA molecules up to several hundred kilobases. *Nat. Methods* 6, 343–345. doi: 10.1038/nmeth.1318

Gocze, P. M., and Freeman, D. A. (1994). Factors underlying the variability of lipid droplet fluorescence in MA-10 Leydig tumor cells. *Cytometry* 17, 151–158. doi: 10.1002/cyto.990170207

Grigorieva, G., and Shestakov, S. (1982). Transformation in the cyanobacterium *Synechocystis* sp. 6803. *Fems Microbiol. Lett.* 13, 367–370. doi: 10.1111/j.1574-6968.1982.tb08289.x

Hauf, W., Schlebusch, M., Hüge, J., Kopka, J., Hagemann, M., and Forchhammer, K. (2013). Metabolic changes in Synechocystis PCC6803 upon nitrogen-starvation: excess NADPH sustains polyhydroxybutyrate accumulation. *Metabolites* 3, 101–118. doi: 10.3390/metabo3010101

Heinrich, A., Maheswaran, M., Ruppert, U., and Forchhammer, K. (2004). The *Synechococcus elongatus* P-II signal transduction protein controls arginine synthesis by complex formation with N-acetyl-L-glutamate kinase. *Mol. Microbiol.* 52, 1303–1314. doi: 10.1111/j.1365-2958.2004.04058.x

Hisbergues, M., Jeanjean, R., Joset, F., Tandeau de Marsac, N., and Bédu, S. (1999). Protein PII regulates both inorganic carbon and nitrate uptake and is modified by a redox signal in Synechocystis PCC 6803. *FEBS Lett.* 463, 216–220. doi: 10.1016/S0014-5793(99)01624-5

Hondo, S., Takahashi, M., Osanai, T., Matsuda, M., Hasunuma, T., Tazuke, A., et al. (2015). Genetic engineering and metabolite profiling for overproduction of polyhydroxybutyrate in cyanobacteria. *J. Biosci. Bioeng.* 120, 510–517. doi: 10.1016/j.jbiosc.2015.03.004

Jiang, P., and Cronan, J. E. Jr. (1994). Inhibition of fatty acid synthesis in *Escherichia coli* in the absence of phospholipid synthesis and release of inhibition by thioesterase action. *J. Bacteriol.* 176, 2814–2821.

Jiang, P., and Ninfa, A. J. (2009). Alpha-ketoglutarate controls the ability of the *Escherichia coli* PII signal transduction protein to regulate the activities of NRII (NrB but does not control the binding of PII to NRII. *Biochemistry* 48, 11514–11521. doi: 10.1021/bi901158h

Joseph, A., Aikawa, S., Sasaki, K., Teramura, H., Hasunuma, T., Matsuda, F., et al. (2014). Rre37 stimulates accumulation of 2-oxoglutarate and glycogen under nitrogen starvation in *Synechocystis* sp. PCC 6803. *FEBS Lett.* 588, 466–471. doi: 10.1016/j.febslet.2013.12.008

Kalscheuer, R., Wältermann, M., Alvarez, M., and Steinbüchel, A. (2001). Preparative isolation of lipid inclusions from *Rhodococcus opacus* and *Rhodococcus ruber* and identification of granule-associated proteins. *Arch. Microbiol.* 177, 20–28. doi: 10.1007/s00203-001-0355-5

Leigh, J. A., and Dodsworth, J. A. (2007). Nitrogen regulation in bacteria and archaea. *Annu. Rev. Microbiol.* 61, 349–377. doi: 10.1146/annurev.micro.61.080706.093409

Liu, X., Sheng, J., and Curtiss, R. III. (2011). Fatty acid production in genetically modified cyanobacteria. *Proc. Natl. Acad. Sci. U.S.A.* 108, 6899–6904. doi: 10.1073/pnas.1103014108

Llácer, J. L., Contreras, A., Forchhammer, K., Marco-Marín, C., Gil-Ortiz, F., Maldonado, R., et al. (2007). The crystal structure of the complex of PII and acetylglutamate kinase reveals how PII controls the storage of nitrogen as arginine. *Proc. Natl. Acad. Sci. U.S.A.* 104, 17644–17649. doi: 10.1073/pnas.0705987104

Llácer, J. L., Espinosa, J., Castells, M. A., Contreras, A., Forchhammer, K., and Rubio, V. (2010). Structural basis for the regulation of NtcA-dependent transcription by proteins PipX and PII. *Proc. Natl. Acad. Sci. U.S.A.* 107, 15397–15402. doi: 10.1073/pnas.1007015107

Lüddecke, J., and Forchhammer, K. (2013). From PII signaling to metabolite sensing, a novel 2-oxoglutarate sensor that details PII-NAGK complex formation. *PLoS ONE* 8:e83181. doi: 10.1371/journal.pone.0083181

Lüddecke, J., and Forchhammer, K. (2015). Energy sensing versus 2-Oxoglutarate dependent ATPase switch in the control of Synechococcus PII interaction with its targets NAGK and PipX. *PLoS ONE* 10:e0137114. doi: 10.1371/journal.pone.0137114

Ma, C. W., Lüddecke, J., Forchhammer, K., and Zeng, A. P. (2014). Population shift of binding pocket size and dynamic correlation analysis shed new light on the anticooperative mechanism of PII protein. *Proteins* 82, 1048–1059. doi: 10.1002/prot.24477

Maheswaran, M., Urbanke, C., and Forchhammer, K. (2004). Complex formation and catalytic activation by the PII signaling protein of N-acetyl-L-glutamate kinase from *Synechococcus elongatus* strain PCC 7942. *J. Biol. Chem.* 279, 55202–55210. doi: 10.1074/jbc.M410971200

Meades, G. Jr., Benson, B. K., Grove, A., and Waldrop, G. L. (2010). A tale of two functions: enzymatic activity and translational repression by carboxyltransferase. *Nucleic Acids Res.* 38, 1217–1227. doi: 10.1093/nar/gkp1079

Merrick, M. (2014). Post-translational modification of P II signal transduction proteins. *Front. Microbiol.* 5:763. doi: 10.3389/fmicb.2014.00763

Merritt, M. V., Rosenstein, S. P., Loh, C., Chou, R. H. S., and Allen, M. M. (1991). A comparison of the major lipid classes and fatty-acid composition of Marine unicellular cyanobacteria with fresh-water species. *Arch. Microbiol.* 155, 107–113. doi: 10.1007/BF00248602

Mo, R., Yang, M., Chen, Z., Cheng, Z., Yi, X., Li, C., et al. (2015). Acetylome analysis reveals the involvement of lysine acetylation in photosynthesis and carbon metabolism in the model cyanobacterium *Synechocystis* sp. PCC 6803. *J. Proteome Res.* 14, 1275–1286. doi: 10.1021/pr501275a

Muro-Pastor, M. I., Reyes, J. C., and Florencio, F. J. (2001). Cyanobacteria perceive nitrogen status by sensing intracellular 2-oxoglutarate levels. *J. Biol. Chem.* 276, 38320–38328. doi: 10.1074/jbc.M105297200

Osanai, T., Oikawa, A., Iijima, H., Kuwahara, A., Asayama, M., Tanaka, K., et al. (2014). Metabolomic analysis reveals rewiring of *Synechocystis* sp. PCC 6803 primary metabolism by ntcA overexpression. *Environ. Microbiol.* 16, 3304–3317. doi: 10.1111/1462-2920.12554

Peramuna, A., and Summers, M. L. (2014). Composition and occurrence of lipid droplets in the cyanobacterium *Nostoc punctiforme*. *Arch. Microbiol.* 196, 881–890. doi: 10.1007/s00203-014-1027-6

Perez, R., Forchhammer, K., Salerno, G., and Maldener, I. (2016). Clear differences in metabolic and morphological adaptations of akinetes of two Nostocales living in different habitats. *Microbiology* 162, 214–223. doi: 10.1099/mic.0.000230

Rippka, R., Deruelles, J., Waterbury, J. B., Herdman, M., and Stanier, R. Y. (1979). Generic assignments, strain histories and properties of pure cultures of cyanobacteria. *J. Gen. Microbiol.* 111, 1–61. doi: 10.1099/00221287-111-1-1

Rodrigues, T. E., Gerhardt, E. C., Oliveira, M. A., Chubatsu, L. S., Pedrosa, F. O., Souza, E. M., et al. (2014). Search for novel targets of the PII signal transduction protein in Bacteria identifies the BCCP component of acetyl-CoA carboxylase as a PII binding partner. *Mol. Microbiol.* 91, 751–761. doi: 10.1111/mmi.12493

Ruiz-López, N., Martínez-Force, E., and Garcés, R. (2003). Sequential one-step extraction and analysis of triacylglycerols and fatty acids in plant tissues. *Anal. Biochem.* 317, 247–254. doi: 10.1016/S0003-2697(03)00139-8

Schägger, H. (2006). Tricine-SDS-PAGE. *Nat. Protoc.* 1, 16–22. doi: 10.1038/nprot.2006.4

Schlebusch, M., and Forchhammer, K. (2010). Requirement of the nitrogen starvation-induced protein Sll0783 for polyhydroxybutyrate accumulation in *Synechocystis* sp. strain PCC 6803. *Appl. Environ. Microbiol.* 76, 6101–6107. doi: 10.1128/AEM.00484-10

Smith, A. C., and Cronan, J. E. (2014). Evidence against translational repression by the carboxyltransferase component of *Escherichia coli* acetyl coenzyme A carboxylase. *J. Bacteriol.* 196, 3768–3775. doi: 10.1128/JB.02091-14

Soriano, A., Radice, A. D., Herbitter, A. H., Langsdorf, E. F., Stafford, J. M., Chan, S., et al. (2006). *Escherichia coli* acetyl-coenzyme A carboxylase: characterization and development of a high-throughput assay. *Anal. Biochem.* 349, 268–276. doi: 10.1016/j.ab.2005.10.044

Stanier, R. Y., Kunisawa, R., Mandel, M., and Cohen-Bazire, G. (1971). Purification and properties of unicellular blue-green algae (order Chroococcales). *Bacteriol. Rev.* 35, 171–205.

Tan, X., Yao, L., Gao, Q., Wang, W., Qi, F., and Lu, X. (2011). Photosynthesis driven conversion of carbon dioxide to fatty alcohols and hydrocarbons in cyanobacteria. *Metab. Eng.* 13, 169–176. doi: 10.1016/j.ymben.2011.01.001

Truan, D., Bjelic, S., Li, X. D., and Winkler, F. K. (2014). Structure and thermodynamics of effector molecule binding to the nitrogen signal transduction PII protein GlnZ from *Azospirillum brasilense*. *J. Mol. Biol.* 426, 2783–2799. doi: 10.1016/j.jmb.2014.05.008

van de Meene, A. M., Hohmann-Marriott, M. F., Vermaas, W. F., and Roberson, R. W. (2006). The three-dimensional structure of the Cyanobacterium *Synechocystis* sp. PCC 6803. *Arch. Microbiol.* 184, 259–270. doi: 10.1007/s00203-005-0027-y

Wang, Z., and Benning, C. (2011). *Arabidopsis thaliana* polar glycerolipid profiling by Thin Layer Chromatography (TLC) coupled with Gas-Liquid Chromatography (GLC). *J. Vis. Exp.* 2518. doi: 10.3791/2518

Wawrik, B., and Harriman, B. H. (2010). Rapid, colorimetric quantification of lipid from algal cultures. *J. Microbiol. Methods* 80, 262–266. doi: 10.1016/j.mimet.2010.01.016

Wolk, C. P., Vonshak, A., Kehoe, P., and Elhai, J. (1984). Construction of shuttle vectors capable of conjugative transfer from *Escherichia coli* to nitrogen-fixing filamentous cyanobacteria. *Proc. Natl. Acad. Sci. U.S.A.* 81, 1561–1565. doi: 10.1073/pnas.81.5.1561

Xiong, W., Lee, T. C., Rommelfanger, S., Gjersing, E., Cano, M., Maness, P. C., et al. (2015). Phosphoketolase pathway contributes to carbon metabolism in cyanobacteria. *Nat. Plants* 2:15187. doi: 10.1038/nplants.2015.187

Yang, L., Ding, Y., Chen, Y., Zhang, S., Huo, C., Wang, Y., et al. (2012). The proteomics of lipid droplets: structure, dynamics, and functions of the organelle conserved from bacteria to humans. *J. Lipid Res.* 53, 1245–1253. doi: 10.1194/jlr.R024117

Zalutskaya, Z., Kharatyan, N., Forchhammer, K., and Ermilova, E. (2015). Reduction of PII signaling protein enhances lipid body production in *Chlamydomonas reinhardtii*. *Plant Sci.* 240, 1–9. doi: 10.1016/j.plantsci.2015.08.019

Zeth, K., Fokina, O., and Forchhammer, K. (2014). Structural basis and target-specific modulation of ADP sensing by the *Synechococcus elongatus* PII signaling protein. *J. Biol. Chem.* 289, 8960–8972. doi: 10.1074/jbc.M113.536557

Zha, W., Rubin-Pitel, S. B., Shao, Z., and Zhao, H. (2009). Improving cellular malonyl-CoA level in *Escherichia coli* via metabolic engineering. *Metab. Eng.* 11, 192–198. doi: 10.1016/j.ymben.2009.01.005

Conflict of Interest Statement: The authors declare that the research was conducted in the absence of any commercial or financial relationships that could be construed as a potential conflict of interest.

7.2 Supplementary information

Supplementary Figure 1: Phosphorylation status of P_{II} during different growth regimes

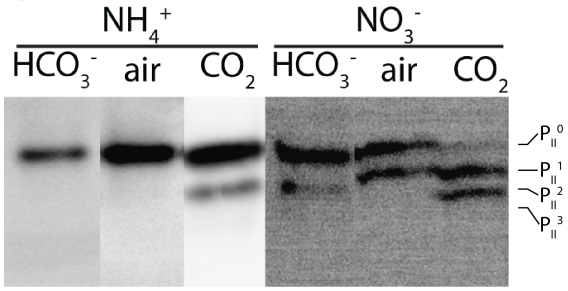

8 Additional results

8.1 Regulatory impact of GlnB on PHB metabolism

8.1.1 Complementation of the P_{II} mutant

8.1.1.1 Localization of P_{II}-Venus during growth

A P_{II} mutant of *Synechocystis* sp. PCC683, created by disrupting the open reading frame of *glnB* (*ssl0707*) with a spectinomycin resistance cassette (Hisbergues et al., 1999), was described to be affected in PHB accumulation upon nitrogen starvation but not during phosphate starvation (Schlebusch, 2012). To determine whether this is due to mutation of *glnB* or a secondary mutation, the P_{II} mutant was complemented with pVZ322-P_{II}. Since P_{II} is highly phosphorylated during nitrogen starvation (Forchhammer and Tandeau de Marsac, 1994) the P_{II} mutant was also complemented with P_{II} phosphomimetic variants P_{II}S49D, P_{II}S49E and a non phosphorylatable P_{II}S49C variant. P_{II}-proteins were translationally fused to Venus (a brighter Yfp variant) to determine whether localization of GlnB *in vivo* behaved as expected from *in vitro* experiments. Complementation was performed as described by Wolk et al. (1984). Expression and translation of GlnB was verified using fluorescence microscopy and is shown in figure 8.1.

P_{II}-Venus was expressed and visible using fluorescence microscopy. Localization of P_{II}-Venus is shown in figure 8.1 A. Venus fluorescence was not equally distributed throughout the cytoplasm and could be divided in three zones. In most cells the center and periphery of a cell harbored a strong fluorescence signal. A weak or no fluorescence intensity signal was seen in the rest of the cell. The strong signal in the center of the cell is the cytoplasm where catabolic and anabolic reactions take place. Some anabolic reactions are regulated by GlnB explaining the high Venus fluorescence (Heinrich et al., 2004). Transport of ammonium in proteobacteria (Gruswitz et al., 2007; Conroy et al., 2007) and nitrate transport in cyanobacteria have been shown to be GlnB regulated (Hisbergues et al., 1999). Hence, localization of GlnB at the periphery shows the *in vivo* interaction of P_{II} with its targets at the cytoplasmic membrane. The area which shows low or no Venus fluorescence is occupied by thylakoid membranes, therefore no fluorescence can be detected there. Surprisingly Venus fluorescence in the P_{II} S49C variant localized more strongly at the cell membrane. It was almost absent in the cytoplasm indicating that this variant might have a higher affinity to a target localized in the cytoplasmic membrane than wild type P_{II} protein (figure 8.1 B). The two phosphomimetic variants S49D/S49E, which were expected to be primarily localized in the cytoplasm were also detected at the cytoplasmic membrane. The S49D variant (figure 8.1 C) was mostly localized in the cytoplasm, but some regions of cytoplasmic membrane were stained as well. The fluorescence signal at the membrane was not as strong as with the wild type protein. The S49E variant had an almost wild type like distribution and was detected in the cytoplasm as well as at the cytoplasmic membrane (8.1 D). Kobayashi et al. (2005) have reported that phosphomimetic variants of P_{II} were able to regulate nitrate uptake in *Synechocystis* sp. PCC 6803 which is consistent

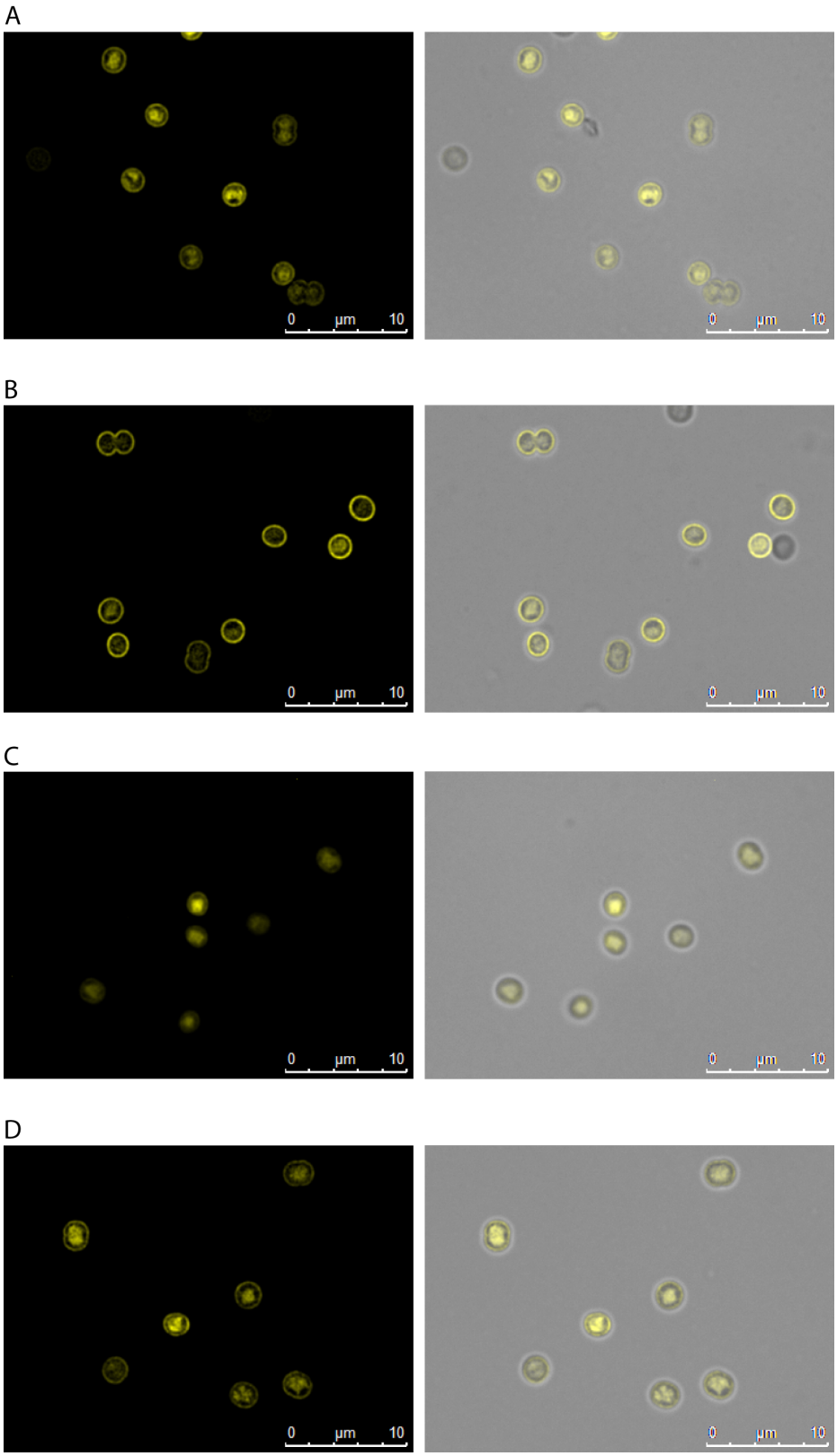

Fig. 8.1: Fluorescence microscopic images of P_{II} -Venus complemented strains during exponential growth, depicts the localization of the P_{II}-Venus fusion protein within the cell. A: P_{II} -Venus, B: P_{II}S49C-Venus, C: P_{II}S49D-Venus, D: P_{II}S49E-Venus.

with S49D/E localization to the cytoplasmic membrane. To exclude that these localization patterns were caused by differential expression of GlnB variants or protein instability, expression of GlnB was investigated using western blot analysis using an α-Gfp primary antibody (figure 8.2). Equal amounts of total protein were loaded and similar amounts of GlnB were present in all strains with slightly reduced levels of the S49D variant.

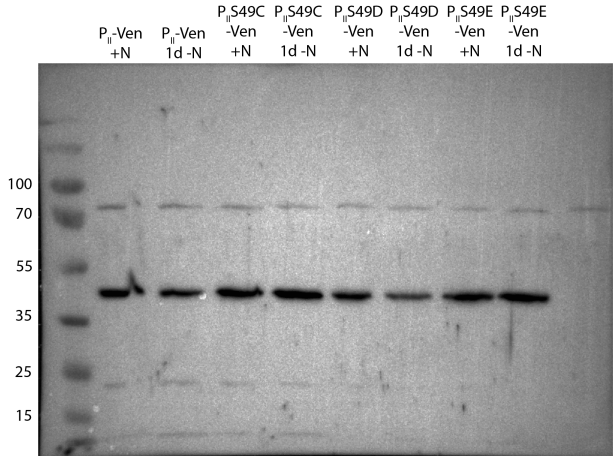

Fig. 8.2: Expression of P_{II} -Venus variants during exponential growth and 1 d nitrogen starvation was tested by western blot with primary antibodies against the P_{II} protein.

8.1.1.2 Localization of P_{II}-Venus during nitrogen starvation

The low PHB phenotype of the P_{II} mutant is observed during nitrogen starvation. Since the role of GlnB during nitrogen starvation remains unclear, localization of P_{II} -Venus was investigated during nitrogen starvation.

To do so, exponentially growing P_{II} complemented strains were transferred in $BG11_{-N}$ to induce chlorosis and imaged using fluorescence microscopy (8.3). Strikingly the distribution of GlnB within the cell changed dramatically. P_{II} was now more evenly distributed throughout the cytoplasm and localization to the cytoplasmic membrane was not as distinct as during exponential growth (figure 8.3 A). This is in agreement with the presumed role of GlnB, which is to inhibit transport of nitrogen sources when nitrogen is abundant. Once the low cellular nitrogen supply is signaled by increasing 2-oxoglutarate levels perceived by P_{II}, it dissociates from its targets. Dissociation reliefs target proteins from inhibition enabling transport of nitrogen sources at full capacity. This explains the reduced fluorescence signal at the cytoplasmic membrane. Another distinct feature is that expression and presence of P_{II} -Venus in individual cell became more heterogeneous. Whilst P_{II} -Venus fluorescence was detectable in almost all cells during exponential growth, this changed upon nitrogen starvation and more cells devoid of Venus fluorescence could be detected. Strikingly localization of GlnB-Venus changed completely in some cells and a spot like localization was visible. These cells are marked with white arrowheads in figure 8.3. Chlorosis involves the degradation of proteins in order to adapt to the low nitrogen

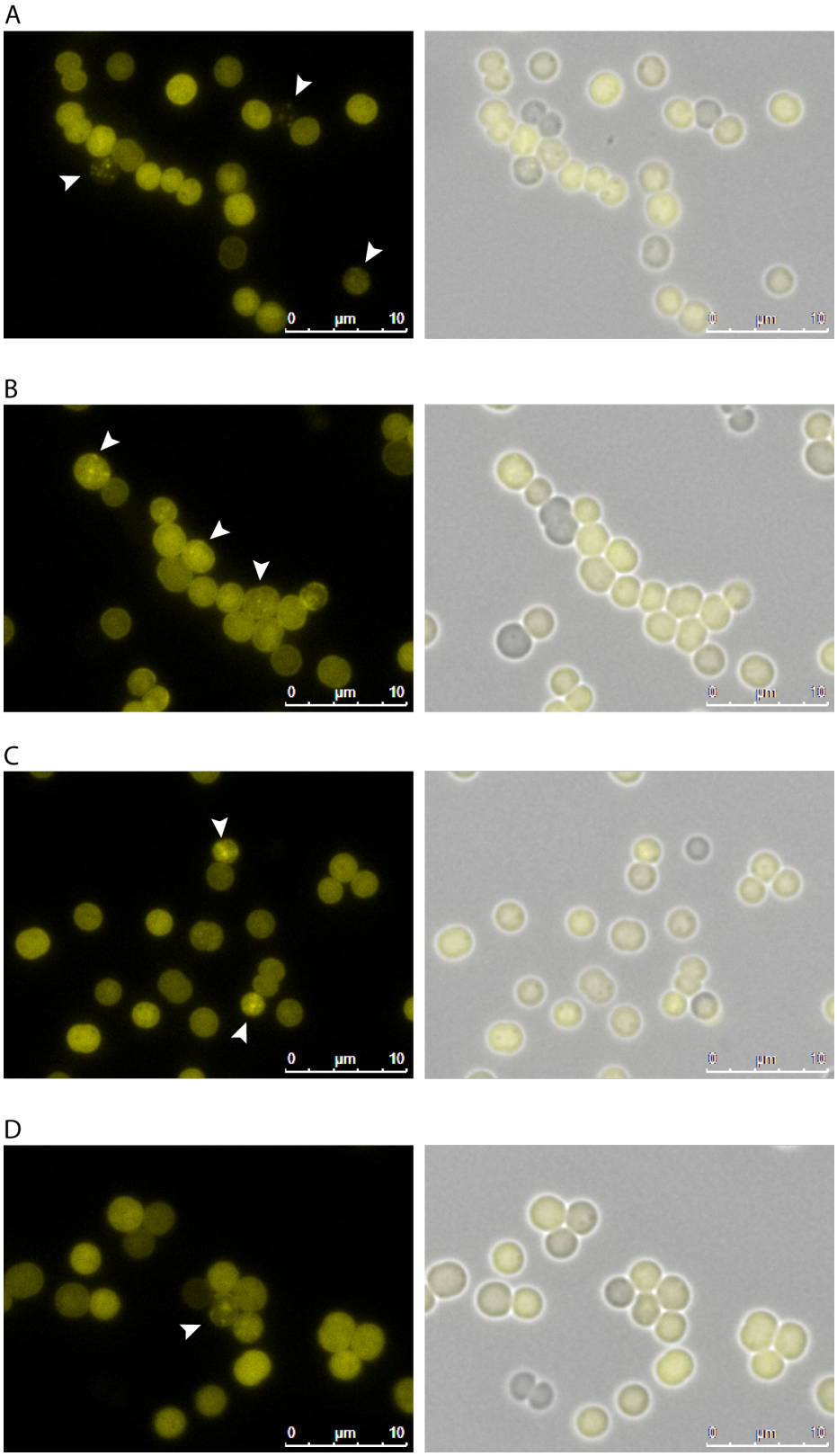

Fig. 8.3: Fluorescence microscopic images of P_{II} -Venus complemented strains after 4 days of nitrogen starvation, shows the localization of the P_{II}-Venus fusion protein within the cell.. A: P_{II} -Venus, B: P_{II}S49C-Venus, C: P_{II}S49D-Venus, D: P_{II}S49E-Venus. Cells with spot-like localization of P_{II} -Venus variants are marked with white arrowheads.

availability. Hence, the observed spot like localization might be degradation of GlnB-Venus. Alternatively the spot like accumulation might be an immobilization of P_{II} in the cytoplasm with a so far unknown target protein. No major differences were visible between the different P_{II} variants. Only the P_{II} S49C variant seemed to be better retained at the cytoplasmic membrane. As GlnB is phosphorylated during nitrogen starvation, no big differences between wild type and phosphomimetic variants were expected. Redistribution of the non phoshporylatable S49C variant in the cytoplasm indicates that binding of 2-oxoglutarate, which accumulates under nitrogen starvation, is physiologically more important for target association than phosphorylation.

8.1.2 PHB metabolism in the P_{II} mutant and complemented strains

8.1.2.1 PHB accumulation in the P_{II} mutant

To test whether complementation of the P_{II} mutant has restored PHB accumulation, complemented strains were subjected to nitrogen starvation and the PHB content was determined. The result is shown in figure 8.4.

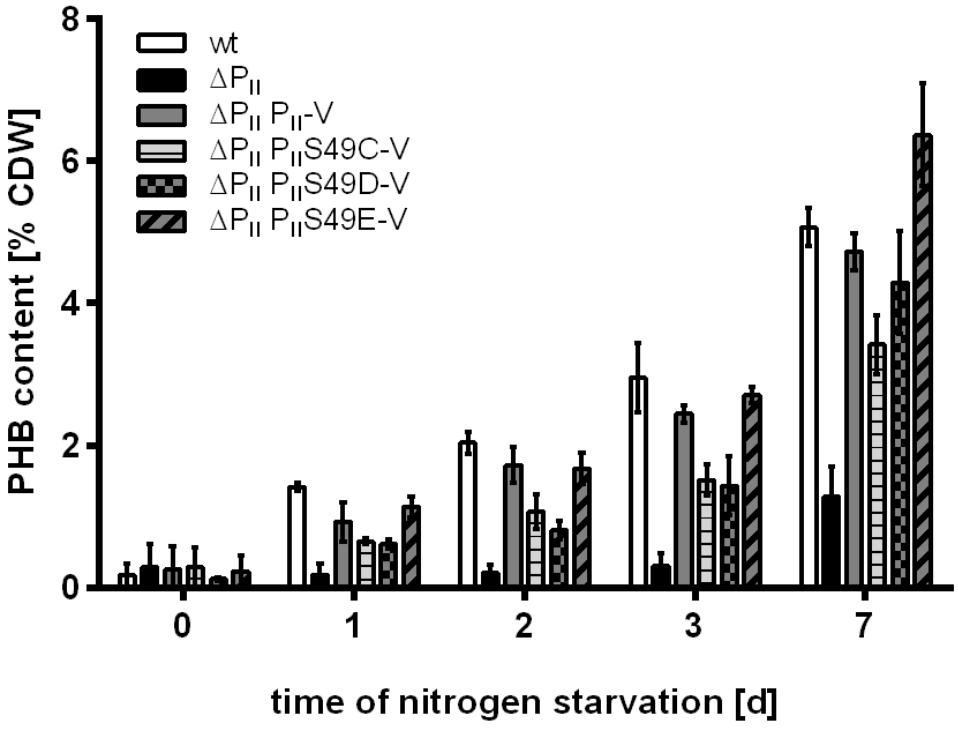

Fig. 8.4: PHB accumulation in wild type and P_{II} mutant complemented strains during nitrogen starvation in. The PHB content is measured in % cell dry weight (CDW). *wild type (white bars), P_{II} mutant (black bars), P_{II}-Venus complemented strain (grey bar), P_{II}S49C-Venus complemented strain (grey horizontal striped bar), P_{II}S49D-Venus complemented strain (grey-black checked bar), P_{II}S49E-Venus complemented strain (grey diagonal striped bar)*

All complemented strains accumulated more PHB than the P_{II} mutant. PHB accu-

mulation in the S49C and S49D variants was slightly delayed whereas the S49E variant accumulated even more PHB than the wild type. As a consequence the mutation of P_{II} is the cause for reduced PHB accumulation. Presence of GlnB is sufficient to complement the observed phenotype. In addition phosphorylation of GlnB is not a major factor regulating PHB accumulation.

8.1.2.2 Influence of GlnB on PHB synthase activity

As PHB accumulation relies on a complex regulatory program to take place, several factors were investigated which have an influence on PHB accumulation. To determine whether low PHB-synthase activities were the reason for reduced PHB accumulation in the P_{II} mutant, PHB-synthase activity was measured during nitrogen starvation.

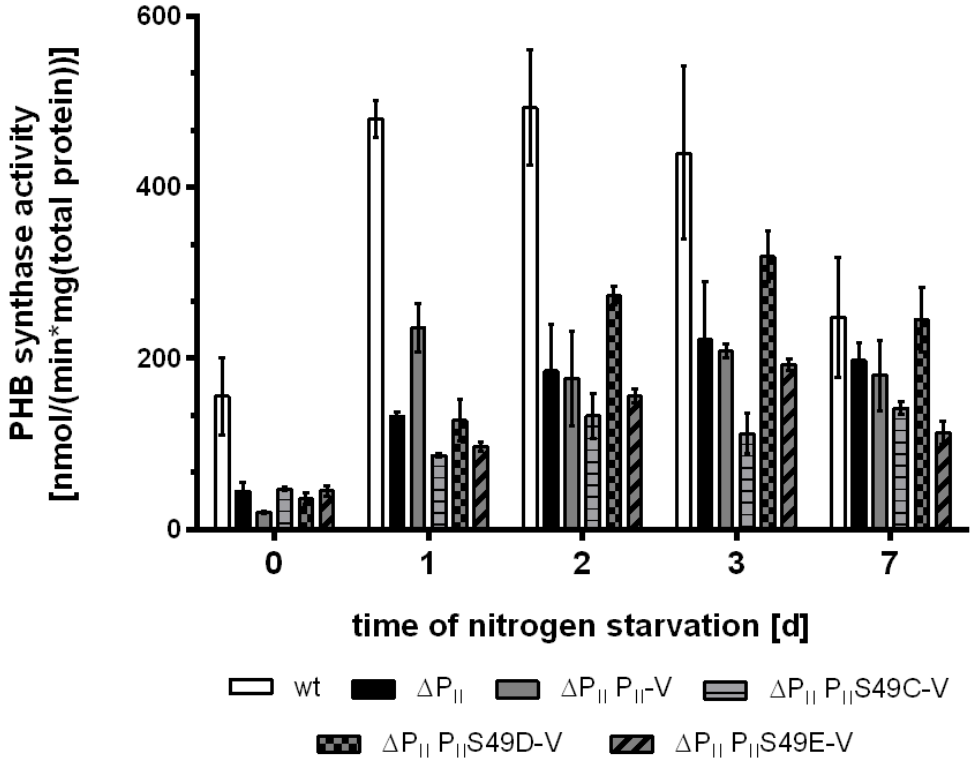

Fig. 8.5: PHB synthase activities in wild type, P_{II} mutant and complemented strains during nitrogen starvation.*wild type (white bars), P_{II} mutant (black bars), P_{II}-Venus complemented strain (grey bar), P_{II}S49C-Venus complemented strain (grey horizontal striped bar), P_{II}S49D-Venus complemented strain (grey-black checked bar), P_{II}S49E-Venus complemented strain (grey diagonal striped bar)*

PHB synthase activities were significantly affected by the deletion of P_{II} and activities were clearly lower than in the wild type (figure 8.5). Nitrogen starvation induced a transient increase in PHB synthase activity which declined with prolonged incubation without nitrogen. Complementation of the P_{II} mutant with all P_{II} variants was not able to increase PHB synthase activities significantly. Mutation of P_{II} in *Synechococcus elongatus*

PCC 7942 induces a loss of function mutation of PipX (Espinosa et al., 2009). Hence, the reduced activity of PHB synthase could be related to an altered transcriptional response during nitrogen starvation. To test this hypothesis the amount of PHB synthase subunit PhaE was estimated using western blot analysis. No differences between wild type and the P_{II} mutant were observed in the soluble fraction and only differences in the insoluble fraction are shown in figure 8.6.

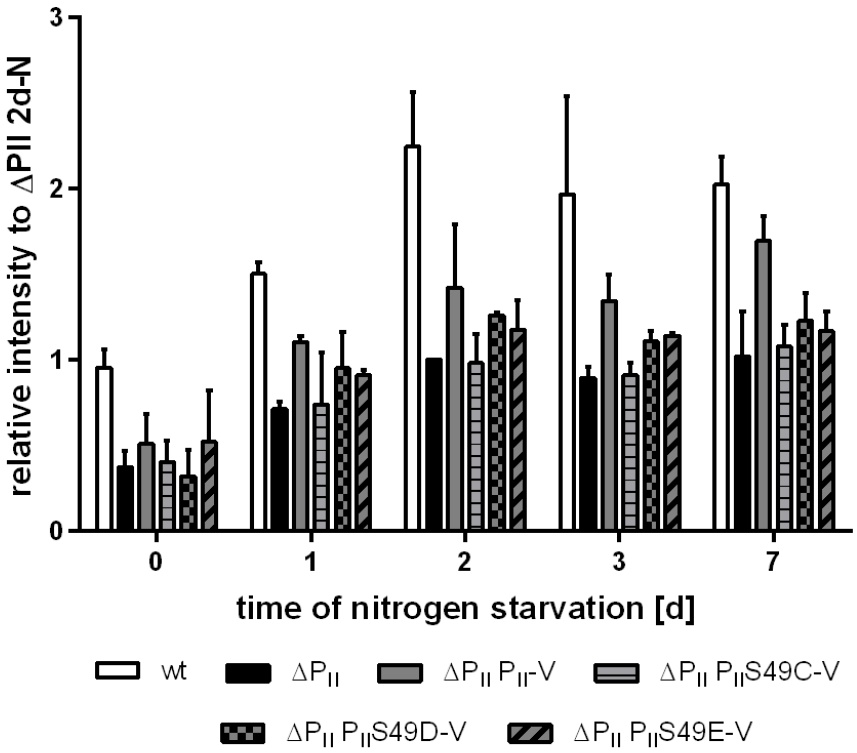

Fig. 8.6: Normalized densiometric estimation of PhaE amount in the P_{II} mutant and P_{II} complemented strains. Normalization was performed to the PhaE amount in the P_{II} mutant 2 d after nitrogen starvation. *wild type (white bars), P_{II} mutant (black bars), P_{II}-Venus complemented strain (grey bar), P_{II}S49C-Venus complemented strain (grey horizontal striped bar), P_{II}S49D-Venus complemented strain (grey-black checked bar), P_{II}S49E-Venus complemented strain (grey diagonal striped bar)*

Roughly 2-3 times higher amounts of PhaE were present in the insoluble fraction after 0, 2, and 3 days of nitrogen starvation. This correlates with increased PHB synthase activity at the dedicated time points (figure 8.5). However PHB synthase activity was roughly five times higher in the wild type at the first day of nitrogen starvation but only twice as much PHB synthase was present. The opposite phenomenon was observed 7 d after nitrogen starvation; while PHB synthase activities between wild type and mutant were similar, the wild type possessed two times more PhaE than the mutant. Consequently an additional mechanism must be present that activates PHB synthase in the early phase of nitrogen starvation, but is able to tune down synthase activity with prolonged nitrogen starvation. Even though the amount of PHB synthase was lower in the P_{II} complemented strains,

PHB accumulation could still be restored. To test whether this difference might be caused by reduced expression of *phaAB* a heterologous system was created to over-express *phaAB* from *Ralstonia eutropha* H16.

8.1.2.3 Expression of *Ralstonia eutropha* H16 *phaAB* in a P_{II} mutant background

To over-express *phaAB* from *R. eutropha* the genes were cloned in pVZ322. Transcription was controlled by the promoter of *sll0783* one of the most strongly expressed genes upon nitrogen starvation. The wild type and P_{II} mutant were transformed with this vector and PHB accumulation was investigated under nitrogen starvation.

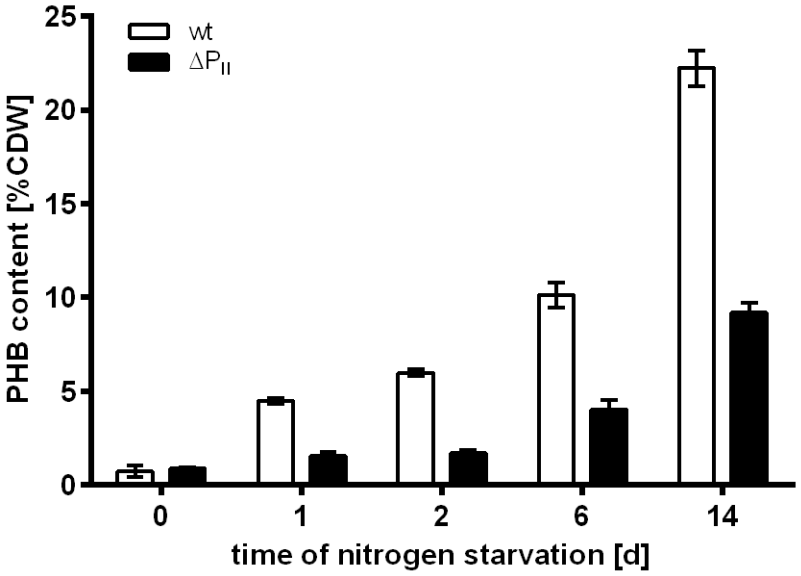

Fig. 8.7: PHB accumulation in wild type and P_{II} mutant upon nitrogen starvation when expressing *phaAB* from *R. eutropha* as % PHB of cell dry weight (CDW).

Strong expression of *phaAB* from *R. eutropha* almost tripled the amount of PHB accumulating under nitrogen starvation than has been reported previously for the wild type (Panda and Mallick, 2007). Expression increased the amount of PHB accumulating in the P_{II} mutant to levels of PHB reported in the literature, but a marked difference between wild type and mutant was still apparent. This demonstrates that expression of *phaAB* is important and might be affected in the P_{II} mutant, but is not the only reason for reduced PHB accumulation. Hence a more detailed expression analysis of *pha* genes was performed.

8.1.2.4 Expression of *pha* genes in the P_{II} mutant

Expression of *phaA*, *phaB*, *phaE* and *phaC* was assayed by qRT-PCR using the $\Delta\Delta C_q$ method to estimate expression during nitrogen starvation relative to expression during

exponential growth.

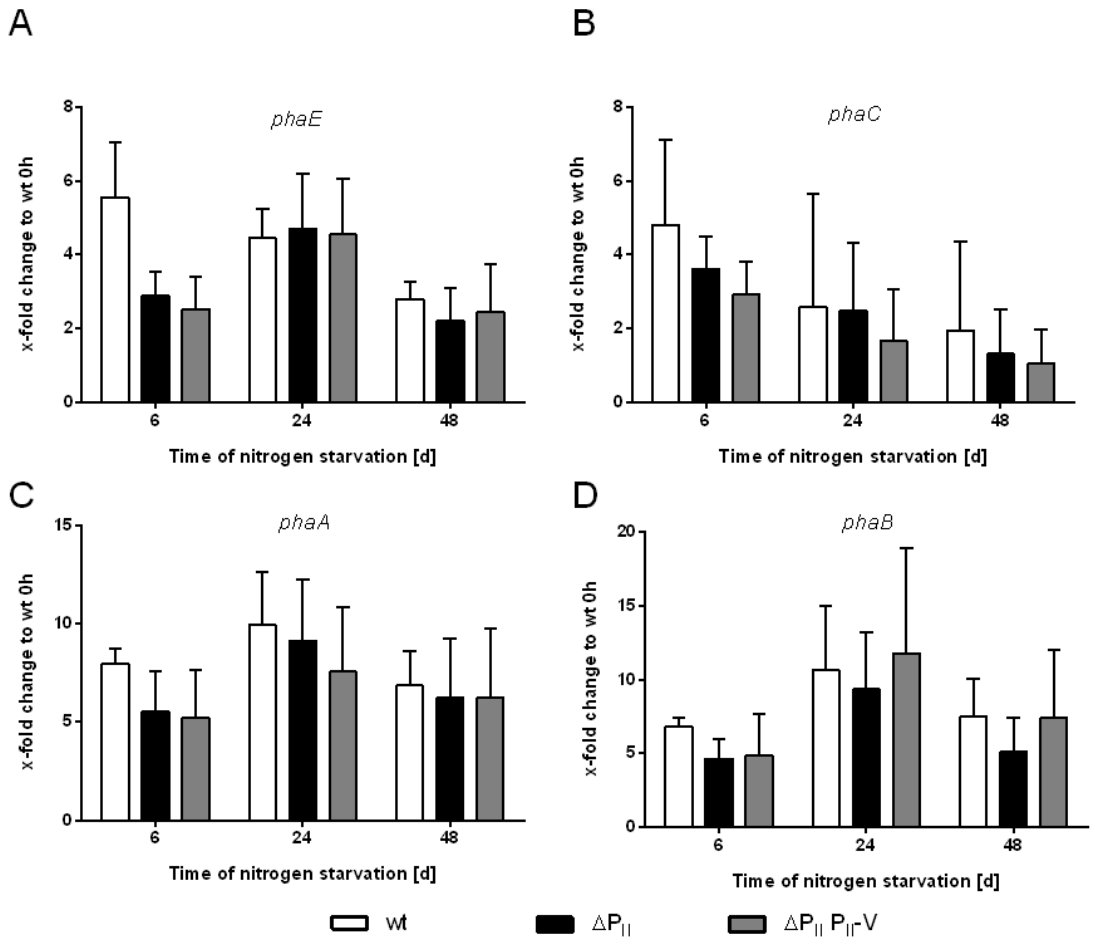

Fig. 8.8: X-fold changes in expression of *pha* biosynthetic genes compared to nitrogen sufficient growth in wild type (white bars), P_{II} mutant (black bars) and P_{II}-Venus complemented mutant (grey bars). A: Expression of *phaE*. B: Expression of *phaC*. C: Expression of *phaA*. D: Expression of *phaB*.

As shown in figure 8.8 expression of the *phaAB* operon was quickly induced within the first six hours of nitrogen starvation. Expression peaked after 24 hours and slowly decreased again 48 hours after nitrogen starvation. Expression of the *phaEC* operon was induced 6 h after nitrogen starvation, but gradually decreased within the observed period. No significant difference could be observed at later stages of nitrogen starvation (24 and 48 h). The biggest difference between wild type, the P_{II} mutant and P_{II} complemented strain was an increased expression of *pha* genes in the wild type at six hours. Expression of *pha* genes in the GlnB complemented strain was almost identical to the mutant. The complemented strain was able to accumulate similar amounts of PHB as the wild type. Hence, a reduced accumulation of PHB due to an altered expression of *pha* biosynthetic genes can be excluded. Interestingly the first 24 h of nitrogen starvation appear to be the period where the majority of PHB synthase is produced. Expression of *phaE* in a later phase does not lead to increased PhaE accumulation (figure 8.6). This indicates that post

transcriptional regulation takes place, possibly through asRNA. As the obtained results were inconclusive with regard to PHB accumulation, a disturbed carbon partitioning between PHB and glycogen was tested as a possible cause for the observed phenotype.

8.1.2.5 Effects of P_{II} mutation on Glycogen accumulation

The P_{II} mutant of *Synechococcus elongatus* PCC 7942 was previously reported to accumulate an increased amount of glycogen (Forchhammer and Tandeau de Marsac, 1995). Glycogen accumulates upon nitrogen starvation therefore the hypothesis that mutation of GlnB alters the carbon flow favoring glycogen accumulation instead of PHB accumulation was tested. To asses whether increased glycogen accumulation occurs during growth in the P_{II} mutant of *Synechocystis* sp. PCC 6803 glycogen content was determined in the exponential growth phase and is shown in figure 8.9.

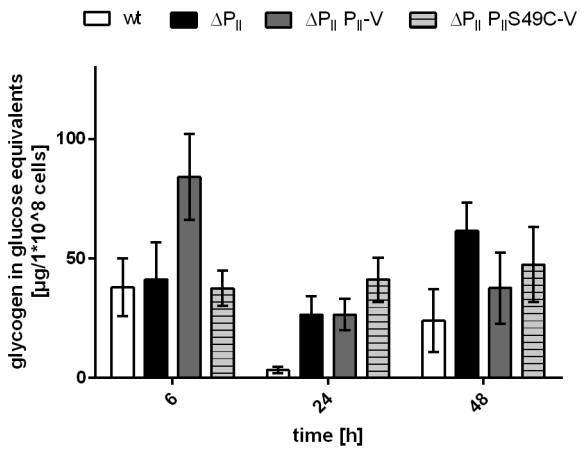

Fig. 8.9: Glycogen accumulation during exponential growth of wild type (white bars), P_{II} mutant (black bars), P_{II} -Venus (grey bars) and P_{II} S49C-Venus (grey horizontally striped bars) complemented strain.

Glycogen levels of the wild type decreased in the 24 hours after inoculation. Most likely glycogen is degraded to provide sufficient energy and carbon to support protein biosynthesis during this stage of growth. Glycogen levels increased after 48 hours to similar levels as 6 hours after the culture was inoculated. Glycogen levels of the P_{II} mutant differed in dynamics: A small decrease of total glycogen could be observed after 24 hours of growth. After 48 hours glycogen levels doubled compared to the wild type. This indicates that either glycogen degradation is strongly reduced in the P_{II} mutant or that an increased glycogen synthesis takes place. The complemented strains differed from the wild type and the P_{II} mutant. The glycogen content did not change in the S49C complemented strain throughout growth. Glycogen content in the GlnB-Venus complemented strain was significantly higher after 6 h than in all other strains, but dropped to P_{II} mutant levels after 24 hours and didn't increase dramatically after 48 hours. As Glycogen levels seemed to be altered as described in the literature and complementation with P_{II} -Venus could

partially restore the dynamics of glycogen turnover, glycogen accumulation was tested during nitrogen starvation in these strains.

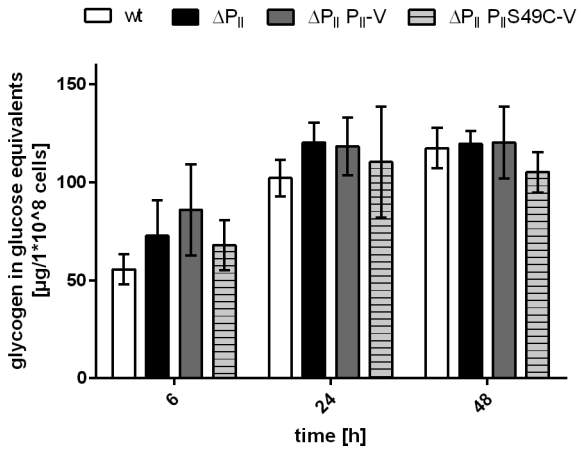

Fig. 8.10: Glycogen accumulation during nitrogen starvation of wild type (white bars), P_{II} mutant (black bars), P_{II} -Venus (grey bars) and P_{II} S49C-Venus (grey horizontally striped bars) complemented strain.

Glycogen accumulation was induced quickly and glycogen content doubled within the first 6 hours of nitrogen starvation (figure 8.10). In all four strains glycogen levels increased after 48 hours of nitrogen starvation, but no significant differences between the strains could be observed. Even though differences in expression and PHB synthase activities could be seen between wild type and P_{II} mutant, expression of GlnB-Venus (or its variants) was able to complement the mutant phenotype. GlnB was previously reported to be involved in acetyl-CoA metabolism through regulation of acetyl-CoA carboxylase (ACC) (Bourrellier et al., 2010; Zalutskaya et al., 2015). Hence, a change in the acetyl-CoA metabolism might have caused the observed phenotype. Consequently the acetyl-CoA metabolism was investigated.

8.1.3 Effects of acetate supplementation on PHB accumulation

8.1.3.1 Acetate supplementation restores PHB accumulation in the P_{II} mutant

To determine whether acetyl-CoA levels were disturbed in the P_{II} mutant during nitrogen starvation, the growth medium was supplemented with 10 mM acetate and PHB accumulation was investigated.

Acetate supplementation increased the amount of PHB accumulating in all strains tested (figure 8.11) compared to incubation without acetate. Acetate supplementation was able to increase the PHB amount in the P_{II} mutant to wild type levels without acetate supplementation. Nevertheless the wild type was able to accumulate more PHB when supplemented with acetate. This result clearly showed that the P_{II} mutant is disturbed in acetate metabolism. The effects of acetate on the metabolism of *Synechocystis* are so far unknown. Hence several hypothesis were tested how acetate might have influenced PHB

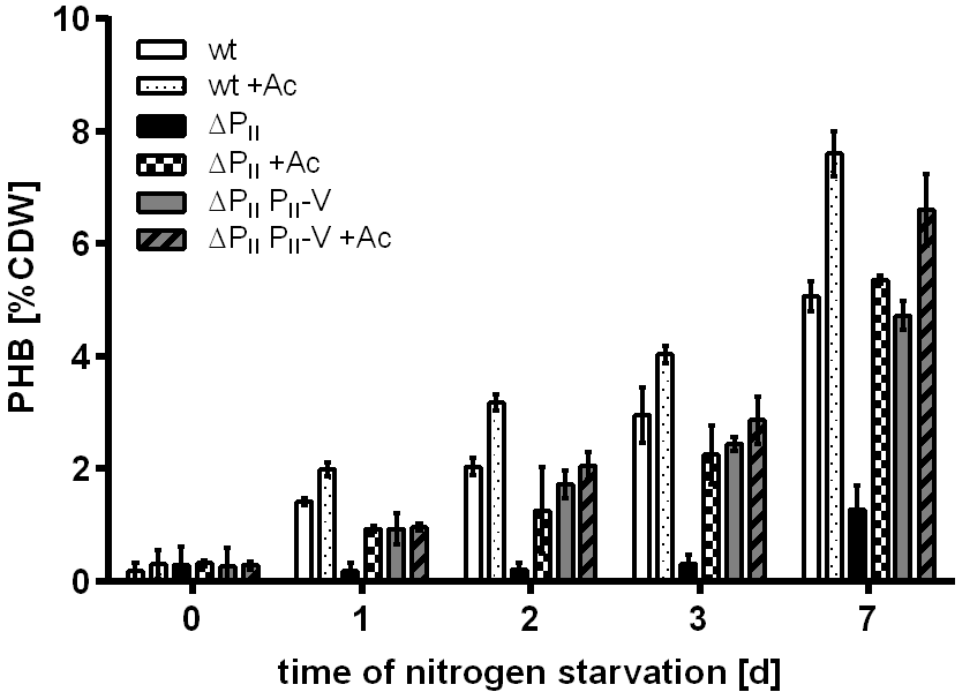

Fig. 8.11: PHB accumulation in wild type (white bars), P_{II} mutant (black bars) and P_{II} -Venus complemented strain (grey bars) during nitrogen starvation without acetate and in wild type (white dotted bars), P_{II} mutant (black checked bars) and P_{II} -Venus complemented strain (grey diagonally striped bars) during nitrogen starvation with 10 mM acetate present in the growth medium.

metabolism.

8.1.3.2 Acetate supplementation changes the transcriptional response of *pha* genes

Expression of *phaAB* was shown to be important for PHB accumulation (figure 8.7), hence a possible stimulating effect of acetate on *pha* gene expression was tested.

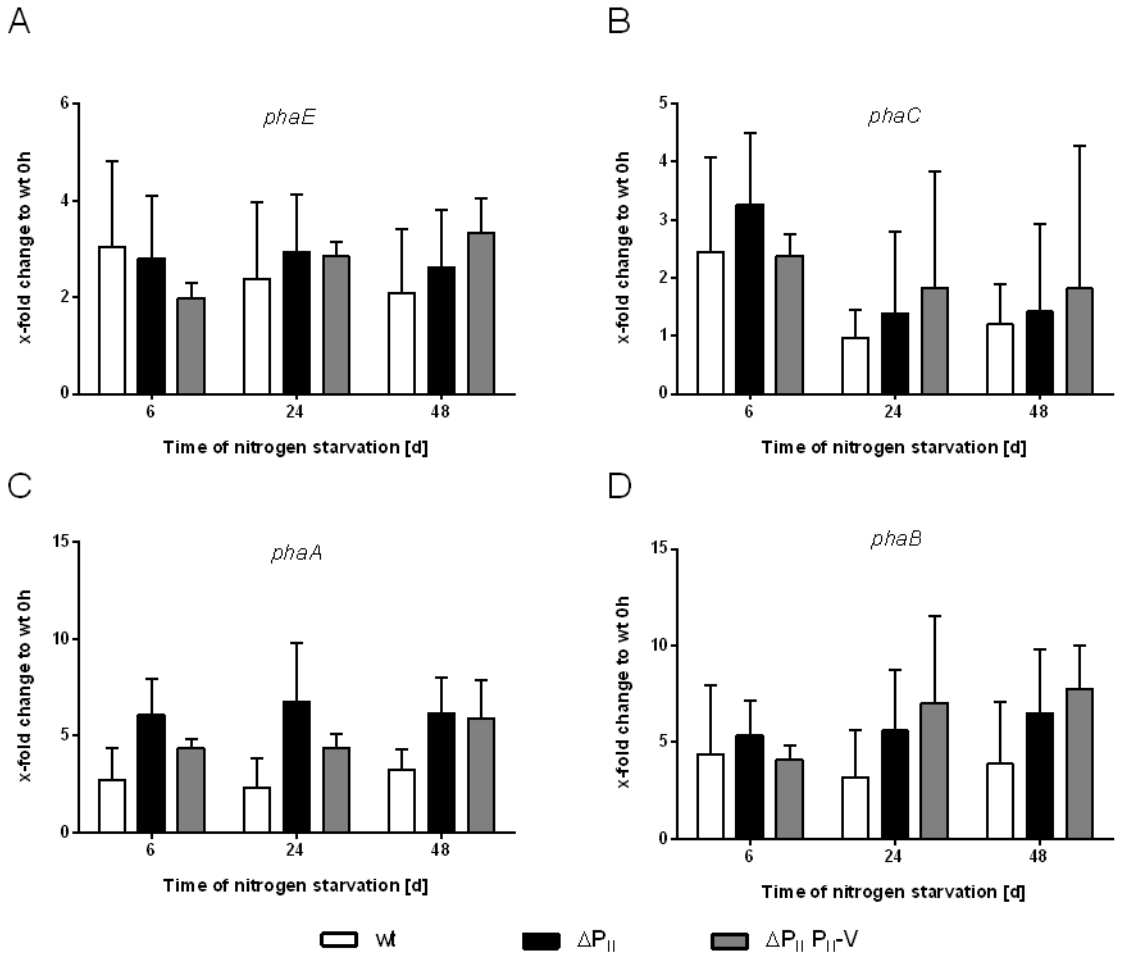

Fig. 8.12: X-fold changes in expression of *pha* biosynthetic genes with 10 mM acetate in the growth medium compared to nitrogen sufficient growth in wild type (white bars), P_{II} mutant (black bars) and P_{II}-Venus complemented mutant (grey bars). A: Expression of *phaE*. B: Expression of *phaC*. C: Expression of *phaA*. D: Expression of *phaB*.

Surprisingly acetate supplementation actually decreased the transcription of all *pha* biosynthetic genes (figure 8.12), when compared to conditions without acetate (figure 8.8). This effect was more profound in the wild type than in the P_{II} mutant or the complemented strain. Looking at the PHB content with acetate supplementation this seems contradictory. It appears that cells are able to respond transcriptionally to the increased availability of acetyl-CoA for PHB synthesis by reducing the transcription of *pha* biosynthetic genes to prevent excessive PHB accumulation.

8.1.3.3 Acetate supplementation influences glycogen accumulation

Utilization of acetate involves the transient formation of acetyl-phosphate (acetyl-P), which acts as signaling molecule in *E. coli*. Acetyl phosphate can act as phospho-group donor or acetylate lysine residues potentially altering carbon flow. Hence, altered accumulation of glycogen in acetate supplemented cultures was investigated.

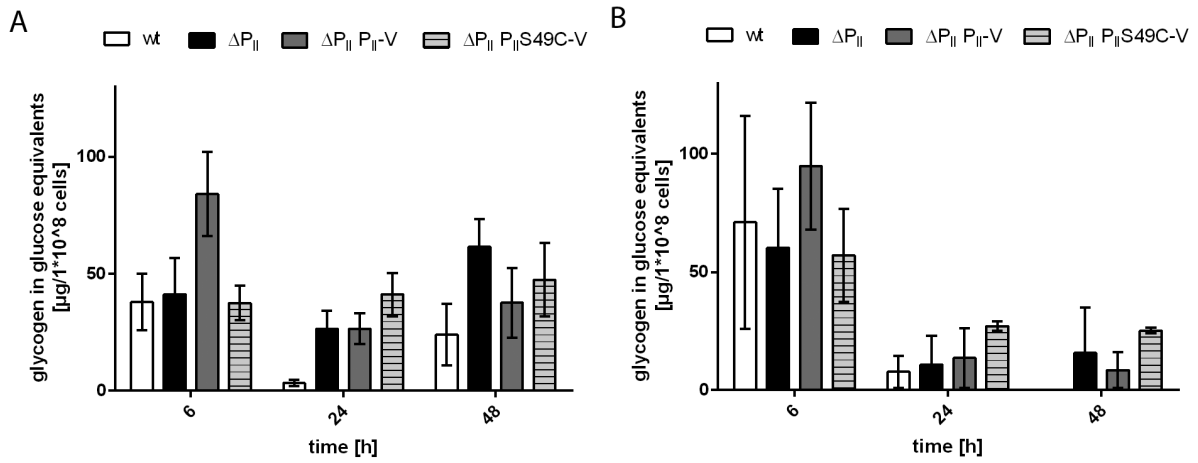

Fig. 8.13: Glycogen accumulation during exponential growth of wild type (white bars), P_{II} mutant (black bars), P_{II} -Venus (grey bars) and P_{II} S49C-Venus (grey horizontally striped bars) complemented strains without acetate (A) and 10 mM acetate (B) in the growth medium.

Acetate in the growth medium had a significant impact on glycogen accumulation (figure 8.13). Glycogen levels 6 hours after inoculation almost doubled when compared to acetate free growth (figure 8.13), but high standard deviation makes interpretation difficult. Stored glycogen was degraded within 24 hours and surprisingly acetate supplementation delayed glycogen accumulation. The delay was also visible when exponentially growing cells were nitrogen starved.

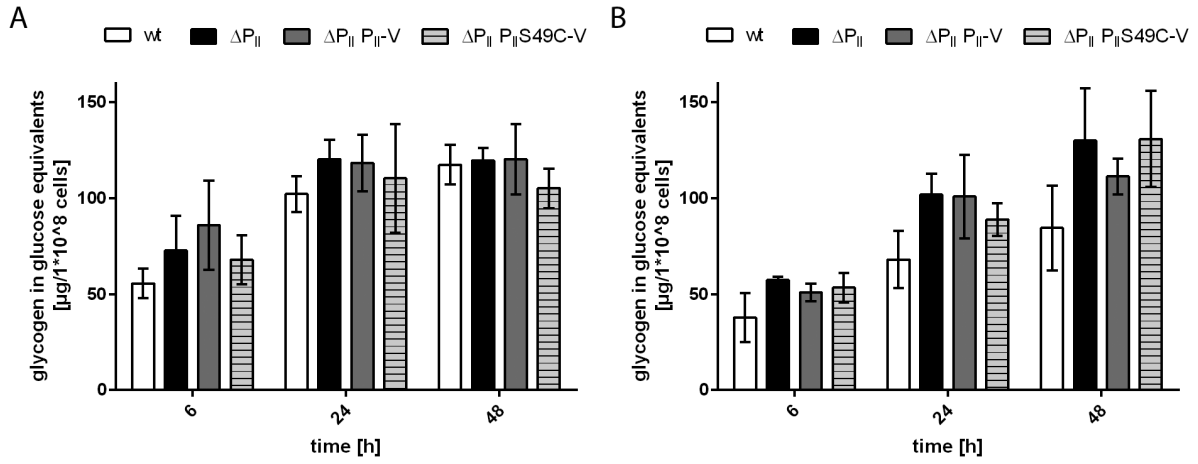

Fig. 8.14: Glycogen accumulation during nitrogen starvation of wild type (white bars), P_{II} mutant (black bars), P_{II} -Venus (grey bars) and P_{II} S49C-Venus (grey horizontally striped bars) complemented strains without acetate (A) and with 10 mM acetate (B) in the growth medium.

Due to cultivation of cells with acetate in the growth medium cells started with lower initial levels of glycogen. Consequently less glycogen was present at the dedicated time points during nitrogen starvation with acetate in the medium (figure 8.14). Acetate clearly delayed glycogen accumulation in wild type but not the P_{II} mutant. This is especially evident 48 hours after nitrogen starvation, where the mutant and complemented strains accumulated more glycogen than the wild type. Taken together acetate enabled the P_{II} mutant to accumulate almost wild type like levels of PHB but did not change the behavior with regard to expression of *pha* genes or glycogen accumulation. Therefore the most likely effect of acetate in the mutant was an increased acetyl-CoA level, that enabled increased PHB accumulation.

8.1.3.4 Changes in acetyl-CoA upon nitrogen starvation

During the course of this work, the P_{II} mutant was shown to have a deregulated ACCase, which lowered the acetyl-CoA pool and favored fatty acid biosynthesis. Complementation with P_{II} -Venus but not the S49E variant reversed this phenotype. Low acetyl-CoA levels would have led to competition between PhaA and ACC for acetyl-CoA leading to reduced PHB accumulation. Hence acetyl-CoA levels during nitrogen starvation were determined.

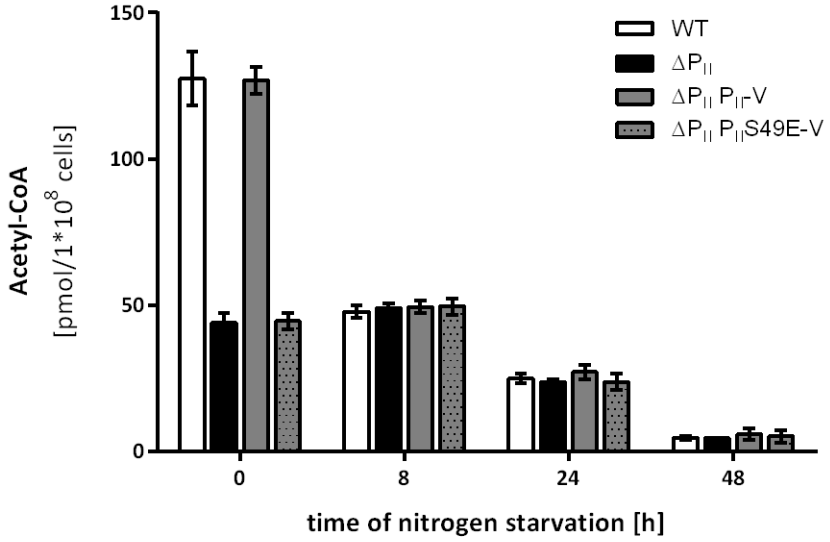

Fig. 8.15: Acetyl-CoA levels of wild type (white bars), P_{II} mutant (black bars), P_{II} -Venus (grey bars) and P_{II} S49E-Venus (grey dotted bars) complemented strains, determined during nitrogen starvation.

In accord with the assumption that ACCase activity is relieved from GlnB inhibition upon nitrogen starvation, acetyl-CoA levels in the wild type dropped P_{II} mutant levels within 8 h of nitrogen starvation (figure 8.15). Acetyl-CoA levels continued to decline but no difference between wild type and all other strains was visible. This refutes the hypothesis that lower acetyl-CoA levels in the P_{II} mutant, compared to wild type, cause reduced PHB accumulation. The same experiment was performed with supplementation

of acetate to the growth medium.

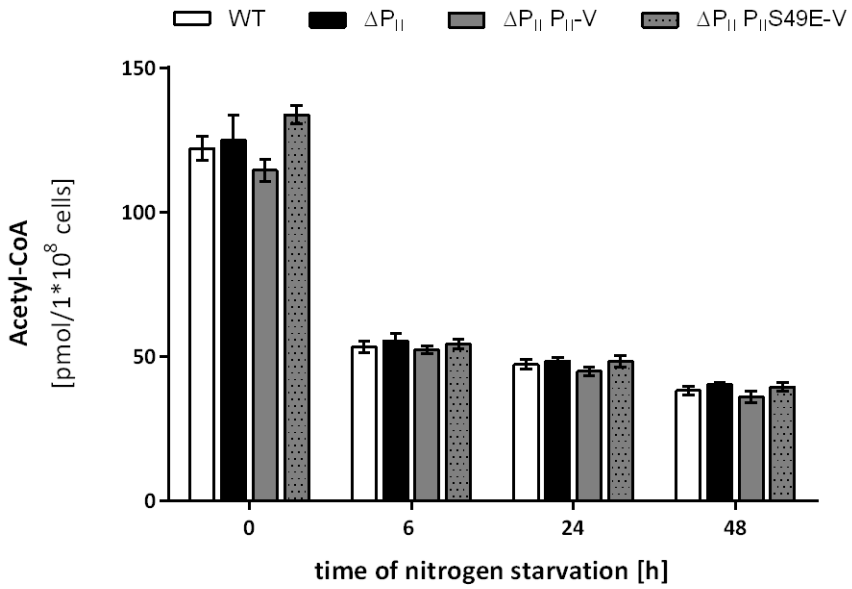

Fig. 8.16: Acetyl-CoA levels of wild type (white bars), P_{II} mutant (black bars), P_{II} -Venus (grey bars) and P_{II} S49E-Venus (grey dotted bars) complemented strains, determined during nitrogen starvation with 10 mM acetate in the medium.

Acetate in the growth medium could restore acetyl-CoA levels in the P_{II} mutant and the S49E complemented strain to wild type levels. Irrespective of acetate being present in the medium, acetyl-CoA levels dropped within six hours of nitrogen starvation in all strains (figure 8.16). Absolute acetyl-CoA levels however remained much higher than without acetate (figure 8.15). These results explain why the P_{II} mutant is able to accumulate near wild type levels of PHB when supplied with acetate. Why PHB accumulation does not take place during nitrogen starvation in the P_{II} mutant, even though acetyl-CoA levels between wild type and mutant are equal, remains puzzling.

8.1.3.5 Acetate supplementation and over-expression of *RephaAB* fully recovers the low PHB phenotype

Acetate supplementation increased acetyl-CoA levels during nitrogen starvation, which resulted in increased PHB accumulation. These conditions were used to determine whether PHB accumulation in a P_{II} mutant background could be fully restored by strong expression of *phaAB* from *R. eutropha*. To do so cultures were nitrogen starved for 2 weeks and the PHB content was examined.

Acetate supplementation was able to complement the P_{II} mutant phenotype as observed in figure 8.11 and over-expression of *phaAB* eliminated the difference between wild type and P_{II} mutant (figure 8.17). As acetyl-CoA levels between wild type and mutant are equal upon nitrogen starvation, the reduced accumulation of PHB in the P_{II} mutant is

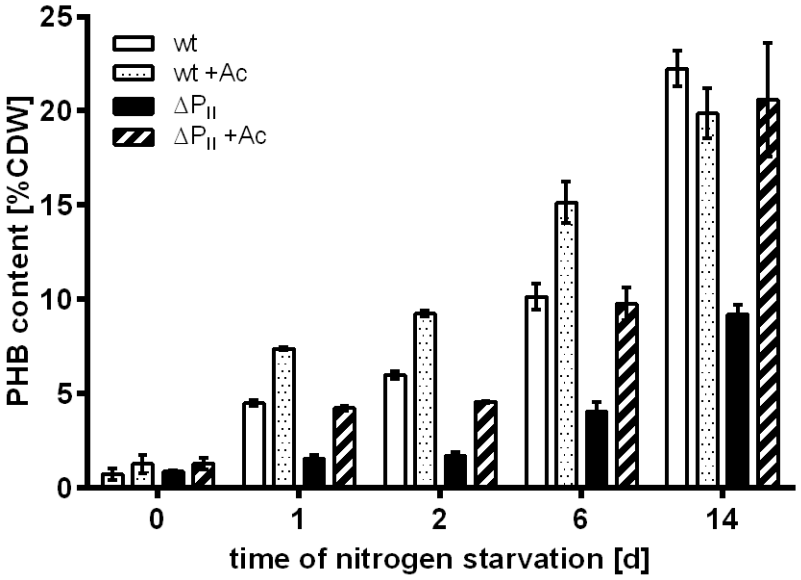

Fig. 8.17: PHB levels of wild type (white bars) or P_{II} mutant (black bars), wild type with 10 mM acetate in the growth medium (white dotted bars) and P_{II} mutant with 10 mM acetate in the growth medium (black diagonally striped bars) over-expressing *phaAB* from *Ralstonia eutropha* during nitrogen starvation.

caused by its inability to channel sufficient carbon towards PHB synthesis.

8.1.4 Resequencing the P_{II} mutant

Results from glycogen accumulation and qRT-PCR indicated that the P_{II} mutant reacts slightly different to acetate in the growth medium and might be affected in perceiving the additional carbon source. To exclude that this is caused by secondary mutations in the P_{II} mutant, the genome of the mutant and the wild type as reference were sequenced.

8.1.4.1 Polymorphisms in the wild type genome sequence

Genomic DNA form the wild type strain used in the laboratory (wild $type_{KF}$ substrain)was isolated as described in the methods section. Genome sequencing and bioinformatic analysis was performed in cooperation with the DSMZ Braunschweig and University of Freiburg. The genome sequence of the laboratory strain was compared to the *Synechocystis* sp. PCC 6803 KAZUSA reference genome (Kaneko et al., 1996). Thirty single nucleotide polymorphisms (SNP) were detected in the wild $type_{KF}$ genome which are listed in table 8.1. Only single nucleotide polymorphisms encoded in the genome are presented, since the poor sequence coverage of plasmids did not allow to make conclusive statements about SNPs on plasmids.

Eleven SNPs were detected in the genome of the wild $type_{KF}$, which were unique and

Tab. 8.1: Single nucleotide polymorphisms (SNP) of the wild type$_{KF}$ compared against the KAZUSA reference genome. NCR: non-coding region

Position	reference	alteration	locus ID	description	effect	known SNP
312085	G	T	*slr1305*	response regulator	D813Y	no
831647	C	T	NCR			no
943495	G	A	*slr1834*	PsaA	V604I	yes
1012958	G	T	NCR			no
1113628	C	T	*sll1271*	carbohydrate selective porin	V208I	no
1204616	G	A	*slr1865*	periplasmic binding protein	C114Y	yes
1260530	C	T	*sll2008*	peptidase	G175R	no
1364187	A	G	*sll0838*	PyrF	silent	yes
1415597	T	C	*slr2058*	TopA	V491A	no
1812419	C	T	*slr1983*	two component sensor and regulator	silent	yes
1819782	A	G	*sll1867*	PsbA3	silent	yes
1819788	A	G	*sll1867*	PsbA3	silent	yes
2066976	C	T	*sll1525*	phosphoribulokinase	silent	no
2092571	A	T	*sll0422*	Asparaginase	L312*	yes
2198893	T	C	*sll0142*	efflux system	silent	yes
2301721	A	G	*slr0168*	unknown protein	K402E	yes
2468395	T	C	*sll0020*	ClpC	T159A	no
2521013	T	C	*slr0222*	Hik25	F897S	yes
2602717	C	A	*slr0468*	unknown protein	H82Q	yes
2602734	T	A	*slr0468*	unknown protein	I88N	yes
2748897	C	T	NCR			no
3014665	T	C	*slr0302*	diguanylate cyclase	silent	yes
3096187	T	C	*ssr1175*	putative transposase	I46T	yes
3098707	T	C	*ssr1176*	putative transposase	C95R	yes
3110189	G	A	NCR			yes
3110343	G	T	*sll0665*	putative transposase	P73Q	yes
3120544	G	C	*sll0659*	FAD dependent oxidoreductase	silent	no
3142651	A	G	*sll0045*	sucrose phosphate synthase (SpsA)	silent	yes
3269419	C	A	*sll0519*	NdhA	G260C	no
3371938	T	A	*slr1564*	SigF	M231K	yes

have not been reported previously. Three of the SNPs were located in non coding regions and two were located in a coding sequence but were silent (*sll0045* and *sll1525*). One SNP led to a conservative point mutation in *sll1271* where valine 208 was replaced by isoleucine, but should not have affected the functionality of the protein. Two SNPs led to amino acid substitutions which replaced a big hydrophaobic amino acid with the small amino acid alanine. The mutations were in DNA topoisomerase I(TopA) and a subunit of the Clp protease ClpC. Mutation of valine 491 to alanine of DNA topoisomerase I (TopA) did not affect a catalytic residue however was in domain IV of topoisomerase. Residues in this domain are highly conserved and the mutation might have an influence on the functionality of TopA. this could cause slower growth due to slower DNA replication. The mutation in ClpC is not positioned in a highly conserved domain and will probably have only minor effects on the fitness of the organism. The other three SNPs led to the substitution of a small amino acid through a bulky amino acid (*slr1305*, *slr1865* and *sll0519*). Mutation of the response regulator *slr1305*, which has homologies to diguanylate cyclases, substituted aspartate 813 to tyrosine at the end of the putative EAL domain. EAL domains are thought to cleave phosphodiester bonds and degrade the second messenger ci-di-GMP, since the mutation is at the end of the conserved domain a adverse effect is less likely to affect the catalytic function of this domain. Mutation in the processing protease (*sll2008*) led to the substitution of glycine 175 to arginine. This mutation is at the end of a peptidase domain and should not have a dramatic effect on the activity of the protease. The SNP in NADH dehydrogenase subunit 1 (NdhA) changed glycine to cysteine in the sixth transmembrane helix. Prediction of the effect this mutation might have is difficult.

8.1.4.2 Insertions and deletions in the wild type genome sequence compared to the reference sequence

Seven insertions and nine deletions were detected in the wild type$_{\mathrm{KF}}$ sequence compared to the reference genome and are shown in table 8.2.

In contrast to SNPs insertions and deletions can have a tremendous influence on the reading frame of a gene. Such mutations were detected twice in untranslated regions. Mutation in the 3' UTR of *sll0528* had likely no effect but insertion at the 5' UTR of *slr2031* likely altered the transcription/translational efficiency of this gene. The majority of mutated genes were involved in shaping the cell surface and interaction with the extracellular matrix. Three genes were an exception *spkA*, *sll1384* and *glpK*. Three insertions/deletions occurred in genes, whose protein function is unknown (*slr0364*, *sll0762* and *ssl787*). The majority of the mutations were most likely loss of function mutation. Either the reading frame was disrupted and premature termination of translation produced a shorter polypeptide, or mutations altered the reading frame extending the poylpeptide at the C-terminus. Mutation at the 5' UTR of *sll0752* shortened the distance between the ribosomal binding site and the start codon by one nucleotide altering translation efficiency.

Tab. 8.2: Inversions and deletions in the wild type$_{KF}$ compared to the KAZUSA reference strain. aas:*amino acid sequence*; RBS: *ribosomal binding site*; NCR: *non coding region*

Position	reference	alteration	locus ID	description	effect
386406	T	TTTGG CTGGG GGAAA AATGT TGGAT TGATA ACCTC GCCCC GGTTA CCATT GAGTC CCATG TGTGT ATTTC CCAGG GCGTT TACCT ATGCA CTGGC AACCA CGA	*slr1084*	WcaF-like	insertion of 34 aa after V77
731366	AT	A	*sll1574*	SpkA	protein fully functional
781618	A	ACCCC GGCTT TAAAC GTCAT GCACC AATCT CTGAT TTACT GGTTT ATTCA TCTAT CAATT CCATA GGCTT TTTGC TTCAT CGCTC CAACT AACTT TTCTG GGATG TCCTC CATGC CCCCC GTGCC TAGCT TACCG TCCAC CGATG CCGTT ATTCC	*slr2031*	insertion in 5' UTR	
1200310	ATC	A	*slr1862*	LarA like	altered aas after E201, premature translational termination
1200313	GT	G	*slr1862*	LarA like	altered aas after E201, premature translational termination
1425468	GT	G	*sll1951*	S-layer protein	D728*
1830443	G	GGTGG TCAAC TACGT CATAA TTAA	*sll1384*	similar to DnaJ	altered aas after H18, premature tanslational termination
1953678	A	AGCCG GGCTA ACGGT GGGAT TTTGG CAAGA CTACC GGGCT TTGGT GGAAA ATCGG GCCAT TGACC GGGTA TTTGA ACCAG GAGTA GGATC CGCCG ATGCC CAGGC AAATT TTTCC GTTTG GCAAG AGGCT GTCC	*slr1672*	GlpK	altered aas from L455
2204575	CG	C	*slr0162*	PilC	altered aas from G142
2350285	T	TA	NCR	upsteram of *sll0350*	
2360245	G	GC	*slr0364*	unknown protein	altered aas from A2975
2409242	TC	T	*sll0762*	unknown protein	altered aas from A99, extended C-terminus
2419397	AT	A	*sll0751*	MlaD-like	altered aas from M165, extended C-terminus
2419397	AT	A	*sll0752*	MlaD-like	RBS 1 nt closer to ATG
2544044	T	TC	*ssl0787*	unknown protein	altered aas from S111, extended C-terminus
3260089	TC	T	NCR	3' UTR of *sll0528*	
3364287	AT	A	*sll1496*	putative sugar transferase	altered aas from K503, premature translational termination

Interestingly *spkA*, a serine/threonine kinase regulating cellular motility, which is disrupted in the reference genome by a frame shift is fully functional. A second noteworthy mutation is in *sll1384* a DnaJ like protein. This mutation alters the reading frame dramatically to the extent that the used wild type is effectively an *sll1384* mutant. Since six homologous *dnaJ* genes are encoded in the *Synechocystis* sp. PCC 6803 genome this mutation can most likely be compensated through DnaJ homologs. The third surprising mutation is in *slr1672* (*glpK*), which is a glycerol kinase (or a carbohydrate kinase). The mutation alters the dimer interface and could lead to a deregulated enzymatic activity. Addition of glycerol (or glucose) to the growth medium has deleterious effects on the growth of wild type$_{KF}$. Mutation of GlpK could alter the metabolic flow when glycerol is present in the medium of wild type$_{KF}$ and therefore explain the observed phenomenon. Accumulation of deleterious mutations in genes shaping the cell surface or interaction with the environment, demonstrate that the wild type$_{KF}$ experiences an altered selective pressure under laboratory conditions than in the environment.

8.1.4.3 Additional deletion around the *ssl0707* (*glnB*) locus

Re-sequencing the wild type and the P_{II} mutant genome was intended to verify that the mutant had no second site mutations in key nitrogen regulators (e.g. NtcA, PipX,...). The analysis identified that the *ssl0707* locus was dramatically changed compared to the intended organization by Hisbergues et al. (1999).

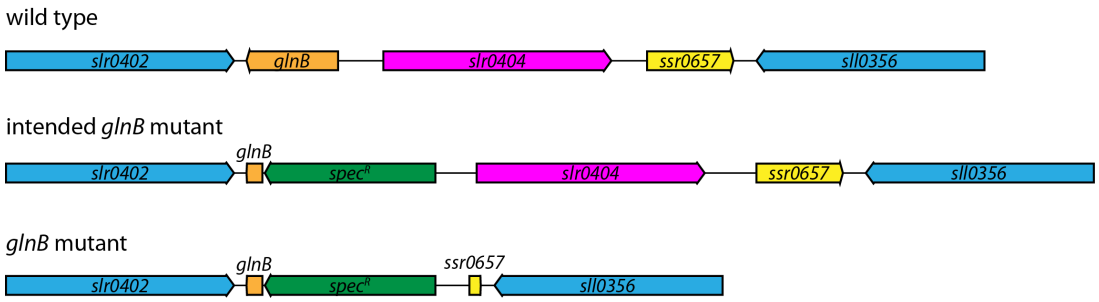

Fig. 8.18: Genome organization of the *ssl0707* locus in wild type, as intended by Hisbergues et al. (1999) and in the *glnB* locus in the P_{II} mutant.

Mutation of *glnB* was intended to delete a major portion of the P_{II} protein without affecting neighboring genes. At the time the mutant was created, available techniques showed that the mutant was indeed devoid of *glnB*. Deletion of *slr0404* and *ssr0657* could not be detected with the applied methods (figure 8.18). Both genes are conserved in cyanobacteria and distant homologs of *slr0404* can even be found in plants. The function of these genes is unknown and based on bioinformatic predictions *slr0404* appears to be a membrane protein. As experimental evidence with complemented strains has shown, these genes do not cause reduced PHB accumulation.

8.1.4.4 Polymorphisms in the P_{II} mutant genome sequence compared to the reference sequence and wild $type_{KF}$

Analysis of the genome sequence of the P_{II} mutant revealed that several SNPs are present in the mutant. Three SNPs are distinct for the P_{II} mutant and not present in the wild $type_{KF}$. Other SNPs are present in the wild $type_{KF}$ but are absent in the P_{II} mutant.

Tab. 8.3: Single nucleotide polymorphisms of the P_{II} mutant compared against the wild $type_{KF}$ genome.

Position	reference	alteration	locus ID	description	mutation	known SNP
733064	A	G	*slr1705*	AspA	Y215C	no
2691388	G	A	*slr0418*	DevT homolog	W285*	no
3423372	C	T	*slr0753*	P protein	L113P	yes

Six single nucleotide polymorphisms present in the wild $type_{KF}$ sequence were absent in the P_{II} mutant (*sll127*, *slr2058*, *sll1525*, *sll020* and *sll0659*). All other described SNPs were present in the genome sequence of the P_{II} mutant. The mutant was obtained from Hisbergues et al. (1999) and derived from the wild type cultivated in that laboratory (wild $type_{TM}$ substrain). The result is not surprising and shows that wild $type_{KF}$ and wild $type_{TM}$ are very closely related but not isogenic. Three unique polymorphisms in the P_{II} mutant were located in genes encoding proteins with diverse functions. Aspartoacylase (AspA) is an enzyme that catalyzes the deacylation of N-acetyl-L-aspartate to acetate and L-aspartate. Tyrosine 215 is not a catalyticly relevant residue but tyrosine residues can be phosphorylated, hence Y215C mutation might alter the regulation of AspA through elimination of the phosphorylation site. The identified DevT homolog is a phosphatase. Introduction of a stop codon instead of W285 deletes 18 amino acids at the C-terminus. Even though the catalytic center of the phosphatase is not affected this could lead to alterations in phosphatase activity. The last SNP is in a transmembrane protein homologous to a Na^+/H^+ antiporter. The mutation replaces leucine 113 to proline and is located in the third transmembrane helix. Due to its structure the amino acid proline is known to break α-helices by disrupting the hydrogen bond network of the polypeptide backbone. This could affect the structure of the transmembrane α-helix affecting Na^+/H^+ antiport. Symport of amino acids or bicarbonate into the cytoplasm should not be affected as six other Na^+/H^+ antiporter are encoded in the genome and would be able to compensate this mutation.

8.1.4.5 Insertions and deletions in the genome sequence of the P_{II} mutant compared to the reference sequence and wild $type_{KF}$

One insertion and two deletions were detected in the P_{II} mutant which were not present in the wild $type_{KF}$ and are shown in table 8.4.

As with single nucletide polymorphisms the P_{II} mutant lacked several insertions detected in the wild $type_{KF}$ (second deletion in LarA *slr1862*, *sll1384* and *sll1496*). Insertion of

Tab. 8.4: Insertions and deletions in the genome of the P_{II} mutant. aas:*amino acid sequence*; RBS: *ribosomal binding site*; NCR: *non coding region*

Position	reference	alteration	locus ID	description	effect
202787	T	TA	*slr1104*	hypothetical protein	altered aas from F78
875190	GC	G	*slr1194*	hypothetical protein	altered aas from P168
2730500	GGTGA GGAAG TTATT ATC-TA GAGGT GT	G	NCR	5' UTR of *slr1099*	

one nucleotide in *slr1104* alters the reading frame after F78 and produces only a 92 amino acid long polypeptide, whereas the full length protein is 613 amino acids long. The protein consists of three conserved domains (FHA-, GGDEF- and EAL-domain) and only the FHA domain is still present in the peptide produced by the P_{II} mutant. The FHA domain is able to bind a phosphopeptide, the GGDEF domain is able to degrade cyclic nucleotides (possibly cyclic diguanosine monophosphate). The EAL domain is thought to stimulate the activity of the GGDEF domain, thereby increasing c-di-GMP turnover. Cyclic di-GMP is thought to regulate adhesion, biofilm formation and phototaxis in *Synechocystis* (Savakis et al., 2012; Agostoni et al., 2016). Consequently the truncated protein in the P_{II} mutant could not degrade c-di-GMP as efficient as the wild type and c-di-GMP levels should be elevated in this strain in conditions *slr1104* is transcribed and active. Deletion of one nucleotide in *slr1194* resulted in a C-terminally truncated protein, whose function is unknown. Hence interpretation of this mutation is difficult. A larger deletion occurred in the non coding region upstream of *slr0199*. The encoded protein has conserved domains homologous to amidotransferases/ergothioneine biosynthesis protein(EgtC), therefore its transcriptional regulation might be altered in the P_{II} mutant. Taken together the sequencing of the wild $type_{KF}$ and the P_{II} mutant revealed interesting adaptations of both strains to laboratory conditions and showed that they are more closely related to each other than to the KAZUSA reference strain. The P_{II} mutant did not show any mutations in key nitrogen regulatory proteins as PipX or NtcA, which was also verified using classic Sanger sequencing. These results exclude the possibility that a secondary mutation is responsible for the reduced PHB accumulation phenotype.

8.1.5 Novel regulatory targets of GlnB

8.1.5.1 Co-immunoprecipitation of P_{II} target proteins

The P_{II} protein is known to interact with various target proteins thereby affecting their metabolic activity or preventing protein-protein interactions. The P_{II} mutant phenotype was recovered by wild type P_{II} and the S49E variant. Hence, pull-down experiments were performed with strains expressing Venus tagged P_{II} protein to identify potential partner proteins, which lead to a recovery of the low PHB phenotype by interacting with P_{II} under

the tested conditions. To do so strains were shifted to $BG11_{-N}$ medium during exponential growth and the analysis was performed with two days nitrogen starved cultures. Pull down experiments were performed in biological duplicates, with cell extracts of the P_{II} mutant, P_{II} complemented and S49E variant complemented strain. The lysis and washing buffer contained 2 mM ATP and 1 mM 2-oxoglutarate to simulate cellular metabolite concentrations during nitrogen starvation. Proteins were co-immuno precipitated using GFP-Trap magnetic beads (Chromotek). Co-extracted proteins were analyzed using mass spectrometry and semi-quantitative analysis was performed to estimate the enrichment of a peptide in the given sample. Enrichment was calculated relative to the intensity in the P_{II} mutant sample. Identified proteins, which were more than fifty fold enriched in extracts of the P_{II}-Venus complemented strain are listed in table 8.5.

Tab. 8.5: Proteins co-precipitated with P_{II}-Venus. EF: *enrichment factor (mean intensity control/mean intensity P_{II}-V)*

locus ID	protein	EF	biol. function
ssr0707	GlnB	∞	nitrogen regulation
sll0920	PepC	∞	pyruvate metabolism
slr0169	CcmP	∞	carbon fixation
sll0398	Dgt	∞	dGTP metabolism
slr1022	ArgD	1002	Arg biosynthesis/ TCA shunt
sll0680	PstB	578	phosphate transport
slr2035	ProB	450	proline biosynthesis
sll1734	CupA	264	CO_2 uptake
slr0520	PurL	100	purine biosynthesis
sll0053	AccC	80	fatty acid biosynthesis
sll1688	ThrC	73	threonine biosynthesis
sll1536	MoeB	66	molybdopterin biosynthesis
sll0245	YchF	58	unknown
slr0752	Eno	57	glycolysis
slr0261	NdhH	56	Complex I
slr1274	PilM	52	motility
sll2008	Prp1	50	protein turnover

Many of the identified proteins are involved in the biosynthesis of amino acids (ArgD, ProB, ThrC), primary carbon metabolism (Eno, PepC), nucleotide metabolism (PurL, Dgt) or CO_2 fixation/acquisition (NdhH, CupA, CcmP). Whether the identified proteins are real regulatory targets of GlnB requires further investigation, as unspecific binding could occur e.g. binding of PstB (periplasmic phosphate binding protein) to phosphorylated serine 49 of GlnB. The S49E variant could complement the P_{II} low PHB phenotype. Therefore the same experiment was performed with cell extracts of the S49E complemented strain. Identified proteins with enrichment factors higher than 50 are listed in table 8.6.

Even though the number of proteins which were significantly enriched is lower, similar categories of proteins were identified. Carbon fixation (CcmP), amino acid biosynthesis

Tab. 8.6: Proteins co-precipitated with P_{II}S49E-Venus. EF: *enrichment factor (mean intensity control/mean intensity P_{II}S49E-V)*

locus ID	protein	EF	biol. function
ssr0707	GlnB	∞	nitrogen regulation
slr0169	CcmP	∞	carbon fixation
slr1476	PyrB	∞	pyrimidine biosynthesis
slr1597	ParA	605	chromosome partitioning
slr1022	ArgD	434	Arg biosynthesis/ TCA shunt
slr0947	RpaB	277	transcription factor
slr2035	ProB	270	proline biosynthesis
sll1994	HemB	131	heme biosynthesis
sll0053	AccC	71	fatty acid biosynthesis
sll1688	ThrC	67	threonine biosynthesis

(ArgD, ProB, ThrC), nucleotide biosynthesis (PyrB). Interestingly a transcription factor (RpaB) and another DNA associated protein (ParA) were identified. Identification of AccC is somewhat surprising as GlnB has been shown to interact with AccB and not with AccC. As ACC is a multi-subunit protein (AccADBC) *in vivo* detection of AccC might be the remnant of the full complex, which was co-precipitated with GlnB.

Proteins identified in both experiments are CcmP, ArgD, ProB and ThrC. These proteins are prime candidates for regulatory targets of GlnB and remain to be identified as such.

8.1.6 Identification of P_{II} related phenotypes

8.1.6.1 Changes in phosphoenolpyruvate carboxylase activity in the PII mutant

PepC was identified as a target of GlnB regulation. Therefore PepC activity was assayed in exponentially grown cells of wild type P_{II} mutant and P_{II}-Venus complemented strain. Results are shown in figure 8.19.

PepC activity was indeed lowered in the P_{II} mutant and even lower in the complemented strain. This supports the result of the pull-down assay. However no information on how much PepC was present in the cell extracts is available. Hence the difference could be linked to altered expression in the P_{II} mutant, which is not overcome by complementation. More biochemical experiments have to be performed to confirm the direct interaction between GlnB and PepC.

8.1.6.2 Disturbed CO_2 fixation

Several proteins involved in CO_2 fixation were identified in pull-down experiments. CcmP, which is a carboxysome shell protein and might provide a pore for 3-phosphoglycerate diffusion in and out of the carboxysome (Cai et al., 2013). CupA is part of the NDH1 complex (Complex I) and is thought to be part of a high affinity CO_2 uptake system (Burnap et al., 2015). Hence growth of the P_{II} mutant (with two complemented strains)

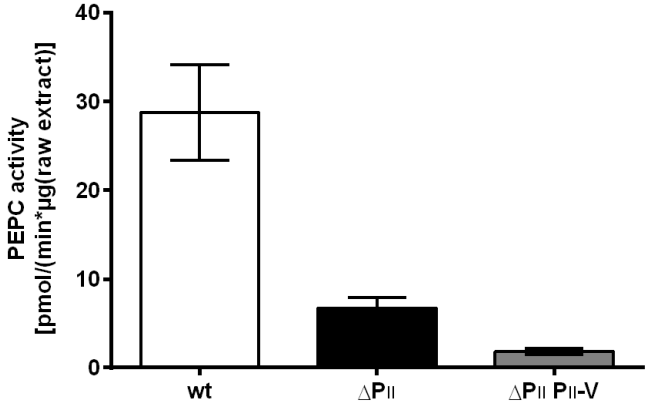

Fig. 8.19: Biosynthetic activity of phosphoenolpyruvate carboxylase in raw cell extracts of wild type (white bar), P_{II} mutant (black bar) and P_{II}-Venus complemented strain (grey bar). Measurements represent the mean of two biological replicates.

was tested under low carbon conditions. No difference was observed when strains were grown on nitrate under low and high CO_2 supplementation. Only when ammonium was used as nitrogen source and cells were grown with high CO_2 supply using high illumination a growth defect could be observed (figure 8.20).

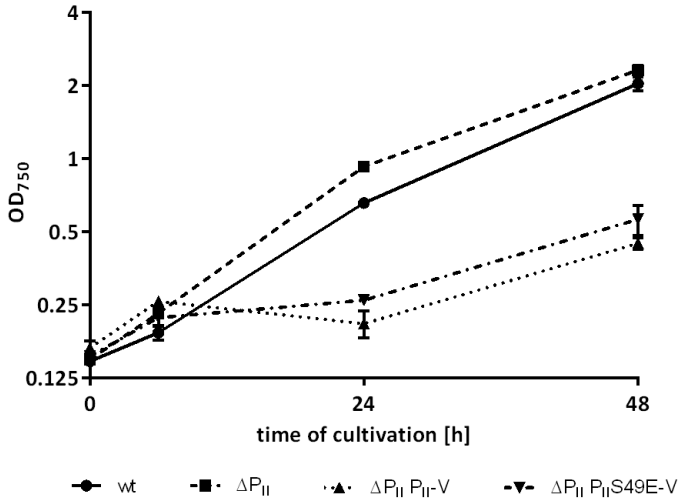

Fig. 8.20: Growth of wild type (circle, continuous line), P_{II} mutant (square, dashed line), P_{II}-Venus (triangle, dotted line) and P_{II}S49E-Venus (inverted triangle, dotted dashed line) complemented strain in BG11 with 5 mM ammonium and vigorous bubbling with CO_2 (2 % v/v). Measurements represent the mean of three biological replicates.

Surprisingly the P_{II} mutant didn't show any phenotype and grew as fast as the wild type, however both complemented strains were not able to grow as fast as the wild type or the P_{II} mutant. As the complemented strains expressed a P_{II} protein that is translationally fused to Venus, the fluorescent protein might have impaired dissociation of P_{II} with its target protein. This could have favored formation of a stable inhibitory complex which

has a negative effect on growth.

8.1.7 Metabolic changes in the P_{II} mutant

Co-immuno precipitation suggested that several enzymes involved in metabolic pathways might be GlnB regulated. Hence, metabolic changes occurring upon nitrogen starvation in wild type, P_{II} mutant and the P_{II} complemented strain were investigated. To do so four biological replicates of each strain were grown to an optical density of OD_{750}=0.6 (t_0) and shifted to $BG11_{-N}$. Cultivation continued for one week and samples were taken 1 and 7 days after nitrogen starvation was induced. Equal amounts of lyophilized cell dry mass were used to extract cellular metabolites. Metabolite abundance was estimated based on the peak area of the chromatogramm. Identification of each metabolite was based on the retention time and mass spectrum. Altogether 30 metabolites from primary metabolism could be identified. Ten lipids, four nucleotide metabolism related compounds and five peptides could not be clearly assigned to a known substance and are not shown. The given values represent the mean of four biological replicates at each time point. Changes in metabolite levels are shown as $\log_2$ fold changes compared to the wild type during exponential growth if not stated otherwise.

8.1.7.1 Metabolites altered upon nitrogen starvation

Nitrogen starvation altered the metabolites pool dramatically mostly leading to a reduction of amino acid pools and accumulation α-ketoacids. Many metabolite pools were not affected by the mutation of P_{II} and behaved like in the wild type.

As reported previously the pools of amino acids decreased for phenylalanine, tyrosine, tryptophane and leucine (figures 8.21 A, B, C, D) (Hauf et al., 2013). The same is true for the polyamine spermidine (figure 8.21 E). All these substances are nitrogen rich and the metabolite pools are lowered due to the inability of the cell to sustain biosynthesis of these. Interestingly levels of 2-C-methyl-D-erythritol-2,4-cyclodiphosphate (MEcPP) an intermediate in the DOXP pathway for isopentenyl pyrophosphate (IPP) and dimethylallyl pyrophosphate (DMAPP) biosynthesis were lowered. IPP and DMAPP are precursors for poly-isoprenoid biosynthesis which are involved in various processes like transport of cell wall sugars across the cell membrane, membrane integrity (hopanoids) and most important for photosynthetic organisms carotenoid biosynthesis. Hence reduced MEcPP levels would dramatically lower carotenoid biosynthesis.

8.1.7.2 Metabolites strongly altered in the P_{II} mutant

Several metabolites which do not group specifically (except proline) in the primary metabolism were altered in the P_{II} mutant. Complementation with P_{II}-Venus could not restore metabolism in the P_{II} mutant to wild type like levels. Metabolite levels strongly

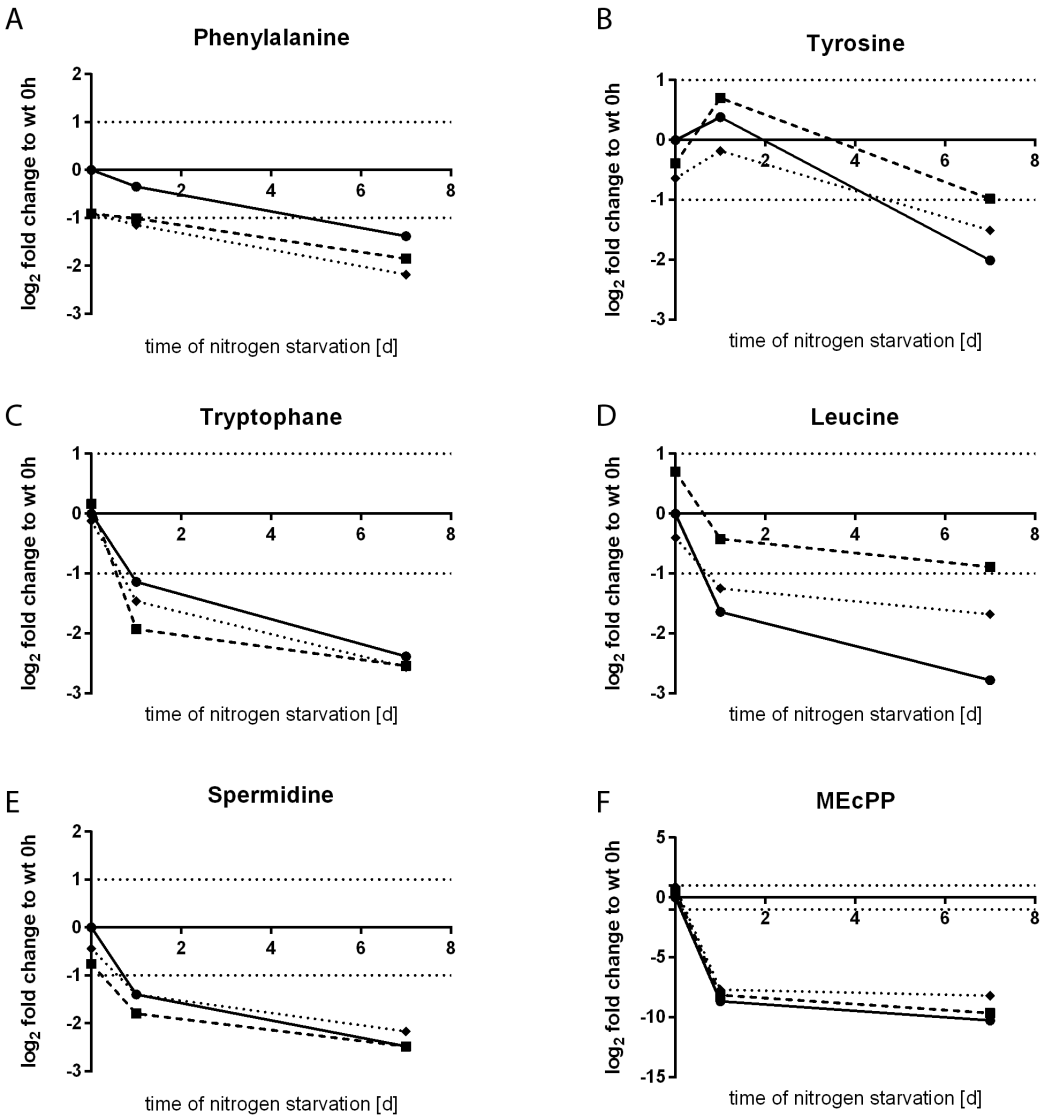

Fig. 8.21: Changes of metabolites upon nitrogen starvation which behaved as in wild type (circles, continuous line) in the P_{II} mutant (squares, dashed line) or the P_{II}-Venus complemented strain (diamonds, dotted lines). Changes are shown as $\log_2$ fold changes compared to levels in wild type during exponential growth.

altered in the P_{II} mutant and the complemented strain are shown in figure 8.22.

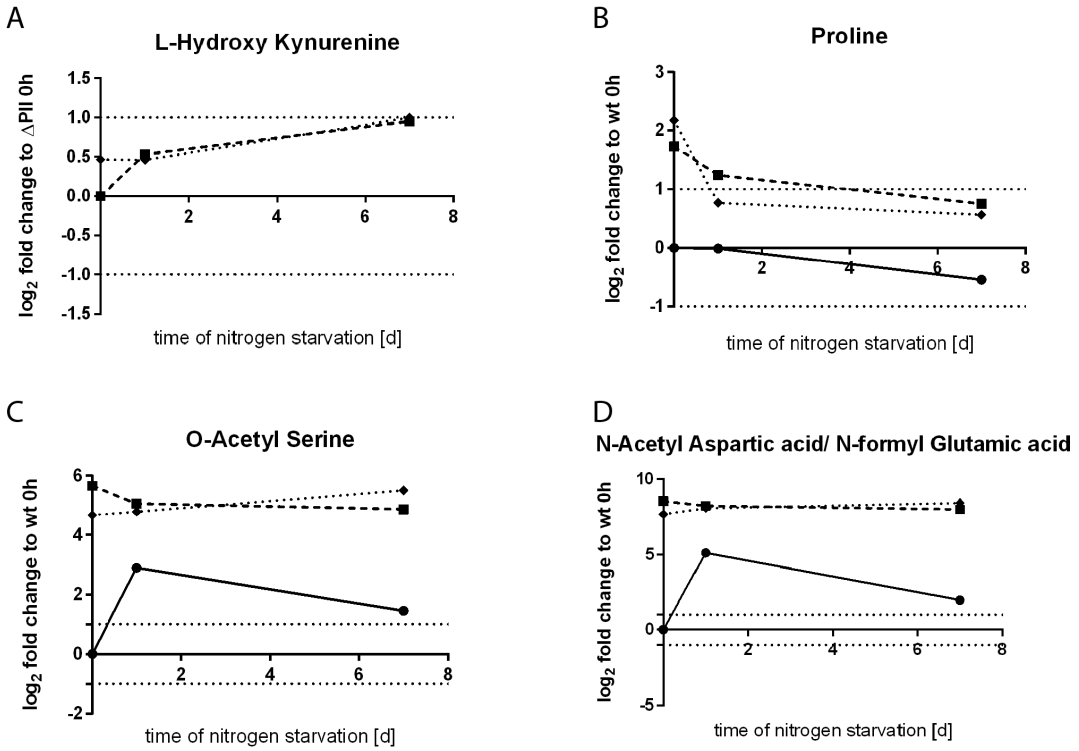

Fig. 8.22: Changes of metabolites upon nitrogen starvation which were strongly elevated in the P_{II} mutant (squares, dashed line) or the P_{II}-Venus complemented strain (diamonds, dotted line) compared to wild type (circles, continuous line). A: Changes are shown as $\log_2$ fold changes compared to levels in the P_{II} mutant during exponential growth as this metabolite was not detected in the wild type. B, C, D: Changes are shown as $\log_2$ fold changes compared to levels in wild type during exponential growth.

3-hydroxy-L-kynurenine is a metabolite in the degradation of tryptophane and is synthesized from tryptophane through an oxidation followed, by a deformylation and transamination reaction. As 3-hydroxy-L-kynurenine can be further metabolized to NAD, increased levels in the P_{II} mutant could be seen as a reaction towards a disturbed NAD and red-ox metabolism. Alternatively a nitrogen starvation like response with increased tryptophane degradation could cause increased 3-hydroxy-L-kynurenine levels (figure 8.22 A). A fourth significantly changed metabolite in the P_{II} mutant and its complemented strain was proline (figure 8.22 B). Whilst the levels decreased upon nitrogen starvation, they were four times higher during exponential growth (note the logarithmic y-axis). This support co-immunoprecipitation experiments, which identified ProB (glutamate kinase) as a protein interacting with P_{II} and indicates that P_{II} might act as a inhibitor of this reaction. Levels of two acetylated amino acids were highly increased in the P_{II} mutant and could not be complemented. One of the amino acids was O-acetyl-serine. Increased accumulation of O-acetyl-serine indicates an increased anabolism of cysteine. Enhanced cysteine synthesis might point in the direction of an altered red-ox balance (possibly oxidative stress), since cysteine is the crucial amino acid in glutathione (figure 8.22 C).

The second amino acid was N-acetylaspartic acid (or n-formyl glutamic acid), which was also detected in wild type samples. A transient increase of this compound was observed in wild type upon nitrogen starvation (figure 8.22 D). Strikingly aspartoaclyase was mutated in the P_{II} mutant. Accumulation of N-acetylaspartic acid could be explained by a reduced activity of aspartoacylase. If this metabolite would be formyl-glutamate an increase in histidine degradation would be expected, but this is not supported by the metabolome data (figure 8.23).

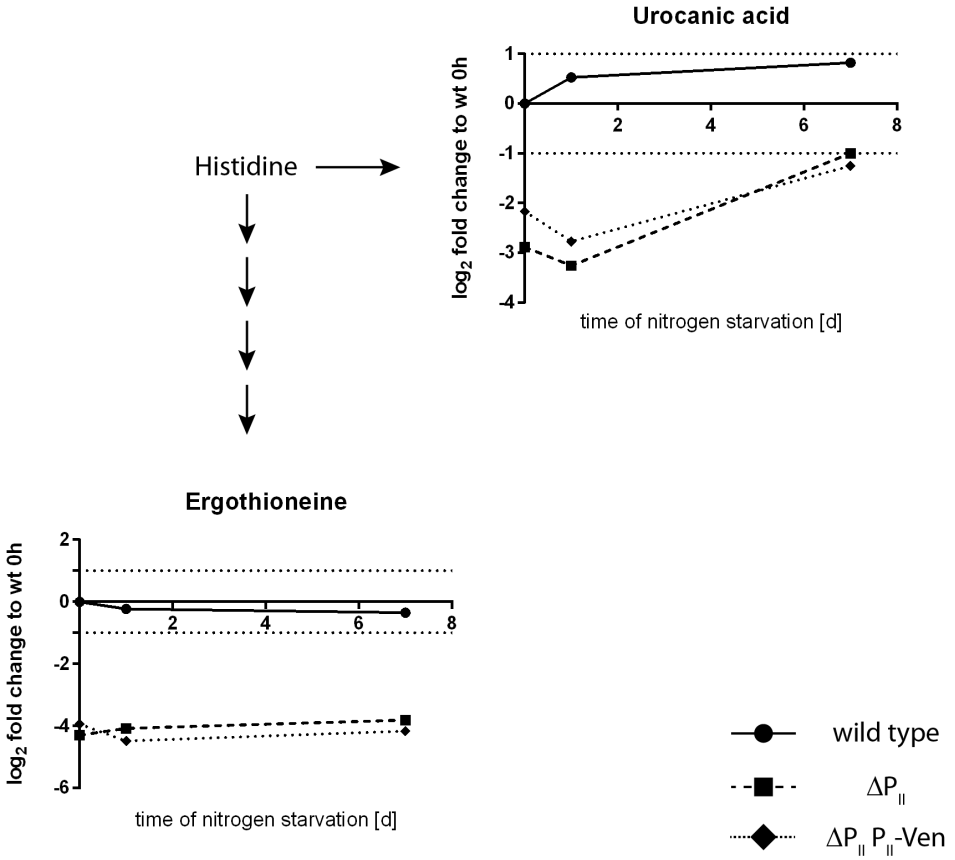

Fig. 8.23: Changes of metabolites upon nitrogen starvation in histidine metabolism. Changes of wild type (dots, continuous line), the P_{II} mutant (squares, dashed line) or the P_{II}-Venus complemented strain (diamonds, dotted line) are shown as $\log_2$ fold changes compared to wild type levels during exponential growth.

Two metabolites derived form histidine were reduced in the P_{II} mutant; urocanic acid and ergothioneine. Ergothioneine is a non proteinogenic amino acid which is believed to be an antioxidant. Sequencing of the P_{II} mutant revealed that transcription of *egtC* could to be affected. Lowered levels of ergothioneine in the mutant confirm this. Urocanic acid is derived from histidine through deamination and can be further degraded to glutamate. Upon nitrogen starvation the wild type catabolizes histidine to urocanic acid, which is reflected by increasing levels of this metabolite with prolonged nitrogen starvation. Reduced levels of urocanic acid in the P_{II} mutant could be caused by reduced histidine levels or reduced catbolism of histidine. Histidine was not detected therefore conclusive statement on

histidine metabolism of the P_{II} mutant can't be made. Histidine biosynthesis begins with ribulose-5 phosphate a key precursor for CO_2 fixation. Several proteins, which are involved in CO_2 acquisition/fixation, were co-immunoprecipitated with GlnB. Alterations in CO_2 fixation in the P_{II} mutant could have led to disturbed ribulose metabolism, potentially affecting histidine levels. This is partially reflected in the levels of C3 carbon metabolites which are shown in figure 8.24.

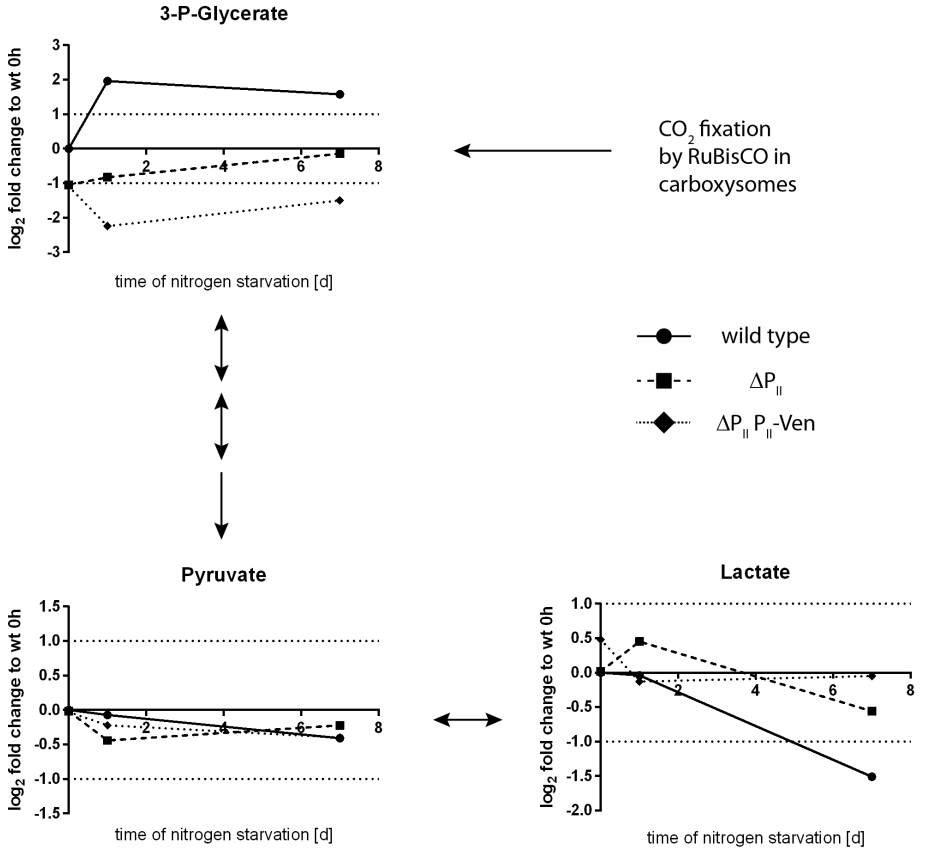

Fig. 8.24: Changes of metabolites upon nitrogen starvation in the lower branch of glycolysis. Changes of wild type (dots, continuous line), the P_{II} mutant (squares, dashed line) or the P_{II}-Venus complemented strain (diamonds, dotted line) are shown as $\log_2$ fold changes compared to wild type levels during exponential growth.

Lowered levels of 3-phosphoglycerate were detected in the P_{II} mutant compared to wild type. This can be interpreted as a result of reduced CO_2 fixation in the mutant, but could also be caused by increased biosynthetic activity of glycogen (figure 8.9) draining this metabolite pool. Interestingly, levels of 3-phosphoglycerate increased upon nitrogen starvation in wild type, but remain lower in the other two strains. Since glycogen pools are strongly increased 24 h after nitrogen starvation the only source for 3-phosphoglycerate at this time point is continuous carbon fixation. Levels of the two other C3 carbon metabolites (pyruvate and lactate) did not change much during nitrogen starvation. Only a small decrease in lactate was observed with prolonged starvation.

8.1.7.3 Effects of the *glnB* deletion on the GS-GOGAT cycle and GABA shunt

2 oxoglutarate is at the interface between carbon and nitrogen metabolism as it is used as substrate by GOGAT for glutamate synthesis. Altered 2-OG levels are reflected in the metabolites of the GS-GOGAT cycle and are shown in figure 8.25.

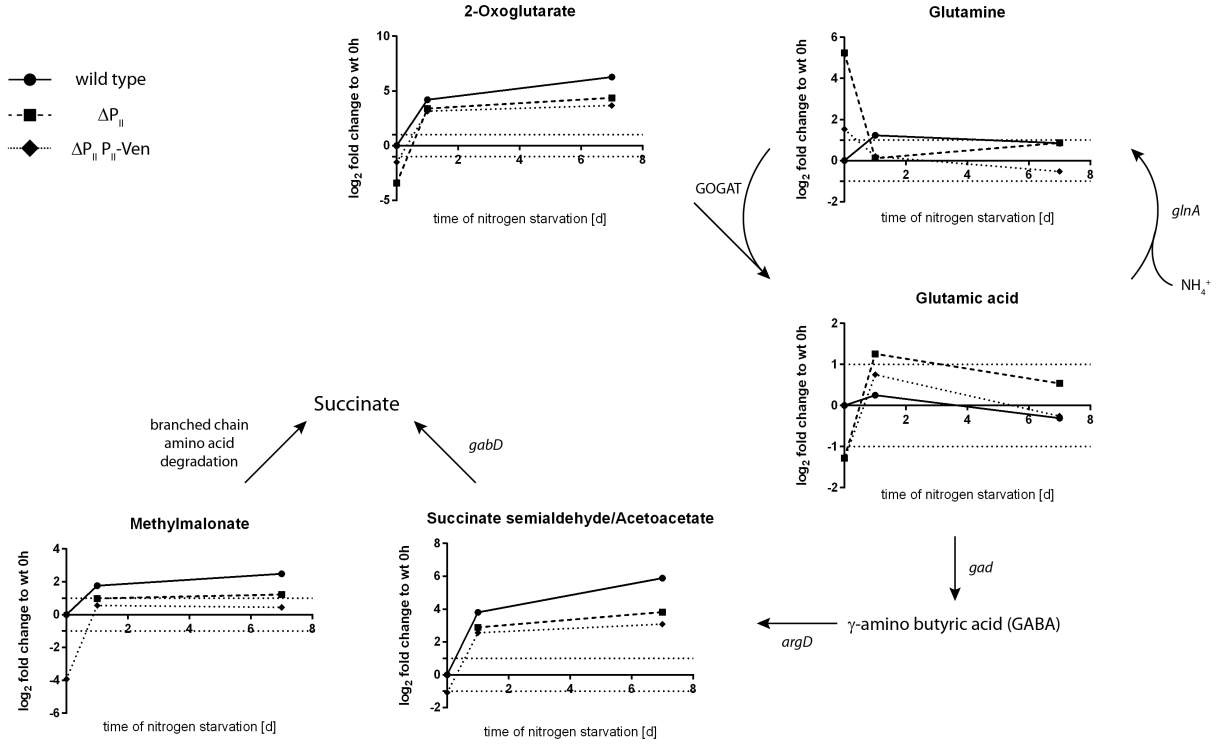

Fig. 8.25: Changes of metabolites upon nitrogen starvation in the GS-GOGAT-cycle and the GABA shunt. Changes of wild type (dots, continuous line), the P_{II} mutant (squares, dashed line) or the P_{II}-Venus complemented strain (diamonds, dotted line) are shown as $\log_2$ fold changes compared to wild type levels during exponential growth.

Strikingly glutamine levels were significantly increased in the P_{II} mutant during exponential growth. In combination with low 2-OG levels this led to lowered glutamate pools. High glutamine synthetase (GS) activity has been reported for the P_{II} mutant (Takatani and Omata, 2006) and offers an explanation for the strongly increased glutamine pool. Glutamate pools in the mutant increased one day after nitrogen starvation which coincides with increased 2-OG levels and decreased glutamine levels. Absence of a nitrogen source reduced efficiency of the GS reaction, leading to lowered glutamate consumption resulting in a strong increase of 2-OG. A second striking effect was visible in the GABA-shunt. Succinate semialdehyde (SSA) was not detectable in the P_{II} mutant during exponential growth and was lower in the complemented strain than in wild type. Levels increased upon nitrogen starvation, but didn't reach wild type levels. SSA is the product of transamination of γ-amino butyric acid (GABA) catalyzed by ArgD, a protein detected by co-immunoprecipitation of GlnB. The role of phosphorylated P_{II} might therefore be to stimulate the reaction upon a carbon/nitrogen imbalance in metabolism. Interestingly

methylmalonate a product of branched chain/pyrimidine degradation was not detectable in the P_{II} mutant during exponential growth. Increased levels could be detected upon nitrogen starvation consistent with degradation of amino acids/nucleotides upon nitrogen starvation.

8.1.7.4 Changes in the TCA-cycle

Mutation of *glnB* had a profound effect on the TCA cycle as shown in figure 8.26.

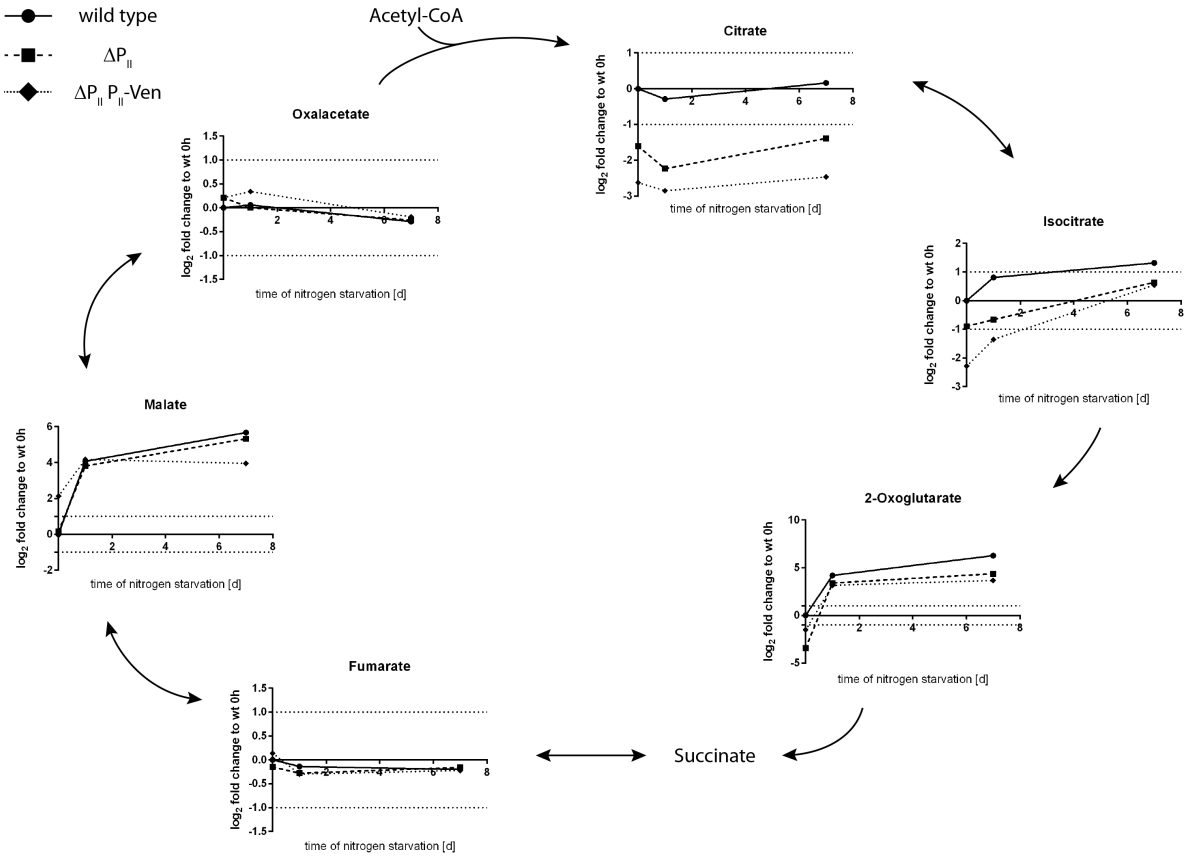

Fig. 8.26: Changes of metabolites upon nitrogen starvation in the TCA-cycle. Changes of wild type (dots, continuous line), the P_{II} mutant (squares, dashed line) or the P_{II}-Venus complemented strain (diamonds, dotted line) are shown as $\log_2$ fold changes compared to wild type levels during exponential growth.

Citrate, isocitrate and 2-oxoglutarate (2-OG) were significantly lower in the P_{II} mutant during exponential growth. Fumarate, malate and oxaloacetate however were hardly affected. Nitrogen starvation led to accumulation of 2-OG, isocitrate and malate, whereas fumarate and oxalacetate levels remained low. Low citrate levels were constantly present in the P_{II} mutant throughout nitrogen starvation and are caused by a combination at least two factors. Lowered 3-phosphoglycerate and lowered acetyl-CoA levels reduced the amount of carbon entering the TCA-cycle during exponential growth, resulting in a depleted citrate pool. Additionally reduced activity of PepC lowers the amount of carbon entering the TCA-cycle through anaplerotic reactions in the P_{II} mutant. The intracellular

red-ox balance shifts to a more reduced cytoplasm upon nitrogen starvation inhibiting malate dehydrogenase. Consequently malate accumulated within the cell in part caused by increased carbon flux through the GABA shunt.

8.1.7.5 Biosynthesis of arginine

GlnB is known to regulate the committed step of arginine biosynthesis through interaction with N-acetyl-glutamate kinase (NAGK) and this deregulation was apparent in the metabolome data shown in figure 8.27.

As expected the levels of N-acetyl glutamic acid were increased during exponential growth, since the absence of P_{II} made NAGK more sensitive to arginine inhibition during exponential growth (Maheswaran et al., 2004). Contrary to the expectation of lowered arginine levels in the P_{II} mutant, arginine levels were even higher than in the wild type. This phenomenon can't be explained by P_{II} mediated regulation of NAGK. The levels of both metabolites dropped upon nitrogen starvation and arginine couldn't be detected after 7 days of starvation in the wild type.

8.1.7.6 Alterations of aspartate derived metabolites

Next to the many changes detected in the other pathways, the levels of aspartate derived metabolites were strikingly increased in the P_{II} mutant and complemented strain. Results are shown in figure 8.28.

Threonine levels were slightly increased in the P_{II} mutant during growth and could be caused by deregulated ThrC detected in co-immunoprecipitation experiments. The two other aspartate derived metabolites were increased: 2-amino 6-oxopimelic acid and lysine. 2-amino 6-oxopimelic acid is in chemical equilibrium with L 2, 3, 4, 5 -tetrahydropicolinate and can be used as proxy to estimate the metabolic flow towards lysine biosynthesis. Lysine levels increased upon nitrogen starvation but accumulation of this metabolite is counter intuitive. Lysine contains an additional amino group and might be synthesized as a medium term nitrogen storage compound. Once an exogenous nitrogen source is available lysine could be used to kick-start the GS-GOGAT cycle. The ϵ-amino group could be used as donor for the synthesis of glutamate from 2-OG through a lysine α-ketoglutarate aminotransferase. Several putative aminotransferases are encoded in the genome of *Synechocystis* sp. PCC 6803 but none has been annotated as lysine α-ketoglutarate aminotransferase. Alternatively this could also be a side reaction of an aminotransferase possibly even ArgD.

8.1.7.7 Conclusive remarks

Mutation of *glnB* strongly alters the metabolic flow during growth and the effects of this are also seen during nitrogen starvation. Unexpectedly the complementation of the P_{II} mutant with fluorescently labeled P_{II} was unable to restore metabolic flows to wild type

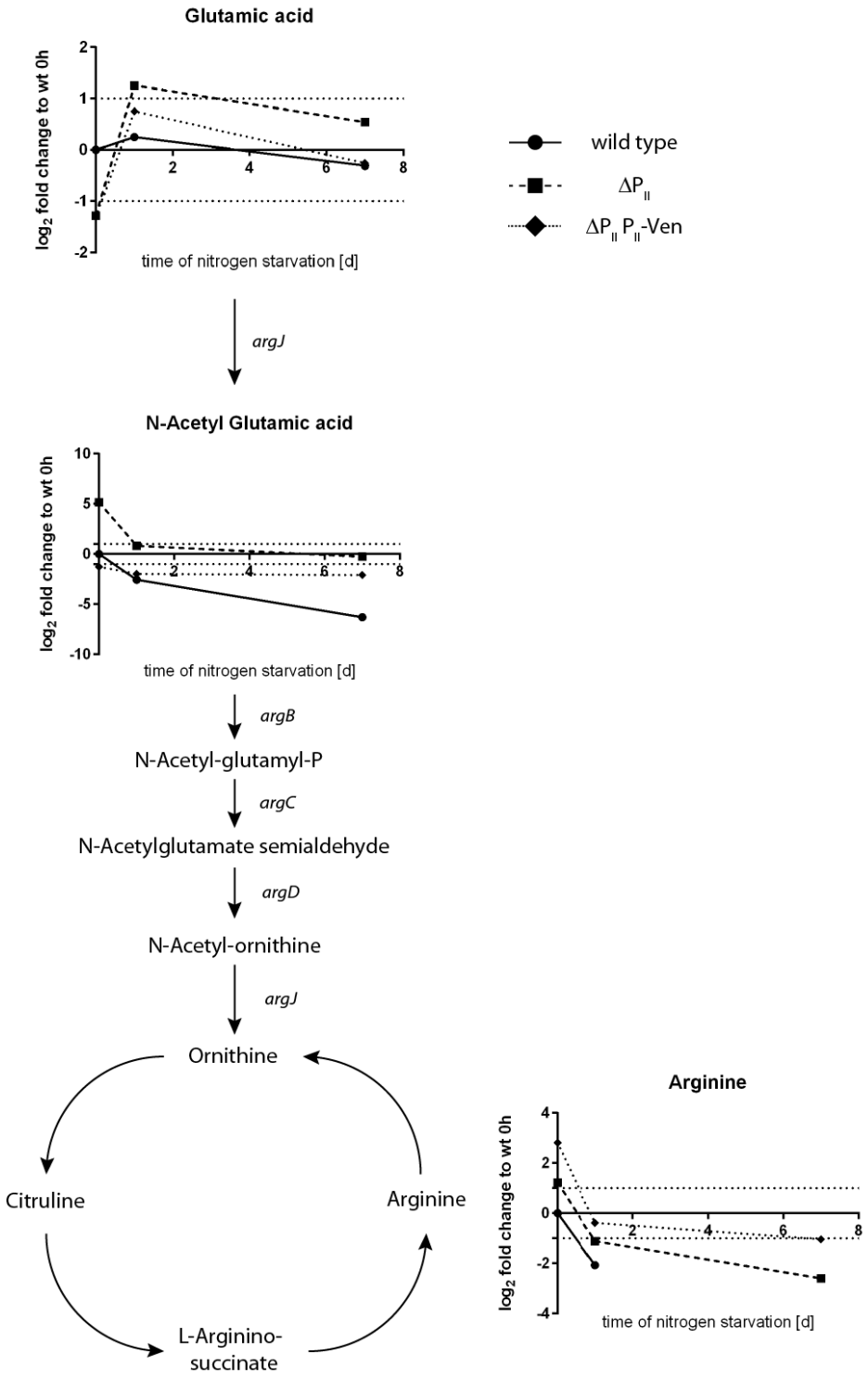

Fig. 8.27: Changes of metabolites upon nitrogen starvation in the biosynthesis of arginine. Changes of wild type (dots, continuous line), the P_{II} mutant (squares, dashed line) or the P_{II}-Venus complemented strain (diamonds, dotted line) are shown as $\log_2$ fold changes compared to wild type levels during exponential growth.

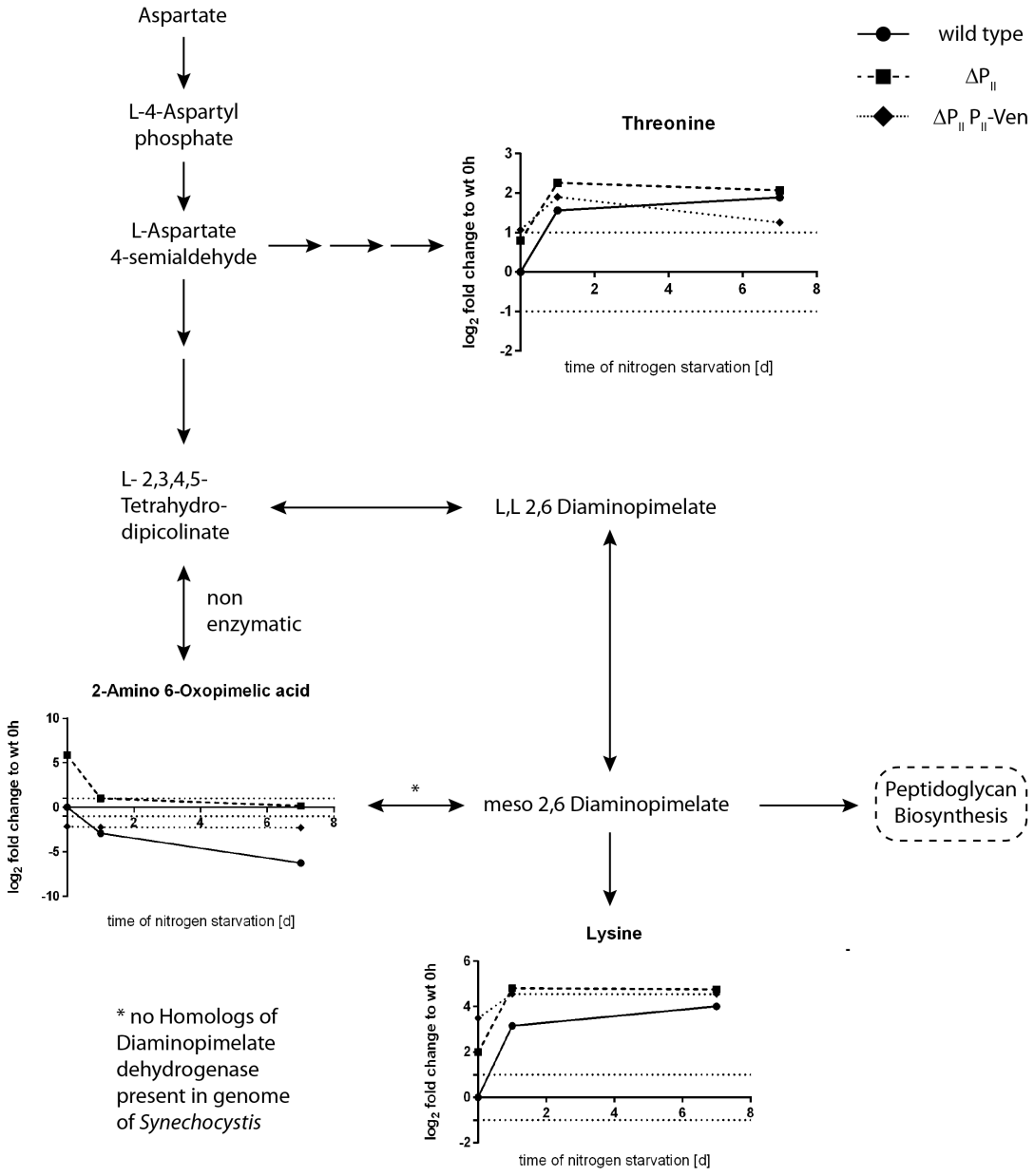

Fig. 8.28: Changes of metabolites upon nitrogen starvation derived from aspartate. Changes of wild type (dots, continuous line), the P_{II} mutant (squares, dashed line) or the P_{II}-Venus complemented strain (diamonds, dotted line) are shown as $\log_2$ fold changes compared to wild type levels during exponential growth.

levels. Only glutamine and N-acetyl glutamic acid levels were similar to wild type levels in the complemented strain. Therefore this complementation is not able to regulate possible targets as the C-terminally added fluorophor has a strong negative effect. Addition of acetate to the growth medium restored steady state acetyl-CoA levels in the P_{II} mutant and enabled wild type like accumulation of PHB in the P_{II} mutant. Upon nitrogen starvation steady state levels of acetyl-CoA were identical in wild type, P_{II} mutant and complemented strains. Nevertheless this complementation restored PHB levels to wild type levels. This strongly suggests that flux through the acetyl-CoA pool is disturbed in the P_{II} mutant, causing reduced PHB accumulation.

8.2 Regulation of PHB synthase

8.2.1 Covalent modification and activation of PHB synthase

PHB synthase has been previously reported to reorganize intracellularly, which coincided with covalent modification and biosynthetic activation (Hauf, 2012). It was suggested that covalent modification could take place at conserved serine residues in PhaE and PhaC. Hence this was investigated more thoroughly.

8.2.1.1 PHB synthase activity and nascent granule formation during exponential growth

PHB synthase activities were measured during exponential growth in wild type and wild type expressing gfp tagged PhaC from a replicative plasmid. Expression of PhaC-Gfp from the exogenous plasmid was described to promote formation of nascent PHB granules during exponential growth.

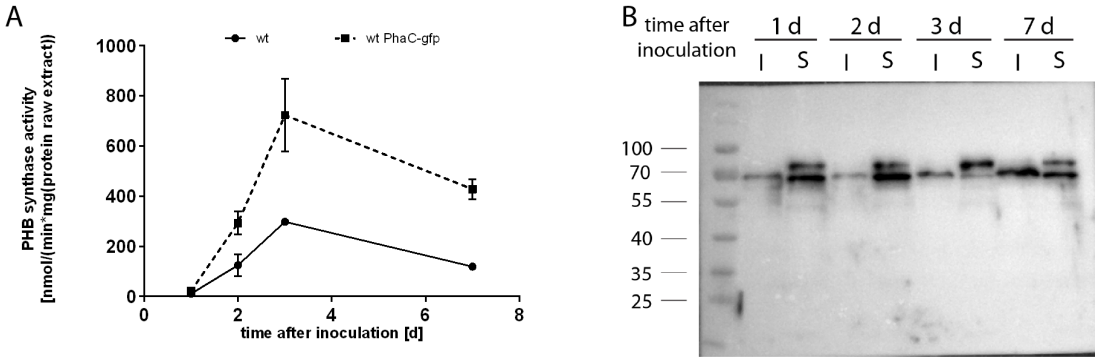

Fig. 8.29: A: Biosynthetic activity of PHB synthase during exponential growth in wild type (circles, continuous line) and PhaC-Gfp (squares, dashed line) expressing strain (mean values of three biological replicates). B: Localization of PhaC-Gfp (66 kDa) in the soluble and insoluble fraction during the growth phase. A second unspecific band with molecular mass above 70 kDa was visible in the soluble fraction and is attributed to a different batch of α-Gfp antibody.

Biosynthetic activity of PHB synthase could be detected throughout the growth phase except at day one. Activity was highest after three days and declined at day seven (figure 8.29 A). Western blot analysis revealed that PhaC-Gfp (66 kDa) localized in both soluble and insoluble fraction throughout growth (figure 8.29 B). An additional unspecific band above 70 kDa was recognized by the antibody in the soluble fraction. The majority of expressed PhaC-Gfp remained soluble throughout growth. Increasing amounts of PHB synthase were detected throughout growth in the insoluble fraction, which correlates with increased biosynthetic activity until day 3. At day 7 PHB synthase was most abundant in the insoluble fraction, but biosynthetic activity was lower than at day 3. Even though PHB synthase was localized in the insoluble fraction, no biosynthetic activity could be detected at day 1. This indicates a mechanism to tune down biosynthetic activity of PHB synthase. As reported previously a small shift was visible between soluble and insoluble PHB synthase, which increased the molecular weight of PhaC in the insoluble fraction.

8.2.1.2 PhaE and PhaC form a stable complex in the nascent PHB grnaule

Class III PHB synthase consists of PhaE and PhaC, both of which are required for catalytic activity. Therefore the insoluble fraction should contain both subunits of PHB synthase and both subunits should be present in the nascent PHB granule. To test this hypothesis cells were grown exponentially for three days and immuno-precipitation experiments were performed with different cellular fractions. Strains expressing either PhaC-Gfp or PhaE-Gfp were used to extract PHB synthase subunits form cell extracts with Gfp-trap magnetic beads (Chromotek).

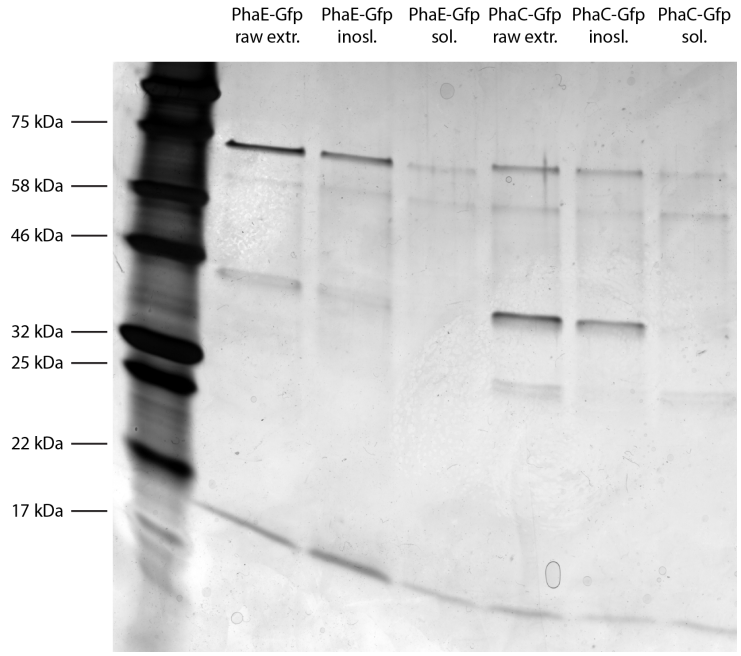

Fig. 8.30: Immuno-precipitation of Gfp-tagged PhaE or PhaC. Different cell fractions were used for immuno-precipitation with the Gfp-trap system.

In all samples a band slightly smaller than 75 kDa is present. This band is most likely PhaE-Gfp in the first three lanes and PhaC-Gfp in lanes four to six (figure 8.30). A second band bigger than 58 kDa was present in all samples and might be unspecific binding to the Gfp-trap. Most interestingly a band below the 46 kDa band was present only in the insoluble fraction and the raw cell extract. The migration in SDS-PAGE corresponds to what would be expected for non tagged PhaE (in case of PhaC-Gfp) or PhaC (in case of PhaE-Gfp). These bands are absent in the soluble fraction which doesn't show catalytic activity. Hence, the nascent granule consists of a stable complex of at least PhaE and PhaC. Several smaller bands could also be detected and might represent additional proteins present in the nascent granule. One of the smaller proteins seen in figure 8.30 might be the recently described phasin protein PhaP (Hauf et al., 2015). To determine whether PhaC and PhaP are both constituents of the nascent PHB granule, a strain expressing PhaP-Venus and PhaC-Cer was constructed. PhaC is translationally fused at the C-terminus with Cerulean (a brighter Cfp variant) and expressed from the native locus

in the genome. PhaP is expressed from a self replicating plasmid and translationally fused to Venus (a brighter Yfp variant) using a flexible linker region between the two proteins.

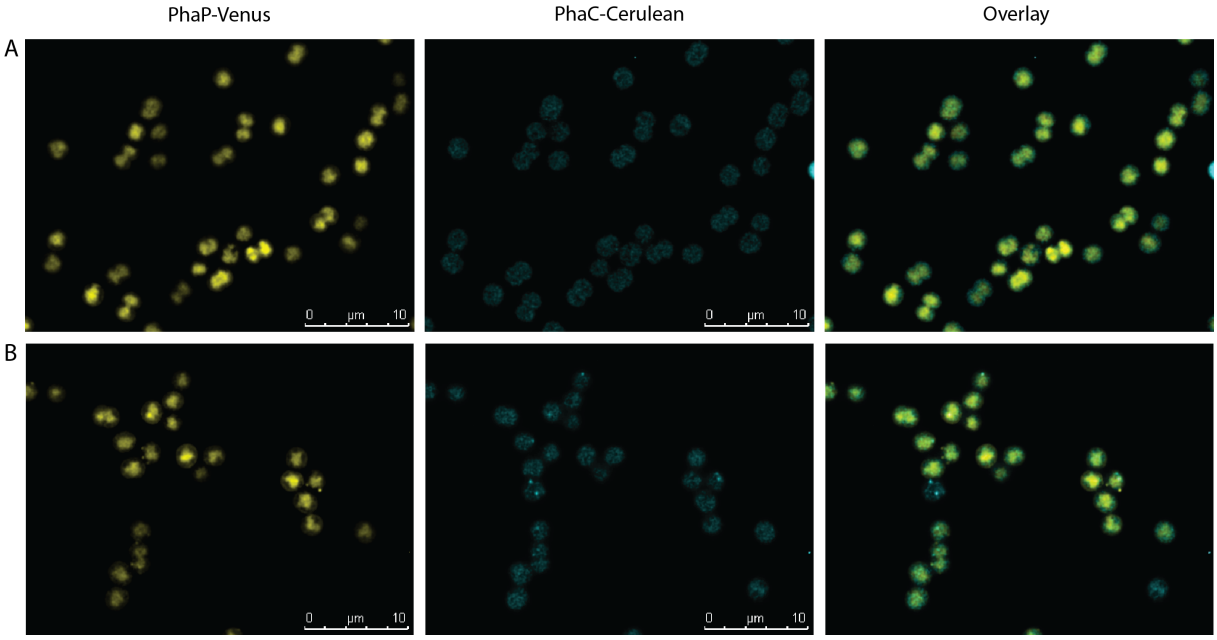

Fig. 8.31: Fluorescence microscopic investigation of PhaC-Cer and PhaP-Ven localization during exponential growth (A) and stationary phase (B).

In contrast to the strain expressing PhaC-Gfp from a plasmid, no nascent granule formation could be observed during exponential growth in the strain expressing PhaC-Cer. Only in later stages of growth (late exponential and stationary phase) nascent PHB granules were formed. PhaC-Cer signal partially co-localized with the PhaP-Ven signal but not all PhaC-Cer spots matched a corresponding spot of PhaP-Ven and vice versa. Biosysnthetic activities of PHB synthase shown in figure 8.29 demonstrated that nascent granules were formed in the strain expressing PhaC-Gfp and the wild type. Otherwise no biosynthetic activity would have been detectable. The absence of distinct PhaC-Cer nascent granules could be caused by low expression of PHB synthase from the native locus in the genome. PhaC-Gfp is expressed form a plasmid and biosynthetic activity of PHB synthase in this strain was 3-4 times higher than in wild type indicating an over-expression of PHB synthase. Nevertheless the strains expressing PhaC-Gfp or PhaE-Gfp present useful systems to study the early formation of PHB granules. Due to the low expression of PhaC-Cer and inferior fluorescence properties of cerulean to Gfp (lower quantum yield, lower fluorescence intensity and faster photobleaching) nascent granules formed in the strain expressing PhaC-Cer might have been below the detection limit of the microscope setup. Hence, absence of a PhaC-Cer signal where a PhaP-Ven signal is present doesn't mean that no PHB synthase is present. Low levels of PhaC are likely present but are below the detection limit of the microscope.

8.2.1.3 Nascent granule formation in the PhaC$_{S105A}$

A conserved serine residue (Ser$_{105}$) was suggested as possible site for covalent modification, which seems to activate the biosynthetic activity of PhaC. Hence, this residue was mutated and its influence on nascent granule formation was tested in a *phaEC*$^-$ background expressing PhaCS105A-Gfp.

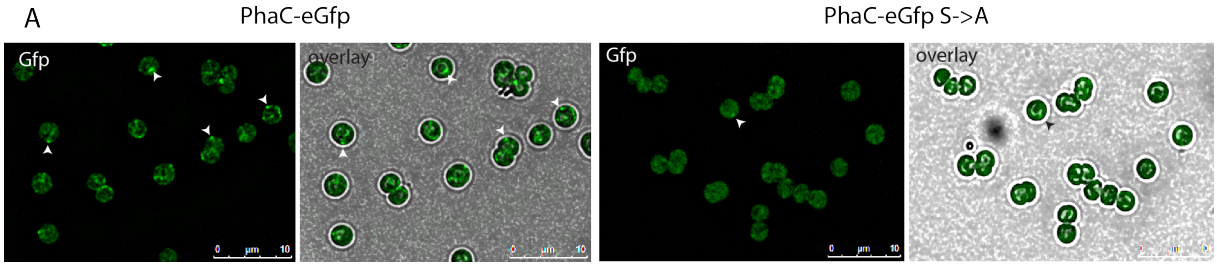

Fig. 8.32: Nascent granule formation of PhaC-Gfp and PhaC$_{S105A}$-Gfp during exponential growth. The position of a nascent granule within the cell is indicated by white arrowheads.

Indeed mutation of Ser105 to alanine strongly reduced the amount of Gfp foci at low and high optical densities, which could have been caused by the inability to covalently modify PhaC (figure 8.32). To test whether PhaC$_{S105A}$-Gfp was still able to produce PHB the strain was subjected to nitrogen starvation to induce strong PHB production.

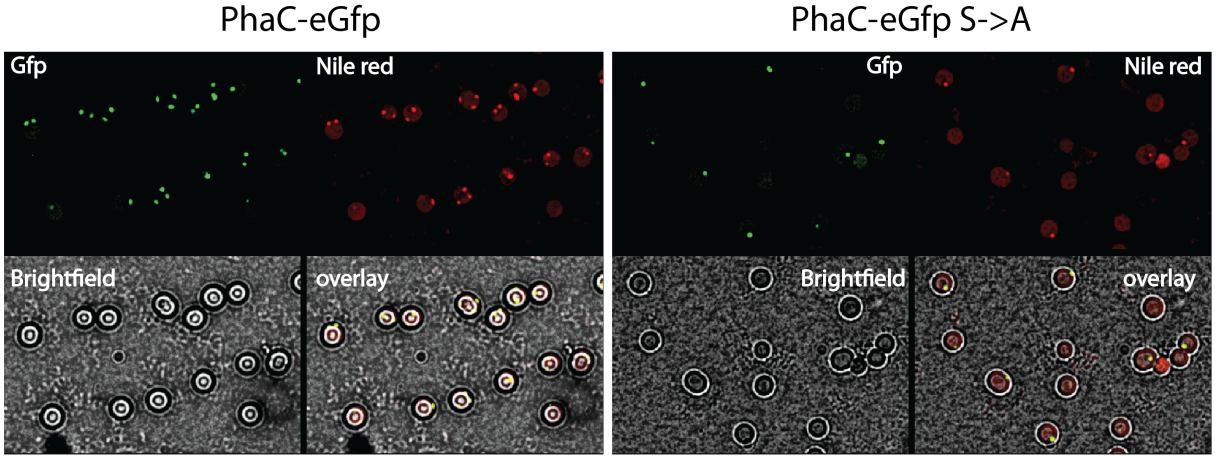

Fig. 8.33: Co-localization of PHB stained with nile red and PhaC-Gfp/PhaC$_{S105A}$-Gfp upon nitrogen starvation.

After 24 hours of nitrogen starvation PHB accumulation was reduced and only one small PHB granule was visible in the strain expressing PhaC$_{S105A}$-Gfp (figure 8.33). Up to three large PHB granules were visible in the control strain. Since microscopic data indicated that PHB accumulation was affected western blot analysis was performed to verify that PHB synthase could still be covalently modified.

Exponentially grown cells expressing PhaC$_{S105A}$-Gfp were used to determine if PhaC$_{S105A}$-Gfp was covalently modified (figure 8.34). The same result as with PhaC-Gfp was obtained. A higher molecular weight PhaC$_{S105A}$-Gfp was detected in the insoluble fraction, while the soluble fraction contained the low molecular weight form. Therefore covalent modification

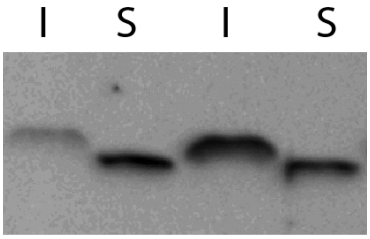

Fig. 8.34: Western blot detection of $PhaC_{S105A}$-Gfp in the soluble and insoluble fraction of cell extracts after 48 and 72 h of growth with α-gfp antibody. I: *insoluble fraction*, S: *soluble fraction*

was not affected by the mutation. Judging by the microscopic images (figure 8.33) less PHB was produced in the strain expressing $PhaC_{S105A}$-Gfp. As this might be linked to reduced PHB synthase levels in the strain this hypothesis was tested by western blot.

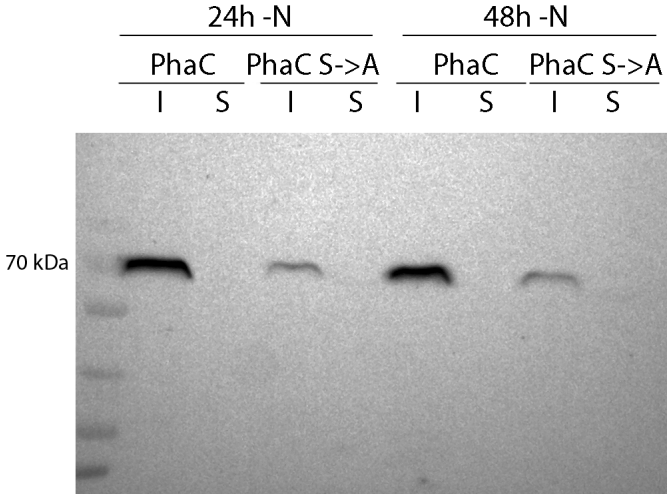

Fig. 8.35: Western blot detection of PhaC-Gfp and $PhaC_{S105A}$-Gfp in the soluble and insoluble fraction of cell extracts after 24 and 48 h of nitrogen starvation with α-gfp antibody. I: *insoluble fraction*, S: *soluble fraction*

Gfp-tagged PhaC was detected in cell extracts of nitrogen starved cultures. Lower levels of $PhaC_{S105A}$-Gfp were present compared to the control strain (figure 8.35). $PhaC_{S105A}$-Gfp levels even declined during nitrogen starvation. Reduced levels of PHB synthase could have been caused by the instability of $PhaC_{S105A}$-Gfp variant. To verify that reduced PHB synthase levels are not linked to protein degradation in raw cell extracts, Gfp fluorescence emission in nitrogen starved cultures was measured *in vivo*.

This measurement confirmed the results of the western blot analysis. Indeed lower Gfp emission of $PhaC_{S105A}$ was detected *in vivo* than in the control strain (figure 8.36). Since the genetic background was identical, reduced PhaC levels can only be explained by reduced stability of the mutated protein. To determine how the mutation could affect protein stability, the secondary structure of PhaC was predicted using the Phyre2 server (Kelley et al., 2015).

PhaC secondary structure was modeled based on gastric lipase. This revealed that

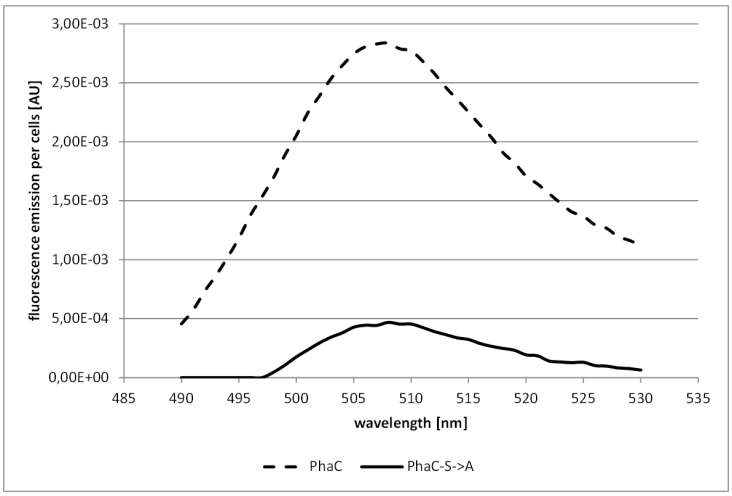

Fig. 8.36: *In vivo* Gfp-fluorescence emission per cell of PhaC-Gfp (dashed line) and $PhaC_{S105A}$-Gfp (continuous line) in arbitrary units [AU].

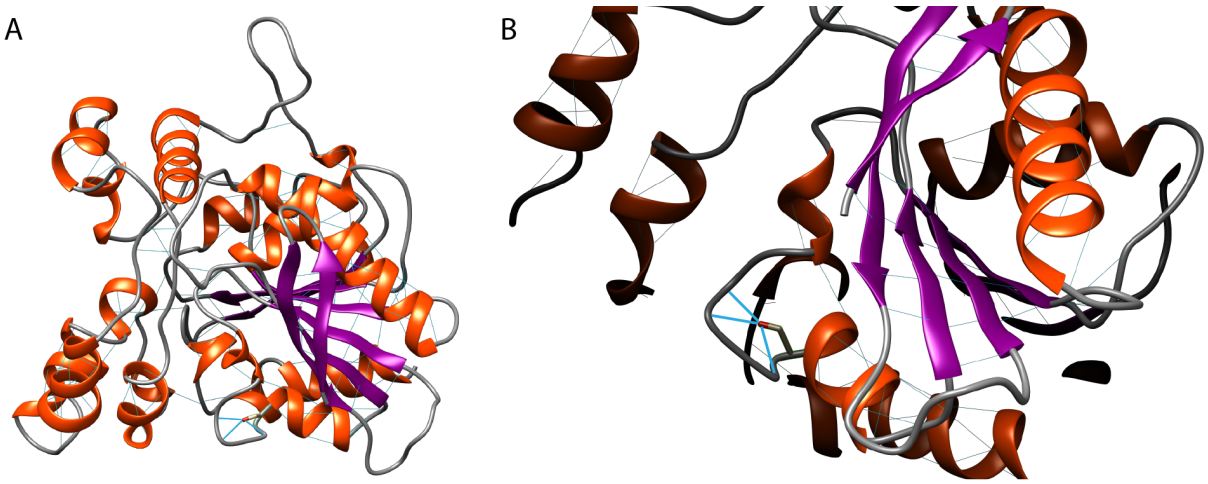

Fig. 8.37: A: Secondary structure prediction of PhaC. Prediction is based on the crystal structure of gastric lipase. B: Zoom in on Serine 105 of PhaC based on secondary structure prediction. Ser 105 is outlined in green and the oxygen atom of serine is shown in red, light blue lines show hydrogen bonds.

Ser_{105} is located within a loop (figure 8.37). The hydroxyl group of serine 105 builds three hydrogen bonds with the peptide backbone and stabilizes the loop structure. Hence, mutation of this conserved residue to alanine, eliminated the stabilizing hydrogen bonds in the loop region making the adjacent α-helices more flexible. The increased flexibility in this region might destabilize the overall α/β-hydrolase fold and make the protein prone to degradation as observed.

8.2.1.4 Nascent granule formation in the $PhaE_{S299A}$

The same set of experiments was performed in a *phaE*$^-$ genetic background expressing either *phaE-gfp* or $phaE_{S299A}$*-gfp* to study the impact of $PhaE_{S299A}$ point mutation.

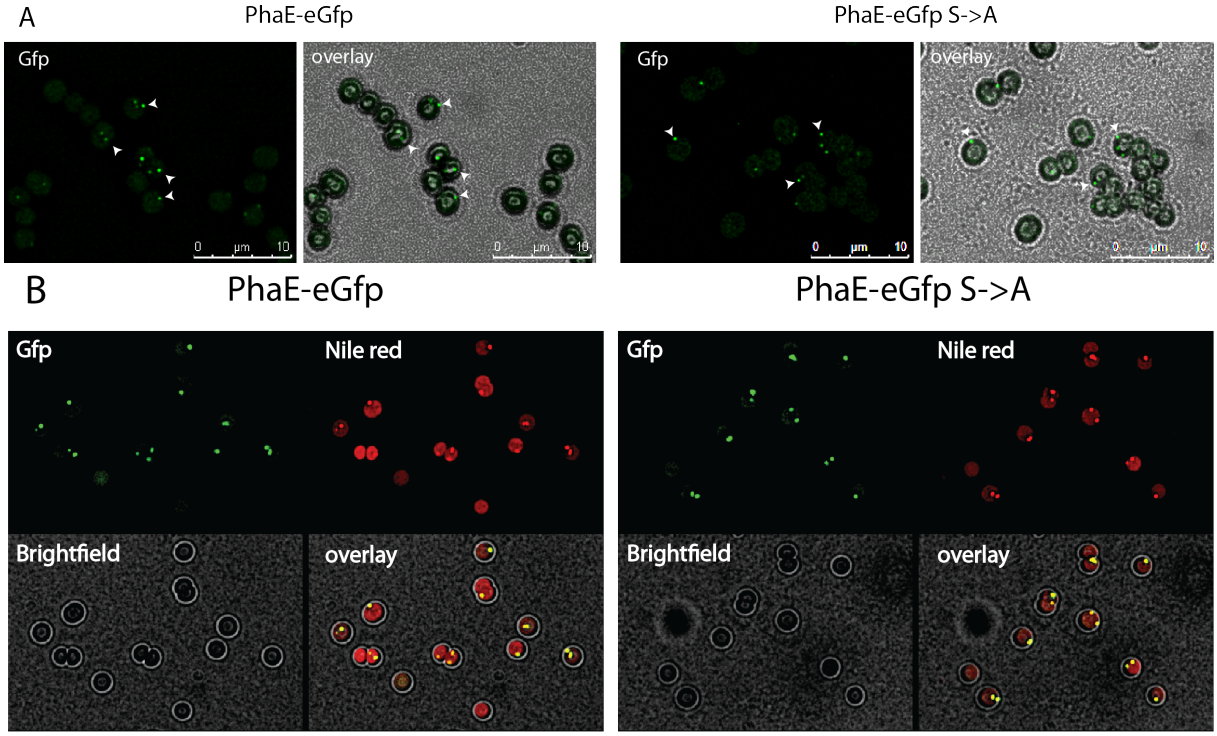

Fig. 8.38: Microscopic images of PhaE-Gfp and $PhaE_{S299A}$ localization during exponential growth (A) and during nitrogen starvation (B). White arrowheads indicate the position of nascent PHB granules.

Nascent granule formation was not affected by the point mutation in PhaE and no differences between wild type and mutated PhaE could be observed during exponential growth (figure 8.38 A). The same is true for nitrogen starvation. No striking difference between wild type and the $PhaE_{S299A}$ variant was visible in the microscopic images (figure 8.38 B). Hence the ability of PhaE to be covalently modified was tested by western blot.

To determine whether covalent modification was still possible, the insoluble and soluble fraction of the cell extract were subjected to SDS-PAGE followed by western blot and detection with an α-Gfp antibody. $PhaE_{S299A}$ could be covalently modified as wild type PhaE, since a distinct high molecular weight band was always present in the insoluble fraction at the same height as in the control (figure 8.39). Therefore serine 299 of PhaE is

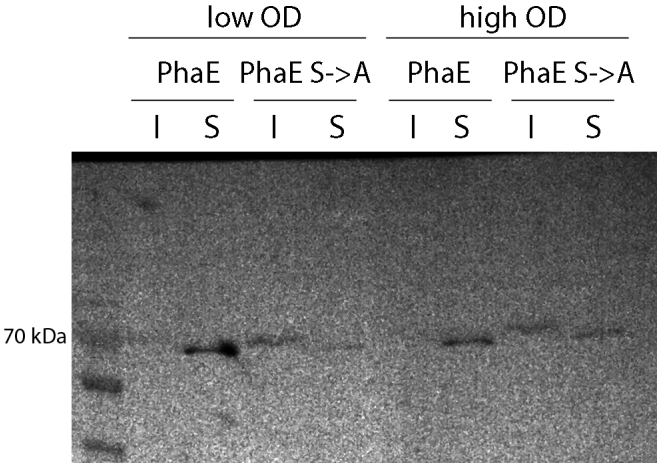

Fig. 8.39: Western blot analysis of PhaE-Gfp and $PhaE_{S299A}$ during exponential growth with an α-gfp antibody. I: *insoluble fraction*, S: *soluble fraction*

not covalently modified and dispensable for catalytic activity.

8.2.1.5 Covalent modification of PhaE and PhaC

The distinct shift of the PhaE and PhaC band in the insoluble fraction was assumed to be caused by a covalent modification. Based on the catalytic mechanism of PhaC a transient thioester is formed between Cys149 and the growing PHB chain. Thioester bonds however are usually hydrolyzed during the preparations of proteins for SDS-PAGE through the presence of a reducing agent (DTT or β-mercaptoethanol) and denaturing protein conditions (75-95 °C for 15-5 minutes). Therefore this covalent modification can be excluded. Nevertheless the modification should be hydrophobic to induce the distinct shift. Acylation and deacylation is a type of covalent modification that could explain the observed shift. Therefore cell extracts expressing either PhaC-Gfp or PhaE-Gfp were subjected to deacylation. PHB synthase was resolved by SDS-PAGE, followed by western blot and detection of the Gfp moiety.

Samples were either treated with 45 mM hydroxylamine for deacylation, a strong reducing environment (500 μM DTT) and without DTT in the sample buffer. The soluble fraction was not treated. The upper band around 70 kDa represents the band corresponding to either PhaE or PhaC in figure 8.40. Independent of the treatment a small shift of the band in the insoluble fraction is always present and acylation and thio-acylation can be excluded as possible covalent modifications of PhaE and PhaC. Signal transduction often involves phosphorylation of target proteins to either activate or inactivate them. Therefore phosphorylation was tested as a possible source of covalent modification using the Phos-tag system.

Raw extracts with PhaE-Gfp and PhaC-Gfp were either treated with alkaline phosphatase for 1 h, which unspecifically cleaves phosphoester bonds, or not. Both proteins in the insoluble fraction were migrating significantly slower in the Phos-tag gel system, but this

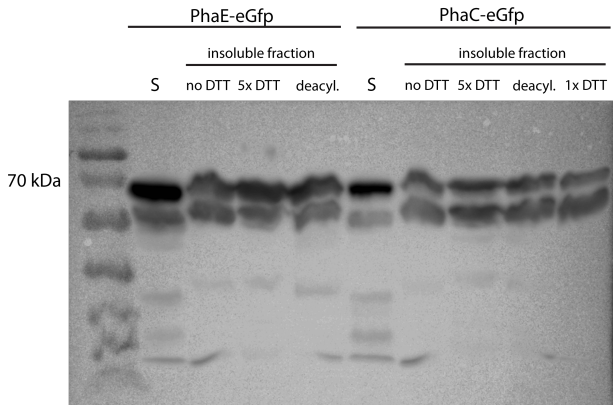

Fig. 8.40: Western blot analysis of PhaE-Gfp and PhaC-Gfp during exponential growth with an α-gfp antibody. Samples were treated with strong reducing reagents to hydrolyze thioester bonds or hydroxylamine for deacylation. I: *insoluble fraction*, S: *soluble fraction*

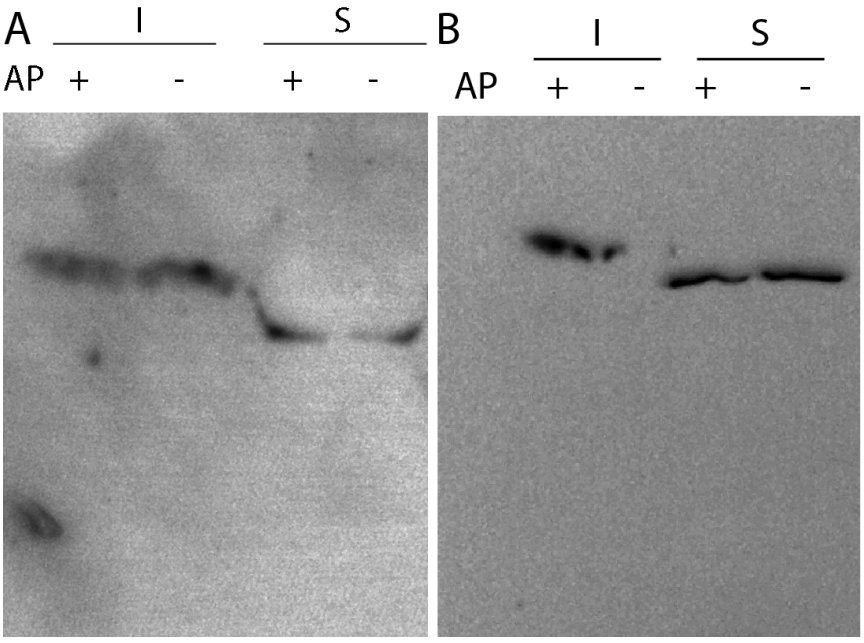

Fig. 8.41: Western blot analysis of PhaE-Gfp (A) and PhaC-Gfp (B) with an α-gfp antibody during exponential growth using the Phos-tag system to detect a possible phosphorylation. I: *insoluble fraction*, S: *soluble fraction* AP: *treated with alkaline phosphatase*

was independent of treatment with alkaline phosphatase. A conclusion of this is, that neither PhaE nor PhaC are phosphorylated. A significantly different migration was observed between the soluble and insoluble fraction; proteins in the insoluble fraction migrated slower than in the soluble fraction. The Phos-tag system increases the retention of negatively charged proteins in SDS-PAGE hence the slower migration. Increased retention can be also interpreted as the loss of a covalent modification (e.g. deacetylation, deformylation) on a negative residue Glu or Asp, but contradicts western blot analysis that suggest an increase of the protein hydrophobicity.

8.2.2 Activation of PHB synthase by acetyl phosphate

8.2.2.1 PHB synthase activation by acetyl phosphate *in vitro*

Miyake et al. (1997) and Sharma et al. (2006) have both reported that acetyl-phosphate stimulates biosynthetic activity of PHB synthase. Acetyl phosphate could act as phosphogroup donor or could be used to acetylate lysine residues thereby activating PHB synthase. As phosphorylation could be excluded, N-acetylation of lysine was tested by western blot using an antibody specifically detecting N-acetyl lysine. Lysine acetylation was examined in raw cell extracts of wild type and *ackA* mutant during exponential growth, stationary phase and nitrogen starvation.

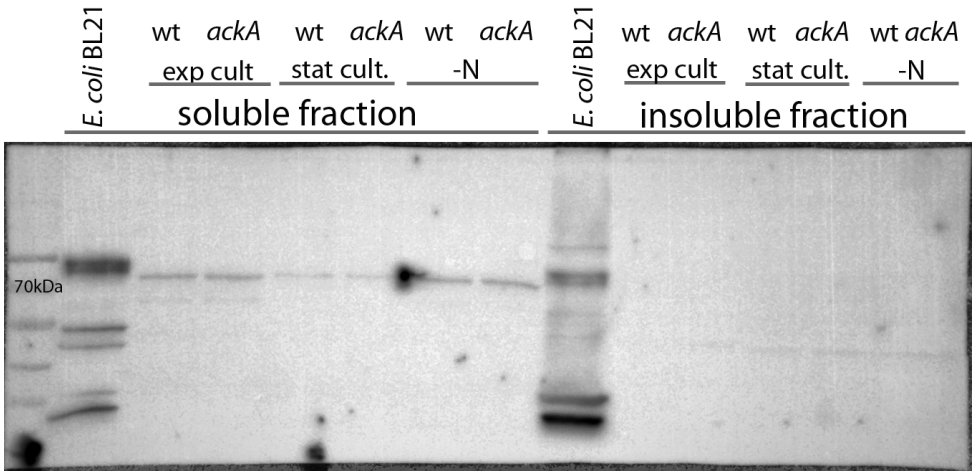

Fig. 8.42: Western blot analysis of N-acetylated lysine residues in raw cell extracts of wild type and *ackA* mutant under different growth conditions using an α-Ac-lysine antibody. I: *insoluble fraction*, S: *soluble fraction*

Several distinct bands were visible in *E. coli* cell extracts and used as positive control (figure 8.42). *Synechocystis* cell extracts did contain only a small fraction of proteins harboring N-acetylated lysine residues. Two distinct protein bands were visible during exponential growth in the soluble fraction. One protein was about 80 kDa and the other about 60 kDa in molecular weight. Acetylation decreased in stationary phase and the 60 kDa band disappeared in stationary phase/nitrogen starvation. The acetylation of the 80 kDa protein seemed to be reduced during stationary phase, but not affected by

nitrogen starvation. The insoluble fraction which harbors active PHB synthase had a very faint band around 50 kDa and is unlikely to be active PHB synthase as it migrates to slow on SDS-PAGE. No differences between acetylation patterns between wild type and *ackA* mutant were visible indicating that acetate signaling as observed in *E. coli* differs in *Synechocystis*. As no indirect activation of PHB synthase through acetylation was visible, the direct effect of acetyl phosphate was tested on raw cell extracts of *Synechocystis*. Cell extracts of wild type grown with 10 mM acetate or without were separated in insoluble and soluble fraction. Different concentrations of acetyl phosphate were added to the reaction mixture and PHB synthase activity was recorded.

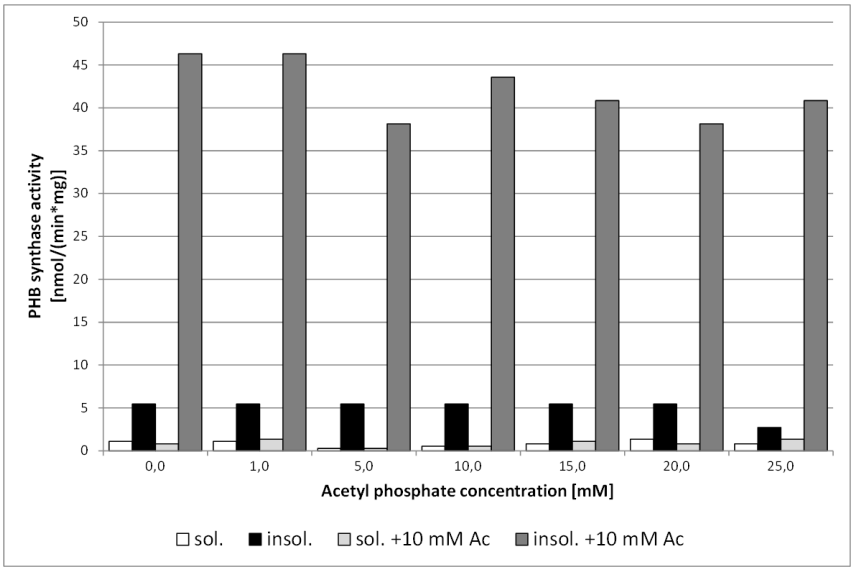

Fig. 8.43: Titration of acetyl phosphate and its influence on PHB synthase activity in the soluble fraction (white bars), insoluble fraction (black bars) of exponentially growing cells, soluble fraction (light grey bars) and the insoluble fraction (dark grey bars) of exponentially growing cells with 10 mM acetate in the growth medium.

PHB synthase activity was higher in the insoluble fractions. Growth with acetate stimulated high PHB synthase activity in the insoluble fraction (figure 8.43). Acetyl phosphate had no effect on PHB synthase activity. Neither the insoluble fraction, where PHB synthase is biosynthetically active and associated in a nascent PHB granule, nor the soluble fraction had increased biosynthetic activities when acetyl phosphate was added. Acetate in the growth medium however stimulated PHB biosynthetic activity possibly due to increased PHB synthase expression. PHB synthesis *in vivo* occurs only after induction of nitrogen starvation. To exclude than an additional factor produced only upon nitrogen starvation stimulates PHB biosynthesis through acetyl phosphate, acetyl phosphate titration was performed with cell extracts of 24 h nitrogen starved cells.

No activity could be measured in the soluble fraction. Acetate supplementation slightly increased PHB synthase activity (figure 8.44). Biosynthetic activity was primarily present in the insoluble fraction. Various concentrations of acetyl phosphate had no effect on PHB synthase activity. High acetyl phosphate activities appeared to actually inhibit biosynthetic

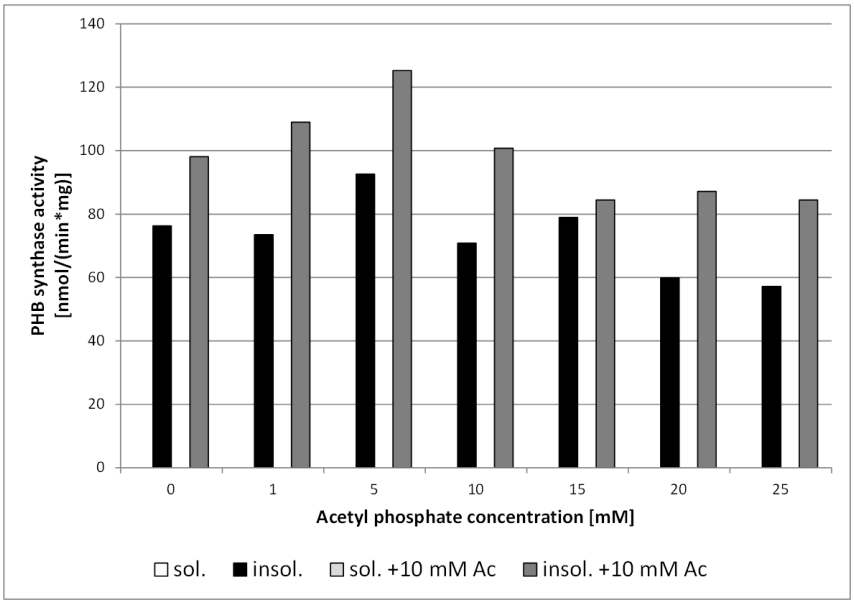

Fig. 8.44: Titration of acetyl phosphate and its influence on PHB synthase activity in the soluble fraction (white bars), insoluble fraction (black bars) of 24 h nitrogen starved cells, soluble fraction (light grey bars) and insoluble fraction (dark grey bars) represent PHB synthase activities of cells cultivated with 10 mM acetate and 24 h nitrogen starved cells.

activity of PHB synthase.

8.2.2.2 PHB synthase activation by acetyl phosphate *in vivo*

Activation of PHB synthase through acetyl phosphate was also tested *in vivo*. To do so, several mutants of acetate metabolism shown in figure 3.3 were generated; single mutants in either acetyl coenzyme A synthetase (*acs*), acetate kinase (*ackA*) or phosphotransacetylase (*pta*), double mutants in *acs*/*ackA*, *acs*/*pta* and a triple mutant in *acs*/*ackA*/*pta*. Deletion of target genes was verified by extraction of genomic DNA and subsequent PCR analysis with one nested primer annealing in region of the gene which should have been deleted. Growth of mutant strains was tested without antibiotics in the medium.

All generated strains did not have an apparent defect in growth as shown in figure 8.45. No prolonged lag phase was visible and growth rates were similar between wild type and mutants. The only difference observed was the lower optical density of the *pta* mutant, which became visible after two weeks of cultivation. This was not pursued any further as no obvious connection to PHB biosynthesis was expected. These mutants were expected to be affected in PHB synthase activities, therefore biosynthetic activity was measured during nitrogen starvation.

Mutation of *acs* did not have any effect on PHB synthase activity. *AckA* and *pta* mutation led to a slightly reduced activity of PHB synthase throughout nitrogen starvation. Differences were more profound after two and three days of nitrogen starvation (figure 8.46 A). The difference between the wild type and mutants was not big and contradicts the

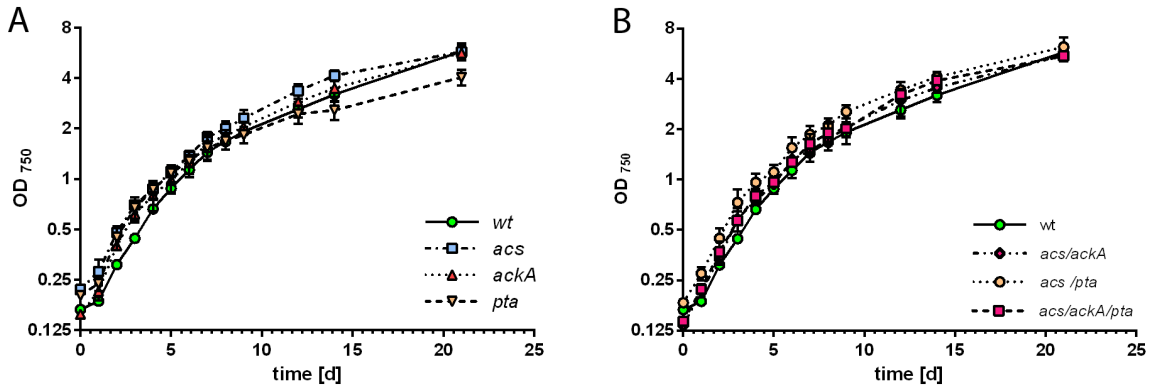

Fig. 8.45: Exponential growth of mutant strains without antibiotics in the growth medium. Measurements represent mean values of three biological replicates. A: wild type (green circles), *acs*- (blue squares), *ackA*- (purple triangles) and *pta*-mutant (orange inverted triangles). B: wild type (green circles), *acs/ackA*- (red diamonds), *acs/pta*- (orange circles) and *acs/ackA/pta*-mutant (purple squares).

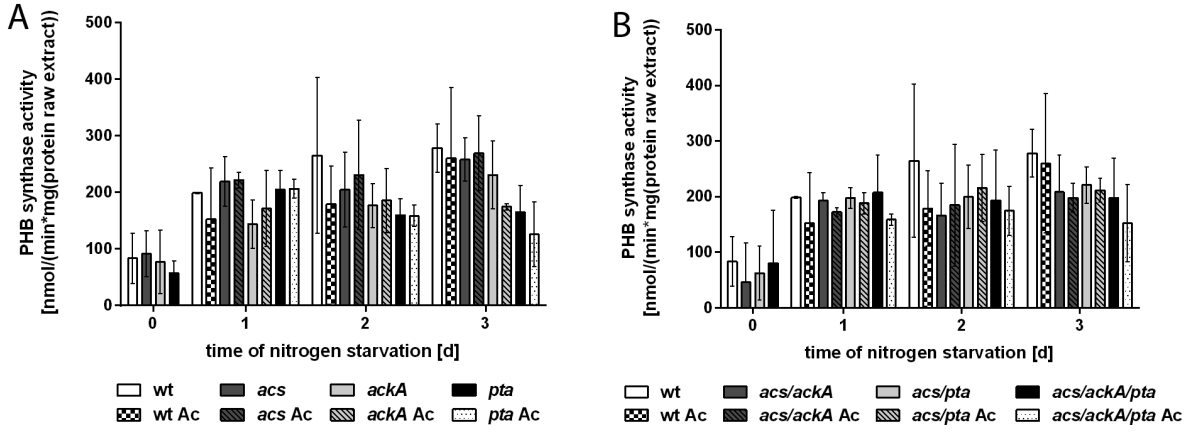

Fig. 8.46: Biosynthetic activity of PHB synthase during nitrogen starvation supplemented with 10 mM acetate or not. Values represent the mean values of three biological replicates. A: wild type (white bars), wild type with acetate (white/black checked bars), *acs*-mutant (dark grey bars), *acs*- mutant with acetate (dark grey, diagonally striped bars), *ackA*-mutant (light grey bars), *ackA*- mutant with acetate (light grey, diagonally striped bars), *pta*-mutant (black bars) and *pta*-mutant with acetate (white dotted bars). B: wild type (white bars), wild type with acetate (white/black checked bars), *acs/ackA*-mutant (dark grey bars), *acs/ackA*-mutant with acetate (dark grey, diagonally striped bars), *acs/pta*-mutant (light grey bars), *acs/pta*-mutant with acetate (light grey, diagonally striped bars), *acs/ackA/pta*-mutant (black bars) and *acs/ackA/pta*-mutant with acetate (white dotted bars).

model proposed by Miyake et al. (1997) and Sharma et al. (2006). According to that model PHB synthase should be activated in the *pta* mutant when acetate is present in the growth medium, due to increased intracellular acetyl phosphate levels. But the opposite was observed. The same is true for the *ackA* mutant, which should have increased intracellular levels of acetyl phosphate without acetate supplementation. Again biosynthetic activity of PHB synthase was reduced and not increased. The same result was observed when double mutants in *ackA/acs*, *pta/acs* or the triple mutant *acs/ackA/pta* were examined (figure 8.46 B). After one day of nitrogen starvation PHB synthase activities were at wild type levels but decreased at day two and three compared to wild type. Oddly PHB biosynthetic activities in the triple mutant were slightly reduced by acetate supplementation, even though acetate uptake should have been abolished and not able to influence synthase activity. To determine whether the small differences in synthase activities would be reflected in total PHB accumulated, the PHB content was determined during nitrogen starvation.

All differences of PHB accumulation were only minor and represent a single biological measurement (figure 8.47). In all strains fed with acetate and a *acs* mutation, the PHB amount was reduced after 7 days of nitrogen starvation when compared to wild type. As expected acetate uptake is facilitated by *acs* in *Synechocystis*, whereas *ackA* and *pta* seem to be dispensable for acetate uptake during nitrogen starvation. No correlation between low PHB synthase activity and PHB accumulation in *pta* or *ackA* mutants was evident. Taken together the experimental evidence demonstrates that acetyl phosphate does not stimulate PHB synthase activity in *Synechocystis*.

8.2.3 Proteins assisting PHB granule formation

In the model organism for PHB accumulation *Ralstonia eutropha* H16 next to PHB synthase up to 9 different phasin proteins are associated with the PHB granule surface. To identify additional proteins at the PHB granule surface in *Synechocystis*, PHB granule formation was induced through 3 d of nitrogen starvation in wild type, a strain expressing PhaC-Gfp or PhaE-Gfp. PHB granules were isolated using the Gfp-trap system and proteins immuno-precipitated were analyzed by mass spectroscopy. 850 Proteins were identified in the different fractions, which roughly corresponds to one fifth of all genes encoded in the genome. Signal intensities between the runs with wild type, PhaC-Gfp and PhaE-Gfp varied and therefore could not be used to calculate enrichment factors. Hence, three criteria were defined to eliminate false positive candidates.

1. False discovery rate > 0 (q-value>0)
2. The number of peptides detected in the control sample was higher than in the PhaE-Gfp sample.
3. Sequence coverage was lower than PhaE in the PhaC-Gfp pull-down experiment, or lower than PhaC in PhaE-Gfp pull down experiment.

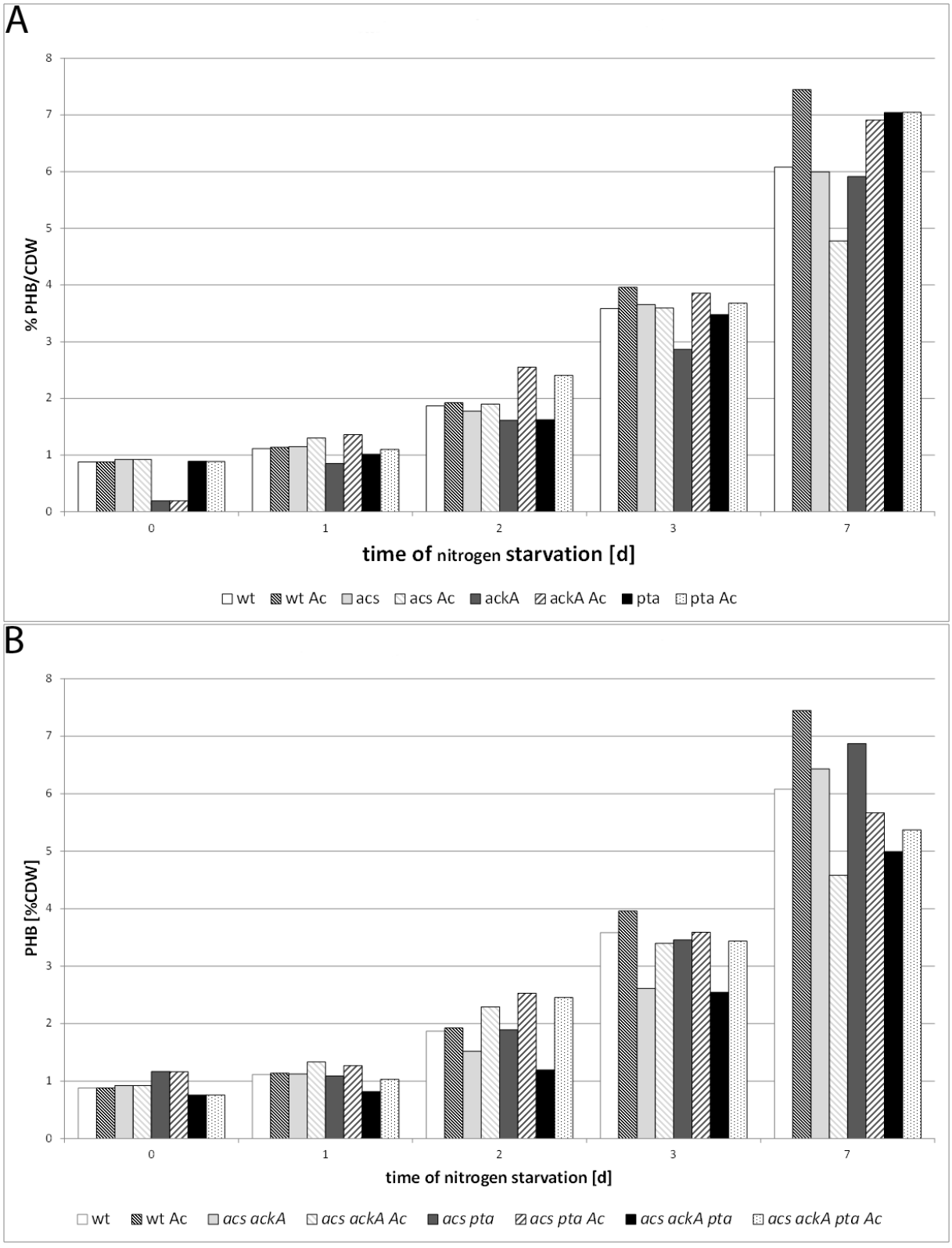

Fig. 8.47: PHB content in % cell dry weight (CDW) upon nitrogen starvation without and with acetate in the growth medium. A: wild type (white bars), wild type with acetate (white/black diagonally striped bars), *acs*$^-$ (light grey bars), *acs*$^-$ with acetate (diagonally striped, light grey bars), *ackA*$^-$ (dark grey bars), *ackA*$^-$ with acetate (diagonally striped, dark grey bars), *pta*$^-$ (black bars) and *pta*$^-$ with acetate (white dotted bars). B: wild type (white bars), wild type with acetate (white/black diagonally striped bars), *acs/ackA*$^-$ (light grey bars), *acs/ackA*$^-$ with acetate (diagonally striped, light grey bars), *acs/pta*$^-$ (dark grey bars), *acs/pta*$^-$ with acetate (diagonally striped, dark grey bars), *acs/ackA/pta*$^-$ (black bars) and *acs/ackA/pta*$^-$ with acetate (white dotted bars).

Results are shown in table 8.7.

Tab. 8.7: Proteins identified in co-immuno-precipitated samples of PhaE- and PhaC-Gfp pull downs.

locus ID	protein	biol. function
slr0455	Slr0455	unknown
slr0058	Slr0058	unknown
slr1839	CcmK4	carbon fixation
slr0585	ArgG	arginine biosynthesis
slr2076	GroL1	chaperone
sll1578	CpcA	photosynthesis
ssr0482	RpsP	ribosomal protein
ssr1399	RpsR	ribosomal protein
ssl3437	RpsQ	ribosomal protein
sll1099	TufA	protein translation
sll0368	PyrR	nucleotide metabolism
slr0623	TrxA	thioredoxin
sll1621	Sll1621	peroxiredoxin

Several proteins of the ribosome were detected as well as proteins involved in photosynthesis. These proteins are highly abundant in the cell and likely represent false positives and were not considered to be associated to the PHB granule surface. Pötter et al. (2004) and others have previously identified chaperones in PHB granule preparations (Han et al., 2001). It has been speculated that chaperones could substitute for phasin proteins possibly explaining the association of GroL1 to the PHB grnaule surface. PHB synthase activities have been reported to respond to the intracellular red-ox balance (Hauf et al., 2013). Therefore detection of thioredoxin and peroxiredoxin might present a regulatory link between red-ox balance and PHB metabolism next to S-glutathionylation of PhaE (Chardonnet et al., 2015). It is unclear how ArgG, CcmK4 and PyrR could be related to PHB metabolism and were not further investigated. The two proteins encoded by *slr0455* and *slr0058* have a PhaF domain which is present in phasin proteins of *Pseudomonads*. PhaF is thought to aid in distributing PHB granules to daughter cells (Maestro et al., 2013; Galan et al., 2011). As these two proteins represented potentially new PHB associated regulatory proteins, they were translationally fused to Venus and expressed in a strain expressing PhaC C-terminally fused to mTurquoise2 (a brighter and more photostable Cfp). Localization of Slr0058 was investigated during stationary phase and nitrogen starvation.

As seen in figure 8.48 Slr0058 primarily localized in the cell periphery close to the cytoplasmic membrane but was also detectable in the cytoplasm. Upon nitrogen starvation the venus signal intensity dropped, which is likely caused by protein degradation upon nitrogen starvation. In several cells the mTurq2 and Ven signal co-localized as indicated by white arrowheads. Co-localization is an indication that Slr0058 might indeed localize to PHB granules but this conclusion requires additional experimental verification. The same experiment was performed to determine Slr0455 localization.

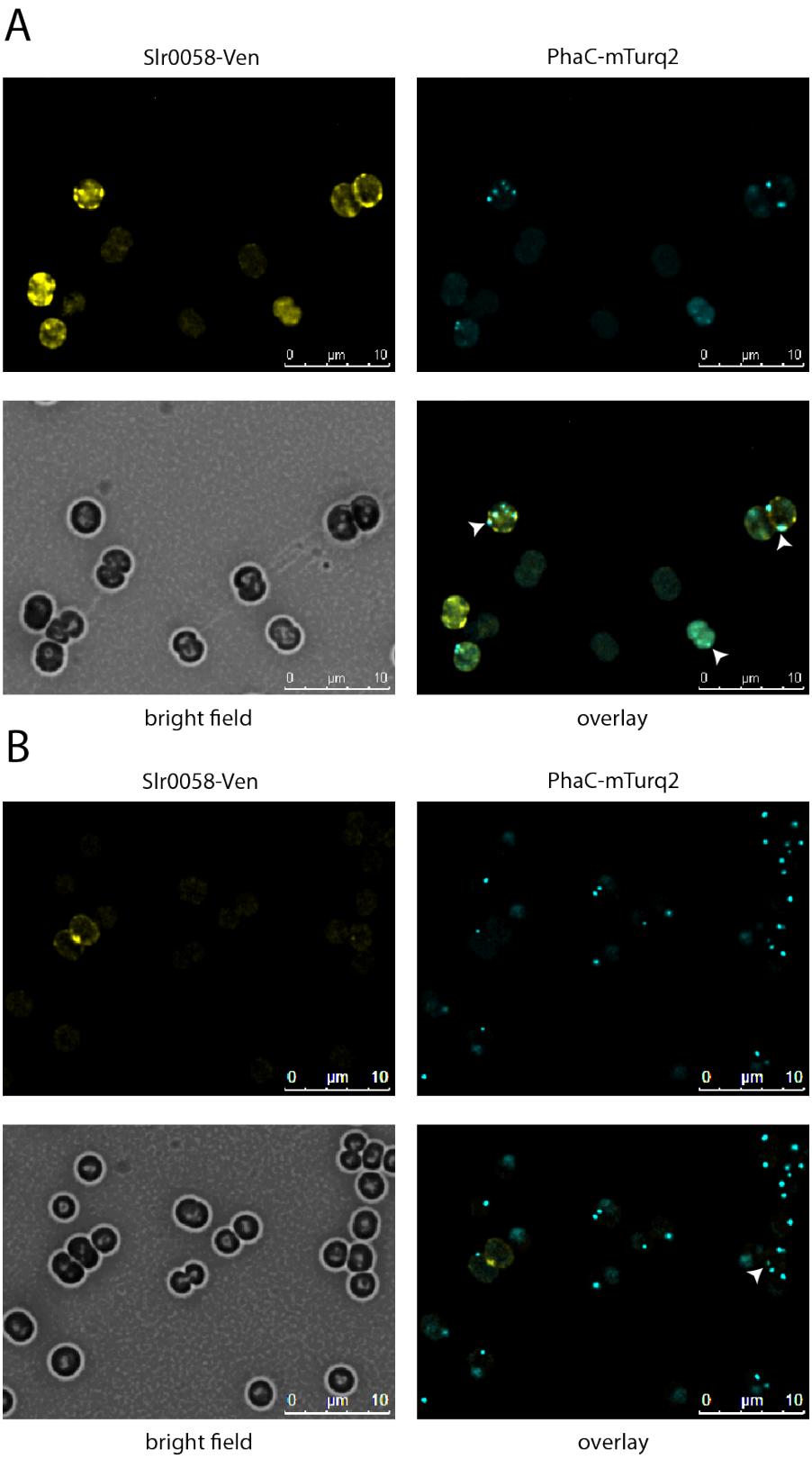

Fig. 8.48: Localization of PhaC-mTurq2 and Slr0058-Ven during stationary phase (A) and nitrogen starvation (B) in *Synechocystis*. Co-localization between Slr0058 and PhaC is indicated by the white arrowheads in the overlay image.

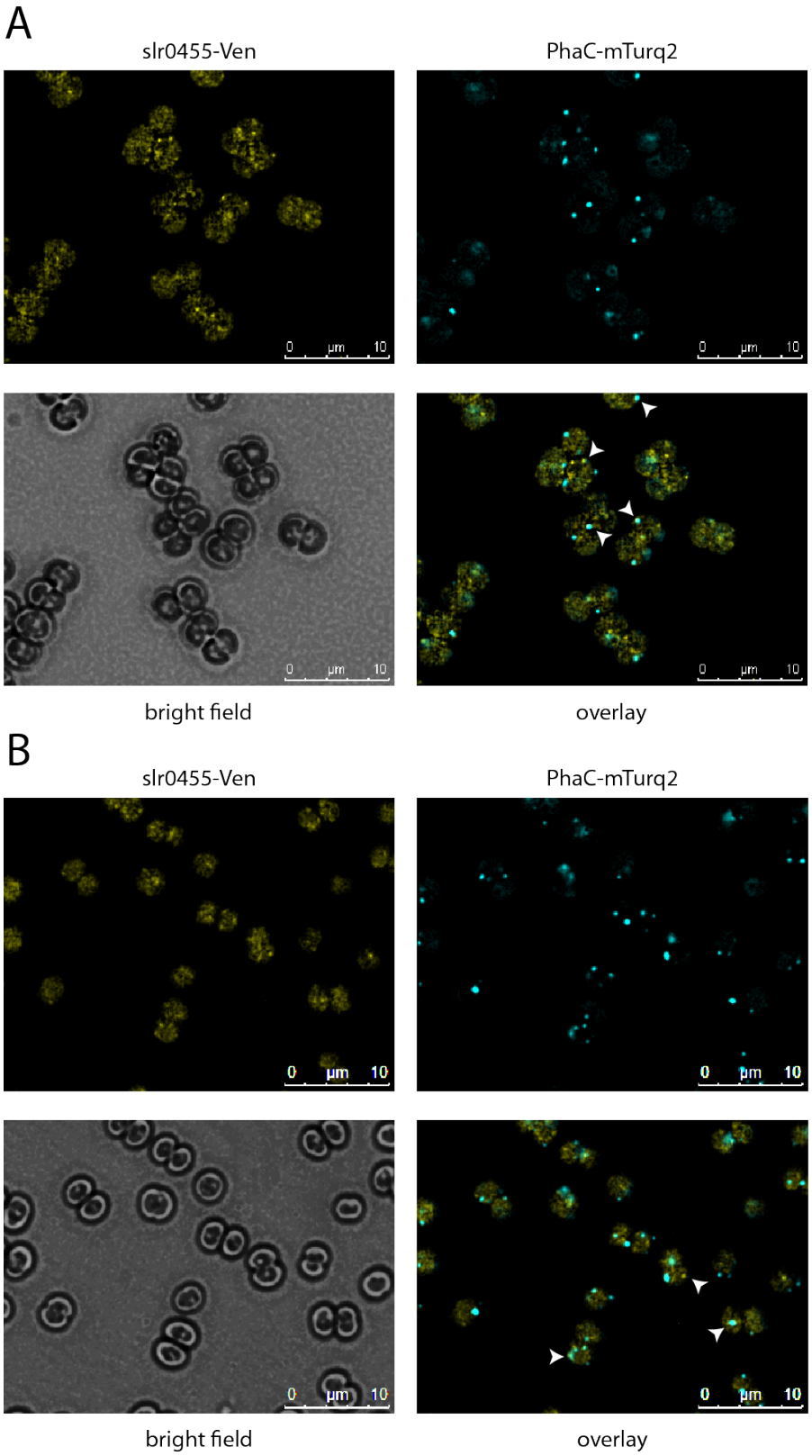

Fig. 8.49: Localization of PhaC-mTurq2 and Slr0455-Ven during stationary phase (A) and nitrogen starvation (B) in *Synechocystis*. Co-localization between Slr0455 and PhaC is indicated by the white arrowheads in the overlay image.

Signal intensities of Slr0455-Ven in stationary phase and nitrogen starvation were low and can be seen in figure 8.49. Slr0455-Ven was visibly concentrated in foci within the cytoplasm during stationary phase and nitrogen starvation. The Slr0455-Ven foci partially co-localized with the PhaC-mTurq2 signal, therefore Slr0455 might be associated to PHB granules *in vivo*. Partial co-localization of both proteins investigated shows that both proteins might be involved in PHB metabolism but requires additional experimental verification.

8.2.4 Increasing PHB production through genetic engineering

As shown in figure 8.7 over-expression of foreign *phaAB* tripled the amount of intracellular PHB. To determine whether this could also be achieved by strong expression of *phaEC* (PHB synthase), native *phaEC* operon was placed under the highly expressed *psbA2* promoter and PHB synthase activity was determined after nitrogen starvation.

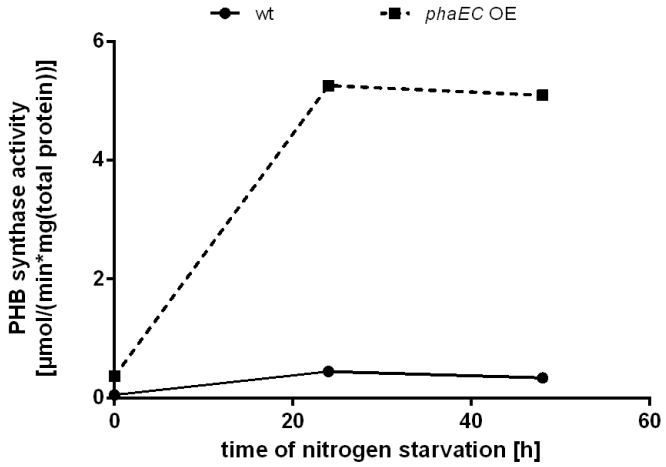

Fig. 8.50: Biosynthetic activity of PHB synthase in wild type (circles, continuous line) and the strain strongly expressing the *phaEC* operon (squares, dashed line) upon nitrogen starvation.

PHB synthase activity was seven fold higher during exponential growth and was roughly 20 fold increased upon nitrogen starvation compared to wild type. Expression of this promoter is not significantly affected by nitrogen starvation (Krasikov et al., 2012). The increase of activity upon nitrogen starvation could be related to the covalent modification described before. To test whether increased biosynthetic activity led to increased PHB accumulation cells were investigated microscopically during nitrogen starvation.

Nile red fluorescence in the wild type stained distinct areas within the cells which correspond to PHB granules. The staining in the *phaEC* over-expressing strain was more dispersed and many small granule like structures were visible (figure 8.51). Much more PHB synthase is present to initiate PHB granules but the precursor biosynthesis is not changed. Hence, the number of PHB granules is strongly increased, wheres the size decreased due to a lack of precursors. To test this hypothesis the PHB content was determined under

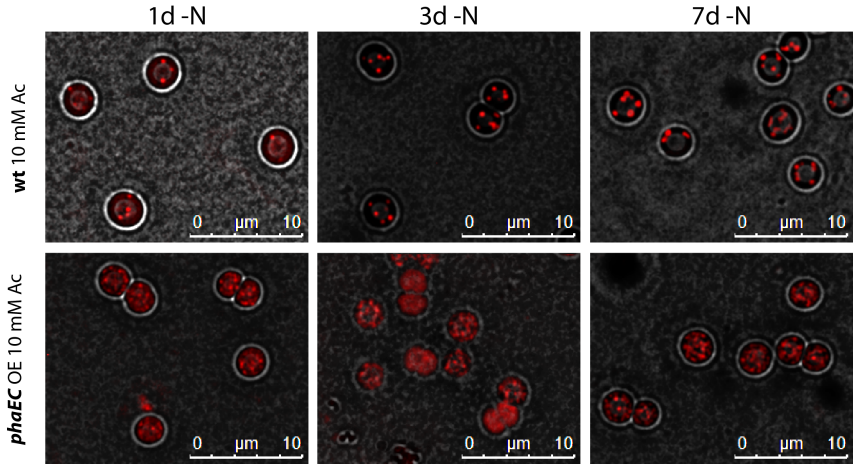

Fig. 8.51: Microscopic investigation of PHB in wild type *Synechocystis* and *phaEC* over-expressing strain. PHB is stained with nile red.

nitrogen starvation.

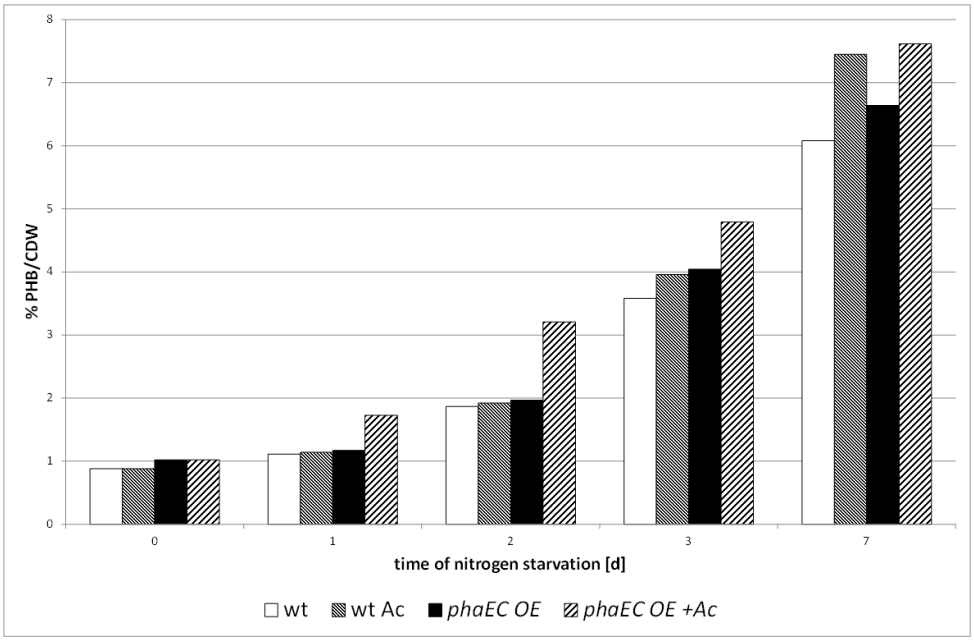

Fig. 8.52: Accumulation of PHB in wild type (white bars), wild type supplemented with acetate (grey dotted bars), *phaEC* over-expressing strain (black bars) and *phaEC* over-expressing strain supplemented with acetate (black diagonally striped bars) upon nitrogen starvation.

Indeed no big difference between the wild type and the *phaEC* over-expressing strain could be detected (figure 8.52), confirming the hypothesis. This demonstrates that precursor supply limits PHB biosynthesis under the tested conditions and regulation of PhaA and PhaB is essential to increase PHB accumulation.

9 Discussion

9.1 Metabolic alterations in *Synechocystis* sp. PCC 6803

9.1.1 Metabolic changes upon nitrogen starvation

Two stages of adaptation towards nitrogen starvation are visible metabolically; a first quick response to supply amino acids for proteome remodeling and a long term response characterized by reduced metabolic activity to sustain survival (e.g. reduced synthesis of isoprenoids) (Görl et al., 1998). A first transient peak of amino acid levels occurs within the first 24 h of nitrogen starvation and coincides with increases in sugar levels, concomitant with accumulation of ketoacids. Chlorosis triggers the degradation of light harvesting complexes within 24 hours, which can make up 50 % of all celluar proteins (Görl et al., 1998; Herrero et al., 2008). Proteolysis liberates amino acids from proteins into the cytoplasm, explaining the transient peak in amino acid levels even though the cellular nitrogen to carbon ratio gradually changes from 1:5 to 1:10 (Krasikov et al., 2012). Long term adaptation to nitrogen starvation leads to a strong reduction of amino acid pools as no external nitrogen source is present to sustain amino acid biosynthesis. An interesting exception to this rule is the accumulation of lysine (and to a lesser extent threonine) upon nitrogen starvation. Even though lysine possesses an additional amino group at the ϵ position, this amino acid accumulates with prolonged nitrogen starvation. Lysine degradation to α-aminoadipatic semialdehyde has been connected with oxidative or osmotic stress resistance in eukaryotes. Expression of this lysine degradation pathway with α-aminoadipatic semialdehyde as intermediate increased osmotic tolerance in *E. coli* (Neshich et al., 2013). Hence, increased levels could be a proxy for the synthesis of α-aminoadipatic semialdehyde to increase stress tolerance in *Synechocystis*. Alternatively the accumulation of lysine during nitrogen starvation could be a medium term response, which enables the cells to boost glutamate synthesis from internal reservoirs once a suitable nitrogen source is present. This would provide sufficient substrate for tetrapyrrole biosynthesis re-initiate photosynthesis and glutamine synthesis through the GS-GOGAT cycle. Intermediates of glycolysis increased within 24 hours of nitrogen starvation to facilitate glycogen synthesis. Glycogen accumulation is crucial for survival under nitrogen deplete conditions and strongly increased under these conditions (Gründel et al., 2012; De Philippis et al., 1992a). Nitrogen starvation therefore redirects the carbon flux favoring gluconeogenesis and glycogen synthesis instead of pentose phosphate pathway, glycolysis and amino acid biosynthesis. Ketoacid levels increased within 24 hours nitrogen starvation especially intermediates of the TCA cycle. Amino acid degradation produces metabolites that enter the TCA cycle as acetyl-CoA, 2-OG, succinyl-CoA, fumarate and oxaloacetate, the latter one being quickly converted to malate due to its chemical instability in aqueous solution. Citrate/isocitrate, 2-OG and malate were exactly the metabolites of the TCA cycle that accumulated during nitrogen starvation. Therefore amino acid degradation contributes to the accumulation of TCA cycle metabolites. This has also implications

for the cellular pH, which would be lowered and might be counteracted by accumulation of lysine. Interestingly nitrogen starvation activates the GABA shunt in *Synechocystis*, which was though to operate in the dark to provide redox equivalents for respiration but is less active under photoautotrophic growth (Xiong et al., 2014). As 2-OG accumulates in the course of nitrogen starvation, the GABA shunt might be triggered to prevent overaccumulation of 2-OG. As a consequence a more reduced intracellular environment is created by enhanced flux through the TCA-cycle.

9.1.2 Altered metabolism of the P_{II} mutant

Deletion of *glnB* has a significant influence on cellular metabolism during growth. A significant drop in acetyl-CoA levels was observed due to the deregulation of acetyl-CoA carboxylase (ACC). Increased substrate turnover of ACC changed the metabolic steady state resulting in low acetyl-CoA levels in the mutant. Lowered acetyl-CoA levels led to reduced citrate pools and therefore reduced the 2-OG levels, hampering carbon flux towards amino acid biosynthesis through the GS-GOGAT cycle. This is also reflected in the reduced glutamate levels of the mutant. P_{II} deletion leads to an increased glutamine synthetase (GS) activity (Takatani and Omata, 2006), which additionally drains the glutamate pool leading to increased glutamine levels. Increased GS activity is most likely a result of enhanced transcriptional activity of NtcA due to the fact that PipX is no longer in complex with P_{II} and can co-activate NtcA mediated transcription. NtcA mediates the transcription of several genes including the transcription factor NrrA (rre37) (Liu and Yang, 2014; Joseph et al., 2014). NrrA has been implied in the regulation of arginine anabolism facilitating the transcription of *argD* and *argG*. Increased transcriptional activity of NtcA should lead to increased NrrA levels. This in turn would activate gene transcription of arginine biosynthesis leading to increased arginine levels as seen in the P_{II} mutant. This also explains why the P_{II} mutant accumulates more glycogen during exponential growth. Metabolic data demonstrate that N-acetyl glutamate (an intermediate of arginine biosynthesis) is accumulating due to a reduced N-acetyl glutamate kinase (NAGK) activity, since P_{II} mediated relief of NAGK inhibition is absent. Nevertheless arginine levels are higher than in the wild type. Therefore reduced NAGK activity is probably compensated by increased transcription of *argD* and *argG* through NrrA, demonstrating the incredible regulatory redundancy of metabolism.

Other metabolic changes were anticipated based on the genomic sequence of the P_{II} mutant. Changes in ergothioneine levels were expected due to mutations in the promoter of *egtC*. This led to 16 fold reduced levels of ergothioneine. Ergothioneine is an antioxdant which reduces reactive oxygen species (ROX) (Saini et al., 2016). Therefore strongly reduced ergothioneine levels likely make the P_{II} mutant more susceptible to oxidative stress, due to formation of ROX under high light illumination at photosystem II or the respiratory machinery (Latifi et al., 2009). Acetyl-serine is a precursor for cysteine, which

in turn is a major component of glutathione. Hence, increased levels of acetyl-serine could be caused by increased cysteine biosynthesis to compensate the loss of ergothioneine by the synthesis glutathione. The point mutation Y215C in aspartoacylase (AspA) suggested possible changes in acetyl-aspartate levels which indeed were tremendous. Even though the mutation is not in a catalytic residue, the strongly increased levels of acetyl-aspartate suggest that tyrosine 215 of AspA is involved in the regulation of catalytic activity. As Tyr can be phosphorylated the mutation of this residue to Cys abolished a putative site for regulation, thereby strongly reducing enzymatic activity. Even though the presented data appear convincing, no phoshopeptide of AspA could be detected in a study that tried to identify potential phosphorylataion sites in *Synechocystis* (Spät et al., 2015). The accumulation of acetyl aspartate could also partially contribute to the lowered acetyl-CoA levels, as the metabolite is not degraded to acetate and aspartate anymore. Acetate supplementation did not inhibit glycogen accumulation during nitrogen starvation as seen in the wild type. It appears that the mutant is not able to perceive acetate or the acetyl-CoA state of the cell.

9.2 Regulation of PHB biosynthesis

9.2.1 Supply of precursors

A factor that favors PHB production upon nitrogen starvation is the continuously increasing reductive power of the cytoplasm. A change in redox balance of the cytoplasm is already visible within 6 hours of nitrogen starvation (Klotz et al., 2015; Salomon et al., 2013), but a clear shift to a more reducing cytoplasm is only seen after 48 hours. Two steps in PHB biosynthesis benefit from this shift. Firstly more reducing power is available to convert acetoacetyl-CoA to 3-hydroxybutyryl-CoA shifting the chemical equilibrium towards formation of 3-hydroxybutyryl-CoA. Secondly PHB synthase responds positively towards a more reducing cellular environment resulting in increased biosynthetic activity. The shifted redox balance might not only be caused by the over-reduction of terminal electron acceptors, but also through increased carbon flux through the TCA cycle sustaining increased biosynthetic activity of PHB synthase. Biosynthesis of PHB occurs upon an imbalanced carbon metabolism that is associated with macronutrient limitation (Panda et al., 2006). PHB biosynthesis is increased upon nitrogen starvation, a simple explanation for increased PHB accumulation would have been increased levels of acetyl-CoA. However exactly the opposite is the case, acetyl-CoA levels decrease. The acetyl-CoA pool is fairly small ($pmol/(1 * 10^8 cells)$) and quickly turned over through various biochemical reactions like the synthesis of citrate or malonyl-CoA for fatty acid synthesis. All of these reactions drain the acetyl-CoA pool upon nitrogen starvation. At the same time the amount of carbon that is available for metabolism declines, due to the fact that carbon fixation is steadily reduced because of lowered photosynthetic activity (Görl et al., 1998). At the

same time carbon flux is redirected towards the synthesis of glycogen reducing carbon flux towards acetyl-CoA. In addition transcription of *pha* genes adds an additional pathway that consumes acetyl-CoA. Hence acetyl-CoA pools decrease. Acetate supplementation can be used to sustain higher acetyl-CoA levels, which favor increased PHB production. Acetate supplementation however does not increase the amount of produced PHB dramatically (roughly 3 % more in wild type after one week). At the same time it actually dampens the expression of PHB biosynthetic genes, which is likely to contribute to the small increase of PHB upon acetate supplementation. This might be overcome if expression of *pha* genes can be uncoupled from the acetate mediated transcriptional repression. Acetate supplementation also reduces the glycogen levels during growth and nitrogen starvation. The same effect was previously observed by De Philippis et al. (1992a). Acetate utilization into carbon metabolism is facilitated through the action of phosphotransacetylase (Pta) in conjunction with acetate kinase (AckA) or the single action of acetyl-CoA synthetase with acetyl-CoA as product. Using the Pta AckA way is energetically more efficient as only one ATP is consumed and acetyl phosphate is formed as an intermediate. Acetyl phosphate is a small metabolite that can acetylate or phosphorylate proteins non enzymatically (Weinert et al., 2013; Klein et al., 2007). Hence, an altered acetylation or phosphorylation pattern of proteins can be expected when cultivating with acetate in the growth medium. This might inhibit glycogen formation due to altered activities of enzymes in glycolysis and gluconeogenesis. A recent report showed that many enzymes of glycolysis, gluconeogenesis, calvin and TCA cycle are acetylated in *Synechocystis* sp. PCC 6803 (Mo et al., 2015). This appears to be conserved throughout the the bacterial kingdom and was also reported for *E. coli* and *B. subtilis* (Kuhn et al., 2014; Kosono et al., 2015). Acetlyation is not restricted to metabolic enzymes but can be detected on ribosomal proteins and RNA polymerase. Therefore altered translation and transcription could be expected, as seen with reduced expression of *pha* genes when acetate is present in the growth medium. This suggest a mechanism by which cells are able to perceive the availability of acetate.

9.2.2 PHB synthase

Biosynthetic activity of PHB synthase is subject to regulation on several levels. Formation of a PhaE and PhaC heterodimer is a prerequisite to obtain catalytically active PHB synthase. Only the catalytic active fraction (insoluble) contains both subunits, whereas the inactive fraction is devoid of the hetero-dimer. Biosynthetic activation goes hand in hand with covalent modification and several types of modifications could be excluded, nevertheless the chemical nature of the modification remains unresolved. Post-translational regulation of PHB synthase is also evident when comparing the increase in biosynthetic activity with increases of PHB synthase in the insoluble fraction. Even though the amount of PHB synthase in the insoluble fraction changes the biosynthetic activity increases or decreases disproportionately. While the amount of PHB synthase only doubles within 48

h of nitrogen starvation the biosynthetic activity is more than tripled. After 7 days of nitrogen starvation the amount of PHB synthase in the insoluble fraction is the same as after 2 days. Biosynthetic activity after 7 days of nitrogen starvation however is 50 % lower than at day 2. As biosynthetic assays were performed under defined conditions, direct influence of metabolites can be excluded due to their dilution throughout the measurement process. Hence, the activating and inactivating factors have to be either associated to the PHB granule surface, or directly attached to PHB synthase. The more reducing redox balance could be translated through S-glutathionylation of PhaE and thereby activate PHB synthase (Chardonnet et al., 2015). Acetyl phosphate can be excluded as activating factor for PHB synthase, since no activating effect of acetyl phsophate on biosynthetic activity of PHB synthase was visible *in vitro* or *in vivo*. Nevertheless high biosynthetic activity of PHB synthase is not necessarily needed to obtain high PHB levels. This has been demonstrated in the P_{II} mutant when supplemented with acetate and the *phaP* mutant which accumulated wild type like levels of PHB.

9.2.3 Increasing PHB production

The observation that *Synechocystis* is able to synthesize up to 25 % (w/w) PHB, when the precursor supply is increased through overexpression of *phaAB* operon was also reported recently (Khetkorn et al., 2016). Overexpression of PHB synthase however did not increase the PHB content confirming the results obtained in the course of this project. Hence, increased precursor supply is a prerequisite for high PHB accumulation. The first step of PHB synthesis is most likely the bottle neck for increased PHB production, due to biochemical parameters of PhaA and the unfavorable $\Delta G^{\circ\prime}$ of 6.8 kcal/mol for the reaction (Lan and Liao, 2012). This could be overcome by synthesizing acetoacetyl-CoA form malonyl-CoA and acetyl-CoA through a ketoacyl-ACP synthase III NphT7 from *Streptomyces* sp.. This enzyme is able to use acetyl-CoA and maolnyl-CoA instead of activated ACP (Okamura et al., 2010) to synthesize acetoacetyl-CoA. This would couple the synthesis of acetoacetyl-CoA to ATP hydrolysis creating a negative $\Delta G^{\circ\prime}$ driving the reaction. Doing this in a genetic background where native *glnB* is substituted through either a GlnBS49D or GlnBS49E variant could additionally boost acetoacetyl-CoA levels, due to a change in the acetyl-CoA to malonyl-CoA ratio in these strains. Creation of a synthetic operon with *nphT7* and *phaB* would ensure similar expression of both genes, potentially increasing efficient conversion of acetoacetyl-CoA to 3-hydroxabutyryl-CoA. Introduction of the 3-hydroxypropionate/4-hydroxybutyrate cycle of archea could potentially further increase 3-hydoxybutyryl-CoA levels. This pathway is originally used by archea to fix carbon dioxide. Part of this pathway uses succinate and converts it in several steps to 3-hydroxybutyryl-CoA (Berg et al., 2007). Using this pathway to redirect the succinic semialdehyde produced by the GABA shunt towards PHB biosynthesis should increase total PHB accumulation. In addition this would provide a second route to fix carbon

dioxide and incoporate it into metabolism. Streamlining PHB production by attaching all biosynthetic enzymes to the PHB surface could further increase PHB production. This could be achieved using protein scaffolds attached to a phasin (Dueber et al., 2009), which would recruit enzymes of PHB precursor biosynthesis in close proximity of the biosyntheticly active PHB synthase. At this point increased expression of PHB synthase might be required to convert all available precursor towards PHB or to provide the desired polymer chain length.

9.2.4 PHB metabolism in the P_{II} mutant

PHB formation is strongly impaired in the P_{II} mutant upon nitrogen starvation. Other stress conditions like phosphate starvation do trigger PHB accumulation and the mutant is indistinguishable from the wild type (Schlebusch, 2012). Hence, deletion of *glnB* obstructs a regulatory event during nitrogen starvation, which is required for high PHB accumulation. The phenotype is complemented by P_{II} and S49 variants, but a negative charge at this position appears to make a difference, since the S49C variant accumulates less PHB than the phosphomimetic variants. The complementation is not achieved by higher biosyntheitc activity of PHB synthase or increased transcription of *pha* genes. Metabolic data indicated an altered redox balance in the mutant, but these alterations were also present in the complemented strain, which accumulated similar levels of PHB as the wild type. Hence, the altered redox balance is not the cause for the observed phenotype. As P_{II} inhibits ACCase activity *in vitro* an initial hypothesis was, that ACCase is relieved form P_{II} mediated inhibition upon nitrogen starvation and efficiently outcompetes PhaA for acetyl-CoA. But this turned out to be not the case as the S49E variant, which is not able to interact with ACCase (no inhibition), could complement the mutant phenotype and even accumulated slightly more PHB than the wild type. The steady state acetyl-CoA levels in the mutant, wild type and complemented strains were identical upon nitrogen starvation therefore reduced levels of this metabolite could be ruled out as cause of the observed phenotype. Acetate supplementation to the growth medium could fully complement the observed phenotype. This shows that the mutant is not able to provide sufficient acetyl-CoA for PHB synthesis. However it is not the steady state of acetyl-CoA but the carbon flux towards of acetyl-CoA that is most likely affected. Acetyl-CoA is either generated through the multiple sugar degradation pathways or through carbon fixation. Sugars are stored intracellularly as glycogen upon nitrogen starvation, therefore catabolism of sugars is the less likely pathway to significantly contribute to acetyl-CoA pools during nitrogen starvation. At the same time carbon fixation slowly ceases and reduced sugar catabolism contributes to a declining acetyl-CoA pool. Interestingly co-immuno precipitation experiments identified the carboxysome shell protein CcmP when GlnB was used as bait. As the carboxysome is the cellular organelle where carbon fixation takes place, absence of P_{II} might alter the permeability of the carboxysome shell for metabolites. Carboxysome shell proteins self

assemble in a disc shaped hexamer with a small pore in the center. The pore diameter formed by CcmP is assumed to facilitate metabolite exchange (Cai et al., 2013). This raises the question whether P_{II} might act on the carboxysome to affect CO2 fixation, especially when 2-OG levels are high. Glycolate, one marker metabolite for photorespiration, has been reported in the P_{II} mutant to be strongly increased (Schwarz et al., 2014). Increased photorespiration in the P_{II} mutant could affect carbon fixation thereby strongly reducing the carbon flux towards acetyl-CoA explaining the low PHB phenotype.

9.3 A revised P_{II} interaction network

The P_{II} regulatory network of *Synechocystis* sp. PCC 6803 could be extended towards acetyl-CoA carboxylase and several other potential interaction partners could be identified. ACC responds towards P_{II} as has been reported for other GlnB proteins and its biosynthetic activity is inhibited by GlnB. 2-OG reliefs this inhibition by modulating T-loop conformation and abolishing the GlnB ACC interaction. The effect of this regulation was clearly visible in the P_{II} mutant *in vivo*, which had lowered steady state levels of acetyl-CoA since ACC was not subject to P_{II} mediated inhibition. Deregulation of ACCase led to slightly increased fatty acid levels under specific growth conditions when 2-OG levels are thought to be low. Increased fatty acid levels were accompanied by transient accumulation of triacyl-glycerols hitherto not known to accumulate in unicellular cyanobacteria. These results implicate that P_{II} mediated regulation of ACCase is an important regulatory mechanism to maintain high acetly-CoA levels. This ensures carbon flow towards the TCA cycle, sustaining amino acid metabolism when carbon supply is limiting. All targets of GlnB known so far are regulated during exponential growth (Heinrich et al., 2004; Espinosa et al., 2006) when P_{II} is needed to balance the C/N metabolism. Upon nitrogen starvation transcription of *glnB* increases and P_{II} is phosphorylated (Krasikov et al., 2012; Forchhammer and Tandeau de Marsac, 1994). This apparent discrepancy between known regulatory targets and transcriptional response upon nitrogen starvation prompted the hypothesis that phosphorylated GlnB might regulate cellular processes important for survival without nitrogen. Co-immuno precipitation of GlnB during nitrogen starvation identified potential target proteins regulated under these conditions. Phosphoenolpyruvate carboxylase (PepC), carboxysome shell protein (CcmP), the bifunctional N-acetylornithine aminotransferase/γ-aminobutyrate aminotransferase (ArgD), glutamate-5 kinase (ProB), and the transcription factor RpaB. As co-immuno precipitation has a high false discovery rate these interactions have to be verified biochemically but initial observations and experiments appear promising.

Measurements of PepC activity in cell extracts of wild type, mutant and complemented strain showed that the PepC activity was reduced in the P_{II} mutant and P_{II} complemented strain. This shows that PepC activity is P_{II} dependent but further experiments need to confirm this. PepC catalyzes the formation of oxalacetate from phosphoenol pyruvate and

carbonate. Oxalacetate is the direct precursor for aspartate synthesis. GlnB sustains the supply of acetyl-CoA under carbon limiting conditions towards the reducing branch of the TCA-cycle. PepC catalyzes the formation of oxaloacetic acid replenishing the TCA-cycle. This reaction sustains formation of citrate through citrate synthase. At the same time it provides carbon backbones for aspartate synthesis. Whereas inhibition of ACC sustains high acetyl-CoA levels, activation of PepC might provide sufficient levels of oxalacetate. Both metabolites are important precursors for amino acid biosynthesis.
Detection of a carboxysome shell protein (CcmP) in the extracts suggest an involvement in carbon fixation. Fluorescence microscopic images during nitrogen starvation show that GlnB-Venus is not equally distributed throughout the cytoplasm but locally concentrated in some of the cells. Spot-like fluorescence demonstrates that free diffusion is inhibited and the protein is immobilized within the cell. As carboxysomes are large protein organelles whose movement is restricted by size and viscosity of the cytoplasm (Yeates et al., 2008), interaction of GlnB with the carboxysome would appear as a spot within a cell. In addition to that both GlnB complemented strains showed impaired growth with excess CO_2. Imunoprecipitation identified several components of the carbon concentrating mechanism (CupA, NdhH) to interact with GlnB. At this stage the observations made remain inconclusive and can't discriminate how GlnB is involved in the regulation of carbon fixation/concentration. The P_{II} complemented strains expressing GlnB variants with Venus at the C-terminus present an attractive toolkit to further study the intracellular dynamics of GlnB. Time lapse fluorescence microscopy could provide information how GlnB localization changes upon ammonia shock treatment. Alternatively expression of GlnB-Ven in an *amtB*$^-$ or a *nrtCD*$^-$ background could clarify whether GlnB regulates ammonia or nitrate import.
Detection of ProB in the co-immunoprecipitated fraction is surprising but nevertheless a promising target for further investigation. As N-acetyl glutamate kinase (NAGK), glutamate kinase is a hexamer and catalyzes the first committed step in proline biosynthesis through phosphorylation of glutamate (Smith et al., 1984). The substrate used differs only slightly and like NAGK, ProB is feedback inhibited by proline. Like arginine, proline levels are increased in the P_{II} mutant possibly due to a similar transcriptional regulation of both pathways. Further biochemical characterization will resolve this issue.
The forth protein identified to potentially interact with P_{II} is the bifunctional N-acetylornithine aminotransferase/γ-aminobutyrate aminotransferase (ArgD). The protein has a fairly broad substrate specificity and transfers an amino group to an oxoacid forming an amino acid or the reverse reaction (Xiong et al., 2014). The intermediate of the GABA shunt succinic semialdehyde is not detected in the P_{II} mutant during exponential growth but accumulates during nitrogen starvation. Interaction of GlnB might modulate the substrate specificity of ArgD allowing the desamination of GABA upon 2-OG binding. This would affect the amount of carbon being directed through the GABA shunt and alter the cellular redox state. As the transamination of GABA might only be a side reaction, lowered levels of glutamate in the mutant may simply reduce the substrate levels to such an extent that

catalytic conversion to succinic semialdehyde is drastically reduced and not detectable with the applied analytical methods.

The transcription factor RpaB was found to interact with GlnB. RpaB is a transcriptional regulator that responds to high light irradiation but is also shown to regulate the expression of *nblA* (Kappell and van Waasbergen, 2007; Kato et al., 2011). The link between the P_{II} regulatory system and the NblS system that responds to environmental stress (phosphorylating RpaB), could be an additional layer of regulatory complexity of the NblS system. If the interaction indeed occurs, P_{II} would most likely obscure the ability of RpaB to bind regulatory sequences on DNA by either preventing dimer formation or inducing changes in secondary structure abrogating DNA binding. A transcriptional activation is less likely as the structural inflexibility of the core P_{II} protein would likely block recruitment of sigma factors or RNA polymerase.

The revised P_{II} interaction network is summarized in figure 9.1 and characterized interactions are depicted. Putative interactions with phosphorylated GlnB are marked with question marks as no direct biochemical evidence is available to confirm the interaction.

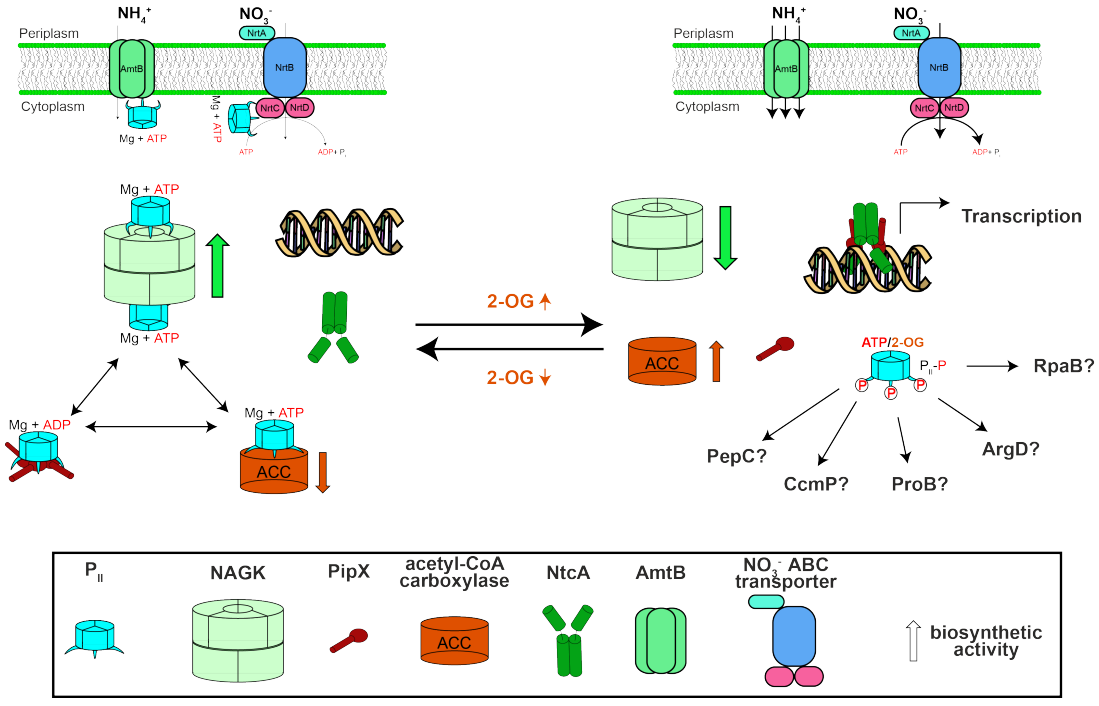

Fig. 9.1: Overview of a revised P_{II} interaction network. The interaction network has been revised and regualtion of acetyl-CoA carboxylase (ACC) has been added. Putative new interaction partners with phosphorylated P_{II} are shown with a question mark as no additional biochemical evidence is present to verify the interaction.

9.4 The PHB granule surface

9.4.1 Identification of phasin proteins

Hein et al. (1998) have identified the PHB synthase of *Synechocystis* sp. PCC 6803 and identified a small protein (Ssl2501) associated to the PHB granule surface. The same protein was also identified in preparations of thylakoid membranes and was therefore always classified as thylakoid associated protein (Wang et al., 2000). This work clearly demonstrated that this protein is not thylakoid associated but localizes to PHB granules *in vivo* and deletion of *ssl2501* resulted in formation of few large PHB granules. A phenotype observed for other phasin deletions therefore *ssl2501* encodes a classical phasin PhaP (Pieper-Fürst et al., 1994). Total PHB amount was not strongly altered by deletion of PhaP, most likely leading to altered mean polymer chain length as phasins are also thought to regulate the processivity of PHB synthase (Jossek et al., 1998). Whether this occurs through stabilization of PHB synthase, mediated by a chaperon like action of phasin proteins or through stabilization of the polymer chain that exits PHB synthase remains to be resolved (Mezzina et al., 2015; Ushimaru et al., 2014). A more detailed structural analysis revealed that PhaP oligomerizes and both α helices of the protein are required for stable attachment to the PHB granule. Nevertheless each α helix was able to bind PHB granules individually *in vivo*.
In an attempt to identify more PHB granule associated proteins two potential phasin proteins were identified in PHB granule preparations. These proteins had homologies to phasin proteins from *Pseudomonas putida* but only partially co-localized to PHB granules *in vivo*. Slr0455 was even degraded upon nitrogen starvation when phasin synthesis would be required. Apparently both proteins were able to associate to a hydrophobic surface but this surface doesn't have to be PHB. Peramuna and Summers (2014) have reported the occurrence of lipid bodies in *Nostoc punctiforme* and formation of lipid bodies was observed in *Synechocystis* in this work. Like PHB granules lipid bodies have proteins associated to their surface (Yang et al., 2012). The phasin like protein Slr0058 was often localized close to the cytoplasmic membrane, whereas Slr0455 was more dispersed within the cell. Instead of binding PHB granules these proteins might associate to lipid bodies forming during growth. Identification of both proteins at PHB granules could be a cross contamination which occurred during the purification procedure. Lipid droplets in eukaryotes are thought to form at the endoplasmatic reticulum where they bud off, consequently triacylglycerols within the droplet are enclosed by a phospholipid monolayer. Partial co-localization of Slr0058 and Slr0455 with PhaC could be explained by the low resolution of fluorescence microscopy. Lipid body synthesis should occur close to the cell periphery as it relies on fatty acid synthesis. PHB granule formation was reported was reported close to the cell periphery (Jendrossek et al., 2007; Hauf, 2012). These could be potential biosynthetic centers within cells where acetyl-CoA metabolism takes place.

9.4.2 Eliminating lipids form the surface

For now almost five decades the scientiffic community has debated whether PHB granules are engulfed by a phospholipid monolayer as early reports have suggested (Griebel et al., 1968). More recent investigations challenged this textbook knowledge (Beeby et al., 2012). Biochemical evidence through PHB granule preparations is not suitable to resolve this question, as unspecific binding of phospholipids to the hydrophobic granule surface can never be fully excluded. Therefore transmission electron microscopy with either chemically fixed or flash frozen cells was applied. Even though electron microscopy has superior resolution to light microscopy differentiation between a monolipid layer or a protein layer is at best difficult if not impossible. Hence, an alternative approach to resolve this question was applied: Fusing the C2 domain of bovine lactadherine (LactC2) with fluorescent proteins to determine the presence of phosphatidyl-serine on the PHB granule surface. LactC2 binds the head group of phosphatidyl-serine with a high affinity (K_d=1.8 nM) and specificity (Shao et al., 2008; Andersen et al., 2000). Expression of various fluorophores (dsRed, sfGfp, mTurq2) fused to LactC2 resulted in localization of this protein to the cell membrane in various microbes like *Escherichia coli*, *Ralstonia eutropha* H16, *Pseudomonas putida* or *Magnetospirillum gryphiswaldense*. Co-localization of LactC2 with PHB granules was only observed in some *E. coli* cells through heterologous expression of the PHB biosynthetic genes. No localization of LactC2 to PHB granules was observed in host which naturally produce PHB even if the majority of phasin proteins was deleted form the genome. Other intracellular organelle like structures the magnetosomes, which are known to be engulfed by a lipid membrane, could be visualized by the LactC2 sensor. Consequently these results demonstrated that PHB granules have no phospholipid membrane *in vivo*. A preparation of PHB granules from *R. eutropha* expressing dsRed-LactC2 could indeed detect phospholipids on a small fraction of PHB granules explaining the results by Griebel et al. (1968) as a preparational artifact. Therefore an updated model of PHB granule formation in *Synechocystis* sp. PCC 6803 is shown in figure 9.2.

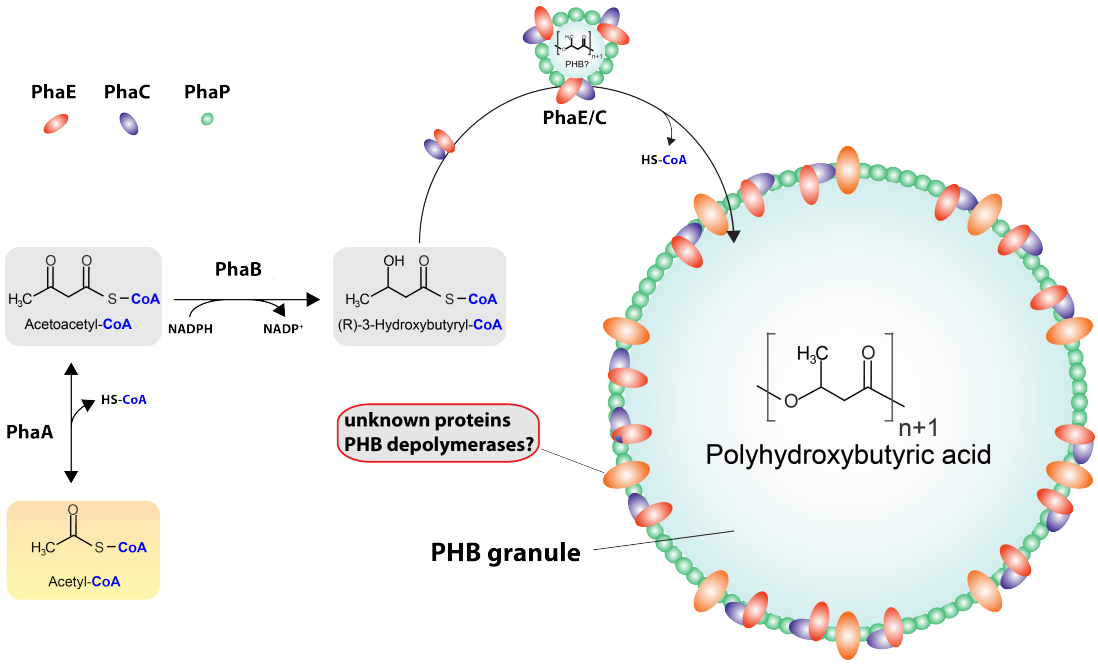

Fig. 9.2: PHB granules in *Synechocystis* sp. PCC 6803 are formed by dimerization of PhaE and PhaC enabling PHB synthesis. Phasin proteins are found associated to growing PHB granules and the PHB granule surface is devoid of phospholipids.

10 Materials and Methods

10.1 Bacterial cultivation

10.1.1 *Escherichia coli* cultivation

E. coli Top10 was routinely used and cultivated in lysogeny broth (LB) (Bertani, 1951) at 37 °C. For growth on plates lysogeny broth was solidified by the addition of 1.5 % agarose (w/v).

Gentamycin, kanamycin, spectinomycin, chloramphenicol and ampicillin were used to select for cells harboring the desired construct on a plasmid. Gentamycin was used with a final concentration of 7.5 µg/ml, kanamycin with 25 µg/ml, spectinomycin with 25 µg/ml, chloramphenicol with 30 µg/ml and ampicillin was added to the growth medium at a final concentration of 100 µg/ml.

10.1.2 *Synechocystis* sp. PCC 6803 cultivation

Synechocystis was grown routinely at 27 °C in 100 ml Erlenmeyer flasks with shaking (120rpm) in $BG11_0$ medium (Rippka et al., 1979) which was supplemented with 5 mM $NaHCO_3$ and 17.3 mM $NaNO_3$ and will be reffered to as $BG11_{+N}$ or BG11. For growth with ammonia as nitrogen source $NaNO_3$ was replaced by 5 mM NH_4Cl and buffered with 5 mM TES NaOH (pH7.8). For feeding experiments with acetate sodium acetate was used at a final concentration of 10 mM if not stated otherwise. For larger scale cultivation cultures were cultivated in 500 ml baffled Erlenmeyer flasks with shaking (120rpm) or 250 ml glass cylinders with vigorous bubbling of ambient air (0.04 % CO_2) or air supplemented with 2 % CO_2. Light intensities were ranged between 40-80 µmol photons m^{-2} s^{-1} (Lumilux de Lux, Daylight, Osram) All minerals present in $BG11_0$ medium are listed in table 10.1. To obtain solid $BG11_{+N}$ medium 1.5 % (w/v) bacto agar (Difco) was added and contained a final concentration of 10 mM TES NaOH (pH 7.8) as buffer. $BG11_{-N}$ medium was prepared as $BG11_{+N}$ but a nitrogen source was omitted.

10.1.3 Strain list

Escherichia coli Top10 was used for standard cloning procedures. The various *Synechocystis* sp. PCC 6803 strains generated and used in this are summarized in table 10.2.

Tab. 10.2: List of bacterial strains

Strain	Strain abbreviation	Genotype	Reference
Synechocystis sp. PCC 6803	wt	wild type	Stanier et al. (1971)
Synechocystis ΔP_{II}	ΔP_{II}	*ssl0707::spec*^{R}	Hisbergues et al. (1999)

Tab. 10.2: List of bacterial strains

Strain	**Strain abbreviation**	**Genotype**	**Reference**
Synechocystis ΔP_{II} PII-V	PII-V	*ssl0707::spec*^{R}(pVZ322-P_{II}-Ven)	this study
Synechocystis ΔP_{II} P_{II}S49C-V	P_{II}S49C-V	*ssl0707::spec*^{R}(pVZ322-P_{II}S49C-Ven)	this study
Synechocystis ΔP_{II} P_{II}S49D-V	P_{II}S49D-V	*ssl0707::spec*^{R}(pVZ322-P_{II}S49D-Ven)	this study
Synechocystis ΔP_{II} P_{II}S49E-V	P_{II}S49E-V	*ssl0707::spec*^{R}(pVZ322-P_{II}S49E-Ven)	this study
Synechocystis ΔP_{II} *phaAB*OE	ΔP_{II} Re*phaAB*OE	*ssl0707::spec*^{R} (pVZ322-p0783RePhaAB)	this study
Synechocystis *phaAB*OE	Re*phaAB*OE	(pVZ322-p0783RePhaAB)	this study
Synechocystis *phaAB*OE2	Re*phaAB*OE2	(pVZ322-ppsbA2RePhaAB)	this study
Synechocystis PhaC-Gfp	PhaC-Gfp	(pVZ322-1830)	Hauf et al. (2013)
Synechocystis PhaE-Gfp	PhaE-Gfp	(pVZ322-1829)	Hauf et al. (2013)
Synechocystis ΔPhaE	ΔPhaE	*slr1829::kan*^{r}	Hauf et al. (2013)
Synechocystis ΔPhaEC	ΔPhaEC	*slr1829::kan*^{r}*::slr1830*	Hauf et al. (2013)
Synechocystis ΔPhaEC PhaCS105A	ΔPhaC-SA	*slr1829::kan*^{r}*::slr1830* (pVZ322-1830SA)	this study
Synechocystis ΔPhaE PhaES299A	ΔPhaESA	*slr1829::kan*^{r} (pVZ322-1829SA)	this study
Synechocystis ΔPhaEC *psbA2::phaEC*	ΔPhaEC-OE	*slr1829::kan*^{r}*::slr1830* (pVZ322-*phaEC*OE)	this study
Synechocystis PhaC-Cr	PhaC-Cr	*slr1830::cerulean::cam*^{R}	this study
Synechocystis PhaC-mTurquoise2	PhaC-mTurq2	*slr1830::mTurquoise2::cam*^{R}	this study

Tab. 10.2: List of bacterial strains

Strain	**Strain abbreviation**	**Genotype**	**Reference**
Synechocystis PhaC-Cr PhaP-Venus	PhaC-Cr PhaP-Ven	*slr1830::cerulean::cam*^{r} (pVZ322-2501-Ven)	this study
Synechocystis slr0058Ven	slr0058-Ven	(pVZ322-slr0058Ven)	this study
Synechocystis slr0455Ven	slr0455-Ven	*slr0455:venus:spec*^{R}*::slr0456*	this study
Synechocystis acs	*acs*	*sll0542::spec*^{R}*::sll0542*	this study
Synechocystis ackA	*ackA*	*sll1299::cam*^{R}*::sll1299*	this study
Synechocystis pta	*pta*	*slr2132::kan*^{R}*::slr2132* (pVZ322-1830)	this study
Synechocystis pta PhaC-PhaC-Gfp	*pta* PhaC-Gfp	*slr2132::kan*^{R}*::slr2132*	this study
Synechocystis acs ackA	*acs ackA*	*sll0542::spec*^{R}*::sll0542, sll1299::cam*^{R}*::sll1299*	this study
Synechocystis acs, pta	*acs, pta*	*sll0542::spec*^{R}*::sll0542, slr2132::kan*^{R}*::slr2132*	this study
Synechocystis acs, ackA, pta	*acs,ackA, pta*	*sll0542::spec*^{R}*::sll0542, sll1299::cam*^{R}*::sll1299, slr2132::kan*^{R}*::slr2132*	this study
Escherichia coli Top10	Top10	F– *mcrA*, Δ(mrr-hsdRMS-mcrBC), Φ80*lac*ZΔM15, Δ*lac*X74, *rec*A1, *ara*D139 Δ*(ara leu)* 7697, *gal*U, *gal*K, *rps*L, (StrR), *end*A1, *nup*G	Invitrogen
Escherichia coli J53 (RP-4)	RP-4	R+ *met, pro* (RP-4: *Ap,Tc, Km, Tra+, IncP*)	Wolk et al. (1984)

10.2 Biochemical Methods

10.2.1 PHB synthase assay

PHB synthase assays were performed as described by Schlebusch and Forchhammer (2010). Briefly, 30 ml cells was harvested by centrifugation at 4,000 × *g* and suspended in lysis buffer (25 mM Tris-HCl [pH 7.4], 50 mM KCl, 5 mM MgCl2, 0,5 mM EDTA, and 1 mM benzamidine). Cells were lysed using FastPrep-24 (MP Biomedical) using 0.1-mm glass beads, and cell debris was removed by centrifugation for 5 s up to 10,000 × *g*. The

Tab. 10.1: Final concentration of minerals in $BG11_0$ medium

	chemical	final concentration in µM
BG11	$MgSO_4$ x $7H_2O$	300
	$CaCl_2$ x $2H_2O$	250
	Citric acid	30
	Ferric ammonium citrate	23
	K_2HPO_4	200
	Na_2CO_3	180
	Na_2EDTA x $2H_2O$	2.5
Trace minerals solution	H_3BO_3	46
	$MnCl_2$ x $4H_2O$	9.2
	$ZnSO_4$ x $7H_2O$	0.77
	Na_2MoO_4 x $2H_2O$	1.6
	$CuSO_4$ x $5H_2O$	0.32
	$CoCl_2$ x $6H_2O$	0.2

resulting cell lysate was separated into a soluble and insoluble fraction by centrifugation at 25,000 × *g* for 30 min at 4°C. The insoluble material was suspended in lysis buffer, and protein concentrations in the fractions were determined as described by Bradford (1976). PHB-biosynthetic activity was monitored by recording the change in absorbance at 412 nm for at least 30 min in the reaction buffer (25 mM Tris-HCl [pH 7.4], 1 mM DTNB [5,5=-dithiobis(2-nitrobenzoic acid)], 20 mM $MgCl_2$, and 100 µM hydroxybutyryl-CoA [Sigma-Aldrich]) after addition of 5 µg protein of the suspended insoluble fraction. The reaction temperature was held constant at 30°C.

10.2.2 PHB quantification

PHB quantification was performed as described by Schlebusch and Forchhammer (2010). Cells were harvested at the dedicated time points by centrifugation (10 min, 4,000 × *g*, 25 °C), washed once with distilled water, and dried for 3 h at 60 °C. Dried pellets were boiled for 1 h in 1 ml concentrated H_2SO_4 diluted with 1 ml 0.014 M H_2SO_4. Cell debris was removed by centrifugation (5 min at 10,000 × *g*), and the supernatant was diluted 10-fold in 0.014 M H_2SO_4. Processed samples were analyzed by high-performance liquid chromatography (HPLC) using a Nucleosil 100 C18 column (125 by 3 mm) and 20 mM phosphate buffer (pH 2.5) as the liquid phase. Crotonic acid was detected at 210 nm, and commercially available PHB processed in parallel was used as a standard.

10.2.3 Glycogen quantification

Glycogen quantification was performed as described by Klotz et al. (2015). Two milliliter culture was harvested and the OD_{750} was measured. Cells were washed twice with sterile H_2O and pelleted. Then the pellet was resuspended in 400 μL 30% (w/v) KOH and

incubated for 2 h at 95 °C. Then, 1.2 ml ice-cold pure ethanol (final concentration 70% (v/v)) was added and incubated for 24 h at -20 °C. Precipitated glycogen was harvested by centrifugation at 4 °C 10,000 × g for 10 min; the pellet was washed with 70% ethanol and centrifuged again at 4 °C at 10,000 × g for 10 min. This step was repeated with 100% ethanol and the pellet was dried in a Speed-Vac at 60 °C for 40 min. Glycogen was digested by the addition of 1 mL of a 100 mM sodium acetate solution (pH of 4.5) to the pellet and incubated for 2 h at 60 °C with $\tilde{3}5$ U amyloglucosidase. 200 μL of this solution was added to 1 ml of a *o*-toluidine reagent (6% *o*-toluidine in 100% acetic acid (v/v); reagent matured for at least 1 week) and incubated at 100 °C. The reaction was cooled for 3 min on ice and the the OD_{635} was measured in a Specord 205 (Analytik Jena). The glycogen content was estimated based on a standard curve with glucose.

10.2.4 Phosphoenolypyruvate carboxylase activity

Fifty milliliter cells were harvested at 4,000 × g for 10 min. Cell Pellets were suspended in lysis buffer (25 mM Tris-HCl [pH 7.4], 50 mM KCl, 5 mM $MgCl_2$, 0,5 mM EDTA, and 1 mM benzamidine). Cells were lysed using FastPrep-24 (MP Biomedical) using 0.1-mm glass beads, and cell debris was removed by centrifugation for 5 s up to 10,000 × g. Enzyme assays were performed with raw cell extracts using 10 mg raw extract for each reaction. Enzyme assays were performed as described by Knowles and Plaxton (2003) with small modifications. The reaction was performed at room temperature in a 1 ml reaction buffer (50 mM TrisHCl pH 7.8, 10 mM $KHCO_3$, 5 mM $MgCl_2$, 4 mM phosphoenolpyruvate, 10 U malate dehydrogenase and 0.2 mM NADPH final concentration) and reaction was started by the addition of the cell extract. The change of optical density at 340 nm was recorded with a Specord 205 (Analytik Jena) for 15 minutes and the slope was used to determine enzyme activity. Enzyme activities were calculated using an extinction coeffcient for NADPH ϵ=6300 $L/(mol * cm)$.

10.2.5 Metabolite extraction and quantification

Metabolite extraction and quantification was performed as desribed by Watzer et al. (2015)with several alterations. For the extraction of metabolites, cells 25 ml of culture at an OD_{750} of 0.8 were shock-cooled by mixing with crushed ice, rapidly harvested by centrifugation, and immediately frozen in liquid nitrogen. Metabolites were extracted from 3.5 mg lyophilized cells twice with 150 µl 80% methanol, 0.1 % formic acid. The two supernatants were combined and 5 µl were injected on a Waters UPLC/Synapt G2 LC/MS system equipped with a Waters Acquity 2.1 mm × 100 mm, 1.8 µm particle size HSS T3 reversed phase column. Metabolites were separated in a gradient from 20 % methanol with 0.1 % formic acid to 100 % methanol with 0.1 % formic acid in 10 min. The mass spectrometer was operated in ESI-positive and -negative modes with a scan range from m/z 50 to 2000 and a dwell time of 0.5 s. Data were evaluated using the MarkerLynx

Software (Waters Cooperation, Milford, MA, USA) in combination with Simca-P (Umetrics AB Umea, Sweden). Compounds (based on formula and MSE fragmentation pattern) that significantly differed (2^4 fold change) between the different samples were identified by principal component analysis (PCA) and orthogonal projections to latent structures (OPLS)—discriminant analysis (DA). Metabolites changes of less than 2^4 were identified manually based on retention time and fragmentation pattern of the metabolite.

10.2.6 Immunoprecipitation with magnetic beads and proteomic analysis

One hundred ml Cell suspension OD_{750}=1 were harvested by centrifugation for 10 min at 4,000 × *g*. Cells were suspended in lysis buffer (25 mM Tris-HCl [pH 7.4], 50 mM KCl, 5 mM $MgCl_2$, 0,5 mM EDTA, and 1 mM benzamidine) that additionally contained 2 mM ATP and 1mM 2-oxoglutarate for immunoprecipitation with GlnB. Lysis was performed using FastPrep-24 (MP Biomedical) using 0.1-mm glass beads. Cell debris and glass beads were removed by short centrifugation for 5 s up to 10,000 × *g*. The supernatant was applied to 50 µl GFP-Trap®MA suspension equilibrated in lysis buffer. The suspension was kept on ice for 1 h an mixed gently every ten minutes. Protein raw extract was separated form magnetic beads and washed 10 times with 300 µl lysis buffer. Magnetic beads were suspended in Laemli buffer and proteins denatured for 5 min at 95 °C. Proteins were directly applied on a precast SDS-PAGE (Serva, TG-Prime4-20%) and separated for 20 min through electrophoresis. Protein bands were visualized using InstantBlue (Expedeon). Due to the short electrophoresis time no separation was achieved and only one band was excised for each sample. Tryptic digestion, LC-MS/MS analysis with Proxeon Easy-nLC coupled to an Orbitrap XL, and bioinformatic analysis was performed at the Proteome center Tübingen.

10.2.7 Analysis of covalent modification

10.2.7.1 Deacylation

Deacylation was performed by addition of 45 mM hydroxylamine (final concentration) to cell raw extracts and incubated for 2 h at room temperature until analyzed by SDS-PAGE and subsequent western blot.

10.2.7.2 Mobility shift of phoshporylated proteins

Phosphorylation mobility shift was used as described by the manufacturer (WAKO Laboratory Chemicals). For this purpose a standard SDS-PAGE was prepared with a final concentration of 50 μmol/l Phos-tag reagent.

10.3 Molecular biological methods

10.3.1 Plasmid list

Several plasmids were created to either make mutants or complement mutant strains, or achieve increased PHB accumulation. These plasmids are summarized in table 10.3.

Tab. 10.3: List of Plasmids

Plasmid	Genetic feature	Reference
pVZ322		Zinchenko et al. (1999)
pVZ322-1829	*slr1829:egfp*	Hauf et al. (2013)
pVZ322-1830	*slr1830:egfp*	Hauf et al. (2013)
pVZ322-2501-Ven	*ssl2501:venus*	Hauf et al. (2015)
pVZ322-1829SA	*slr1829:egfp*	this study
pVZ322-1830SA	*slr1830:egfp*	this study
pVZ322-P_{II}-Ven	*ssl0707:strep-tag:venus*	this study
pVZ322-P_{II}S49C-Ven	*ssl0707S49C:strep-tag:venus*	this study
pVZ322-P_{II}S49D-Ven	*ssl0707S49D:strep-tag:venus*	this study
pVZ322-P_{II}S49E-Ven	*ssl0707S49E:strep-tag:venus*	this study
pVZ322-slr0058Ven	*slr0058:venus*	this study
pVZ322-*phaEC*OE	*ppsbA2:slr1829*	this study
pVZ322-p0783RePhaAB	*psll0783:RephaAB*	this study
pVZ322-ppsbA2RePhaAB	*ppsbA2:RephaAB*	this study
pVZ322-ptrcRePhaAB	*ptrc:RephaAB*	this study
pJetsll1299KO	*sll1299::cat^R::sll1299*	this study
pJetsll0542KO	*sll0542::spec^R::sll0542*	this study
pJetsll0529KO	*sll0529::gen^R::sll0529*	this study
pJetslr0453KO	*slr0453::cat^R::slr0453*	this study
pJetslr2132KO-1	*sl2132::kan^R::slr2132*	this study
pUC19PhaCmTurq2	*slr1830:mTurq2:cat^R::sll1736*	this study
pUC19PhaCCer	*slr1830:cerulean:cat^R::sll1736*	this study
pUCphaABKO	*slr1993::cat^R::slr1994*	this study
pUC19slr0058KO	*slr0058::cat^R::slr0059*	this study
pUC19slr0455KO	*slr0455::spec^R::slr0456*	this study
pUC19slr0455Ven	*slr0455:venus:spec^R::slr0456*	this study

10.3.2 RNA extraction

RNA extraction was adopted from Pinto et al. (2009). All consumables used for the experiments were either purchased RNasee free, or RNase was inactivated through diethylpyrocarbonate treatment. Ten ml cell culture were harvested through rapid filtration (Supor800, 0.8 µm, 47 mm) and the filter with cells was quickly dissolved in in 0.85 ml PGTX (4% (w/v) phenol; glycerol 6.9% (v/v); 8-hydroxyquinoline 0.1 % (w/v); 20 mM EDTA; 100 mM NaAc; guanidine thiocyanate 9.5 % (w/v); guanidine hydrochloride 4.6% (w/v); Triton X100 2% (v/v)). Harvested cells were frozen in liquid nitrogen and stored

at -80 °C until processed further. All further steps were carried out at 4 °C. Cells were homogenized in a FastPrep-24 (MP Biomedical) using 0.1-mm glass beads (3* 6.5 m/s for 20 s at 4). Samples were heated for 5 min at 95 °C and transferred on ice to precipitate proteins. Chloroform:IAA (24:1) was added in a ration 1:2 to the sample and inverted several times. Phase separation was induced through centrifugation for 5 minutes at full speed and 4 °C. The aqueous phase was transferred in a new tube and mixed with 1 part Chloroform:IAA (24:1), mixed by inversion and phase separation by centrifugation for 5 minutes at full speed and 4 °C was induced. The aqueous phase was transferred in a new tube and RNA grade glycogen was added to a final concentration of 0.1 µg/µl. The samples were mixed with equal volumes isopropanol and stored for at least 2 h at -80 °C (or -20 °C overnight). RNAwas pelleted at 4 °C for 30 min maximum speed. The supernatant was removed and the pellet washed with ice cold 70% ethanol (v/v) once. RNA was precipitated through centrifugation for 5 min at full speed and 4 °C. The pellet was air dried and suspended in RNase free water and stored at -80 °C until further used.

10.3.3 cDNA synthesis

Prior to cDNA synthesis gDNA was degraded using the DNA-free™DNA removal kit (Ambion, thermo Fischer). The nucleic acid concentration was adjusted to 200 ng/µl and DNA was degraded according to the manufacturers instruction. DNA degradation was verified through gel electrophoresis. Synthesis of cDNA was performed with the applied biosystems High capacity cDNA reverse transcription kit with random primers included in the kit. For cDNA synthesis 1.5 µg total RNA was used and reactions were performed according to the manufacturers recommendations. Synthesized cDNA was diluted 1:10 and stored at -20 °C until further used.

10.3.4 Quantitative PCR (qPCR)

Quantitative PCR was performed using the high ROX qPCR master Mix (Genaxxon Biosciences), with the Agilent Aria MX real time PCR system using a three step cycling protocol shown in table 10.4.

Tab. 10.4: Three step cycling protocol for qPCR

Step	**temperature °C**	**time**
Initial denaturation	95	10 min
Denaturation	95	15 s
Annealing	52	15 s
Extension	72	30 s
Final extension	72	2 min
melting curve analysis	starting from 50 °C 2°C per minute to 95 °C	

C_q values were calculated in the AriaMX software. Linearity of the qPCR reaction was tested and efficiency of the qPCR reaction for each gene of interest was determined to be above 95%. Normalization was performed according to Vandesompele et al. (2002) using the $\Delta\Delta C_q$ method.

10.3.5 Primer used for qPCR

Primer used for qPCR reactions are summarized in table 10.5.

Tab. 10.5: Primer used for qPCR

Name	Sequence	Gene of interest
q1829fw	AGTCCTTTGAGTCTTTGCCC	*phaE*
q1829rv	CGCCGAACCATTATCCAATTTAG	*phaE*
q1830fw	GTGTTACGCTTCTCTATTCCCG	*phaC*
q1830rv	CAATATCTACTGCTTCGGCTCC	*phaC*
q1993fw	GCCAGAAACTGTTAGCAAAGC	*phaA*
q1993rv	CCACCGTTCACATTCAACTTG	*phaA*
q1994fw	ACTATTCCGCCACTAAAGCTG	*phaB*
q1994rv	GGATCGCCAAAGTCATTTCG	*phaB*
qslr1265fw	AGGTATCGAAGTGGGCATTG	*rpoC1*
qslr1265rv	CAGACGTTTAATCAGCTTGGC	*rpoC1*
qsll1868fw	CCGAGTTTTAGTGTCAGTCCAG	*dnaG*
qsll1868rv	TTGGATTTGATAGCGACGGG	*dnaG*
qslr1731fw	CAGAACCATGATTTGGCAAGG	*kdpD*
qslr1731rv	ACTCATCCACTAACGCCAAC	*kdpD*

10.3.6 gDNA extraction and next generation sequencing

Genomic DNA was extracted form 10 ml *Synechocystis* liquid culture. Cells were harvested through centrifugation for 10 min at room temperature. The cell pellet was washed once with TE buffer (50 mM TrisHCl pH 7.8, 5 mM EDTA) and suspended in 300 µl TE buffer. Cells were lysed using FastPrep-24 (MP Biomedical) using 0.1-mm glass beads. After cell lysis proteins were denatured by addition of 250 µl Phenol:Chloroform:IAA (25:24:1) and vortexed vigorously. Phase separation was induced by centrifugation for 5 min at 20,000 × *g* and the aqueous phase was transferred to a new tube. Phenol traces were removed by addition of equal amounts of chloroform:IAA (24:1), vortexing and phase separation by centrifugation for 5 min at 20,000 × *g*. DNA was precipitated from the aqueous phase by addition of 0.7 volumes isopropanol, storage at -20 °C for 1 h followed by centrifugation for 5 min at 20,000 × *g* and 4°C. The DNA pellet was washed once with pure ethanol, followed by washing with 70 % (v/v) ethanol and dried on air. The DNA pellet was suspended in nuclease free water. Library preparation and sequencing was performed in Dr. Anne-Kristin Kaster lab at the DSMZ Braunschweig, with an Illumina

MiSeq. Bioinformatic analysis was performed in cooperation with Dr. Anne-Kristin Kaster and Prof. Dr. Wolfgang Hess in Freiburg.

10.4 Microscopic techniques

10.4.1 Fluorescence microscope setup

Microscopy was performed with the Leica DM5500 B microscope using the 100x/1.3 oil objective lens (Leica Microsystems). Depending of fluorophore spectral properties fluorescence microscopy was performed with either of four filter cubes. In order to detect eGfp an excitation filter BP 470/40 and suppression filter BP 525/50 nm were used. To detect cyanobacterial auto fluorescence and nile red fluorescence a filter cube with excitation filters BP 535/50 and suppression filter BP 610/75 was used. To detect Cerulean and mTurquoise2 fluorescence a filter cube with excitation filter ET436/20x and emission filter ET480/40m. Venus fluorescence was detected with excitation filter 500/20x, and emission filter ET535/30m. Image acquisition was done with a Leica DFC360FX black and white camera. Bright field images were exposed for 5 ms, eGfp for 100 ms, auto fluorescence for 80-120 ms, nile red 100 ms, Venus for 150 ms, cerulean for 200 ms and 100 ms for mTurquoise2. Black and white pictures were colored through the software Leica Application Suite (LAS AF) provided by Leica Microsystems. Z-stacks, in which every 0.25 µm a picture was recorded, were processed with LAS AF. Processing involved 3D deconvolution using the blind approach with 10 iterations.

10.4.2 Cell immobilization

Microscope slides were layered with 1 ml 1.5 % agarose solution (w/v) and dried over night. Ten micro liter of cell suspension were put on agarose coated microscope slides and a cover glass was placed over the sample prior to microscopy. Alternatively 2 µl cell suspension was applied to commercially acquired poly-lysine covered microscope slide (Thermo Fischer) and cell suspension was covered with a cover glass.

10.4.3 Staining with Nile red

When only PHB staining was of interest a cell suspension of a 20 µl, 10 µl nile red solution (1 µg/ml in ethanol) was added, ten 10 µl of the resulting cell suspension was dropped on an agarose coated slide and investigated under the microscope. For co-localization experiments 1 µl nile blue saturated solution in DMSO was added to 200 µl cell suspension and incubated for 5 minutes at room temperature. Afterwards cells were pelleted by centrifugation at 10,000 $\times$ g for 2 minutes and room temperature. The cell pellet was suspended in an appropriate volume of phosphate buffered saline (137 mM NaCl, 2.7 mM KCl pH7.4).

10.4.4 Staining with Bodipy

To 100 µl *Synechocystis* sp. PCC 6803 cell suspension 1 µl Bodipy®493/503 (10 mg/ml in DMSO) was added and incubated for five minutes. Cells were pelleted at 10,000 × g for 2 minutes and cell pellets were suspended in PBS. Two microliter were dropped on a poly-lysine coated glass slide and examined using a Leica DM5500B microscope.

10.4.5 Image adjustments

Image adjustments were performed with Adobe Photoshop CS5 by adjusting the input levels of the red, green and blue channel. Input levels were adjusted based on two criteria; avoiding loss of information due to low input levels of the upper input value and increased color intensities to visualize fluorophor emission. If two images were intended to be compared to each other identical upper and lower input values were set to reflect the native signal intensities.

List of Abbreviations

$\times g$	gravitational acceleration
2-OG	2-oxoglutarate
2-OG	2-oxoglutarate
3-PGA	3-phosphoglycerate
ACC	Acetyl-coenzyme A carboxylase
AckA	Acetate kinase
Acs	Acetyl-coenzymeA synthetase
ADP	Adenosine diphosphate
ATP	Adenosine triphosphate
cDNA	complementary DNA
Cer	Cerulean
CO_2	carbon dioxide
CoA	Coenzyme A
DNA	Desoxyribonucleic acid
DTT	Dithiothreitol
EDTA	Ethylenediaminetetraacetic acid
Ga	10^9 years
GABA	γ-amino butyric acid
gDNA	genomic DNA
Gfp	Green fluorescent protein
GOGAT	Glutamine oxoglutarate aminotransferase
GS	Glutamine synthetase
HCO_3^-	Bicarbonate
K_M	Michaelis constant
kDa	kilo Dalton
M	mol/l
mM	mmol/l
mTurq2	mTurquoise2
NAD^+	Nicotinamide adenine dinucleotide
NADH	reduced Nicotinamide adenine dinucleotide
$NADP^+$	Nicotinamide adenine dinucleotide phosphate
NADPH	reduced Nicotinamide adenine dinucleotide phosphate
NCR	Non coding region
PCC	Pasteur culture collection
PepC	Phosphoenolpyruvate carboxylase
PhaA	β-ketothiolase
PhaB	Acetoacetyl-CoA reductase
PhaC	PHB synthase subunit C
PhaE	PHB synthase subunit E
PHB	Polyhydroxybutyric acid
PSI	Photosystem I
PSII	Photosystem II
Pta	Phosphotransacetylase
qRT-PCR	quantitative real-time reverse transcriptase polymerase chain reaction
RBS	Ribosomal binding site
RubisCO	Ribulose-1,5-bisphosphate carboxylase/oxygenase
SDS	Sodium dodecyl sulfate
SNP	single nucleotide polymorphism
TCA	tricarboxylic acid/citric acid/Krebs cycle
TES	N-[Tris(hydroxymethyl)methyl]-2-aminoethanesulfonic acid
Tris	Tris(hydroxymethyl)aminomethane
UTR	Untranslated region
Ven	venus
XFPK	Xylulose-5-phosphate/fructose-6-phosphate phosphoketolase
XPK	Xylulose 5-phosphate phosphoketolase

References

Agostoni, M., Waters, C. M., and Montgomery, B. L. (2016). Regulation of biofilm formation and cellular buoyancy through modulating intracellular cyclic di-gmp levels in engineered cyanobacteria. *Biotechnology and Bioengineering*, 113(2):311–319.

Andersen, M. H., Graversen, H., Fedosov, S. N., Petersen, T. E., and Rasmussen, J. T. (2000). Functional analyses of two cellular binding domains of bovine lactadherin. *Biochemistry*, 39(20):6200–6206.

Baier, A., Winkler, W., Korte, T., Lockau, W., and Karradt, A. (2014). Degradation of phycobilisomes in *Synechocystis* sp. PCC6803: Evidence for essential formation of an NblA1/NblA2 heterodimer and its codegradation by a Clp protease complex. *Journal of Biological Chemistry*, 289(17):11755–11766.

Baier, K., Nicklisch, S., Grundner, C., Reinecke, J., and Lockau, W. (2001). Expression of two *nblA*-homologous genes is required for phycobilisome degradation in nitrogen-starved *Synechocystis* sp. PCC6803. *FEMS microbiology letters*, 195(1):35–39.

Battchikova, N., Eisenhut, M., and Aro, E.-M. (2011). Cyanobacterial NDH-1 complexes: Novel insights and remaining puzzles. *Biochimica et Biophysica Acta (BBA) - Bioenergetics*, 1807(8):935 – 944. Regulation of Electron Transport in Chloroplasts.

Bauwe, H., Hagemann, M., and Fernie, A. R. (2010). Photorespiration: players, partners and origin. *Trends in plant science*, 15(6):330–336.

Beeby, M., Cho, M., Stubbe, J., and Jensen, G. J. (2012). Growth and localization of polyhydroxybutyrate granules in *Ralstonia eutropha*. *Journal of bacteriology*, 194(5):1092–1099.

Berg, I. A., Kockelkorn, D., Buckel, W., and Fuchs, G. (2007). A 3-hydroxypropionate/4-hydroxybutyrate autotrophic carbon dioxide assimilation pathway in archaea. *Science*, 318(5857):1782–1786.

Bertani, G. (1951). STUDIES ON LYSOGENESIS: The mode of phage liberation by lysogenic *Escherichia coli*. *Journal of bacteriology*, 62(3):293.

Bourrellier, A. B. F., Valot, B., Guillot, A., Ambard-Bretteville, F., Vidal, J., and Hodges, M. (2010). Chloroplast acetyl-coa carboxylase activity is 2-oxoglutarate-regulated by

interaction of P_{II} with the biotin carboxyl carrier subunit. *Proceedings of the National Academy of Sciences*, 107(1):502–507.

Bradford, M. (1976). A rapid and sensitive method for the quantitation of microgram quantities of protein utilizing the principle of protein-dye binding. *Analytical Biochemistry*, 72(1):248 – 254.

Burnap, R. L., Hagemann, M., and Kaplan, A. (2015). Regulation of CO_2 concentrating mechanism in cyanobacteria. *Life*, 5(1):348.

Cai, F., Sutter, M., Cameron, J. C., Stanley, D. N., Kinney, J. N., and Kerfeld, C. A. (2013). The structure of CcmP, a tandem bacterial microcompartment domain protein from the β-carboxysome, forms a subcompartment within a microcompartment. *Journal of Biological Chemistry*, 288(22):16055–16063.

Carr, N. and Whitton, B. (1982). *The Biology of cyanobacteria*. Botanical monographs. University of California Press.

Chardonnet, S., Sakr, S., Cassier-Chauvat, C., Maréchal, P. L., Chauvat, F., Lemaire, S. D., and Decottignies, P. (2015). First proteomic study of S-glutathionylation in cyanobacteria. *Journal of Proteome Research*, 14(1):59–71. PMID: 25208982.

Charng, Y.-y., Kakefuda, G., Iglesias, A. A., Buikema, W. J., and Preiss, J. (1992). Molecular cloning and expression of the gene encoding ADP-glucose pyrophosphorylase from the cyanobacterium *Anabaena* sp. strain PCC 7120. *Plant Molecular Biology*, 20(1):37–47.

Chen, C., Cao, R., Shrestha, R., Ward, C., Katz, B. B., Fischer, C. J., Tomich, J. M., and Li, P. (2015). Trapping of intermediates with substrate analog HBOCoA in the polymerizations catalyzed by class III polyhydroxybutyrate (phb) synthase from *Allochromatium Vinosum*. *ACS chemical biology*, 10(5):1330–1339.

Chen, X., Schreiber, K., Appel, J., Makowka, A., Fähnrich, B., Roettger, M., Hajirezaei, M. R., Sönnichsen, F. D., Schönheit, P., Martin, W. F., and Gutekunst, K. (2016). The Entner–Doudoroff pathway is an overlooked glycolytic route in cyanobacteria and plants. *Proceedings of the National Academy of Sciences*.

Colby, G. D. and Chen, J. S. (1992). Purification and properties of 3-hydroxybutyryl-coenzyme a dehydrogenase from *Clostridium beijerinckii* ("*Clostridium butylicum*") NRRL B593. *Applied and Environmental Microbiology*, 58(10):3297–3302.

Conroy, M. J., Durand, A., Lupo, D., Li, X.-D., Bullough, P. A., Winkler, F. K., and Merrick, M. (2007). The crystal structure of the *Escherichia coli* AmtB–GlnK complex reveals how GlnK regulates the ammonia channel. *Proceedings of the National Academy of Sciences*, 104(4):1213–1218.

Cooley, J. W., Howitt, C. A., and Vermaas, W. F. J. (2000). Succinate:Quinol oxidoreductases in the cyanobacterium *Synechocystis* sp. strain PCC 6803: Presence and function in metabolism and electron transport. *Journal of Bacteriology*, 182(3):714–722.

De Philippis, R., Ena, A., Guastiini, M., Sili, C., and Vincenzini, M. (1992a). Factors affecting poly-β-hydroxybutyrate accumulation in cyanobacteria and in purple non-sulfur bacteria. *FEMS Microbiology Letters*, 103(2-4):187–194.

De Philippis, R., Sili, C., and Vincenzini, M. (1992b). Glycogen and poly-β-hydroxybutyrate synthesis in *Spirulina maxima*. *Microbiology*, 138(8):1623–1628.

Diamond, S., Jun, D., Rubin, B. E., and Golden, S. S. (2015). The circadian oscillator in *Synechococcus elongatus* controls metabolite partitioning during diurnal growth. *Proceedings of the National Academy of Sciences*, 112(15):E1916–E1925.

Díaz-Troya, S., López-Maury, L., Sánchez-Riego, A. M., Roldán, M., and Florencio, F. J. (2014). Redox regulation of glycogen biosynthesis in the cyanobacterium *Synechocystis* sp. PCC 6803: Analysis of the AGP and glycogen synthases. *Molecular plant*, 7(1):87–100.

Ding, X., Matsumoto, T., Gena, P., Liu, C., Pellegrini-Calace, M., Zhong, S., Sun, X., Zhu, Y., Katsuhara, M., Iwasaki, I., Kitagawa, Y., and Calamita, G. (2013). Water and CO_2 permeability of SsAqpZ, the cyanobacterium *Synechococcus* sp. PCC7942 aquaporin. *Biology of the Cell*, 105(3):118–128.

Dueber, J. E., Wu, G. C., Malmirchegini, G. R., Moon, T. S., Petzold, C. J., Ullal, A. V., Prather, K. L., and Keasling, J. D. (2009). Synthetic protein scaffolds provide modular control over metabolic flux. *Nature biotechnology*, 27(8):753–759.

Espinosa, J., Castells, M. A., Laichoubi, K. B., and Contreras, A. (2009). Mutations at *pipX* suppress lethality of P_{II}-deficient mutants of *Synechococcus elongatus* PCC 7942. *Journal of Bacteriology*, 191(15):4863–4869.

Espinosa, J., Forchhammer, K., Burillo, S., and Contreras, A. (2006). Interaction network in cyanobacterial nitrogen regulation: PipX, a protein that interacts in a 2-oxoglutarate dependent manner with P_{II} and NtcA. *Molecular Microbiology*, 61(2):457–469.

Fokina, O., Chellamuthu, V.-R., Forchhammer, K., and Zeth, K. (2010a). Mechanism of 2-oxoglutarate signaling by the *Synechococcus elongatus* P_{II} signal transduction protein. *Proceedings of the National Academy of Sciences*, 107(46):19760–19765.

Fokina, O., Chellamuthu, V.-R., Zeth, K., and Forchhammer, K. (2010b). A novel signal transduction protein P_{II} variant from *Synechococcus elongatus* PCC 7942 indicates a two-step process for NAGK-P_{II} complex formation. *Journal of molecular biology*, 399(3):410–421.

Fokina, O., Herrmann, C., and Forchhammer, K. (2011). Signal-transduction protein P_{II} from *Synechococcus elongatus* PCC 7942 senses low adenylate energy charge *in vitro*. *Biochemical Journal*, 440(1):147–156.

Forchhammer, K. and Lüddecke, J. (2016). Sensory properties of the P_{II} signalling protein family. *FEBS Journal*, 283(3):425–437.

Forchhammer, K. and Tandeau de Marsac, N. (1994). The P_{II} protein in the cyanobacterium *Synechococcus* sp. strain PCC 7942 is modified by serine phosphorylation and signals the cellular N-status. *Journal of Bacteriology*, 176(1):84–91.

Forchhammer, K. and Tandeau de Marsac, N. (1995). Functional analysis of the phosphoprotein P_{II} (glnB gene product) in the cyanobacterium *Synechococcus* sp. strain PCC 7942. *Journal of Bacteriology*, 177(8):2033–40.

Galan, B., Dinjaski, N., Maestro, B., De Eugenio, L., Escapa, I., Sanz, J., Garcia, J., and Prieto, M. (2011). Nucleoid-associated PhaF phasin drives intracellular location and segregation of polyhydroxyalkanoate granules in *Pseudomonas putida* KT2442. *Molecular microbiology*, 79(2):402–418.

Görl, M., Sauer, J., Baier, T., and Forchhammer, K. (1998). Nitrogen-starvation-induced chlorosis in *Synechococcus* PCC 7942: Adaptation to long-term survival. *Microbiology*, 144(9):2449–2458.

Griebel, R., Smith, Z., and Merrick, J. M. (1968). Metabolism of poly(-hydroxybutyrate). purification, composition, and properties of native poly(-hydroxybutyrate) granules from *Bacillus megaterium*. *Biochemistry*, 7(10):3676–3681.

Gründel, M., Scheunemann, R., Lockau, W., and Zilliges, Y. (2012). Impaired glycogen synthesis causes metabolic overflow reactions and affects stress responses in the cyanobacterium *Synechocystis* sp. PCC 6803. *Microbiology*, 158(12):3032–3043.

Gruswitz, F., O'Connell, J., and Stroud, R. M. (2007). Inhibitory complex of the transmembrane ammonia channel, AmtB, and the cytosolic regulatory protein, GlnK, at 1.96 Å. *Proceedings of the National Academy of Sciences*, 104(1):42–47.

Han, M.-J., Yoon, S. S., and Lee, S. Y. (2001). Proteome analysis of metabolically engineered *Escherichia coli* producing poly(3-hydroxybutyrate). *Journal of Bacteriology*, 183(1):301–308.

Hauf, W. (2012). Polyhydroxybutyrate (PHB) metabolism and PHB granule formation in *Synechocystis* sp. PCC 6803.

Hauf, W., Schlebusch, M., Hüge, J., Kopka, J., Hagemann, M., and Forchhammer, K. (2013). Metabolic changes in *Synechocystis* PCC6803 upon nitrogen-starvation: Excess NADPH sustains polyhydroxybutyrate accumulation. *Metabolites*, 3(1):101.

Hauf, W., Watzer, B., Roos, N., Klotz, A., and Forchhammer, K. (2015). Photoautotrophic polyhydroxybutyrate granule formation is regulated by cyanobacterial phasin PhaP in *Synechocystis* sp. strain PCC 6803. *Applied and Environmental Microbiology*, 81(13):4411–4422.

Hein, S., Tran, H., and Steinbüchel, A. (1998). *Synechocystis* sp. PCC6803 possesses a two-component polyhydroxyalkanoic acid synthase similar to that of anoxygenic purple sulfur bacteria. *Archives of microbiology*, 170(3):162–170.

Heinrich, A., Maheswaran, M., Ruppert, U., and Forchhammer, K. (2004). The *Synechococcus elongatus* P_{II} signal transduction protein controls arginine synthesis by complex formation with N-acetyl-l-glutamate kinase. *Molecular Microbiology*, 52(5):1303–1314.

Herrero, A., Flores, E., and Flores, F. (2008). *The cyanobacteria: molecular biology, genomics, and evolution*. Caister Academic Press.

Herrero, A., Muro-Pastor, A. M., and Flores, E. (2001). Nitrogen control in cyanobacteria. *Journal of Bacteriology*, 183(2):411–425.

Hisbergues, M., Jeanjean, R., Joset, F., de Marsac, N. T., and Bédu, S. (1999). Protein P_{II} regulates both inorganic carbon and nitrate uptake and is modified by a redox signal in *Synechocystis* PCC 6803. *FEBS letters*, 463(3):216–220.

Jendrossek, D. (2009). Polyhydroxyalkanoate granules are complex subcellular organelles (carbonosomes). *Journal of bacteriology*, 191(10):3195–3202.

Jendrossek, D. and Pfeiffer, D. (2014). New insights in the formation of polyhydroxyalkanoate granules (carbonosomes) and novel functions of poly(3-hydroxybutyrate). *Environmental Microbiology*, 16(8):2357–2373.

Jendrossek, D., Selchow, O., and Hoppert, M. (2007). Poly(3-hydroxybutyrate) granules at the early stages of formation are localized close to the cytoplasmic membrane in *Caryophanon latum*. *Applied and Environmental Microbiology*, 73(2):586–593.

Joseph, A., Aikawa, S., Sasaki, K., Teramura, H., Hasunuma, T., Matsuda, F., Osanai, T., Hirai, M. Y., and Kondo, A. (2014). Rre37 stimulates accumulation of 2-oxoglutarate and glycogen under nitrogen starvation in *Synechocystis* sp. PCC 6803. *FEBS letters*, 588(3):466–471.

Jossek, R., Reichelt, R., and Steinbüchel, A. (1998). In vitro biosynthesis of poly (3-hydroxybutyric acid) by using purified poly (hydroxyalkanoic acid) synthase of *Chromatium vinosum*. *Applied microbiology and biotechnology*, 49(3):258–266.

Kaneko, T., Sato, S., Kotani, H., Tanaka, A., Asamizu, E., Nakamura, Y., Miyajima, N., Hirosawa, M., Sugiura, M., Sasamoto, S., et al. (1996). Sequence analysis of the

genome of the unicellular cyanobacterium *Synechocystis* sp. strain PCC6803. II. sequence determination of the entire genome and assignment of potential protein-coding regions. *DNA research*, 3(3):109–136.

Kappell, A. D. and van Waasbergen, L. G. (2007). The response regulator RpaB binds the high light regulatory 1 sequence upstream of the high-light-inducible *hliB* gene from the cyanobacterium *Synechocystis* PCC 6803. *Archives of microbiology*, 187(4):337–342.

Kato, H., Kubo, T., Hayashi, M., Kobayashi, I., Yagasaki, T., Chibazakura, T., Watanabe, S., and Yoshikawa, H. (2011). Interactions between histidine kinase NblS and the response regulators RpaB and SrrA are involved in the bleaching process of the cyanobacterium *Synechococcus elongatus* PCC 7942. *Plant and Cell Physiology*, 52(12):2115–2122.

Kelley, L. A., Mezulis, S., Yates, C. M., Wass, M. N., and Sternberg, M. J. (2015). The Phyre2 web portal for protein modeling, prediction and analysis. *Nature protocols*, 10(6):845–858.

Khetkorn, W., Incharoensakdi, A., Lindblad, P., and Jantaro, S. (2016). Enhancement of poly-3-hydroxybutyrate production in *Synechocystis* sp. PCC 6803 by overexpression of its native biosynthetic genes. *Bioresource technology*, 214:761–768.

Klein, A. H., Shulla, A., Reimann, S. A., Keating, D. H., and Wolfe, A. J. (2007). The intracellular concentration of acetyl phosphate in *Escherichia coli* is sufficient for direct phosphorylation of two-component response regulators. *Journal of Bacteriology*, 189(15):5574–5581.

Klotz, A., Reinhold, E., Doello, S., and Forchhammer, K. (2015). Nitrogen starvation acclimation in synechococcus elongatus: Redox-control and the role of nitrate reduction as an electron sink. *Life*, 5(1):888.

Knowles, V. L. and Plaxton, W. C. (2003). From genome to enzyme: Analysis of key glycolytic and oxidative pentose-phosphate pathway enzymes in the cyanobacterium *Synechocystis* sp. PCC 6803. *Plant and Cell Physiology*, 44(7):758–763.

Kobayashi, M., Takatani, N., Tanigawa, M., and Omata, T. (2005). Posttranslational regulation of nitrate assimilation in the cyanobacterium *Synechocystis* sp. strain PCC 6803. *Journal of Bacteriology*, 187(2):498–506.

Kosono, S., Tamura, M., Suzuki, S., Kawamura, Y., Yoshida, A., Nishiyama, M., and Yoshida, M. (2015). Changes in the acetylome and succinylome of *Bacillus subtilis* in response to carbon source. *PloS one*, 10(6):e0131169.

Krasikov, V., Aguirre von Wobeser, E., Dekker, H. L., Huisman, J., and Matthijs, H. C. P. (2012). Time-series resolution of gradual nitrogen starvation and its impact on

photosynthesis in the cyanobacterium *Synechocystis* PCC 6803. *Physiologia Plantarum*, 145(3):426–439.

Kuhn, M. L., Zemaitaitis, B., Hu, L. I., Sahu, A., Sorensen, D., Minasov, G., Lima, B. P., Scholle, M., Mrksich, M., Anderson, W. F., et al. (2014). Structural, kinetic and proteomic characterization of acetyl phosphate-dependent bacterial protein acetylation. *PloS one*, 9(4):e94816.

Laichoubi, K. B., Espinosa, J., Castells, M. A., and Contreras, A. (2012). Mutational analysis of the cyanobacterial nitrogen regulator PipX. *PloS one*, 7(4):e35845.

Lan, E. I. and Liao, J. C. (2012). ATP drives direct photosynthetic production of 1-butanol in cyanobacteria. *Proceedings of the National Academy of Sciences*, 109(16):6018–6023.

Latifi, A., Ruiz, M., and Zhang, C.-C. (2009). Oxidative stress in cyanobacteria. *FEMS microbiology reviews*, 33(2):258–278.

Lee, H.-M., Flores, E., Forchhammer, K., Herrero, A., and Tandeau de Marsac, N. (2000). Phosphorylation of the signal transducer P_{II} protein and an additional effector are required for the P_{II}-mediated regulation of nitrate and nitrite uptake in the cyanobacterium *Synechococcus* sp. PCC 7942. *European Journal of Biochemistry*, 267(2):591–600.

Levi, C. and Preiss, J. (1976). Regulatory properties of the ADP-Glucose pyrophosphorylase of the blue-green bacterium *Synechococcus* 6301. *Plant Physiology*, 58(6):753–756.

Liu, D. and Yang, C. (2014). The nitrogen-regulated response regulator NrrA controls cyanophycin synthesis and glycogen catabolism in the cyanobacterium *Synechocystis* sp. PCC 6803. *Journal of Biological Chemistry*, 289(4):2055–2071.

Llacer, J. L., Espinosa, J., Castells, M. A., Contreras, A., Forchhammer, K., and Rubio, V. (2010). Structural basis for the regulation of NtcA-dependent transcription by proteins PipX and P_{II}. *Proceedings of the National Academy of Sciences*, 107(35):15397–15402.

Lüddecke, J. and Forchhammer, K. (2013). From P_{II} signaling to metabolite sensing: A novel 2-oxoglutarate sensor that details P_{II}-NAGK complex formation. *PloS one*, 8(12):e83181.

Maestro, B., Galán, B., Alfonso, C., Rivas, G., Prieto, M. A., and Sanz, J. M. (2013). A new family of intrinsically disordered proteins: Structural characterization of the major phasin PhaF from *Pseudomonas putida* KT2440. *PLoS ONE*, 8(2):1–15.

Maheswaran, M., Urbanke, C., and Forchhammer, K. (2004). Complex formation and catalytic activation by the P_{II} signaling protein of N-acetyl-l-glutamate kinase from *Synechococcus elongatus* strain PCC 7942. *Journal of Biological Chemistry*, 279(53):55202–55210.

Mayer, F., Madokour, M. H., Pieper-Fürst, U., Wieczorek, R., Liebergesell, M., and Steinbüchel, A. (1996). Electron microscopic observations on the macromolecular organization of the boundary layer of bacterial PHA inclusion bodies. *The Journal of General and Applied Microbiology*, 42(6):445–455.

Mezzina, M. P., Wetzler, D. E., Almeida, A., Dinjaski, N., Prieto, M. A., and Pettinari, M. J. (2015). A phasin with extra talents: a polyhydroxyalkanoate granule-associated protein has chaperone activity. *Environmental microbiology*, 17(5):1765–1776.

Miyake, M., Kataoka, K., Shirai, M., and Asada, Y. (1997). Control of poly-β-hydroxybutyrate synthase mediated by acetyl phosphate in cyanobacteria. *Journal of Bacteriology*, 179(16):5009–13.

Mo, R., Yang, M., Chen, Z., Cheng, Z., Yi, X., Li, C., He, C., Xiong, Q., Chen, H., Wang, Q., et al. (2015). Acetylome analysis reveals the involvement of lysine acetylation in photosynthesis and carbon metabolism in the model cyanobacterium *Synechocystis* sp. PCC 6803. *Journal of proteome research*, 14(2):1275–1286.

Montesinos, M. L., Muro-Pastor, A. M., Herrero, A., and Flores, E. (1998). Ammonium/methylammonium permeases of a cyanobacterium: Identification and analysis of three nitrogen-regulated *amt* genes in *Synechocystis* sp. PCC 6803. *Journal of Biological Chemistry*, 273(47):31463–31470.

Neshich, I. A., Kiyota, E., and Arruda, P. (2013). Genome-wide analysis of lysine catabolism in bacteria reveals new connections with osmotic stress resistance. *The ISME journal*, 7(12):2400–2410.

Ninfa, A. J. and Jiang, P. (2005). P_{II} signal transduction proteins: sensors of α-ketoglutarate that regulate nitrogen metabolism. *Current opinion in microbiology*, 8(2):168–173.

Oeding, V. and Schlegel, H. G. (1973). β-ketothiolase from *Hydrogenomonas eutropha* H16 and its significance in the regulation of poly-β-hydroxybutyrate metabolism. *Biochemical Journal*, 134(1):239–248.

Oh, D.-H., Chung, C.-W., Kim, J. Y., and Rhee, Y. H. (1997). Partial purification and characterization of β-ketothiolase from *Alcaligenes* sp. SH-69. *Journal of Microbiology-Seoul-*, 35:360–364.

Ohashi, Y., Shi, W., Takatani, N., Aichi, M., Maeda, S.-i., Watanabe, S., Yoshikawa, H., and Omata, T. (2011). Regulation of nitrate assimilation in cyanobacteria. *Journal of Experimental Botany*, 62(4):1411–1424.

Okamura, E., Tomita, T., Sawa, R., Nishiyama, M., and Kuzuyama, T. (2010). Unprecedented acetoacetyl-coenzyme A synthesizing enzyme of the thiolase superfamily

involved in the mevalonate pathway. *Proceedings of the National Academy of Sciences*, 107(25):11265–11270.

Panda, B., Jain, P., Sharma, L., and Mallick, N. (2006). Optimization of cultural and nutritional conditions for accumulation of poly-β-hydroxybutyrate in *Synechocystis* sp. PCC 6803. *Bioresource Technology*, 97(11):1296 – 1301.

Panda, B. and Mallick, N. (2007). Enhanced poly-β-hydroxybutyrate accumulation in a unicellular cyanobacterium, *Synechocystis* sp. PCC 6803. *Letters in Applied Microbiology*, 44(2):194–198.

Pattanayak, G. K., Phong, C., and Rust, M. J. (2014). Rhythms in energy storage control the ability of the cyanobacterial circadian clock to reset. *Current Biology*, 24(16):1934 – 1938.

Peramuna, A. and Summers, M. L. (2014). Composition and occurrence of lipid droplets in the cyanobacterium *Nostoc punctiforme*. *Archives of microbiology*, 196(12):881–890.

Peschek, G. A., Obinger, C., and Renger, G. (2011). *Bioenergetic processes of Cyanobacteria*. Springer.

Pfeiffer, D. and Jendrossek, D. (2014). Pham is the physiological activator of poly(3-hydroxybutyrate) (PHB) synthase (PhaC1) in *Ralstonia eutropha*. *Applied and Environmental Microbiology*, 80(2):555–563.

Pieper-Fürst, U., Madkour, M. H., Mayer, F., and Steinbüchel, A. (1994). Purification and characterization of a 14-kilodalton protein that is bound to the surface of polyhydroxyalkanoic acid granules in *Rhodococcus ruber*. *Journal of bacteriology*, 176(14):4328–4337.

Pinto, F. L., Thapper, A., Sontheim, W., and Lindblad, P. (2009). Analysis of current and alternative phenol based RNA extraction methodologies for cyanobacteria. *BMC Molecular Biology*, 10(1):1–8.

Ploux, O., Masamune, S., and Walsh, C. T. (1988). The NADPH-linked acetoacetyl-CoA reductase from *Zoogloea ramigera*. *European Journal of Biochemistry*, 174(1):177–182.

Pötter, M., Müller, H., Reinecke, F., Wieczorek, R., Fricke, F., Bowien, B., Friedrich, B., and Steinbüchel, A. (2004). The complex structure of polyhydroxybutyrate (PHB) granules: four orthologous and paralogous phasins occur in *Ralstonia eutropha*. *Microbiology*, 150(7):2301–2311.

Preiss, J. (1984). Bacterial glycogen synthesis and its regulation. *Annual Review of Microbiology*, 38(1):419–458. PMID: 6093684.

Quintero, M. J., Montesinos, M. L., Herrero, A., and Flores, E. (2001). Identification of genes encoding amino acid permeases by inactivation of selected orfs from the *Synechocystis* genomic sequence. *Genome Research*, 11(12):2034–2040.

Radchenko, M. V., Thornton, J., and Merrick, M. (2010). Control of AmtB-GlnK complex formation by intracellular levels of ATP, ADP, and 2-oxoglutarate. *Journal of Biological Chemistry*, 285(40):31037–31045.

Rehm, B. (2006). *Microbial bionanotechnology: biological self-assembly systems and biopolymer-based nanostructures*. Horizon Bioscience.

Rippka, R., Deruelles, J., Waterbury, J., Herdman, M., and Stanier, R. Y. (1979). Generic assignments, strain histories and properties of pure cultures of cyanobacteria. *Journal of General Microbiology*, 111(1):1–61.

Saha, R., Liu, D., Hoynes-O'Connor, A., Liberton, M., Yu, J., Bhattacharyya-Pakrasi, M., Balassy, A., Zhang, F., Moon, T. S., Maranas, C. D., and Pakrasi, H. B. (2016). Diurnal regulation of cellular processes in the cyanobacterium *Synechocystis* sp. strain PCC 6803: Insights from transcriptomic, fluxomic, and physiological analyses. *mBio*, 7(3).

Saini, V., Cumming, B. M., Guidry, L., Lamprecht, D. A., Adamson, J. H., Reddy, V. P., Chinta, K. C., Mazorodze, J. H., Glasgow, J. N., Richard-Greenblatt, M., Gomez-Velasco, A., Bach, H., Av-Gay, Y., Eoh, H., Rhee, K., and Steyn, A. J. (2016). Ergothioneine maintains redox and bioenergetic homeostasis essential for drug susceptibility and virulence of *Mycobacterium tuberculosis*. *Cell reports*, 14(3):572–585.

Salomon, E., Bar-Eyal, L., Sharon, S., and Keren, N. (2013). Balancing photosynthetic electron flow is critical for cyanobacterial acclimation to nitrogen limitation. *Biochimica et Biophysica Acta (BBA)-Bioenergetics*, 1827(3):340–347.

Sauer, J., Görl, M., and Forchhammer, K. (1999). Nitrogen starvation in *Synechococcus* PCC 7942: Involvement of glutamine synthetase and NtcA in phycobiliprotein degradation and survival. *Archives of microbiology*, 172(4):247–255.

Sauer, J., Schreiber, U., Schmid, R., Völker, U., and Forchhammer, K. (2001). Nitrogen starvation-induced chlorosis in *Synechococcus* PCC 7942. Low-level photosynthesis as a mechanism of long-term survival. *Plant physiology*, 126(1):233–243.

Savakis, P., De Causmaecker, S., Angerer, V., Ruppert, U., Anders, K., Essen, L.-O., and Wilde, A. (2012). Light-induced alteration of c-di-GMP level controls motility of *Synechocystis* sp. PCC 6803. *Molecular Microbiology*, 85(2):239–251.

Schirrmeister, B. E., Gugger, M., and Donoghue, P. C. J. (2015). Cyanobacteria and the great oxidation event: Evidence from genes and fossils. *Palaeontology*, 58(5):769–785.

Schlebusch, M. (2012). *Analysis of the Sll0783 function in PHB synthesis in Synechocystis PCC 6803: A crucial role of NADPH in N-starvation*. PhD thesis, Universität Tübingen.

Schlebusch, M. and Forchhammer, K. (2010). Requirement of the nitrogen starvation-induced protein Sll0783 for polyhydroxybutyrate accumulation in *Synechocystis* sp. strain PCC 6803. *Applied and Environmental Microbiology*, 76(18):6101–6107.

Schwarz, D., Orf, I., Kopka, J., and Hagemann, M. (2014). Effects of inorganic carbon limitation on the metabolome of the *Synechocystis* sp. PCC 6803 mutant defective in *glnB* encoding the central regulator P_{II} of cyanobacterial C/N acclimation. *Metabolites*, 4(2):232–247.

Sendersky, E., Kozer, N., Levi, M., Garini, Y., Shav-Tal, Y., and Schwarz, R. (2014). The proteolysis adaptor, NblA, initiates protein pigment degradation by interacting with the cyanobacterial light-harvesting complexes. *The Plant Journal*, 79(1):118–126.

Shao, C., Novakovic, V. A., Head, J. F., Seaton, B. A., and Gilbert, G. E. (2008). Crystal structure of lactadherin C2 domain at 1.7 Å resolution with mutational and computational analyses of its membrane-binding motif. *Journal of Biological Chemistry*, 283(11):7230–7241.

Sharma, L., Panda, B., Singh, A. K., and Mallick, N. (2006). Studies on poly-β-hydroxybutyrate synthase activity of *Nostoc muscorum*. *The Journal of General and Applied Microbiology*, 52(4):209–214.

Shen, J.-R. (2015). The structure of photosystem II and the mechanism of water oxidation in photosynthesis. *Annual Review of Plant Biology*, 66(1):23–48. PMID: 25746448.

Smith, C., Deutch, A., and Rushlow, K. (1984). Purification and characteristics of a gamma-glutamyl kinase involved in *Escherichia coli* proline biosynthesis. *Journal of bacteriology*, 157(2):545–551.

Spät, P., Macek, B., and Forchhammer, K. (2015). Phosphoproteome of the cyanobacterium *Synechocystis* sp. PCC 6803 and its dynamics during nitrogen starvation. *Regulatory potential of post-translational modifications in bacteria*, page 20.

Stanier, R., Kunisawa, R., Mandel, M., and Cohen-Bazire, G. (1971). Purification and properties of unicellular blue-green algae (order Chroococcales). *Bacteriological reviews*, 35(2):171.

Suzuki, E., Ohkawa, H., Moriya, K., Matsubara, T., Nagaike, Y., Iwasaki, I., Fujiwara, S., Tsuzuki, M., and Nakamura, Y. (2010). Carbohydrate metabolism in mutants of the cyanobacterium *Synechococcus elongatus* PCC 7942 defective in glycogen synthesis. *Applied and environmental microbiology*, 76(10):3153–3159.

Takatani, N. and Omata, T. (2006). Effects of P_{II} deficiency on expression of the genes involved in ammonium utilization in the cyanobacterium *Synechocystis* sp. strain PCC 6803. *Plant and cell physiology*, 47(6):679–688.

Taroncher-Oldenburg, G., Nishina, K., and Stephanopoulos, G. (2000). Identification and analysis of the polyhydroxyalkanoate-specific β-ketothiolase and acetoacetyl coenzyme A reductase genes in the cyanobacterium *Synechocystis* sp. strain PCC6803. *Applied and Environmental Microbiology*, 66(10):4440–4448.

Ushimaru, K., Motoda, Y., Numata, K., and Tsuge, T. (2014). Phasin proteins activate *Aeromonas caviae* polyhydroxyalkanoate (PHA) synthase but not *Ralstonia eutropha* PHA synthase. *Applied and environmental microbiology*, 80(9):2867–2873.

Valladares, A., Montesinos, M. L., Herrero, A., and Flores, E. (2002). An ABC-type, high-affinity urea permease identified in cyanobacteria. *Molecular microbiology*, 43(3):703–715.

Vandesompele, J., De Preter, K., Pattyn, F., Poppe, B., Van Roy, N., De Paepe, A., and Speleman, F. (2002). Accurate normalization of real-time quantitative RT-PCR data by geometric averaging of multiple internal control genes. *Genome biology*, 3(7):1–12.

Wahl, A., Schuth, N., Pfeiffer, D., Nussberger, S., and Jendrossek, D. (2012). PHB granules are attached to the nucleoid via PhaM in *Ralstonia eutropha*. *BMC microbiology*, 12(1):262.

Wang, Y., Sun, J., and Chitnis, P. R. (2000). Proteomic study of the peripheral proteins from thylakoid membranes of the cyanobacterium *Synechocystis* sp. PCC 6803. *Identification and functional analysis of thylakoid membrane proteome*, 1050:50.

Watzer, B., Engelbrecht, A., Hauf, W., Stahl, M., Maldener, I., and Forchhammer, K. (2015). Metabolic pathway engineering using the central signal processor P_{II}. *Microbial Cell Factories*, 14(1):1–12.

Weinert, B. T., Iesmantavicius, V., Wagner, S. A., Schölz, C., Gummesson, B., Beli, P., Nyström, T., and Choudhary, C. (2013). Acetyl-phosphate is a critical determinant of lysine acetylation in *E. coli*. *Molecular cell*, 51(2):265–272.

Whitton, B. and Potts, M. (2000). *The ecology of cyanobacteria: their diversity in time and space*. Kluwer Academic.

Wieczorek, R., Pries, A., Steinbüchel, A., and Mayer, F. (1995). Analysis of a 24-kilodalton protein associated with the polyhydroxyalkanoic acid granules in *Alcaligenes eutrophus*. *Journal of Bacteriology*, 177(9):2425–2435.

Wolk, C. P., Thomas, J., Shaffer, P. W., Austin, S. M., and Galonsky, A. (1976). Pathway of nitrogen metabolism after fixation of 13N-labeled nitrogen gas by the cyanobacterium, *Anabaena cylindrica*. *Journal of Biological Chemistry*, 251(16):5027–5034.

Wolk, C. P., Vonshak, A., Kehoe, P., and Elhai, J. (1984). Construction of shuttle vectors capable of conjugative transfer from *Escherichia coli* to nitrogen-fixing filamentous cyanobacteria. *Proceedings of the National Academy of Sciences*, 81(5):1561–1565.

Xiong, W., Brune, D., and Vermaas, W. F. (2014). The γ-aminobutyric acid shunt contributes to closing the tricarboxylic acid cycle in *Synechocystis* sp. PCC 6803. *Molecular microbiology*, 93(4):786–796.

Xiong, W., Lee, T.-C., Rommelfanger, S., Gjersing, E., Cano, M., Maness, P.-C., Ghirardi, M., and Yu, J. (2015). Phosphoketolase pathway contributes to carbon metabolism in cyanobacteria. *Nature plants*, 2:15187.

Yang, L., Ding, Y., Chen, Y., Zhang, S., Huo, C., Wang, Y., Yu, J., Zhang, P., Na, H., Zhang, H., et al. (2012). The proteomics of lipid droplets: structure, dynamics, and functions of the organelle conserved from bacteria to humans. *Journal of lipid research*, 53(7):1245–1253.

Yeates, T. O., Kerfeld, C. A., Heinhorst, S., Cannon, G. C., and Shively, J. M. (2008). Protein-based organelles in bacteria: Carboxysomes and related microcompartments. *Nature Reviews Microbiology*, 6(9):681–691.

Zakhia, F., Jungblut, A.-D., Taton, A., Vincent, W. F., and Wilmotte, A. (2008). Cyanobacteria in cold ecosystems. In *Psychrophiles: from biodiversity to biotechnology*, pages 121–135. Springer.

Zalutskaya, Z., Kharatyan, N., Forchhammer, K., and Ermilova, E. (2015). Reduction of P_{II} signaling protein enhances lipid body production in *Chlamydomonas reinhardtii*. *Plant Science*, 240:1–9.

Zeth, K., Fokina, O., and Forchhammer, K. (2014). Structural basis and target-specific modulation of ADP sensing by the *Synechococcus elongatus* P_{II} signaling protein. *Journal of Biological Chemistry*, 289(13):8960–8972.

Zinchenko, V., Piven, I., Melnik, V., and Shestakov, S. (1999). Vectors for the complementation analysis of cyanobacterial mutants. *Russian Journal of Genetics*, 35(3):228–232.

Acknowledgements

I am thankful to Prof. Forchhammer for the constant support and his inspiring optimism through the ups and downs of a PhD. It was a pleasure to work in an atmosphere where I was granted the freedom to pursue my ideas.

I am thankful to Prof. Jendrossek for fruitful discussions and his enthusiasm towards microbial cell biology.

Furthermore I want to thank my lab mates Björn and Alex for the special lab environment, with off project fermentation experiments. I want to also thank Jan L., Klaus, Jan B. and Philipp for the activities outside the lab.

Last but not least, I want to thank my family and my wife Ksenia for the support throughout the years.